Nonperturbative Aspects of Kaon Structure

Parada Tobel Paraduan Hutauruk

Thesis submitted for The Degree of Doctor of Philosophy
in Theoretical Physics

Thesis Supervisors:
Prof. Anthony. W. Thomas
Dr. Ian Christhoper Cloet
A/Prof. Ross Young

THE UNIVERSITY
of ADELAIDE

Faculty of Sciences

School of Chemistry & Physics

Adelaide, 12 January 2016

Contents

List of Tables

List of Figures

Signed Statement

I certify that this work contains no material which has been accepted for the award of any other degree or diploma in my name, in any university or other tertiary institution and, to the best of my knowledge and belief, contains no material previously published or written by another person, except where due reference has been made in the text. In addition, I certify that no part of this work will, in the future, be used in a submission in my name, for any other degree or diploma in any university or other tertiary institution without the prior approval of the University of Adelaide and where applicable, any partner institution responsible for the joint-award of this degree.

I give consent to this copy of my thesis, when deposited in the University Library, being made available for loan and photocopying, subject to the provisions of the Copyright Act 1968.

I also give permission for the digital version of my thesis to be made available on the web, via the University's digital research repository., the Library Search and also through web search engines, unless permission has been granted by the University to restrict access for a period of time.

SIGNED: DATE:

Acknowledgements

I would like to thank to my Lord Jesus for pouring on me His "*infinite*" blessings and knowledge in order to finish my Ph.D in His time. Glory to God in the highest.

I would like to thank to my supervisor Prof. Tony Thomas for giving me a great opportunity to pursue my Ph.D at the CSSM. Your patient, support and encouragement always make me feeling great and enjoyable during my Ph.D time.

I would also like to thank to my second supervisor A/Prof. Ross Young, who while not directly involved with the research in this thesis but he always helped when it was needed. I thank my other supervisor, Dr. Ian Cloet, for his patience, attention, advice and discussion while he was in Adelaide (before moving to Argonne). It was absolutely amazing, incredible and unforgettable moment for me. I hope we will continue this collaboration in the future.

Most importantly, I would like to thank to my *inspiration* and *beautiful* wife, Dina and beloved daughters, Tania and Atta for their *infinite* love, spirit, patience, support and prayer. I dedicate this thesis to my wife, daughters and my big family, St. R. Hutauruk and M. Hutabarat and Niken Pratindyastuti.

I also thank my roommate Daniel Whittenbury for our friendship and discussion about many things, I really enjoyed our discussion.

Last but not the least, I would like to thank Prof. Terry Mart for always helping me and being my *physics inspiration*. Also I would like to thank to A/Prof. Anto Sulaksono and Dr. Laksana. T. Handoko for their assistance and support. Thank you for their help and support to find my destiny being a *good physicist*.

Finally I thank to Physics Postgraduate Coordinator Dr. Rodney Crewther for helping me during the ASI (Adelaide Scholarship International) process and the University of Adelaide for awarding me an ASI to pursue my PhD at CSSM.

Adelaide, 12 January 2016.
Sincerely Yours,

Parada Tobel Paraduan Hutauruk, M.Sc

Dedication

Tetapi firman ini sangat dekat kepadamu, yakni di dalam mulutmu,
dan didalam hatimu, untuk dilakukan
(Ulangan 30:14) [ITB]
But the word is very nigh unto thee, in thy mouth, and in thy heart,
that thou mayest do it
(Deuteronomy 30 :14) [KJV]

Kupersembahkan untuk:
Ayahanda dan ibunda tersayang (St. R. Hutauruk dan M. Br. Hutabarat)
Isteriku tercinta (Eva Dina Sakti) dan anak-anakku tersayang (Tania dan Atta),
Adik-adikku terkasih (Johardi, Johanes, Lena, Yanti dan Jonni).

Abstract

In this thesis we have studied the structure of the kaon using the Nambu-Jona-Lasinio (NJL) model with the proper-time regularisation scheme to simulate the effect of quark confinement. The separate contributions of each flavour to the elastic form factor are calculated with and without the effect of dressing at the quark-photon vertex. In comparison with the existing experimental data, our model shows a remarkable agreement. We found the contribution of the anti-strange quark sector form factor of the kaon dominates for $Q^2 \geq 1.\ 6\ \mathrm{GeV}^2$, whereas the contribution of the u-quark sector form factor of the kaon is larger for $Q^2 \leq 1.6\ \mathrm{GeV}^2$. Clearly the difference in quark masses leads to a dramatic difference between the anti-strange quark and the up quark contribution to the kaon form factors.

We observed the structure of the kaon with a particular interest in the effects of the larger mass of the strange quark. At present, a detailed understanding of the pion and kaon structure is hampered by the rather small sample of experimental data. It is known that u_K is somewhat at softer that u_π in large-x valence region, which we will show is a natural consequence of the larger mass of the spectator strange quark in the K^+. While at the present time, one does not know the separate flavor contributions to the kaon elastic form factor and one may hope that it will prove possible to measure them in future. Given the phenomenological importance of the Drell-Yan-West relation (DYWR), it is certainly of considerable theoretical interest to compare the flavour dependence of the large-x PDFs with corresponding large-Q^2 behaviour of the separate flavour contributions to the elastic form factors.

We also investigate the effect of the spectator quark mass on the PDF for a given quark flavor, finding satisfactory agreement with the experimental ratio $\dfrac{u_{K^+}(x)}{u_{\pi^+}(x)}$. We conclude with a discussion of the relationship of the large-x behaviour of a PDF and the high-Q^2 behaviour of the contribution to the elastic form factor from the same quark.

The comparison of the asymptotic behaviour of the individual flavour form factors and parton distributions is fascinating. While all elastic form factors in the NJL model behave as $\dfrac{1}{Q^2}$ at larger Q^2, as already noted, the total K^+ and π^+ form factors only differ by about 10 % in that region. As a reflection of the DYWR, we conclude that this dominance of the elastic form factor for the $\bar{s}$-quark at large Q^2 is mirrored in the dominance of the strange PDF at large-x, with $\bar{s}_{K^+}(x)/u_{K^+}(x)$ $3:1$ at large-x.

List of Publications

- **P. T. P. Hutauruk**, I. .C .Cloet and Anthony. W. Thomas *Charge Symmetry Violation Effects in Parton Distributions*, Phys. Lett. **B**–(to be submmited).
- **P. T. P. Hutauruk**, I. .C .Cloet and Anthony. W. Thomas *Flavor Dependence of the Pion and Kaon Elastic Form Factors and Parton Distribution Functions*, Phys. Rev. **C**–(to be submitted).

1 Introduction

The standard model (SM) of particle physics was constructed almost 50 years ago [1–3]. For our purpose the SM is a theory of fundamental strongly interacting particles. There are four known types of fundamental interaction forces in nature. They are gravitation [1], electromagnetic (γ), nuclear strong (g) and nuclear weak ($W^{\pm}$, Z^0) forces and all the phenomena of physics in nature are described by these four fundamental forces. On July 2012, the Higgs Boson particle was confirmed independently at the LHC (Linear Hadron Collider) experiment by ATLAS [4] and CMS collaborations [5]. The elementary particles, which are the building blocks of matter, in the SM are classified into fermions and bosons. Fermions are divided into two types: leptons ($e, \mu, \tau, \nu_e, \nu_\mu, \nu_\tau$) and quarks ($u, c, t, d, s, b$). Leptons have spin $\frac{1}{2}$ and interact only via electromagnetic and weak interactions. Quarks can interact via the electromagnetic, weak and strong interactions, however a free quark has never been observed in nature. Historically, quarks [2] were firstly proposed by Gell-Mann [6] and Zweig [7–9] in 1964 and only three flavors of quarks (u, d, s) were known at that time. They stated that the physical hadrons are composite objects which consist of three quarks for the baryon and of a quark-antiquark pair for the mesons. Thus hadrons in nature can generally be categorized into baryons and mesons in nowadays. In this thesis we will concentrate on the pseudoscalar mesons: kaon and pion and strong interaction (QCD).

Quantum Chromodynamics (QCD) [3] [11], which is a part of the SM, is universally believed to be a robust quantum field theory for describing the strong interaction

[1] The gravitation force is not yet fully understood and included in the SM.

[2] The word "quark" firstly emerged in the novel Finnegan's Wake written by the Irish author James Joyce (18821941). The protagonist of the book is a publican named Humphrey Chimpden Ear-wicker who dreams that he is serving beer to a drunken seagull (no joke). Instead of asking for "three quarts for Mister Mark" the inebriated bird says "three quarks for Muster Mark". Since the pre-standard model theory was complete with only three quarks, the name made some sense. The full standard model today consist of six quarks. That hasn't made the word any less fun to say. Quark!

[3] The QCD name appears for the first time in general reviewed by Marciano and Pagels [10]

between quarks and gluons forming hadrons. QCD was firstly suggested by Fritzsch, Gell-Mann and Leutwyler [12]. The strong interaction governs the nuclear forces within and between hadrons and the nuclear forces ultimately arise through gluon dynamics. The gluon is both a color gauge field and the mediator of the force among quarks, isolating quarks inside the colorless compound systems called hadrons in the low energy regime. In low energy nuclear physics the strong nuclear force plays at relatively large distances. This is because the potential between quarks increases linearly and hence quarks cannot be separated. This phenomena is called as *confinement* [4]. To break the gluonic tubes between quarks, more external energy is required to disturb the system and the breaking mechanism involves the creation of a quark-antiquark pair. This confinement topic will be discussed later in more details in Chapter 2. There are numerous reasons to believe that QCD generates nuclear forces are so strong that less than 2% of the hadron mass can be attributed to the so-called current quark masses that appear in the QCD Lagrangian; viz., forces capable of generating mass from almost nothing, a phenomenon known as dynamical chiral symmetry breaking (DCSB). The color confinement is an interesting feature of the strong interaction at large distances. In this regime the interaction field among the quarks is very strong as indicated by its large effective strong coupling constant. With such a large effective strong coupling constant, it is not possible to employ a perturbative QCD approach. That is, the strong coupling constant grows in the infrared region and the predictive power of perturbation theory breaks down. This is the so-called *infrared slavery*. Nonperturbative QCD has hideous infrared singularities which prevent the quarks and gluons being released from a hadron.

At that time, some theorists attempted to model the non-Abelian theories by adding gluon field interaction terms into Lagrangian with the universal coupling constant g_s. However, such developments take us in an inappropriate direction, which goes far way from the real world. That perspective changed when Gross and Wilczek [13, 14] and Politzer [5] [15] found the effective coupling constant g_s disappears at short distance (large Q^2) and increases at long distances (low Q^2) as illustrated in Fig. 1.0.1. This successful theory paved the way to confinement and provided a bridge between the confinement of quarks within the hadron at low energy and the quasi-free behavior of quarks in the parton model. In contrast, in the short distances or high energy scale ($\sim$ 1 GeV), QCD has an asymptotic freedom feature where the effective strong coupling constant is relatively small. In the other words, when the quarks and gluons interaction decreases at short distances, QCD is asymptotically free. The running coupling constant decreases with increasing the energy scale, Q [16]. With such small strong coupling constant, α_s, perturbative QCD calculation can be performed. The formula for the effective strong coupling constant or one-loop running coupling constant

[4] This is one of unsolved problem which is part of the Yang Mills Theory and one of the 7 millennium prize problems given by the Clay Mathematics Institute. They offer a prize of US$ 1 million to the one who solves the problem.

[5] They were awarded a Nobel Prize in Physics 2004 for the discovery of asymptotic freedom in the strong interaction.

(*running* means it varies with the energy scale) is expressed by

$$\alpha_S(Q^2) = \frac{g_s^2}{(4\pi)} = \frac{12\pi}{(33-2N_f)ln[\frac{Q^2}{\Lambda^2_{QCD}}]} = \frac{4\pi}{\beta_0 ln[\frac{Q^2}{\Lambda^2_{QCD}}]}. \tag{1.0.1}$$

Here $\beta_0 = \dfrac{11N_C - 2N_f}{3}$ is a constant, N_f denotes the number of quark flavors, $N_C = 3$ stand for the number of colours and Λ_{QCD} is the fundamental scale of QCD. An implication of the feature of the running coupling constant in Eq.(1.0.1) is that different scales have different degrees of freedom.

DCSB, another dynamical property of the QCD, has the responsibility for generating the constituent quark mass of the hadron at a low energy scale (below $\sim$ 1 GeV). By taking massless quarks the chiral symmetry is realized in the Goldstone mode broken spontaneously. The effective strong coupling constant is defined as $\alpha_S(Q^2)$, where $\beta_0 > 0$ and Λ_{QCD} is renormalization scale. The quarks are asymptotically free if $\alpha_S(Q^2) \to 0$ as $Q^2 \to \infty$. The magnitude of Λ_{QCD} is determined by the typical hadron size. By taking the radius of proton $\sim$ 1 fm, it yields the $\Lambda_{QCD} \sim 300$ MeV and this is close to the experimental result [16]. A plot of the running coupling constant as a function of energy scale, Q in Eq. (1.0.1), is depicted in Fig. 1.0.1.

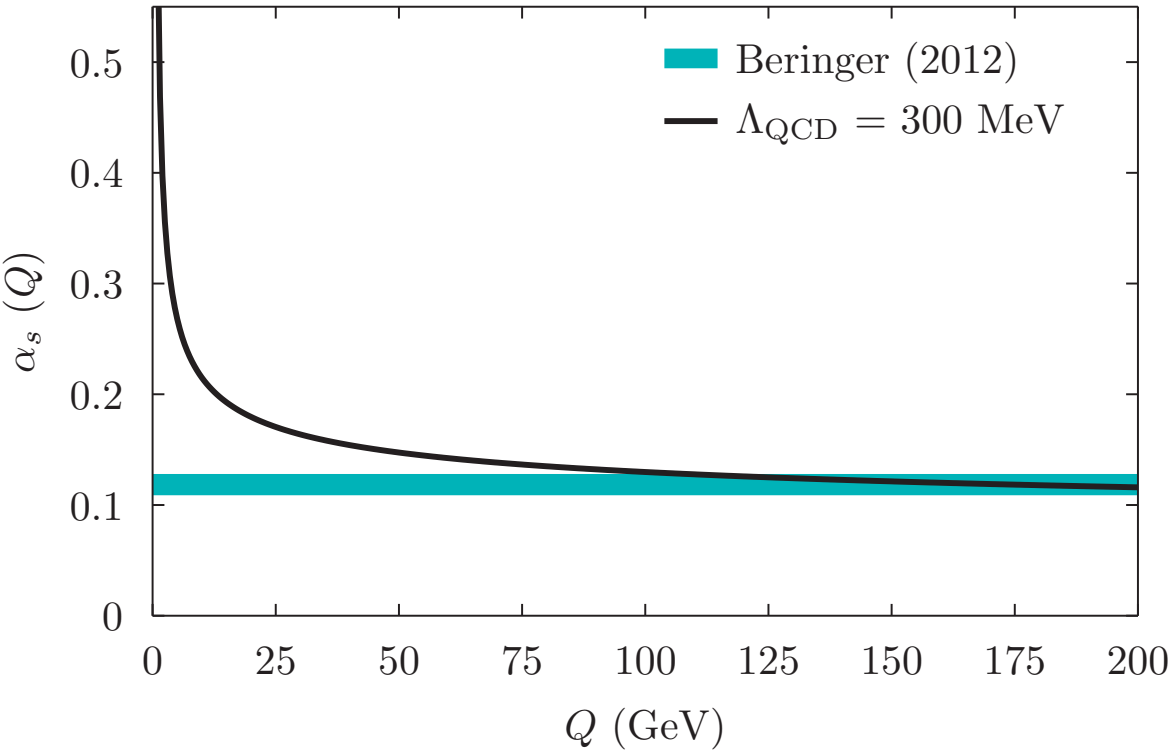

Figure 1.0.1: Running coupling constant, $\alpha_S(Q)$ as a function of energy scale, Q. The running coupling constant is shown as a black solid lines and the prediction value of the $\alpha_S(M_Z^2) = 0.1184 \pm 0.0007$ is blue solid lines [16].

QCD is unable to directly predict structure functions of hadrons. This is due

to the nonperturbative effect of QCD [6] i.e. confinement and dynamical symmetry breaking (DSB). Understanding confinement and DSB give us a remarkable perspective to understand hadron physics. This is because DSB is responsible for existence of pions, kaons, and eta as well as generating quark mass from vacuum state via interactions. At the moment the most direct method with which to gain access to the long distance behavior of QCD is lattice QCD [17–20]. However it is restricted to the first and second moments when it is used to compute the moments of parton distribution functions (PDF) [18]. With this in mind, another possible way is to use a hadronic model that adopts QCD features. Such a model should possess the same symmetries as QCD and hence we call it a "*QCD insipired*" model. In mimicking the features of QCD, some studies of the structure of hadrons have been performed and tremendous progress achieved. However, the structure of hadrons (baryon and meson) is not yet fully understood and hence we do not really understand the QCD theory itself. In a realistic calculation, it is very difficult to derive the hadronic observable from the first principles of QCD. In this stage to overcome this intricate task, hadronic models like Dyson-Schwinger equation (DSE) [21–25], QCD sum rules [26–29], Nambu-Jona Lasinio model [30–44, 47–57] are used to model the quarks interaction within the hadron. Lattice QCD is expected to be one possible way for studying the internal hadron properties and hadron internal structure from the first principles of QCD. In lattice QCD, the equations of motion (EOM) are numerically computed after it is discretized onto a space-time lattice. However, this lattice method also has a serious problem with the computing power needed to compute with physical quark masses. For this reason, the majority of lattice calculations use unphysically large quark masses. Therefore the extrapolations are required to reach the physical regime. Moreover, lattice QCD also has a problem at small momenta because of the finite volume effects. Therefore another extrapolation method is needed to obtain infinite volume limit.

Another way is to use a hadronic model. The Nambu-Jona-Lasinio (NJL) model is adopted in this thesis. This is an effective theory, which mimics many of the key features of QCD and is used as a tool to help understand non-perturbative phenomena in low energy QCD [34–38]. This model describes the chiral symmetry breaking, which gives rise to dynamically generated constituent quark masses. The NJL model has successfully been used to investigate a broad range of phenomena, from the properties of individual hadrons [39] to heavy ion collisions [40] and neutron stars [39, 41, 42]. In addition, to baryon properties such as masses and axial charges [43, 44] the model has also been used to study more complex phenomena such quark fragmentation functions [45, 46] and transverse momentum dependent (TMD) phenomena [47, 48]. Moreover, the NJL model was widely used to study the structure of hadrons [30–35]. The model has also been used to compute the properties of a diquark, such as its mass and electromagnetic form factor. These, in turn, are required for a description of nucleon [30–44, 47–57] and hyperon [51]. Also, it has been used to investigate the properties of mesons [50, 52] and properties of meson propagators [53]. However, the NJL model has mostly been applied to investigate nucleon structure and properties [31–33, 49, 54, 55]. In some applications, the NJL model employing the proper time regularization (PTR) scheme has been used to study nucleon quark distributions in relation to the proton spin crisis [56]

[6] In this regime, $Q^2 \sim 1$, $\alpha_S \sim 1$ and perturbative QCD is broken.

and nuclear matter [31, 57]. Furthermore, the NJL model also has been used to study the electromagnetic form factor of hadrons [31, 49, 55, 58, 181] and the hadronization process [59]. However, the NJL model is a considerable simplification as it has no gluon interaction. Therefore, several attempts have been suggested to improve the NJL model by including scalar, pseudoscalar, vector, axial-vector terms in the meson interactions as well as in the diquark interaction part. This approach is well known as Bosonization of the NJL model [60–65]. We do not discuss the latter model in this work but for readers who are interested, we refer to Refs. [60–65]. We only focus to the NJL model. The NJL model is not renormalizable and does not confine the quarks, therefore it suffers from nonphysical $q-\bar{q}$ thresholds [60]. The model must be regulated to render it finite. We employ the proper time regularization scheme to regularize the divergent integrals. In fact, there are several regularizations available in the market, like 3D non-covariant regularization [35, 52], dimensional regularization [66–70], 4D covariant regularization [35, 52], Pauli-villars regularization [35, 51] and proper-time regularization [23–25, 30–32, 34–38, 41, 43, 44, 47–57]. Each regularization has its advantages and disadvantages. In this work we choose a proper time regularization scheme, as mentioned earlier, because it was very successful in many applications [30–44, 47–57]. A comprehensive review of the proper time regularization can be found in Refs. [23–25, 30–32, 34–38, 41, 43, 44, 47–57]. More details and systematics of the NJL model and its QCD symmetries will be discussed in Chapter 3.

As pointed out earlier, the NJL model with help of the proper-time regularization scheme has been applied in some applications either in the pion and nucleon case, however, this is the first calculation for studying the parton distribution functions of the kaon in the NJL model with the proper-time regularization scheme. However, for the kaon form factor, this is not a first calculation because, very recently, a new paper for the pion and kaon form factors in Ref. [78] has been published. In their paper, they studied the kaon form factor with the vector mesons and including the pion loop. However, we compute the kaon form factor with completely different method with their work. In this thesis, the dressed quark and vector mesons are automatically included by modifying a quark-photon vertex. More details and systematics of the kaon form factor and the results will be discussed in Chapter 4.

As mentioned in the first paragraph, in the SM the kaon (mesons) consist of a quark-antiquark pair. It indicates that the structure of the kaon is simpler than the nucleon, therefore the dynamics of quarks inside the kaon may be easier to study than inside the nucleon. This gives us a great opportunity to gain useful information about the dynamics of quarks within the kaon and it may eventually be applied to observe the dynamics of quarks inside the nucleon, which is a more complicated case and not yet fully understood. Understanding quark dynamics in hadrons will lead us to extract new knowledge of QCD as the underlying theory. Nowadays we are still far from fully understanding the behavior of the kaon internal structure due to the lack of experimental data. The most extensive sets of experimental data have been collected for the pion and nucleon form factors and their valence quark distributions.

The best and cleanest method to extract information from hadrons as complex systems is by means of a known probe which does not interact strongly with hadrons. Such a probe will give a good resolution of the internal structure of hadron at short

distance. In deep inelastic scattering (DIS), the common probes used is a lepton, in practice an electron, neutrino and muon. An important knowledge in respect to the internal structure of the hadrons can be inferred from the PDF and form factor (FF). The PDF and FF are unique tools to access the nonperturbative region of QCD. PDF is described by a diagonal matrix elements of a bi-local operator in the light cone framework, where the initial and final state are the same. The parton distribution function is one of the nonperturbative properties which can be measured along with the form factors and generalized parton distributions (GPD). Substantial progress on parton distributions and form factors has been achieved in recent years. The PDF and FF studies have been performed to observe the structure of the hadrons and their properties using hadronic models [79–92, 94–101, 103, 180]. However the internal hadron structure and their properties are not yet fully understood.

As mentioned earlier, nowadays our knowledge and understanding of the structure of hadrons is that the hadrons consist of quarks and gluons, the nucleon bound state is made of three quarks and mesons consist of quark and anti-quark pairs. Within a hadron the quarks interact with one another by exchanging the gluons that carry colour quantum numbers. Three valence quarks in the baryon i.e. Δ^{++} (uuu), Δ^{-} (ddd) and Ω^{-} (sss) leads to a new problem associated with the Pauli exclusion principle which states that the quarks (fermions) are not allowed to occupy the same state. In order to distinguish the three quarks, color was introduced as a new degree of freedom. Since the color degree of freedom is not directly observed in the nature, it is assumed that the hadronic phenomena be unchanged under the exchange of color. Color was firstly suggested by Greenberg [104] in order to recover the Pauli exclusion principle. Thus dynamics of gluon was proposed by Moo Young Han and Yoichiro Nambu [105, 106] in 1965. They identified the gluons as gauge bosons in a non-abelian gauge theory. In the symmetry group, color was adopted in SU(3) as non abelian group with a single quark assigned to the fundamental triplet, 3, of SU(3), and the gluons self-interacting. All observed hadrons are color neutral. Thus nucleon made of *partons* (hard point-like objects, which were identified as the quarks and gluons) has been detected via the first experiment of the DIS at Stanford linear accelerator (SLAC) in the late 1960s [107, 108]. This indicates that the nucleon is not structureless. In the same time this is also first evidence for the quarks.

Furthermore at high energy the PDF is a great way to extract information of the internal hadron structure. These distribution can be experimentally determined for a relatively high value of the momentum transfer Q^2. Most of the experimental data on PDF has been collected for the nucleon and for the pion but it is not so for the kaon case. The experimental data for the kaon is very limited. This is one of our motivations for doing this work, but we only focus on the kaon (unequal masses) and pion (equal masses) cases. In addition, PDF allow us to observe the dynamics of quarks at short distances and allow us to obtain a good resolution of the hadron structure. From the knowledge of PDF calculation will be straightforwardly extended to GPD. However, the present study is restricted to the PDF and FF of the kaon and pion. This independent study can also lead us to link the parton distribution function at higher Q^2 and form factor at higher x indirectly via DYWR as in GPD at forward limit. This relation explains the link between longitudinal and transverse momentum of the valence

quark behavior at higher Q^2 and x, respectively. In the large momentum transfer regime, QCD demonstrated that asymptotic freedom allows a perturbative expansion approximation. In deep inelastic scattering, the short distances means $Q^2 \to \infty$ and $\nu \to \infty$ when x is fixed, where $x = \dfrac{Q^2}{2M\nu}$ is the Bjorken variable. Note that, in deep inelastic scattering, hadrons are assumed to be made up of *partons* which do not interact among themselves.

With these problems in mind, in this thesis, we concentrate on investigating the internal structure of the pseudoscalar mesons (kaon and pion) via FF and PDF [7]. The kaon internal structure will be studied by means of the PDFs within the NJL model. Using the Lagrangian of NJL model, the dynamical mass of quark and anti-quark is generated by quark interaction with the vacuum state and a chiral spontaneously symmetry breaking (chiral limit) is realized. However the NJL model has a divergence in the loop momentum integrals and a specific regularization will be performed in order to cure the divergence. In this study the PTR scheme is chosen. It preserves the Lorentz covariance. In addition, in this regularization, the infrared cutoff removes the imaginary part of the loop integral to eliminate the nonphysical domain for hadron decay into quarks and thus simulates confinement. Thus these dynamical properties of the kaon in the NJL model are used as an input into PDFs to describe the structure of the kaon.

From experimental side, in the near future, new experimental data for the kaon are expected from JLAB, J-PARC at Japan as well as COMPASS at CERN. The theoretical results of this thesis will be tested using that new experimental data. On the other hand, the comparison between our model prediction and experimental data will lead us to a new understanding of the structure of the kaon and QCD itself as the underlying theory. From this calculation, the dynamics of quarks inside the kaon and pion are studied by modeling their interaction dynamics in the NJL model. Later on, this knowledge will be accustomed to study and to investigate the dynamics of quarks inside the pion and kaon using FF and PDF which is the ultimate goal of this thesis. In addition the charge symmetry breaking is also investigated in parton distribution functions and form factors of the kaon and pion. Charge symmetry breaking emerges due to the mass difference between up and down quarks.

The outline of this thesis is as follows: In Chapter 2 we briefly review QCD as the underlying theory of the strong interaction and deep elastic scattering as an experiment tool to investigate the parton distribution functions.

In Chapter 3 the SU(3) NJL model, which is a chiral effective theory, will be introduced. The Bethe-Salpeter equation (BSE) will be used to compute the mesons as bound states of a quark- antiquark pair. In addition, the PTR scheme is introduced as a regularization theory to cure an integral divergence in the NJL model. Later, the static and dynamic properties of the pseudoscalar mesons and the structure of the kaon and pion is presented. The properties of the kaon and pion are computed in the NJL model.

In Chapter 4 the electromagnetic form factor of the kaon (unequal masses) and pion (unequal masses) are presented. The elastic form factor of the kaon and pion are also

[7] The FF and PDF observables can be measured in experiment.

calculated using NJL model. The form factor of the quark constituents of the pion and kaon results are also presented. The electromagnetic form factor of the pion and kaon at large Q^2 are provided.

In Chapter 5 the valence quark distributions of the kaon and pion are reported. The valence quark distributions are calculated by using proper time regularization scheme in the NJL model. Additionally the valence quark distributions of the constituents of the pion and kaon results are observed. Moreover the ratio between valence quark distributions of the kaon and pion are observed in order to understand the behavior of the valence quark and to study their nuclear environment sensitivity. Finally a comparison our results to available experimental data is presented. The valence quark distributions of the pion and kaon in the large x are presented. The link of PDF and FF are accessed using the DYWR. This relation corresponding to the scaling behavior of the kaon in the NJL model.

In Chapter 6 the charge symmetry violation (CSV) or charge symmetry breaking (CSB) in the PDF and FF of the pion and kaon are presented. Last but not least, in Chapter 7 a summary and outlook of this thesis will be presented.

2

QCD and Deep Inelastic Scattering

In this chapter QCD and its properties are reviewed. QCD is a gauge theory based on the non-Abelian color symmetry group SU(3). In QCD the gluon is a mediator particle of color interactions carrying color charge, in contrast with the photon in Quantum Electrodynamics (QED). In this review, starting from the Lagrangian of QCD, both perturbative QCD and nonperturbative QCD are presented. In the high energy region, the perturbative QCD approach is a very powerful method to link elementary quantities and physical quantities through a factorization theorem in order to be able to interpret the theoretical results and experimental data. In the factorization theorem, the differential cross section is factorized based upon all orders of the running coupling constants, $\alpha_S(Q^2)$. A summary review of QCD and its properties, the quark parton model (QPM), DIS, factorization theorem, and QCD evolution is presented in the next sections.

2.1 Quantum Chromodynamics

QCD poses a fundamental theory of the strong interaction, where quarks and gluons are its degrees of freedom and it is a part of the SU(3) $\times$ SU(2) $\times$ U(1) standard model of particle physics. The dynamical interaction of the quarks and gluons renders the color interactions. QCD is constructed based upon the gauge group $SU(3)_C$ in color space which is non-Abelian gauge group. In group theory, SU(3) means the special unitary group in 3 dimensions which involves the unitary set of 3×3 matrices with determinant one. The set has nine linearly independent unitary complex matrices [1]. One has determinant -1 and there are a total of eight independent component matrices in the matrix space. This corresponds to eight different generators of SU(3) [2]. In QCD, the quark-quark interaction and gluons interaction as potential part and kinetic (free)

[1] A complex matrix has $2N^2$ degrees of freedom. Unitary has N^2 constraints

[2] The number of generators of the SU(N) is $N^2 - 1$. Hence the number generators is 8 for SU(3).

part are described by QCD Lagrangian. The free fermion Lagrangian is expressed by

$$\mathcal{L} = \bar{q}_f^i(i\gamma^\mu\partial_\mu - \hat{m})q_f^j, \tag{2.1.1}$$

where q_f^i denotes a quark field with fundamental color index i, $q_f = (q_f^R, q_f^G, q_f^B)^T$ and f is six active flavors ($u,\ d,\ s,\ c,\ b,\ t$). γ^μ is a Dirac matrix. The mass matrices in the flavor space is symbolized as $\hat{m} = \mathrm{diag_f}\ (\mathrm{m_u},\ \mathrm{m_d},\ \mathrm{m_s}, ...\mathrm{m_{N_F}})$. The free Lagrangian in Eq. (2.1.1) is invariant under arbitrary global [3] SU $(3)_c$ gauge transformation in color space, it then has form

$$q_f^i \to (q_f^i)' = U_\beta^i q_f^i; \qquad UU^\dagger = U^\dagger U = 1; \qquad Det(U) = 1, \tag{2.1.2}$$

where U, which is a 3×3 unitary matrix acting on color index, can be expressed by

$$U = \exp^{\left(-ig_s\frac{\lambda^a}{2}\Theta_a\right)}, \tag{2.1.3}$$

with λ^a are 3×3 hermitian matrices and are the so-called the SU(3) generators of the Gell-Mann matrices of the SU $(3)_c$ representation, and Θ_a denotes real arbitrary parameters with $a = 1, 2, 3, ..., 8$. $\mathrm{SU}(3)_c$ denotes generators of the strong interaction gauge group which commute with $\mathrm{SU}(3) \otimes \mathrm{SU}(3)$ current and mix quarks with the same hyper-charge and isospin but different color. g_s denotes the strong coupling constant ($g_\mathrm{s}^2 = 4\pi\alpha_\mathrm{S}$) which is dimensionless strength coupling. This is analogous with e in QED. The Gell-mann matrices, λ^a are trace-less and satisfy the commutation rules,

$$[\lambda^a, \lambda^b] = 2if^{abc}\lambda^c. \tag{2.1.4}$$

To obtain the free QCD Lagrangian in Eq. (2.1.1) which is invariant under local $\mathrm{SU}(3)_c$ gauge invariance. This implies replacing the partial derivative, ∂_μ by the covariant derivative, D_μ. To fulfill the invariance requirement, one should have

$$\begin{aligned} D_\mu q_f^i &= [\partial_\mu - ig_s\frac{\lambda^a}{2}A_\mu^a(x)]q_f^i \\ &= [\partial_\mu - ig_s[A_\mu^a(x)]_{\alpha\beta}]q_f^i = U(D_\mu U), \end{aligned} \tag{2.1.5}$$

where a form of the $\mathrm{SU}(3)_c$ gauge field, $[A_\mu^a(x)]_{\alpha\beta}$ [4] with a Lorentz index $\mu = 0,\ 1,\ 2,\ 3$ is introduced by

$$[A_\mu^a(x)]_{\alpha\beta} \equiv \left(\frac{\lambda^a}{2}\right)_{\alpha\beta} A_\mu^a(x), \tag{2.1.6}$$

where A_μ^a is also well known as a four component vector (gauge) potential.

$$A_\mu^a \to (A_\mu^a)' = U[A_\mu^a U^\dagger - \frac{i}{g_s}\partial_\mu U]U^\dagger. \tag{2.1.7}$$

[3] Global means the field is transformed in the same way at all space-time points.

[4] $\mathrm{SU}(3)_c$ gauge field can also written as $\sum_{a=1}^{8}\frac{\lambda^a}{2}A_\mu^a(x)$.

Under an infinitesimal $SU(3)_c$ gauge transformation, where U can be expanded using a Taylor series, U becomes,

$$U = \exp^{\left(-ig_s\frac{\lambda^a}{2}\Theta_a\right)} \equiv 1 - ig_s\frac{\lambda^a}{2}\Theta_a(x) + \ldots, \tag{2.1.8}$$

it then gives

$$\begin{aligned} q_f^i \to (q_f^i)' &= q_f^i - ig_s\left(\frac{\lambda^a}{2}\right)_{\alpha\beta}\delta\Theta_a q_f^{i\beta} \\ A_\mu^a \to (A_\mu^a)' &= A_\mu^a - \partial_\mu(\delta\Theta_a) + g_s f_{abc}\delta\Theta^b A_\mu^c, \end{aligned} \tag{2.1.9}$$

Gluons are physical degrees of freedom and carry energy and momentum. Then to construct a kinetic term for gluon fields satisfying gauge invariance, an additional term must be added to the gluon field tensor. This additional term is taken analogous to successful theory of QED, however anti-symmetric field strength tensor in QED is not gauge invariant. Therefore the gluon field tensor is introduced as

$$\begin{aligned} F_{\mu\nu}^a &\equiv \frac{i}{g_s}[D_\mu, D_\nu] \\ &= \partial_\mu A_\nu^a - ig_s[A_\mu^a, A_\nu^a] \equiv \frac{\lambda^a}{2}F_{\mu\nu}^a(x) \\ &= \partial_\mu A_\nu^a - \partial_\nu A_\mu^a + g_s f_{abc}A_\mu^b A_\nu^c. \end{aligned} \tag{2.1.10}$$

Under a gauge transformation, that is

$$F_{\mu\nu}^a \to (F_{\mu\nu}^a)' = UF_{\mu\nu}^a U^\dagger, \tag{2.1.11}$$

the trace over color, $Tr_C[F_{\mu\nu}F^{\mu\nu}] = \frac{1}{2}F_{\mu\nu}^a F_a^{\mu\nu}$, remains invariant. A_μ^a denote the gluon fields (gauge bosons) with color index a, λ^a are the SU(3) generators of the Gell-Mann matrices. f^{abc} is the anti-symmetric structure constants of the $SU(3)_c$. The non-Abelian character of the gauge group is revealed in the pure gluonic interactions which come from the gluon covariant field strength tensors. Finally a complete Lagrangian of QCD, which satisfies local $SU(3)_c$ gauge invariance can be written as

$$\begin{aligned} \mathcal{L}_{\rm QCD} &= -\frac{1}{4}F_{\mu\nu}^a F_a^{\mu\nu} + \bar{q}_f^i(i\gamma^\mu D_\mu - \hat{m})q_f^i \\ &= -\frac{1}{4}[\partial_\mu A_\nu^a - \partial_\nu A_\mu^a][\partial^\mu A_a^\nu - \partial^\nu A_a^\mu] + \bar{q}_f^i(i\gamma^\mu\partial_\mu - \hat{m})q_f^i \\ &+ g_{\rm s}A^a\bar{q}_f^i\gamma_\mu(\frac{\lambda^a}{2})q_f^i - \frac{g_{\rm s}}{2}f_{abc}[\partial_\mu A_\nu^a - \partial_\nu A_\mu^a]A_b^\mu A_c^\nu \\ &- \frac{g_{\rm s}^2}{4}f^{abc}f_{ade}A_\mu^a A_\nu^b A_d^\mu A_e^\nu, \end{aligned} \tag{2.1.12}$$

where the first term in the QCD Lagrangian contains the the kinetic terms of the different fields. The second term of the QCD Lagrangian describes the color interaction of quarks and color octet gluons. The cubic and quadratic gluon self-interactions arise from the $F_{\mu\nu}^a F_{\mu\nu}^a$ Yang-Mills terms. The coupling constant, g_s in the Lagrangian

decreases with increasing energy scales. Extensive reviews of QCD can be found in Refs. [10, 11] or in textbooks [109, 110]. The elementary properties of QCD at both low energy (nonperturbative) such as color confinement, chiral symmetry breaking and high energy (perturbative) such as asymptotic freedom are briefly recapitulated in the subsection below. These crucial QCD properties are required to describe the structure of hadrons at different energy scales.

2.2 Asymptotic Freedom

One unique property of the strong interaction at short distance, which has an important key role in this region, is asymptotic freedom. At large transfer momentum, Q^2, or short distance, the interaction strength, α_S, becomes logarithmically small. In other words, the $\alpha_S \to 0$ for $Q^2 \to \infty$. This is in contrast with the QED behavior, where $\alpha_{em} = \frac{e^2}{2\epsilon_0 hc} \sim \frac{1}{137}$ denotes the fine structure constant, which decreases with decreasing Q or with increasing $r = \frac{1}{Q}$. In QCD [5], the strength of the strong interactions, α_S decreases with increasing Q^2 and vanishes asymptotically. This indicates that quarks behave as free particles at large energy scale (short distances), as depicted in Fig. 1.0.1. The effective strength of the coupling constant interaction will vanish in this energies limit. Notice that to investigate the asymptotic freedom, it is enough to study the behavior of the β-function in the vicinity of the origin of the coupling constant space (one loop approximation) [10]. The QCD running coupling, α_S in Eq. (1.0.1) indicates the number of flavor, N_F [6] gives a positive contribution to QCD running coupling constant via β-function. This arises from $q\bar{q}$ loops, as depicted in Figs. 2.2.1 and 2.2.3. The gluon self-interactions [7] gives a negative contribution to the QCD running coupling constant. It is so called an anti-screening effect when the gluon self-interaction blows up the QCD charge. The illustration of the anti-screening effect is shown in Figs. 2.2.2 and 2.2.3.

The asymptotic freedom of QCD was discovered independently by David Gross [10] and Frank Wilczeck [13, 14], David Politzer [15], and Gerard t'Hooft [111]. The consequence of the asymptotic freedom of QCD is that the perturbative approach behaves well at higher energies due to the effective coupling constant decreasing. This behavior is very important at high energies. This leads to remarkable success of the DIS experiment at high energy regime. In addition, this indicates that the color interaction effects may be computed perturbatively at small distances or at large transfer momentum, Q^2.

[5] In QCD, the vacuum state is not empty space but consists of the virtual quark-antiquark ($q\bar{q}$) pairs. Aside from this virtual quark-antiquark pairs, the vacuum also consists of the virtual gluon pairs. This occurs due to the gluon self-coupling interaction. In the vacuum state, the quark-antiquark pairs yields a charge screening, which has a positive β-function. This gives a positive contribution to α_S. In contrary, the gluon pairs give a negative contribution to α_S. Once the negative contribution is large than the positive contribution, consequently the β- function is negative.

[6] This can be clearly seen in the second term, $\frac{-2N_F}{3}$ in β_0 in Eq. (1.0.1), arises from Fig. 2.2.1. This causes screening.

[7] This comes from the first term, $\frac{11N_C}{3}$ in β_0. This causes anti-screening.

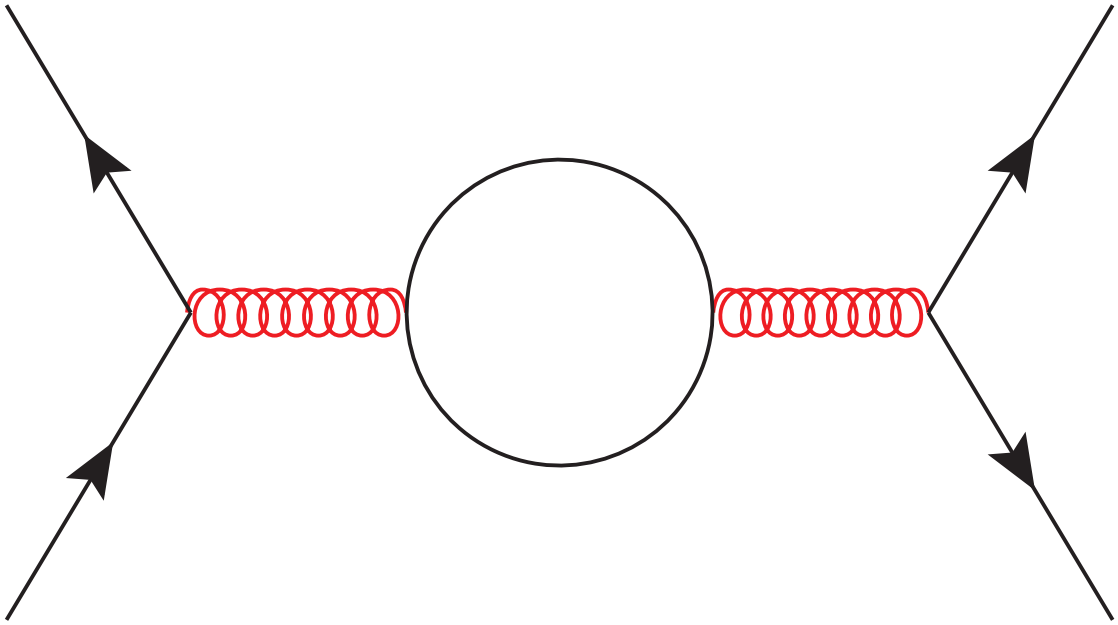

Figure 2.2.1: The quark (loop) interaction has a screening effect, where has a positive β-function. The gluons are represented by red color and the quarks are represented by black.

Consequently QCD can be potentially tested in high energy experiments. From recent calculations the QCD predictions in this regime shows excellent agreement with the experimental data.

2.3 Color Confinement

Hadron structure and QCD is characterized by two emergent phenomena at low energy: confinement and DCSB. The confinement conjecture states that particles carrying a color charge cannot be isolated and can therefore not be directly observed in nature. In Fig. 1.0.1 the color interactions increases at low energies, therefore the perturbative approach is unreliable. This implies that the quarks form bound states as the running coupling constant increases. In the past many attempts have been performed to understand nonperturbative QCD behavior at low energies. For example, in phenomenology the linear potential between quark and anti-quark which is in color singlet state, has a form

$$V(r) \equiv kr, \tag{2.3.1}$$

where V(r) denotes the potential between quark and anti-quark and the quark-antiquark system is connected by a string. The potential between the quark-antiquark pair becomes stronger when the quark-antiquark pair is forced to separate by pulling them apart (external force). This indicates that the strong color interaction increases with separation distance between the quark-antiquark and that quarks are isolated inside the hadrons. At some larger separation, it becomes energetically more favorable for

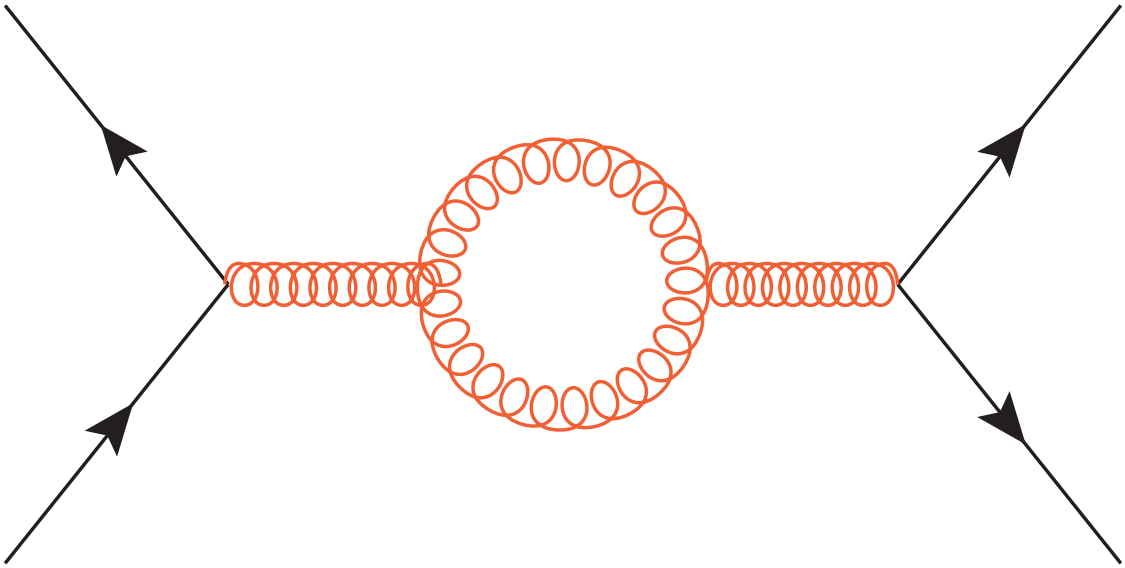

Figure 2.2.2: As in Fig. 2.2.1, but for the gluon (loop) interaction has an anti-screening effect.

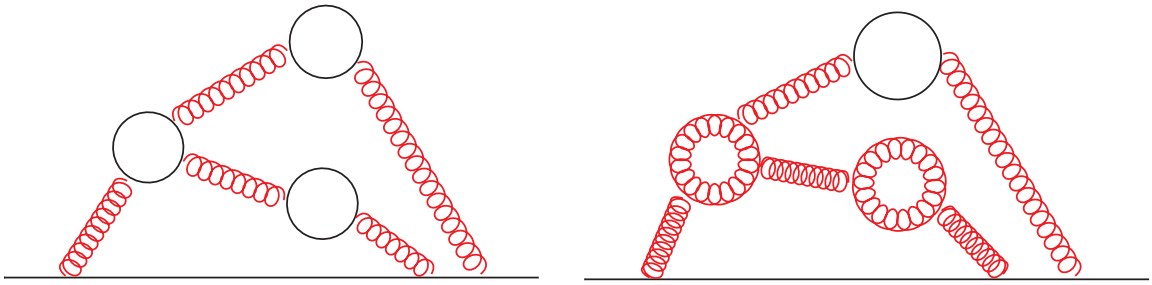

Figure 2.2.3: . Diagrammatic representation of the cloud of virtual $q\bar{q}$ pairs around a quark (left), where diagrammatic representation of the cloud of virtual gluons due to gluon self-interactions (right).

a quark-antiquark pair to split into a two quark-antiquark pairs. This is called as *confinement*. This phenomenon is consistent with experimental facts. In this region all particles appear to be color neutral, which is why we have never see free quarks. However, once the quarks leave the nonperturbative region, they will dress themselves and convert into hadrons. This phenomena is analogous with the normal superconductor where the flux of the magnetic is expelled from the interior of the metal. This is so called Meissner effect [112]. The illustration of the linear potential of the gluon interaction is depicted in Fig. 2.3.1

2.4 Chiral Symmetry

The chiral symmetry is a very important QCD feature to understand the phenomena in low energy strong physics. In the chiral symmetry, in principle the current quark masses

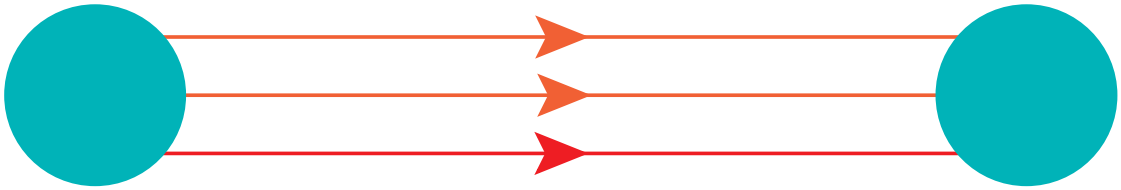

Figure 2.3.1: The linear potential of gluon interaction (flux tube) between quark-antiquark pair yielded by dual Meissner effect [112, 113].

has necessarily to be small. If the spin of the quark is in the direction of momentum, it is called $right-handed$ and in opposite direction, it is called $left-handed$. The QCD Lagrangian satisfies this chiral symmetry. By defining the projection operator of the left- and right-handed quark fields,

$$q_{R,L} = \frac{1}{2}\left(1 \pm \gamma_5\right) q, \tag{2.4.1}$$

where plus for the right-handed field and negative for the left-handed field and $\frac{1}{2}(1\pm\gamma_5)$ denotes the projection operators. Substituting the expression of left- and right-handed quark fields in Eq. (2.4.1) into QCD Lagrangian in Eq. (2.1.12), the QCD Lagrangian can be rewritten as

$$\mathcal{L}_{\text{QCD}} = \bar{q}_L i\not{D} q_L + \bar{q}_R i\not{D} q_R - \bar{q}_R \hat{m} \bar{q}_L - \bar{q}_L \hat{m} \bar{q}_R - \frac{1}{4} F^a_{\mu\nu} F^{\mu\nu}_a, \tag{2.4.2}$$

By considering $\hat{m} = diag(m_u, m_d, ..., m_{N_F}) \to 0$, the QCD Lagrangian has a chiral symmetry, $SU(N_f)_L \times SU(N_f)_R$ and it is then decomposed as

$$\mathcal{L}_{\text{QCD}} = \bar{q}_L i\not{D} q_L + \bar{q}_R i\not{D} q_R - \frac{1}{4} F^a_{\mu\nu} F^{\mu\nu}_a, \tag{2.4.3}$$

where the quark fields of the left-handed and righ-handed are separated and do not connect. The left- and right-handed fields in the Lagrangian fulfill the chiral transformations,

$$\begin{aligned} q_L &= \begin{pmatrix} u_L \\ d_L \\ s_L \end{pmatrix} \to U_L \begin{pmatrix} u_L \\ d_L \\ s_L \end{pmatrix} = e^{-i\omega^a_L T^a} \begin{pmatrix} u_L \\ d_L \\ s_L \end{pmatrix}, \\ q_R &= \begin{pmatrix} u_R \\ d_R \\ s_R \end{pmatrix} \to U_R \begin{pmatrix} u_R \\ d_R \\ s_R \end{pmatrix} = e^{-i\omega^a_R T^a} \begin{pmatrix} u_R \\ d_R \\ s_R \end{pmatrix}, \end{aligned} \tag{2.4.4}$$

where $T_a = \frac{\lambda^a}{2}$. In the limit of chiral symmetry (vanishing quark masses), the Lagrangian preserves the full symmetry under $SU(N_f)_V \times SU(N_f)_A \times U(1)_V \times U(1)_A$ which fulfills symmetric transformation, $q \to e^{-i\omega^a_V T^a} q$ and $q \to e^{-i\omega^a_A T^a \gamma_5} q$, respectively. The invariance of $\mathcal{L}_{QCD}$ under $U(1)_V$ transformation relates to a conserved

baryon number current with charge conservation. The expression of baryon number is formulated as

$$\mathcal{B} = \frac{1}{3}\int d^3x q^\dagger q. \tag{2.4.5}$$

The invariance of $\mathcal{L}_{QCD}$ under chiral symmetry implies $N_F^2 - 1$ conserved vector currents,

$$\begin{aligned}\mathcal{J}^\mu_{V,a}(x) &= \bar{q}(x)\gamma^\mu T_a q(x), \qquad with \qquad \partial_\mu \mathcal{J}^\mu_{V,a}(x) = 0 \\ &= \bar{q}_R\gamma^\mu T_a q_R + \bar{q}_L\gamma^\mu T_a q_L,\end{aligned} \tag{2.4.6}$$

and $N_F^2 - 1$ conserved axial currents,

$$\begin{aligned}\mathcal{J}^\mu_{A,a}(x) &= \bar{q}(x)\gamma^\mu\gamma_5 T_a q(x), \qquad with \qquad \partial_\mu \mathcal{J}^\mu_{A,a}(x) = 0 \\ &= \bar{q}_R\gamma^\mu T_a q_R - \bar{q}_L\gamma^\mu T_a q_L,\end{aligned} \tag{2.4.7}$$

here T_a denotes the generators of the SU(3) Lie algebra, where $a = 1, 2, ..., 8$. The charge conservation is also evaluated using Noether's theorem, it then gives,

$$\mathcal{Q}^a_V = \int d^3x \mathcal{J}^\mu_{V,0}(x) \qquad \frac{d\mathcal{Q}^a_V}{dt} = 0, \tag{2.4.8}$$

$$\mathcal{Q}^a_A = \int d^3x \mathcal{J}^\mu_{A,0}(x) \qquad \frac{d\mathcal{Q}^a_A}{dt} = 0, \tag{2.4.9}$$

Furthermore the charge conservation of the singlet Noether vector currents and Noether axial currents are given by

$$\begin{aligned}\mathcal{J}^\mu_V &= \bar{q}_R\gamma^\mu q_R + \bar{q}_L\gamma^\mu q_L \\ &= \bar{q}\gamma^\mu q, \qquad with \qquad \partial^\mu \mathcal{J}^\mu_V = 0,\end{aligned} \tag{2.4.10}$$

$$\mathcal{J}^\mu_A = \bar{q}_R\gamma^\mu q_R - \bar{q}_L\gamma^\mu q_L = \bar{q}\gamma^\mu\gamma_5 q. \tag{2.4.11}$$

This equation implies that the singlet vector current, $U(1)_V$, is conserved because the left-handed and right-handed fields have the same phase under a transformation. In contrast, the singlet axial vector current has a different phase between the left-handed and the right-handed fields. The singlet axial vector current is not conserved on the quantum level since $U(1)_A$ is broken due to the axial anomaly. This is because of the mass term in $\mathcal{L}_{\mathrm{QCD}}$. This will discussed in more detail in Section 2.5.

2.5 Spontaneous Chiral Symmetry Breaking

In this section, we present the dynamical (spontaneous) chiral symmetry breaking, which is one of the nonperturbative features of QCD as explained in Section 1. This generates mass from nothing (vacuum) and is very useful to understand the dynamics of the nonperturbative region. In general, the realization of the chiral symmetry is

manifest as two possibilities, a Wigner-Weyl conjecture and Nambu-Goldstone conjecture [114, 115]. The broken symmetry indicates that the Lagrangian is invariant under all symmetries but the vacuum is not. A system which has Lagrangian and the vacuum are invariant under a continuous chirality transformation is the so-called as the $Wigner - Weyl$ conjecture. In the Wigner-Weyl conjecture, the vacuum (ground) state invariant under $SU(3)_L \times SU(3)_R$ transformation realized by acting the generators of symmetry on the vacuum state, it then gives,

$$\mathcal{Q}_A^a \mid 0\rangle = \mathcal{Q}_V^a|0\rangle = 0, \tag{2.5.1}$$

where $|0\rangle$ stands for the ground state of QCD. It is symmetric only under the subgroup $\mathrm{SU}(3)_V$. This also shows that the vacuum expectation value (VEV) of the vacuum state subject to a set of linear relations. It implies that the vacuum state has zero VEV [114, 115]. In addition, it would indicates that parity doublets emerge in the hadron spectrum. The implication is that the spectra of pseudoscalar ($J^P = 0^-$) and scalar ($J^P = 0^+$) mesonic transitions would be undistinguished, but this degeneracy is not be observed in the real world. Therefore one can conclude that $\mathcal{Q}_V^a|0\rangle \sim 0$ and $\mathcal{Q}_A^a \mid b\rangle \neq 0$. In the other words, a system which has a Lagrangian is invariant under a continuous chiral transformation but the vacuum is not is the so-called a Nambu-Goldstone chiral symmetry realization. This conjecture implies that the symmetry is spontaneously broken and there exists massless Goldstone bosons. An expression of the broken symmetry is given by

$$\mathcal{Q}_A^a|0\rangle \neq 0. \tag{2.5.2}$$

This broken symmetry is associated with the existence of the massless Nambu-Goldstone bosons which coupled to the axial current, $\mathcal{J}_\mu^a$ generated quantum numbers of the corresponding axial charges. For $N_F = 3$, the candidates of the massless Nambu-Goldstone bosons are identified with the octet lightest pseudoscalar mesons (π, K and η). They have a small mass arising because an explicit broken symmetry which is impact of the non-vanishing quark masses.

Based on QCD, the dynamical symmetry breaking is exhibited by the non-vanishing of a singlet scalar quark condensate which can be written as

$$\langle 0|\bar{q}q|0\rangle = \langle 0|\bar{q}_R q_L + \bar{q}_L q_R|0\rangle, \tag{2.5.3}$$

where this is not chirally invariant under the continuous transformation because the mixing the left-handed and right-handed quark field operators. This is different from the $\mathrm{SU}(3)_V$ where the left-handed and right-handed quark field simultaneously. The chiral symmetry will be restored once the finite expectation value of the scalar quark condensate melts away at high temperatures and densities. Thus the symmetry is realized as Wigner-Weyl conjecture. Moreover the ground state of QCD, defined as the vacuum, is generated by a condensate of scalar quark-antiquark pairs. This is shown by a nonzero VEV [8] of the composite operator, $\bar{q}q$, ($\langle 0|\bar{q}q|0\rangle \equiv \langle \bar{q}q\rangle$). Assuming $N_F = 3$, one has,

$$\langle \bar{q}q\rangle = \langle 0|\bar{q}q|0\rangle = \langle 0|\bar{u}u|0\rangle + \langle 0|\bar{d}d|0\rangle + \langle 0|\bar{s}s|0\rangle, \tag{2.5.4}$$

[8] In QCD, the light quark operator $\bar{q}q$ has a nonzero VEV, which can be written as $\langle \mid \bar{q}q \mid\rangle = \langle 0 \mid (\bar{u}u + \bar{d}d) \mid 0\rangle \equiv -(250MeV)^3$.

where u, d, s denotes a field for up, down and strange quarks, respectively and $\langle\bar{q}q\rangle$ is the chiral condensate. This exact definition of chiral condensate is written as,

$$\langle\bar{q}q\rangle = -iTr \lim_{y\to x^+} \left[S_F(x,y) - S_F^0(x,y)\right], \tag{2.5.5}$$

with $S_F(x,y$ and $S_F^0(x,y)$ are the full and the bare (perturbative) quark propagators, respectively. Obviously, the chiral condensate in Eq. (2.5.5) is a purely nonperturbative phenomenon. $S_F(x,y) = -i\langle 0 \mid T\left[q(x)\bar{q}(x)\right] \mid 0\rangle$. Using the Wick's theorem which states that the time product $T\left[q(x)\bar{q}(x)\right]$ can reduce to the normal product $:\bar{q}q:$ plus contraction of two field operators.

2.6 Low Energy Theorems

In Section 2.5 , the broken symmetry corresponds to the non-conserved of the axial current. Herein the weak pion decay is examined. The weak pion decay is a purely isovector transition. The chiral symmetry is broken down to $SU(3)_V$ giving rise to pseudscalar Goldstone field $|\pi_a\rangle$ as explained in Section 2.5. The Nambu-Goldstone boson state is written as

$$\langle 0 \mid \mathcal{J}^\mu_{A,a}(x) \mid \pi_b(p)\rangle = if_\pi p^\mu e^{-ip.x}\delta_{ab}, \tag{2.6.1}$$

with f_π the pion decay constant, a and b isospin indices and p^μ denotes four momentum. The physical value of the pion decay constant, f_π, which is deduced from lifetime (decay) of the charge pions, it then gives (PDG) [116],

$$f_\pi = (130.41 \pm 0.03 \pm 0.20)\text{MeV}. \tag{2.6.2}$$

Using the divergence of the axial current, which is also well know as partially conserved axial vector current (PCAC), one obtains for two flavors, $N_F = 2$, case and isospin component, a =1,

$$\partial_\mu \mathcal{J}^\mu_{A,1} = (m_u + m_d)\bar{q}i\gamma_5\frac{\tau_1}{2}q, \tag{2.6.3}$$

where τ_1 is an isospin Pauli matrix. The divergence of the axial current in Eq. (2.6.3) can be solved by using the canonical anti-commutation relations for fermions [9]. Then considering the axial vector current operator symbolized by $\hat{\mathcal{P}}_a = \bar{q}(x)\gamma_5\tau_a q(x)$, the canonical commutation relation between $\hat{\mathcal{Q}}^a_A$ and $\hat{\mathcal{P}}_b$ can be expressed by

$$\left[\hat{\mathcal{Q}}^a_A, \hat{\mathcal{P}}_b\right] = -\delta_{ab}\bar{q}q. \tag{2.6.4}$$

By combining the divergence of the axial current in Eq. (2.6.3) and charge, one then obtains

$$\langle 0 \mid \left[\hat{\mathcal{Q}}^1_A, \partial_\mu \mathcal{J}^\mu_{A,1}\right] \mid 0\rangle = -\frac{i}{2}(m_u + m_d)\langle\bar{u}u + \bar{d}d\rangle, \tag{2.6.5}$$

[9] The canonical anti-commutation relations, $[\hat{A}, \hat{B}] = \{\hat{A}, \hat{B}\} - 2\hat{B}\hat{A}$.

(2.6.6)

After substituting a complete set of pseudoscalar states in canonical commutator relation, the terms on the left hand side in Eq. (2.6.5) can straightforwardly computed from Eq. (2.6.1). By truncating the relation by one pion states, $|\pi\rangle$, one has

$$m_\pi^2 f_\pi^2 = -m\langle\bar{q}q\rangle + \mathcal{O}(m^2), \tag{2.6.7}$$
$$m_K^2 f_K^2 = -m\langle\bar{q}q\rangle + \mathcal{O}(m^2), \tag{2.6.8}$$
$$\tag{2.6.9}$$

where $m = m_u \sim m_d \sim m_s$ by considering the isospin limit. This result is the so-called $Gell - Mann - Oakes - Renner - relation$ (GMOR) [117]. One notes that involving pions in the low energy theorems are a consequence of the PCAC relation. In Chapter 3, one will show that the NJL model also satisfies the GMOR relations.

2.7 Deep Inelastic Scattering

DIS is a process of a lepton (electron, muon, neutrino) scatters a nucleus target by transferring a large amounts of energy and four-momentum transferred squared $q = (\nu, \vec{q})$ [118, 119, 121–123]. The deep inelastic process takes place, when $Q^2 \to \infty$ and the energy of the exchange boson in lab frame [10] $q^0_{Lab} = \nu \to \infty$, in order to keep their ratio finite. The DIS reaction process can be written as

$$\ell(k, s) + A(P, S) \to \ell'(k', s') + X(P_X), \tag{2.7.1}$$

with ℓ, ℓ' and A denote the initial lepton, scattered lepton and the target (nucleon), respectively. X is the unobserved final hadronic state. The initial and final four momentum of the lepton are symbolized by k, k', respectively. The initial momentum of target is labeled by P. The small letter of S and s' denote the spin of corresponding particle.

In DIS process, the target breaks up and forms an infinite number of feasible hadronic final states which remain unobserved. Therefore only lepton will be detected and then one measures its final energy of the lepton as well as the scattering angle θ relative to the incoming lepton beam of fixed energy. The lowest order approximation diagram for DIS is shown in Fig. 2.7.1.

[10] In the lab frame, the target is at rest, then the target four momentum is written as $P = (M_A, 0, 0, 0)$, where M_A is the target mass.

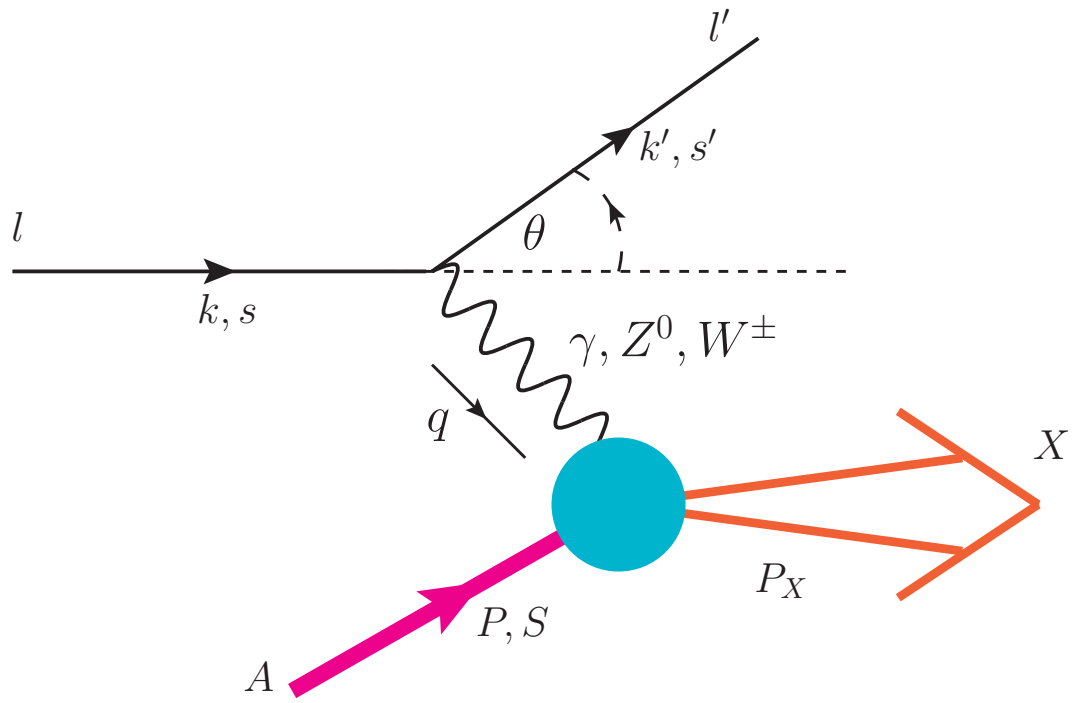

Figure 2.7.1: The initial and final four momentum and spin are denoted by k, s and k', s', respectively. P, S is four momentum and spin of the target (magenta line), $q = (k - k')$ is a momentum transferred to the target by exchanged vector bosons (γ, Z^0, and, $W^{\pm}$). The angle between an incoming and outcoming lepton (black lines) in the target rest target is denoted by θ. The blue blob denotes the nonperturbative dynamics.

Based upon the diagram in Fig. 2.7.1, the invariant amplitude, $\mathscr{M}$ can be written as

$$\mathscr{M} = \sum_{s'} \bar{u}(k', s')\gamma^{\mu}u(k, s)\frac{ie^3 g_{\mu\nu}}{q^2}\langle X|\mathcal{J}^{\nu}(0)|P, S\rangle, \tag{2.7.2}$$

where $u(k)$ and X are a field of the particle and unobserved particle, respectively. $\mathcal{J}(0)$ stands for the operator of hadronic electromagnetic current. In the reaction process, X is not observed, the DIS differential cross section, $d\sigma$ can be written as

$$d\sigma = \frac{1}{4J}\frac{d^3k'}{2E'(2\pi)^3}\sum_X \prod_{i=1}^{nX}\int \frac{d^3p_i}{(2\pi)^3 2E_i}|\mathscr{M}|^2(2\pi)^4\delta^4(P + q - \sum_{i=1}^{nX} p_i), \tag{2.7.3}$$

with $J = P.k$ stand for the flux factor. The DIS differential cross section which can be written as the product of leptonic and hadronic tensors

$$d\sigma = \frac{1}{4J}\frac{d^3k'}{2E'(2\pi)^3}\frac{e^4}{Q^4}2\pi L_{\mu\nu}\mathcal{W}^{\mu\nu}. \tag{2.7.4}$$

From Eqs. (2.7.3) and (2.7.4), the leptonic tensor, $L_{\mu\nu}$ can be defined by

$$\begin{aligned} L^{\mu\nu} &= \sum_{s'} |\bar{u}(k',s')\gamma^{\mu}u(k,s)|^2 \\ &= \frac{1}{2}Tr\left[(\not{k}'+m)(1+\gamma_5\not{s}')\gamma^{\mu}(\not{k}'+m)\gamma^{\nu}\right] \\ &= 2(k^{\mu}k'^{\nu}+k^{\nu}k'^{\mu}+g^{\mu\nu}k.k'+i\epsilon^{\mu\nu\lambda\sigma}q_{\lambda}k_{\sigma}). \end{aligned} \tag{2.7.5}$$

In Eq. (2.7.5) the polarization effect is taken into account. However it can straightforwardly be reduced to the unpolarized beam and unpolarized target case by ignoring the fourth term in Eq. (2.7.5), which are spin contributions from the both beam and target.

On the other hand, the hadronic tensor, $\mathcal{W}_{\mu\nu}$, has the form

$$\begin{aligned} \mathcal{W}_{\mu\nu} &= \frac{1}{2\pi}\sum_{X}\prod_{i=1}^{nX}\int\frac{d^3p_i}{(2E_i2\pi)^3}\delta^4(p+q-px) \mid \langle X_i|\mathcal{J}_{\nu}(0)|P,S\rangle \mid^2 \\ &= \frac{1}{2\pi}\int d\xi e^{iq.\xi}\langle P,S \mid \mathcal{J}_{\mu}(\xi)\mathcal{J}_{\nu}(0) \mid P,S\rangle \\ &= \frac{1}{2\pi}\int d\xi e^{iq.\xi}\langle P,S \mid [\mathcal{J}_{\mu}(\xi),\mathcal{J}_{\nu}(0)] \mid P,S\rangle, \end{aligned} \tag{2.7.6}$$

where the states are normalized. [11]

In the target rest frame, where $P^{\mu}=(M_A,0,0,0)$, and neglecting lepton masses, the differential cross section in Eq. (2.7.3) can rewritten as

$$\frac{d\sigma}{d\Omega dE'} = \frac{\alpha_{em}^2}{2M_AQ^4}\frac{E'}{E}L_{\mu\nu}\mathcal{W}^{\mu\nu}, \tag{2.7.7}$$

with $\alpha_{em}=\dfrac{e^2}{4\pi}$ and Ω stand for the solid angle.

A diagrammatic representation of the leptonic and hadronic tensors is depicted in Fig. 2.7.2. This indicates that the leptonic tensor is purely perturbative. Therefore QED can be applied in this part, whereas the hadronic tensor is nonperturbative which contains a quark-gluon interactions inside the target (nucleon).

[11] $\langle p \mid p'\rangle = 2p^0(2\pi)^3\delta^3(\overrightarrow{p}-\overrightarrow{p'})$, and $(2\pi)^4\delta^4(p+q-pX) = \int d^4\xi e^{i(p+q-pX).\xi}$.

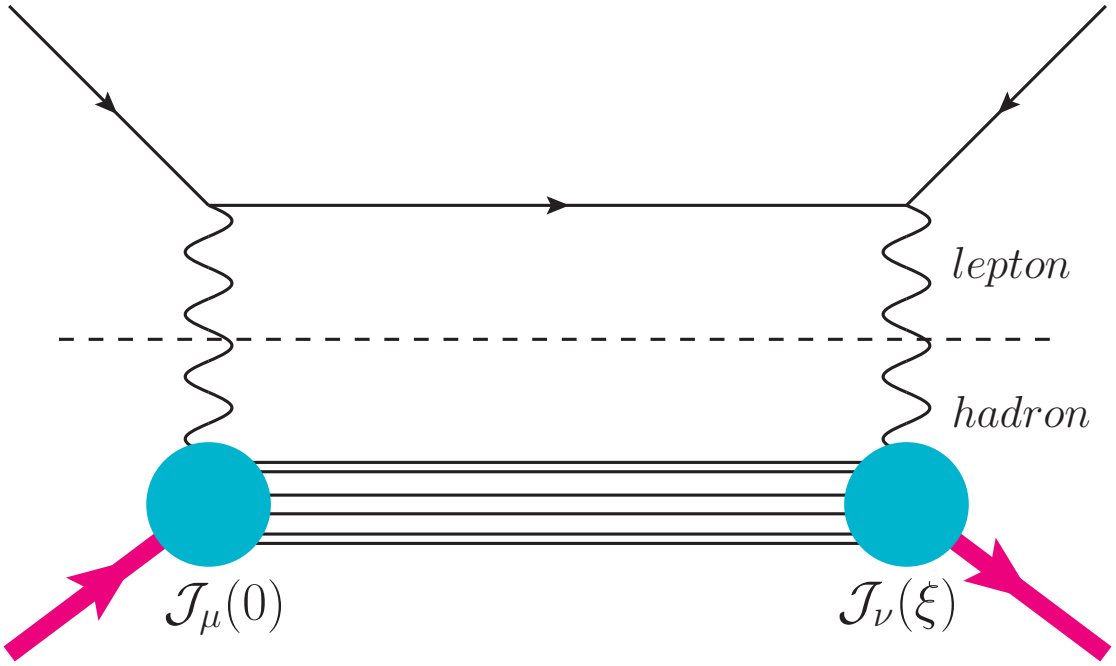

Figure 2.7.2: Diagrammatic representation of the leptonic and hadronic tensors in the one boson exchange. The leptonic tensor is a purely perturbative and the hadronic tensor is a non-perturbative.

Figure 2.7.1 exhibits that each of the three electroweak gauge bosons play a role in DIS. The squared amplitude changes when the neutral gauge boson, Z^0, is considered in the DIS processes. The total squared amplitude has a form

$$\begin{aligned} \mid \mathcal{M} \mid^2 &= \mid \mathcal{M}_\gamma + \mathcal{M}_Z \mid^2 \\ &= \mid \mathcal{M} \mid^2 + \mid \mathcal{M}_Z \mid^2 + \mathcal{M}_\gamma \mathcal{M}_Z^* + \mathcal{M}_Z \mathcal{M}_\gamma^*, \end{aligned} \tag{2.7.8}$$

where $\mid \mathcal{M}_\gamma \mid^2$ is a purely electromagnetic contribution term, $\mid \mathcal{M}_Z \mid^2$ denotes a purely weak contribution term and $\mathcal{M}_\gamma \mathcal{M}_Z^* + \mathcal{M}_Z \mathcal{M}_\gamma^*$ is an interference contribution term. Therefore the differential cross section for including both γ and Z^0 exchange, similar steps as differential cross section in Eq. (2.7.7), can be written as

$$\frac{d\sigma_{nc}}{d\Omega dE'} = \frac{\alpha_{em}^2}{2M_A Q^4} \frac{E'}{E} \sum_{i=\gamma,\gamma Z,Z} L_{\mu\nu}^i \mathcal{W}_i^{\mu\nu} \eta^i, \tag{2.7.9}$$

with the η for both γZ and Z can be defined as

$$\eta^\gamma = 1, \tag{2.7.10}$$

$$\eta^{\gamma Z} = \left(\frac{G_F M_Z^2}{2\sqrt{2}\pi\alpha_{em}} \right) \left(\frac{Q^2}{Q^2 + M_Z^2} \right), \tag{2.7.11}$$

$$\eta^Z = \left(\left(\frac{G_F M_Z^2}{2\sqrt{2}\pi\alpha_{em}} \right) \left(\frac{Q^2}{Q^2 + M_Z^2} \right) \right)^2, \tag{2.7.12}$$

and $L_{\mu\nu}$ for both γZ and Z have a form

$$L^{\gamma Z}_{\mu\nu} = (g_V - \lambda g_A) L^{\gamma}_{\mu\nu}, \qquad L^{Z}_{\mu\nu} = (g_V - g_A)^2 L^{\gamma}_{\mu\nu}. \tag{2.7.13}$$

where λ denotes the helicity of the incoming lepton. The values of the helicity, $\lambda = \pm 1$. The formula in Eq. (2.7.13) hold for negative charge of the incoming lepton, therefore the sign of the g_A is changed from positive becomes negative, where the expression of g_A is

$$g_V = -\frac{1}{2} + 2\sin^2\theta_W, \qquad g_A = -\frac{1}{2}. \tag{2.7.14}$$

In analogy to the differential cross section expression in Eq. (2.7.9), the differential cross section for the charged current [12] can be formulated as

$$\eta^W = \frac{1}{2}\left(\frac{G_F M_W^2}{4\pi\alpha_{em}}\right)\left(\frac{Q^2}{Q^2 + M_Q^2}\right), \qquad L^{W^\pm}_{\mu\nu} = (1 \pm 2\lambda)^2 L^{\gamma}_{\mu\nu}. \tag{2.7.15}$$

In general the compact form of the hadronic tensor, which is Lorentz and CP invariant, can be written in terms of eight independent structure functions, F_1^i, F_2^i, F_3^i, g_1^i, g_2^i, g_3^i, g_4^i, and g_5^i and has a form

$$\begin{aligned}\mathcal{W}^i_{\mu\nu} = &-2g_{\mu\nu}F_1^i + \frac{2P_\mu P_\nu}{P.q}F_2^i + i\frac{\epsilon_{\mu\nu\alpha\beta}}{P.q}P^\alpha q^\beta F_3^i + i\frac{2M_A\epsilon_{\mu\nu\alpha\beta}}{P.q}\left[q^\alpha S^\beta g_1^i - 2xP^\alpha S^\beta g_2^i\right] \\ &- \frac{2M_A}{P.q}\left[P_\mu S_\nu + S_\mu P_\nu\right] + 2M_A\frac{S.q}{(P.q)^2}P_\mu P_\nu g_4^i + 2M_A\frac{S.q}{P.q}g_{\mu\nu}g_5^i,\end{aligned} \tag{2.7.16}$$

where $i \in \gamma, \gamma Z, Z, W^\pm$. In Eq. (2.7.16), the terms are proportional to q^μ and q^ν vanish because they do not contribute to the differential cross section. This is because the lepton tensor satisfies a conservation law, $q^\mu L_{\mu\nu} = q^\nu L_{\mu\nu} = 0$. Thus the differential cross section can be written in terms of the dimensionless structure functions, F_1^i (x, Q^2), F_2^i (x, Q^2) , g_1^i (x, Q^2), and g_2^i (x, Q^2) [13], where $x = \dfrac{Q^2}{2P.q}$ is well known as the Bjorken variable. In addition, from Eq. (2.7.16), one finds

$$F_3^\gamma = g_3^\gamma = g_4^\gamma = g_5^\gamma = 0. \tag{2.7.17}$$

This is because the electromagnetic interaction is parity conserving. The weak interaction is parity violating, therefore the second rank tensors and pseudo-tensors can be found in Eq. (2.7.16). Then the unpolarized differential cross section in Eq. (2.7.3) can be written in terms of the structure function and it has form [14]

$$\frac{d\sigma}{dxdyd\phi} = \frac{e^4}{4\pi^2 Q^2}\left[\frac{y}{2}F_1(x,Q^2) + \frac{1}{2xy}\left(1 - y - \frac{y^2}{4}(\kappa - 1)F_2(x,Q^2)\right)\right], \tag{2.7.18}$$

[12] The sum is over suitable W bosons (W^+ or W^-).

[13] F(x, Q^2) for pseudoscalar mesons.

[14] We sum over the initial electron helicities.

with $\kappa = 1 - \dfrac{4x^2 M_A^2}{Q^2}$ and the spin-dependent differential cross section [15] is written as

$$\frac{\Delta\sigma}{dxdyd\phi} = \frac{e^4}{4\pi^2 Q^2}\left[\left(1 - \frac{y}{2} - \frac{y^2}{4}(\kappa - 1)\right) g_1(x, Q^2) - \frac{y}{2}(\kappa - 1) g_2(x, Q^2)\right], \tag{2.7.19}$$

where the target is polarized parallel to the lepton beam is assumed [16]. In this thesis, we will focus on structure functions of the pseudoscalar mesons, such as the kaon and pion, which relates to the unpolarized differential cross section in Eq. (2.7.18).

2.8 Quark Parton Model

QPM assumes that the current $\mathcal{J}_\mu$ couples to quarks. It was proposed firstly by Feynman [120] in the late 1960's to explain Bjorken scaling. Excellent reviews are given by Roberts [118] and Jaffe [121, 122]. Consequently QPM contribution to forward Compton scattering amplitude can be divided into flow and interaction of quark lines. Second assumption is that the currents may be treated as in free field theory at large Q^2 (asymptotic freedom). Therefore the final state interaction and vertex corrections can be neglected. Then residual contributions come from the parton diagram and interference, respectively. However the interference will be disappear by power of Q^2 and then only the incoherent elastic scattering of the virtual photon off the target quarks survives.

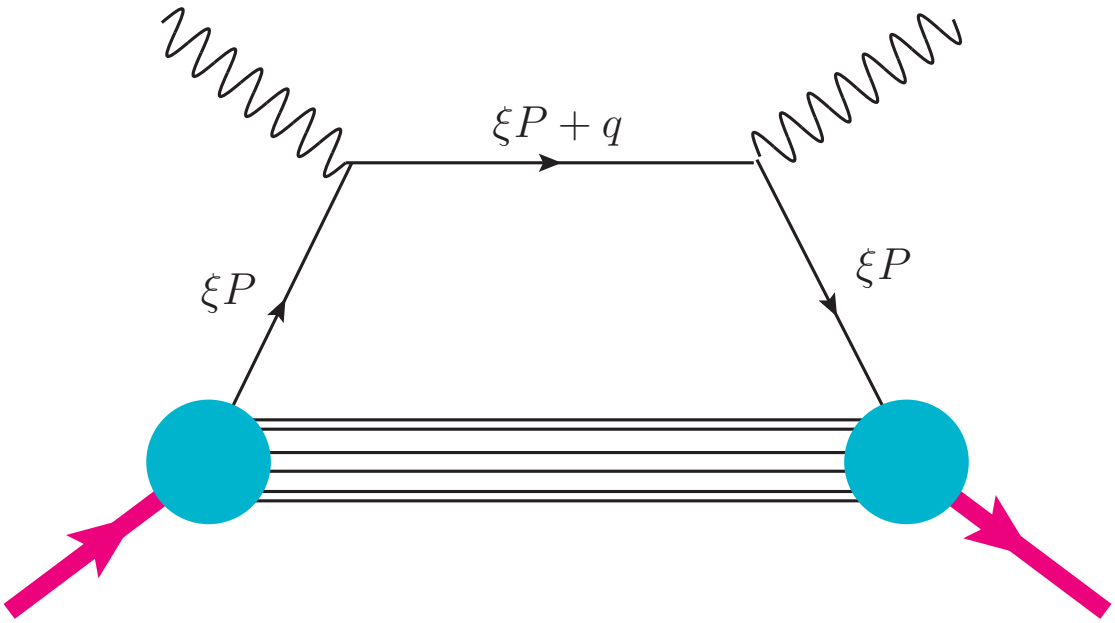

Figure 2.8.1: Diagrammatic representation of the Quark Parton Model.

[15] The difference between the positive and negative helicities of the lepton is taken into account.

[16] $\dfrac{d\sigma}{dxdyd\phi} = \dfrac{M_A \nu}{E'} \dfrac{d\sigma}{dE' d\Omega}$

According to free quark theory model, the current commutator, $\mathcal{J}_\mu\ (\xi)$, in $\mathcal{W}_{\mu\nu}$ of the structure function can be reduced. A derivation of QPM based on the currents [121, 122] are given as

$$\mathcal{J}_\mu(\xi) = \bar{\psi}(\xi)\mathcal{Q}\gamma_\mu\psi(\xi), \tag{2.8.1}$$

with $\mathcal{Q}$ denotes the quark charge matrices (=$diag\ \left(\frac{2}{3}, -\frac{1}{3}, -\frac{1}{3}, \dots\right)$). The current commutator in the definition of $\mathcal{W}_{\mu\nu}$ in Eq. (2.7.6), can be written as

$$\begin{aligned}\left[\mathcal{J}^\dagger_\mu(\xi), \mathcal{J}_\nu(0)\right] &= \bar{\psi}(\xi)\gamma_\mu\{\psi(\xi), \bar{\psi}(\xi)\}\mathcal{Q}^2\gamma_\nu\psi(0) \\ &\quad - \bar{\psi}(0)\gamma_\nu\{\psi(0), \bar{\psi}(\xi)\}\mathcal{Q}^2\gamma_\mu\psi(\xi),\end{aligned} \tag{2.8.2}$$

with the anti-commutator definition is

$$\{\psi(\xi), \bar{\psi}(0)\} = \frac{1}{2\pi}\gamma_\rho\frac{\partial}{\partial\xi_\rho}\left[\epsilon(\xi^0)\delta(\xi^2) + \mathcal{O}\left(\frac{m^2}{Q^2}\right)\dots\right], \tag{2.8.3}$$

where $\{\psi(\xi), \bar{\psi}(0)\}$ [17] is the anti-commutator relation. A second term containing the quark masses in Eq. (2.8.3) is ignored because quark masses only generate a small correction of the $\mathcal{O}\left(\frac{m^2}{Q^2}\right)$ in the Bjorken limit. The Dirac matrix identity are introduced and inserted into Eq. (2.8.2), one obtains,

$$\begin{aligned}\frac{1}{2}(\gamma_\mu\gamma_\rho\gamma_\nu + \gamma_\nu\gamma_\rho\gamma_\mu) &= (g_{\mu\rho}g_{\nu\sigma} + g_{\mu\sigma}g_{\nu\rho} - g_{\mu\nu}g_{\rho\sigma})\gamma^\sigma \\ &\equiv \mathcal{S}_{\mu\rho\nu\sigma}\gamma^\sigma,\end{aligned} \tag{2.8.4}$$

then putting them together Eqs. (2.8.2)- (2.8.4) into the hadronic tensor, $\mathcal{W}_{\mu\nu}$ in Eq. (2.7.6), one obtains

$$\begin{aligned}\lim_{Bj}\mathcal{W}_{\mu\nu} = \frac{1}{8\pi^2}\mathcal{S}_{\mu\rho\nu\sigma}\int d^4\xi e^{iq.\xi}\left[\frac{\partial}{\partial\xi_\rho}\epsilon(\xi^0)\delta(\xi^2)\right] \\ \times\langle p \mid \bar{\psi}(\xi)\gamma^\sigma\mathcal{Q}^2\psi(0) - \bar{\psi}(0)\gamma^\sigma\mathcal{Q}^2(\xi) \mid p\rangle_c,\end{aligned} \tag{2.8.5}$$

where " $\lim_{Bj}$ " remind us that QPM assumption in Eq. (2.8.5) are only valid as $Q^2 \to \infty$ at fixed $x = \frac{Q^2}{2M_A\nu}$. Then employing the integration by parts, the term in which $\frac{\partial}{\partial\xi_\rho}$ acts on matrix element will be dropped as it generates factors p^ρ or $\xi^\rho\mu^2$, both of which are negligible with respect to q^ρ in the Bjorken limit [18].

Introducing the light-cone coordinates in the rest frame, one then has

$$\lim_{Bj}\mathcal{W}_{\mu\nu} = \lim_{q^-\to\infty}\frac{-i}{8\pi^2}\mathcal{S}_{\mu\rho\nu\sigma}q^\rho\int d\xi^+d\xi^-e^{iq^+\xi^- + iq^-\xi^+}$$

[17] $\{\psi(\xi), \bar{\psi}(0)\} = \{\psi(-\xi), \bar{\psi}(0)\}$

[18] ξ^ρ Fourier transform into $\frac{q^\rho}{q^2}$

$$\times \delta\left(2\xi^+\xi^- - \xi_\perp^2\right)\epsilon\left(\xi^+ - \xi^-\right)$$
$$\times \langle p \mid \bar{\psi}\gamma^\sigma \mathcal{Q}^2\psi(0) - \bar{\psi}(0)\gamma^\sigma\mathcal{Q}^2\psi(\xi) \mid p\rangle_c. \tag{2.8.6}$$

Note that the form of $\mathcal{S}_{\mu\rho\nu\sigma}$ indicates that the coefficient of $g_{\mu\nu}$ in $\mathcal{W}_{\mu\nu}$ equals half the trace of $\mathcal{W}_{\mu\nu}$. Through the decomposition of hadronic tensor, $\mathcal{W}_{\mu\nu}$ in Eq. (2.7.6), it then gives

$$\begin{aligned}\mathcal{W}_1 &= \frac{1}{2}\left[3\mathcal{W}_1 - \left(1 + \frac{\nu}{2M_A x_A}\right)\mathcal{W}_2\right] \\ &= \frac{1}{2}\left[3F_1 - \left(1 + \frac{\nu}{2M_A x_A}\right)F_2\right],\end{aligned} \tag{2.8.7}$$

note that $1 \ll \dfrac{\nu}{M_A}$ and with the help of the structure function definition in Eq. (2.7.18), one obtains

$$F_2(x_A) = 2x_A F_1(x_A). \tag{2.8.8}$$

which is known as the Callen-Gross relation [124] and follows from the quark spin being $\dfrac{1}{2}$. By applying the δ-function in Eq. (2.8.6) to perform the $\xi_\perp^2$ integral using $\displaystyle\int d^2\vec{\xi}_\perp^2\,\delta(\vec{\xi}_\perp^2 - 2\xi^+\xi^-) = \pi$, the structure function, $F_2(x_A)$ can be rewritten as

$$\begin{aligned}F_2(x_A) = 2x_A \lim_{q^-\to\infty} \frac{-iq^-}{8\pi}\int d\xi^+ d\xi^- e^{iq^+\xi^- + iq^-\xi^+} \\ \times \left[\theta(\xi^+)\theta(\xi^-) - \theta(-\xi^+)\theta(-\xi^-)\right] \\ \times \langle p \mid \bar{\psi}(\xi)\gamma^+\mathcal{Q}^2\psi(0) - \bar{\psi}(0)\gamma^+\mathcal{Q}^2\psi(\xi) \mid p\rangle_c \mid_{\vec{\xi}_\perp^2 = 2\xi^+\xi^-},\end{aligned} \tag{2.8.9}$$

where the indices ρ and σ can be $-$ and $+$, respectively [19]. Then applying an integration by parts over ξ^+ in Eq. (2.8.9)and keeping only the leading term at large q^-, it then gives

$$\begin{aligned}F_2(x_A) = \frac{x_A}{4\pi}\int d\xi^- e^{iq^+\xi^-}\langle p \mid \bar{\psi}(\xi^-)\gamma^+\mathcal{Q}^2\psi(0) \\ - \bar{\psi}(0)\gamma^+\mathcal{Q}^2\psi(\xi^-) \mid p\rangle_c \mid_{\xi^+ = \vec{\xi}_\perp = 0}\end{aligned} \tag{2.8.10}$$

where $q^+ = \dfrac{-M_A x_A}{\sqrt{2}}$. To further simplify Eq. (2.8.10) using the projection matrix in terms of the light-cone γ matrices that is

$$\psi_\pm = \mathscr{P}^\pm\psi, \tag{2.8.11}$$
$$\mathscr{P}^\pm = \frac{1}{2}\gamma^\mp\gamma^\pm = \frac{1}{2}\left(1 \pm \alpha^3\right), \tag{2.8.12}$$

with $\mathscr{P}^+ + \mathscr{P}^- = 1$, $\mathscr{P}^\pm\mathscr{P}^\pm = \mathscr{P}^\pm$ and $\mathscr{P}^\pm\mathscr{P}^\mp = 0$. Inserting $\psi_\pm$ into Eq. (2.8.10), it can be rewritten as

$$F_2(x_A) = \frac{x_A}{2\sqrt{2}\pi}\int d\xi^- e^{iq^+\xi^-}$$

[19] $g^{++} = g_{--} = 0$.

$$\times \langle p \mid \psi_+^\dagger(\xi^-)\mathcal{Q}^2\psi_+(0) + \psi_+(\xi^-)\mathcal{Q}^2\psi_+^\dagger(0) \mid p\rangle_c \mid_{\xi^+=\vec{\xi}_\perp=0}, \tag{2.8.13}$$

In order to interchange the quark fields in second term of Eq. (2.8.13), we use the connected matrix element, that is

$$\begin{aligned}\langle p \mid \bar\psi(\xi)\psi(0) \mid p\rangle_c &= \langle p \mid : \bar\psi(\xi)\psi(0) : \mid p\rangle \\ &= -\langle p \mid \psi(0)\bar\psi(\xi) \mid p\rangle_c,\end{aligned} \tag{2.8.14}$$

where $\langle p \mid : \cdots : \mid p\rangle$ is a normal ordering. This removes the singularity [20] in the product operator of the fields, so it does not contribute to a connected element matrix.

To obtain the familiar parton model, inserting a complete set of states between the quark fields [21], translating the $x-^-$ dependence out of ψ_+ or $\psi_+^\dagger$, integrating over ξ^- and summing over quark flavors [22], it then gives

$$\begin{aligned}F_2^A(x_A) &= x_A \sum_a e_a^2 \sum_n \frac{1}{\sqrt{2}}\delta(p^+ + q^+ - p_n^+)\{\mid \langle n \mid \psi_{a+}(0) \mid p\rangle \mid^2 \\ &\quad + \mid \langle n \mid \psi_{a+}^\dagger(0) \mid p\rangle \mid^2\} \\ &= x_A \sum e_a^2 (f_{a/A}(x_A) + f_{\bar a/A}(x_A)),\end{aligned} \tag{2.8.15}$$

where a superscript A to F is to show us that F_2 depends on the target, e_a is the charge of a quark flavor a and the summation indicates that we have summed explicitly over quark flavors. Note that for a target of mass M_A, one has $q^+ = -\dfrac{x_A M_A}{\sqrt{2}}$, where $x_A = \dfrac{Q^2}{2M_A\nu}$, and $p^+ = \dfrac{M_A}{\sqrt{2}}$. Substituting p^+ to q^+, one has $q^+ = -x_A p^+$. This indicates that we work in the nuclear rest frame. Therefore the distribution $f(x_A)$ in Eq. (2.8.15) can be expressed by

$$f_{a/A}(x_A) = \frac{1}{\sqrt{2}}\sum_n \delta(p^+ - x_A p^+ - p_n^+) \mid \langle n \mid \psi_{a+} \mid p\rangle \mid^2, \tag{2.8.16}$$

$$f_{\bar a/A}(x_A) = \frac{1}{\sqrt{2}}\sum_n \delta(p^+ - x_A p^+ - p_n^+) \mid \langle n \mid \psi_{a+}^\dagger \mid p\rangle \mid^2, \tag{2.8.17}$$

where $f_{a/A}(x_A)$ describes the probability per unit x_A to remove from the target a quark of flavor a with plus component of momentum,$x_A p^+$, leaving behind a physical state ($\mid n\rangle$) with plus component momentum, $p_n^+ = (1-x_A)p^+$. Similarly, $f_{\bar a/A}$ is the probability to remove an anti-quark with plus component momentum, $x_A p^+$, leaving behind a physical state with $p_n^+ = (1-x_A)p^+$. The illustration of quark distributions, $f_{a/A}(x_A)$ and anti-quark distributions, $f_{\bar a/A}(x_A)$ are depicted in Fig. 2.8.2 and Fig. 2.8.3.

[20] The singularity is a C-number. It occurs when $\xi \to 0$.

[21] A complete set of states denoted by $\sum_n \mid n\rangle\langle n \mid = 1$

[22] quark flavors, $a = u, d, s, \cdots$, where u, d and s are up, down and strange quarks, respectively.

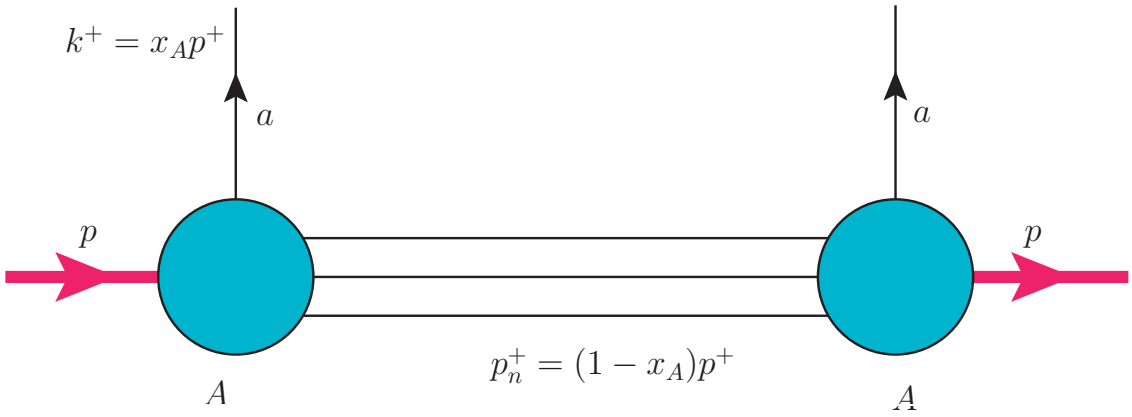

Figure 2.8.2: The quark distribution function, $f_{a/A}(x_A)$.

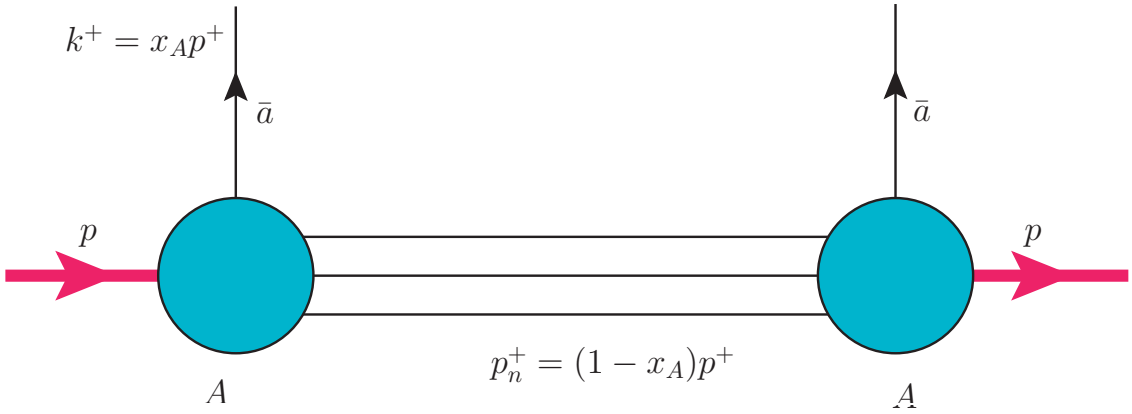

Figure 2.8.3: The anti-quark distribution function, $f_{\bar{a}/A}$.

On the other hand, the quark distribution function $f(x_A)$ has a connection with the forward amplitude for quark-target scattering, $\mathcal{A}_{\mu\nu}(p,k)$. The virtual quark-target forward scattering amplitude in the $A^+ = 0$ gauge, as illustrated in Fig. 2.8.4, is defined by

$$\mathcal{A}_{\mu\nu}(k,p) \equiv \int d^4\xi e^{-ik.\xi} \langle p \mid T\left(\bar{\psi}_\mu(\xi)\psi_\nu(0)\right) \mid p\rangle_c. \tag{2.8.18}$$

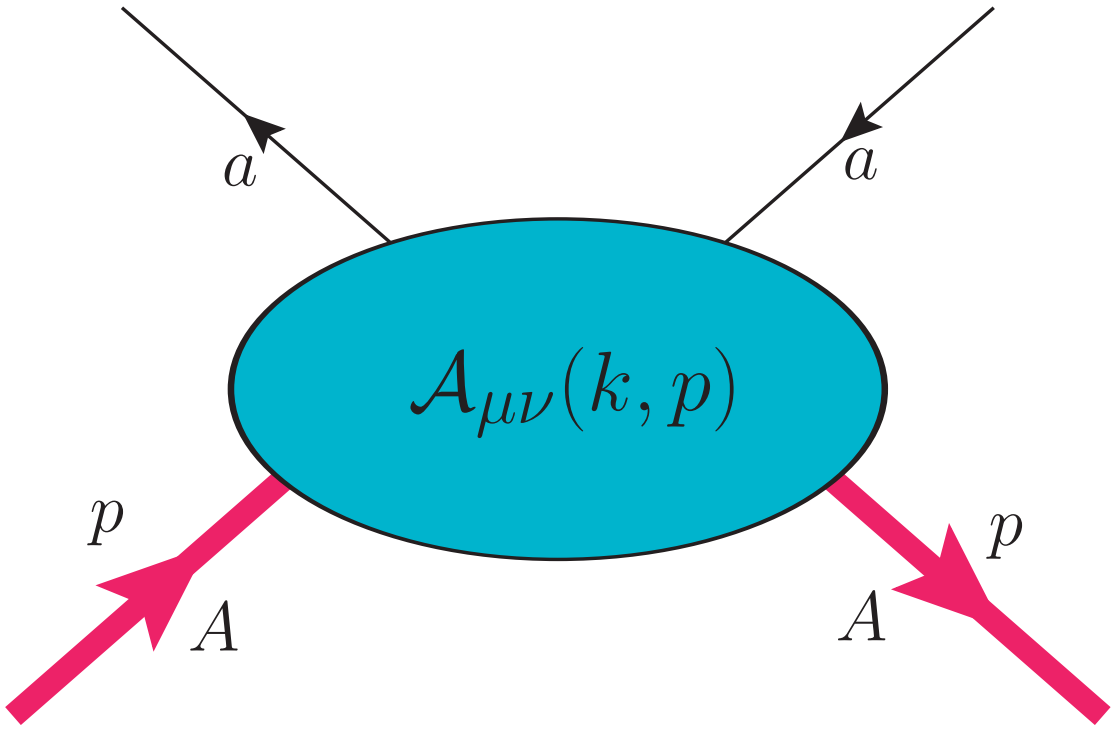

Figure 2.8.4: The virtual quark hadron scattering amplitude, $\mathcal{A}_{\mu\nu}(k,p)$.

Tracing the Dirac indices with γ^+ in the amplitude for quark hadron scattering, $\mathcal{A}_{\mu\nu}(k,p)$, and integrating over all components k at fixed , $k^+ = x_A p^+$, yields a distribution function, $f(x_A)$,

$$\begin{aligned} f(x_A) &= \int \frac{d^4k}{(2\pi)^4}\delta\left(\frac{k^+}{p^+} - x_A\right) Tr\left[\gamma^+ \mathcal{A}_{\mu\nu}(k,p)\right] \\ &= \frac{1}{p^+}\int \frac{d^4k}{(2\pi)^4}\delta\left(k^+ - x_A p^+\right) Tr\left[\gamma^+ \mathcal{A}_{\mu\nu}(k,p)\right]. \end{aligned} \tag{2.8.19}$$

where $\delta\left(\frac{k^+}{p^+} - x_A\right) = \frac{1}{p^+}\left(k^+ - x_A p^+\right)$.

The distribution function, $f(x_A)$ has some significant properties such as positivity, and normalization constraints. The state, $\mid n\rangle$ in Eq. (2.8.16) is physical and therefore its plus component of momentum must be positive ($p^+ > 0$). Thus $f(x_A)$ equals zero, for $x_A \geq 1$ or $x_A \geq \frac{M_A}{M_N}$, where the subscript A denotes a nucleus target. In addition, in Eq. (2.8.16), the quark distribution, $f(x_A)$ is manifestly positive for $0 < x_A < 1$. For $x_A < 0$, the $f(x_A)$ is given by

$$\begin{aligned} f_{a/A}(x_A) &= \frac{1}{2\sqrt{2}\pi}\int d\xi^- e^{iq^+\xi^-}\langle p \mid \psi^\dagger_{a+}(\xi)\psi_{a+}(0) \mid p\rangle_c \mid_{\xi^+=\vec{\xi}_\perp=0} \\ &= -\frac{1}{2\sqrt{2}\pi}\int d\xi^- e^{iq^+\xi^-}\langle p \mid \psi^\dagger_{a+}(0)\psi^\dagger_{a+}(\xi) \mid p\rangle_c \mid_{\xi^+=\vec{\xi_\perp}=0}, \end{aligned} \tag{2.8.20}$$

then performing the connection matrix element in Eq. (2.8.14) to Eq. (2.8.20), one has

$$f_{a/A}(x_A) = -\frac{1}{2\sqrt{2}\pi}\int d\xi^- e^{iq^+\xi^-}\langle p \mid \psi^\dagger_{a+}(xi)\psi^\dagger_{a+}(0) \mid p\rangle_c \mid_{\xi^+=\vec{\xi_\perp}=0}, \tag{2.8.21}$$

replacing $\xi^- \to -\xi^-$ and translating the matrix element into Eq. (2.8.21), one finds

$$f_{a/A}(x_A) = -f_{\bar{a}/A}(-x_A). \tag{2.8.22}$$

The result in Eq. (2.8.22) indicates that the quark distribution function does not vanish for $x < 0$ and is determined by the anti-quark distribution for $x > 0$. In addition, it shows us that x_A is limited to $-1 \geq x_A \leq 1$ and that the measurements in the physical region $0 < x_A < 1$, determine the distribution function everywhere. Practically the quark distribution formulas in Eqs. (2.8.16)- (2.8.22) will be used in Chapter 5.

Later, the quark distribution in Eqs. (2.8.21)-(2.8.22) are integrated over all x_A [23] and one obtains,

$$\begin{aligned}\int_{-\infty}^{\infty} dx_A f_{a/A}(x_A) &= \int_0^1 \big(f_{a/A}(x_A) - f_{\bar{a}/A}(x_A)\big) \\ &= \frac{1}{2\pi M_A}\int dq^+ d\xi^- e^{iq^+\xi^-}\langle p \mid \psi^\dagger_{a+}(\xi)\psi_{a+}(0) \mid p\rangle_c \mid_{\xi^+=\vec{\xi}_\perp=0} \\ &= \frac{1}{M_A}\langle p \mid \psi^\dagger_{a+}(0)\psi_{a+}(0) \mid p\rangle_c,\end{aligned} \tag{2.8.23}$$

where $\psi^\dagger_{a+}(0)\psi_{a+}(0) = \frac{1}{\sqrt{2}}\mathcal{J}^+_a$ and $\mathcal{J}^\mu_a$ is a conserved current. The expectation value of $\mathcal{J}^\mu_a$ is equal to the number of quarks of flavor a minus the quark number of anti-quarks of flavor a. Using this definition, Eq. (2.8.23) can be rewritten as

$$\begin{aligned}\int_{-\infty}^{\infty} dx_A f_{a/A}(x_A) &= \frac{1}{M_A}\langle p \mid \psi^\dagger_{a+}(0)\psi_{a+}(0) \mid p\rangle_c \\ &= \frac{1}{M_A}\langle p \mid \mathcal{J}^\mu_a \mid p\rangle_c \\ &= N_{a/A} - N_{\bar{a}/A},\end{aligned} \tag{2.8.24}$$

here $N_{a/A}$ and $N_{\bar{a}/A}$ are the number of quarks and anti-quarks, respectively. This is the so-called the quark number sum rules.

By definition, the quark and anti-quark distributions ($f_{a/A}(x_A)$ and $f_{\bar{a}/A}(x_A)$) are interpreted as a probability per unit x_A to find a quark or anti-quark of flavor a with $k^+ = x_A p^+$ in the nucleus target, A, it then can be formulated by

$$f_{a/A}(x_A) = \frac{dP_{a/A}}{dx_A}. \tag{2.8.25}$$

This interpretation is the advantages of the QPM sum rules. Similarly, the momentum sum rules for quark distribution can be derived by following QPM sum rules. The

[23] Note that $x_A = -\frac{\sqrt{2}q^+}{M_A}$.

momentum sum rules for quark distribution, as ultimate goal for the structure function, is given as

$$\int_0^1 dx_A x_A \left[f_{a/A}(x_A) - f_{\bar{a}/A}(x_A) \right] = \epsilon_{a/A} + \epsilon_{\bar{a}/A}, \tag{2.8.26}$$

with $\epsilon_{a/A}$ ($\epsilon_{\bar{a}/A}$) is the fraction of the target nucleus p^+ carried by quarks (antiquarks) of flavor a. Assuming that the hadron contained only valence quarks, then $\sum_a \epsilon_{a/A}$ in Eq. (2.8.26) would be equal 1. At large transfer momentum, Q^2, it is typically $\frac{1}{2}$, indicating that substantial momentum and energy of the hadrons is carried by gluons.

2.9 Light-cone Dominance Behavior

It is very useful to understand the distance scales in DIS, as in Section 2.8. It can be obviously seen in hadronic tensor, $\mathcal{W}_{\mu\nu}$, in Eq. (2.7.6). To examine the distance scales [24] in the context of a space-time description, we recall the hadronic tensor,

$$\mathcal{W}_{\mu\nu} = \frac{1}{2\pi} \int d\xi e^{iq.\xi} \langle P, S \mid [\mathcal{J}_\mu(\xi)\mathcal{J}_\nu(0)] \mid P, S \rangle. \tag{2.9.1}$$

The distance scales between the two current insertions ($\mathcal{J}_\mu(\xi)$ and $\mathcal{J}_\nu(0)$) in Eq. (2.9.1) are dominated by ξ. The commutator of the currents in Eq. (2.9.1) are weighted by a factor $\exp(iq.\xi)$. [25] The dot-product $q.\xi$ are require to be finite. For the sake of the simplicity, we choose to work in the target rest frame [26] where the incoming virtual photon moving in the z-direction, that is

$$q = \left(\nu, 0, 0, -\sqrt{\nu^2 + Q^2} \right). \tag{2.9.2}$$

In the Bjorken limit, $Q^2 \to \infty$ and $x_A = \dfrac{Q^2}{2M_A\nu}$ is fixed [27], Eq. (2.9.2) can be rewritten as

$$q = \left(\nu, 0, 0, -\nu - M_A x_A \right). \tag{2.9.3}$$

Later, the light-cone coordinates is introduced as

$$q^\pm \equiv \frac{q^0 \pm q^3}{\sqrt{2}}, \tag{2.9.4}$$

[24] The distance referred to the space-time separation, ξ_λ between the points at which currents $\mathcal{J}_\mu$ and $\mathcal{J}_\nu$ act.

[25] The dot-product of $q.\xi$ is given by $q.\xi = q^+\xi^- + q^-\xi^+$.

[26] In the target rest frame, we also have $p = (M, 0, 0, 0)$.

[27] In the Bjorken limit, we have $\dfrac{Q^2}{\nu^2} \to 0$.

Using Eq. (2.9.4), one obtains that $q^- \to \infty$ and $q^+ \to -\frac{M_A x_A}{\sqrt{2}}$ in the Bjorken limit. Therefore a finite $q.\xi$ requires $\xi^+ \to 0$ and $\mid \xi^- \mid < \frac{\sqrt{2}}{M_A x_A}$, where $M_A x_A = M_A x = \frac{Q^2}{2\nu}$, so it means the limiting value of q^+ is independent of the nucleus mass, M_A.

The commutator in Eq. (2.9.1) is causal, therefore $\xi^2 = 2\xi^+\xi^- - \vec{\xi}_\perp^2$ is positive ($\xi^2 \geq 0$). Thus $\xi^+ \to 0$ with ξ^- finite requires $\vec{\xi}_\perp \to 0$. Notice that all components of $\xi^\mu \to 0$, except ξ^- vanish in the Bjorken limit. Thus DIS is not a short distance physics phenomenon ($\xi^\mu \to 0$), but rather a light-cone ($\xi^2 \to 0$) dominated process. To understand the dynamics and nuclear effects in inclusive electron scattering, the two constraints $\xi^+ \to 0$ and $\xi^- < \frac{\sqrt{2}}{M_A x_A}$ imply $\mid \xi^0 \mid < \frac{1}{M_A x_A}$ and $\mid \xi^3 \mid < \frac{1}{M_A x_A}$. In the Bjorken limit, the correlation length probed by DIS becomes light-like [28] but may extend to very large spatial distances and times in the small x limit.

2.10 Factorization Scale

A hadronic cross section contains mass singularities [125–128] at the short distances and infrared divergent [130] at the long distances physics. Therefore, hadronic cross sections cannot be calculated using perturbative QCD. The separation of short distance and long distance factors using factorization scale leads us to generalization of calculable partonic cross section to physical measurable hadronic cross section. Extensive reviews of the factorization scale can be found in Refs [131–137].

The factorization theorem states that the inclusive cross section can be factorized as a convolution of a renormalized soft nonperturbative part and a hard scattering part that is free of long distances singularities. This indicates that factorization concerns isolating the singularities as universal factors associated with long distance interactions. In addition, the singularities will be absorbed into non-perturbative parton distribution and fragmentation functions. In the same way, UV divergences in the perturbative calculations associated with short distance interactions are isolated into universal renormalization constants and absorbed into measurement physical constant in renormalized field theory. The factorization can be illustrated by the following identity

$$1 + \alpha \ln\left(\frac{q^2}{p^2}\right) + \cdots = \quad \left[1 + \alpha \ln\left(\frac{\mu_f^2}{p^2}\right) + \cdots\right]\left[1 + \alpha \ln\left(\frac{q^2}{\mu_f^2}\right) + \cdots\right], \quad (2.10.1)$$

with μ_f denotes collectively the renormalization and the factorization scale. All Feynman diagrams contribution to DIS in terms of order of α_S are illustrated in Fig. 2.10.1.

[28] The light-like means that space-time distance equal zero.

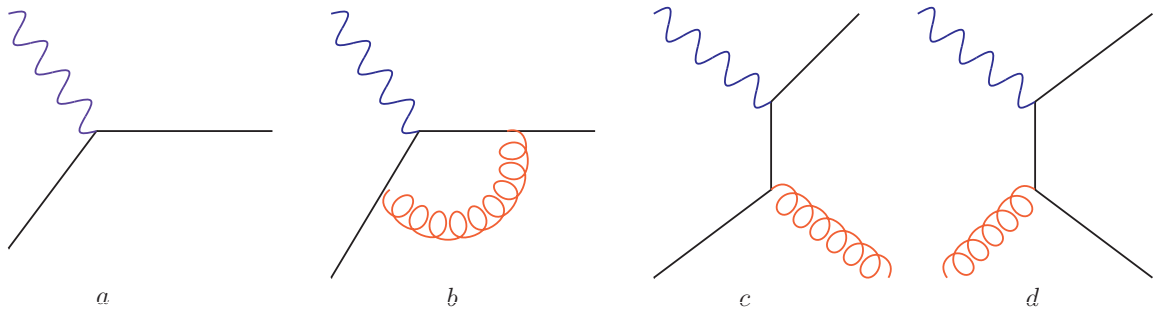

Figure 2.10.1: Feynman diagrams contribution to DIS to order α_S : (a) Leading order (LO) quark scattering; (b) Next leading order (NLO) vertex correction; (c) NLO quark scattering; and (d) NLO gluon fusion.

Through the interpretation of the factorization theorem, the structure function in the inclusive DIS cross section can be written as

$$F_a^\lambda(x,Q^2) = \sum_a f_A^a(x,\mu) \otimes \hat{F}_A^\lambda(x, \frac{Q}{\mu}, \frac{Q}{m}, \alpha_s(\mu)) + \cdots , \tag{2.10.2}$$

where $f_A^a(x,\mu)$ denotes the distribution of the parton a inside hadron A, $\hat{F}_a^\lambda$ is the perturbatively calculable hard cross section and μ is the factorization scales. The ellipsis $(\cdots)$ is higher twist contribution, symbolized by $\mathcal{O}\left(\frac{\Lambda}{Q}\right)^r$ where r is a positive number. A superscript λ denotes a helicity index and $\otimes$ is the convolution integral [29].

The definitions of the PDF and the factorization formulation depend on the magnitudes of the factorization scale, μ. This respects to the quark masses. Therefore the factorization scales are necessarily non-trivial. The DIS cross-section factorization has been proven to all orders in perturbation theory and is the basis of all other cross section factorization like the Drell-Yan reactions and semi-inclusive DIS, as shown in Fig. 2.10.1. Note that in a leading order (LO), the gluon structure function, F_g^λ vanishes and quark structure function contributes.

The term on the right hand side in Eq. (2.10.2) shows that the factorized term consisting of the convolution integral as a function of the momentum fraction variable.This is only leading twist approximation, which includes all algorithmic effects such as $\log\left(\frac{Q}{\mu_f}\right)$ and $\log\left(\frac{\mu_f}{m}\right)$. The factorization shows the separation of the parton structure function into a long distance physics factor with the confinement scale and a short distance factor with the large momentum scale, Q. Once the parton distribution functions are known, then it would be extended to evolve the parton distribution to arbitrary high energies by using the QCD evolution. This issues will be discussed further in Subsection 2.11.

[29]The convolution integral is formally introduced as $f(z) \otimes g(z) \equiv \int_z^1 \frac{dy}{y} f(\frac{z}{y}) g(y)$.

2.11 QCD Evolution

QCD evolution was proposed by Dokshitzer [138], Gribov and Lipatov [139] as well as Altarelli and Parisi [92] (DGLAP) to evolve the parton distribution functions as a function of longitudinal momentum, x and initial model scale, Q_0 to parton distribution functions as a function x and QCD scale, Q^2. In QCD evolution, the model scale means the momentum transfer scale that comes from the hadronic model (NJL model in our case), whereas the QCD scale means the evolution scale matching between model scale and the experimental scale. In hadronic model the quark distribution is not a function of Q^2 , whereas in QCD the quark distribution function depends logarithmically on Q^2. Therefore the scaling of perturbative QCD are performed through the QCD evolution which is called DGLAP. From now on, we just called the QCD evolution as DGLAP evolution.

In this thesis, the initial scale of the NJL model for parton distribution function is chosen to be, Q_0^2= 0.16 GeV^2. This initial model is expected to be good choice in describing quark distribution in QCD (high energy). Several previous calculations have used this initial scale in the NJL model [48, 56, 140–142]. One important constraint is that the momentum sum rule of the valence quark at the initial model scale, Q_0, must be equal to unity, whereas others are zero. For example the gluon and sea quark momentum sum rule equal to zero. The mathematical expression of momentum sum rule for the valence quark, gluon and sea quark, respectively, can be written as

$$\langle x\rangle_V(Q^2) = \int dx x f(x,Q^2) = 1, \tag{2.11.1}$$

$$\langle x\rangle_g(Q_0^2) = 0, \tag{2.11.2}$$

$$\langle x\rangle_S(Q_0^2) = 0, \tag{2.11.3}$$

here Q^2 denotes the four transfer momentum, $f(x,Q^2)$ is the quark distribution as a function of longitudinal momentum and four transfer momentum. In the DGLAP evolution the valence quark distribution can be evolved to LO, to next leading order (NLO) and next-next leading order (NNLO). These depend on order of the running coupling constant, α_S (Q^2).

In general the quark distributions in the hadrons are classified into three types in DGLAP evolution; the gluon distribution, quark distribution and the sea quark distribution. The quark distribution, which is well known as the valence quark distribution is called as the non-singlet quark distribution. The non-singlet quark distribution is defined as the quark distribution minus the antiquark distribution which can be expressed by

$$q_v(x) = q(x) - \bar{q}(x), \tag{2.11.4}$$

where q_v (x) denotes the valence quark distribution as a function of longitudinal momentum, q (x) is a quark distribution and $\bar{q}$ (x) is an antiquark distribution.

The evolution of the non-singlet quark distribution in DGLAP are defined by

$$\frac{\partial q_{NS}(x,Q^2)}{\partial \ln(Q^2)} = \mathcal{P}_{qq}(x,\alpha_S(Q^2)) \otimes q_{NS}(x,Q^2), \tag{2.11.5}$$

where $\mathcal{P}_{qq}$ denotes the splitting of the q-q (quark-quark) function. The physics interpretation of $\mathcal{P}_{qq}$ is the probability for a quark of type q with momentum fraction z to emit quark and becomes a quark of new type q with momentum fraction x. The $\mathcal{P}_{qq} \otimes q_{NS}$ means the convolution product between splitting function and the non-singlet quark distributions. This has a from

$$\mathcal{P}_{qq} \otimes q_{NS} = \int_x^1 \frac{dz}{x} \mathcal{P}\left(\frac{x}{z}\right) q_{NS}. \tag{2.11.6}$$

The non-singlet quark distribution in DGLAP can be written as

$$\frac{\partial}{\partial \ln Q^2} \int_0^1 dx q_{NS}(x, Q^2) = 0. \tag{2.11.7}$$

The other type of quark distribution is called a singlet quark distribution under DGLAP evolution. It is defined by

$$q_s(x) = \sum_i q_i^+ = \sum_i q_i(x) + \bar{q}_i(x), \tag{2.11.8}$$

where i denotes quark flavor. Commonly these quark distributions appear in hadrons which have structure functions of F_1, F_2 and g_1, respectively. The singlet quark distribution in DGLAP are expressed by

$$\frac{\partial}{\partial \ln Q^2} \begin{pmatrix} q_s(x, Q^2) \\ g(x, Q^2) \end{pmatrix} = \begin{pmatrix} \mathcal{P}_{qq} & \mathcal{P}_{qg} \\ \mathcal{P}_{gq} & \mathcal{P}_{gg} \end{pmatrix} \otimes \begin{pmatrix} q_s(x, Q^2) \\ g(x, Q^2) \end{pmatrix}, \tag{2.11.9}$$

In analogy to Taylor expansion series, the splitting functions can also be expanded on the running coupling constant, α_S (Q^2) in perturbative QCD region, it then takes a form

$$\mathcal{P}(z, Q^2) = \left(\frac{\alpha}{2\pi}\right) \mathcal{P}^{(0)}(z) + \left(\frac{\alpha}{2\pi}\right)^2 \mathcal{P}^{(1)}(z) + \left(\frac{\alpha}{2\pi}\right)^3 \mathcal{P}^{(2)}(z) + ..., \tag{2.11.10}$$

where the first term in $\mathcal{P}^{(0)}(z)$ is the LO, the second term in $\mathcal{P}^{(1)}(z)$ denotes the NLO and the last term in $\mathcal{P}^{(2)}(z)$ is the NNL0. However in this thesis we limit our interest only for LO [143–145] and NLO [146, 147]. Therefore, for the readers interested in NNLO, we refer to Refs [148–150]. On the other hand, the Feynman diagrams contribute to LO are depicted in Fig 2.11.1.

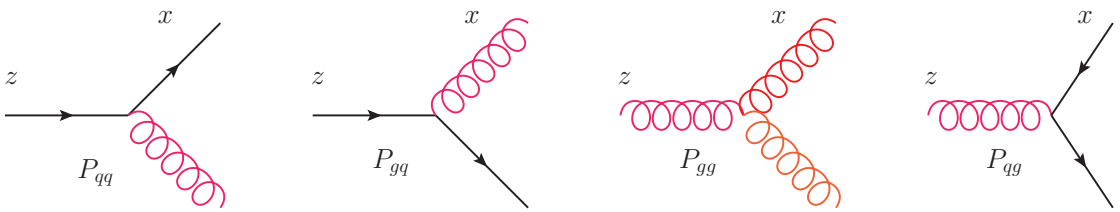

Figure 2.11.1: All diagrams contributions to LO splitting function in the kernel of QCD evolution. $P_{p'p}$ pose the probability for a parton of type p with momentum fraction z to emit particle quark or gluon and being a parton of type p' with momentum fraction x.

The NLO is very important for yielding consistent solution of the DGLAP equation. The NLO result is expressed by

$$\alpha_s = \frac{4\pi}{\beta_0}\frac{1}{\ln(Q_\Lambda)}\left[1 - \frac{\beta_1}{\beta_0}\frac{\ln\ln(Q_\Lambda)}{\ln(Q_\Lambda)} + \mathcal{O}\left(\frac{1}{\ln^2(Q_\Lambda)}\right)\right], \tag{2.11.11}$$

with

$$Q_\Lambda = \frac{Q^2}{\Lambda^2_{QCD}}, \qquad \beta_0 = \frac{11}{3}N_C - \frac{4}{3}T_f, \qquad \beta_1 = \frac{34}{3}N_C^2 - \frac{10}{3}N_C N_F - 2C_F N_F. \tag{2.11.12}$$

here N_C denotes the number of colors, N_F is the number of active flavors and $C_F = \frac{4}{3}$. The value of Λ_{QCD} depends on the number of active flavors and the renormalization scheme, in the $\overline{MS}$, the value of $\Lambda_{QCD}^{N_F=3,4,5,6} = (0.248, 0.200, 0.131, 0.050)$ GeV [149].

2.12 Summary

In this chapter a brief overview of QCD and its properties such as asymptotic freedom, color confinement, chiral symmetry and the spontaneous chiral symmetry breaking, have already been introduced starting from the Lagrangian of QCD, both perturbative QCD and nonperturbative QCD. The latter properties of the QCD is very important to help us to build an *inspired model* like NJL model in our studies, which will discuss later in Chapter 3. Later on we demonstrated how to obtain a GMOR in QCD.

In addition, we have demonstrated that in high energy region perturbative QCD approach is very powerful method to link elementary quantities and physical quantities through a factorization theorem in order to be able to interpret the theoretical result and experimental data via DIS. In factorization theorem, the differential cross section is factorized based upon all orders of the running coupling constants, $\alpha_S(Q^2)$.

Finally, the quark parton model, DIS, factorization theorem, and QCD evolution has been presented. Moreover, we have also demonstrated how to derive the valence quark distribution of the composite particle and how to evolve the valence quark distribution using DGLAP evolution. In DGLAP evolution, the model scale comes from the hadronic model, whereas the QCD scale means the evolution scale matching between model scale and the experimental data. Note that the intial scale of the NJL model for parton distribution function is chosen to be $Q_0^2 = 0.16$ GeV^2.

3
Nambu-Jona-Lasinio Model

The NJL model was proposed by Yoichiro Nambu [1] and Giovanni Jona-Lasinio in 1961 [151, 152], in the pre QCD era, to model the nucleon-nucleon interaction. Later on, it was used to describe the quark-quark interaction [32, 34–38] [2]. Historically, in fact, this model was inspired by the BCS theory of superconductivity [153], which was used to compute the energy gap in the excitation spectrum of the electron.

With this interaction, we show how the NJL model can be used to describe the kaon and pion in terms of quark degrees of freedom. To describe the bound state of the two body interaction like a kaon, we use the Bethe-Salpeter equation. The NJL model shares the same global symmetry properties as QCD, such as DCSB and its Lagrangian has been constructed satisfying the basic symmetries of QCD. From this Lagrangian, the EOM will be derived through the Euler-Lagrangian equation. However, it is not a gauge theory model, which does not include the gauge bosons (gluons) and cannot describe confinement. The NJL model exhibits spontaneous chiral symmetry breaking in vacuum because of the attractive interaction in the quark-antiquark channel. The DCSB gives rise to dynamically generated dressed quark masses. The NJL model has a long story of remarkable success in the study hadron properties [30–44, 47–57, 154–157].

In this chapter, we give a brief introduction to the NJL model, including the Lagrangian, dynamical quark mass and gap equation, proper time regularization scheme and the Bethe-Salpeter equation (BSE), yielding a bound state of the quark-antiquark pair in the kaon used in this work.

[1] Yoichiro Nambu just passed away on July 5, 2015, while the author was writing this thesis.

[2] The fermionic field is used to describe interaction between the quarks in the effective Lagrangian, which is simplified to be a four-point (contact) interaction.

3.1 The Lagrangian of NJL model

As already mentioned in Section 2.1, the non-renormalized QCD Lagrangian can be written as

$$\mathcal{L}_{\rm QCD} = \bar{\psi}\left(i\not{D} - m_q\right)\psi - \frac{1}{4}\mathcal{F}^a_{\mu\nu}\mathcal{F}^{\mu\nu}_a, \tag{3.1.1}$$

with $\not{D}$ denotes the covariant derivative, m_q is the quark mass matrix ($q = u, d, s, \cdots$) and $\mathcal{F}^a_{\mu\nu}$ is the gluon field strength tensor. ψ and $\bar{\psi} = \psi^\dagger\gamma_0$ denote the initial and final quark fields. The QCD Lagrangian in Eq. (3.1.1) satisfies the fundamental QCD symmetries, that is

$$\mathcal{S}_{\rm QCD} = SU(N_F)_{\rm L} \otimes SU(N_F)_{\rm R} \otimes SU(N_C) \otimes U(1)_{\rm V} \otimes \mathcal{F}, \tag{3.1.2}$$

with the number of flavors and colors are denoted by N_F and N_C, respectively, The chiral group $SU(N_F)_{\rm L} \otimes SU(N_F)_{\rm R}$ poses a chiral symmetry [3] ($m_u \sim m_d \sim m_s = m_q \to 0$, for 3-flavors case), $U(1)_{\rm V}$ is the symmetry of baryon number, $SU(N_c)$ is the color gauge symmetry. The $\mathcal{F}$ is the set of discrete symmetries charge (C), parity (P) and time (T), respectively [154]. The local non-Abelian $SU(N_C)$ color determines the quark-gluon and the gluon-gluon couplings.

The NJL model is an chiral effective theory that mimics many of the key features of QCD in Eq. (3.1.2) and is therefore a useful tool to help understand non-perturbative phenomena in low energy. The NJL model has a chirally invariant four-fermion interaction. This indicates that the NJL model involves only quark degrees of freedom and the gluon degrees of freedom have been absorbed into effective coupling constant, G_π, where G_π is dimensionful with dimension $[\text{mass}]^{-2}$. The model is then an effective non-renomalizable theory. For simplicity, we focus only on the case of the three flavor NJL model. Extension to larger number of flavors can be done straightforwardly. Implementing the symmetry group in Eq. (3.1.2), the Lagrangian density of the three flavor NJL model can be compactly written as

$$\mathcal{L}_{\rm NJL} = \bar{\psi}\left(i\partial\!\!\!/ - m_q\right)\psi + \mathcal{L}_{\rm four-fermion} + \mathcal{L}_{\rm six-fermion}, \tag{3.1.3}$$

where $\psi = (u, d, s)$ for $N_F = 3$ denotes the light quark fields, $m_q = diag(m_u, m_d, m_s)$ is the current quark mass matrix. The quark-quark interactions consist of the four-fermion interaction, $\mathcal{L}_{\rm four-fermion}$ and the six-fermion interaction, $\mathcal{L}_{\rm six-fermion}$. The four-fermion interaction contains the features of the dynamical chiral symmetry breaking and the six-fermion interaction is introduced to break the axial $U(1)$ symmetry in the $SU(3)_F$ NJL model. Note that the NJL Lagrangian in Eq. 3.1.3 does not allow for anomolous magnetic coupling, since the Fierz transforms of the two four-fermion terms give the same contribution to $\sigma^{\mu\nu}\sigma_{\mu\nu}$ up to sign [155–157].

The effective four-fermion interaction,$\mathcal{L}_{\rm four-fermion}$ in Eq. (3.1.3), has the form,

$$\mathcal{L}_{\rm four-fermion} = G\sum_{a=0}^{8}\left[\left(\bar{\psi}\lambda^a\psi\right)^2 + \left(\bar{\psi}\gamma_5\lambda^a\psi\right)\right], \tag{3.1.4}$$

[3] $SU(N_F)_L \otimes SU(N_F)_R$ is broken down to $SU(N_F)_{\rm V} \otimes SU(N_F)_{\rm A}$ with the appearance of $N_F^2 - 1$ Goldstone bosons, where A and V denote axial and vector. For the three flavor case, the light pseudoscalar mesons, π, K and η emerge.

where λ^a denotes the Gell-Mann matrices in the isospin space and γ_5 is the Dirac matrix. The first term is the scalar interaction and the second term denotes the pseudoscalar interaction. This term is invariant under $U(3)$ and responsible for the dynamical chiral symmetry breaking (DCSB) and thence the generation of quark masses.

The 't Hooft determinant [158], $\mathcal{L}_{\rm six-fermion}$, in Eq. (3.1.3) can be written as

$$\mathcal{L}_{\rm six-fermion} = -K\{\det{}_{\rm f}\left[\bar{\psi}(1+\gamma_5)\psi\right] + \det{}_{\rm f}\left[\bar{\psi}(1-\gamma_5)\psi\right]\}, \tag{3.1.5}$$

where determinant $\det_{\rm f}$ has to be taken in flavor space, K [4] denotes the effective coupling. The six-fermion interaction was first time suggested by Kobayashi and Maskawa to explain the $\eta - \eta'$ mass splitting. In the same time, 't Hooft used the six-fermion interaction to describe the instanton interaction. Since then the six-fermion interaction is called as Kobayashi-Maskawa-'t Hooft interaction. This interaction is signed by three incoming fields and three outcoming fields, i.e. $(u\bar{u})$, $(d\bar{d})$, $(s\bar{s})$ or (ud), $(\bar{u}\bar{d})$, $(s\bar{s})$. In addition, the six-fermion interaction has been used in the NJL model to study hadron physics connecting to the η' mass problem [38, 39].

After a Fierz transformation (see Appendix A.5), the Lagrangian density of the NJL model for three flavors in Eq. (3.1.3) – containing just four-fermion interactions– takes the form [5] [159]

$$\begin{aligned}\mathcal{L}_{\rm NJL} &= \bar{\psi}(i\partial\!\!\!/ - \hat{m})\psi \\ &\quad + G_\pi\left[(\bar{\psi}\,\lambda_a\,\psi)^2 - (\bar{\psi}\,\lambda_a\,\gamma_5\,\psi)^2\right] \\ &\quad - G_\rho\left[(\bar{\psi}\,\lambda_a\,\gamma^\mu\,\psi)^2 + (\bar{\psi}\,\lambda_a\,\gamma^\mu\gamma_5\,\psi)^2\right],\end{aligned} \tag{3.1.6}$$

where the quark field has the flavour components $\psi = (u, d, s)$, $\hat{m} = \mathrm{diag}(m, m, m_s)$ denotes the current quark mass matrix, and G_π, G_ρ are four-fermion coupling constants. A sum over $a = 0, \ldots, 8$ is implied in Eq. (3.1.6), where $\lambda_1, \ldots, \lambda_8$ are the Gell-Mann matrices in flavor space and $\lambda_0 \equiv \sqrt{\frac{2}{3}}\,\mathbb{1}$.

3.2 Dynamical Mass and Gap Equation

In this section we briefly present the vacuum properties of quarks and the kaon and pion described in the NJL model. The gap equation describes the interaction of the particle with the vacuum. It is generated by following the quark self-energy [6] expression, corresponding to the Feynman diagram in Fig. 3.2.1. The standard NJL gap equation, illustrated in Fig. 3.2.1, provides the dressed quark propagator. The general solution of this gap equation has the form

$$M_q = m_q - 2G_\pi\langle\bar{\psi}\psi\rangle, \tag{3.2.1}$$

[4] The effective coupling, K, has dimension $[\text{mass}]^{4-3N_F}$

[5] In principle the flavor singlet and octet pieces of the G_v term in Eq. (3.1.6) can appear in the NJL interaction Lagrangian with separate coupling constants, as they are individually chirally symmetric. Our choice of identical coupling constants avoids flavor mixing, giving the flavour content of the ω meson as $u\bar{u} + d\bar{d}$ and the ϕ meson as $s\bar{s}$.

[6] The quark self-energy, arises from the quark-antiquark interaction term, is calculated by means of Hartree or Hartree-Fock approximation. It shifts the the constituent quark mass with a constant value if the self-energy has a local properties.

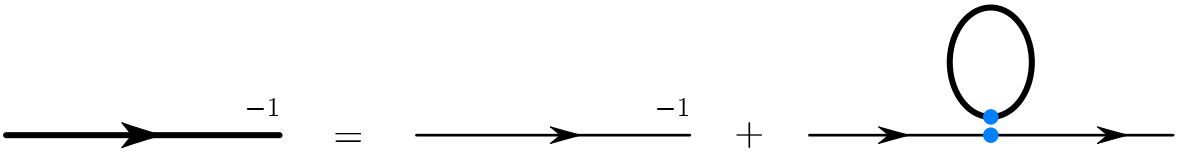

Figure 3.2.1: The NJL gap equation in the Hartree–Fock approximation. The thin line is bare quark propagator, $S_0^{-1}(k) = \not{k} - m + i\epsilon$, whereas the thick line is the dressed Euclidean quark propagator, $S_q(k)$. The shaded circle is the $q\bar{q}$ interaction kernel is given by Eq. (3.4.2).

where M denotes the dynamical (constituent) mass, m_q is the current quark mass in the NJL Lagrangian. The Tr is to be taken in Dirac, color and flavor spaces. G_π [7] is the effective coupling in the scalar channel. Using the mean field (Hartree) approximation (MFA), the two-quark condensate is generally defined as

$$\langle\bar{\psi}\psi\rangle = -\int \frac{d^4k}{(2\pi)^4}\mathrm{Tr}\left[\mathrm{S_q(k)}\right], \tag{3.2.2}$$

where $S_q(k)$ is the dressed quark propagator at momentum space in the NJL model obtained from the gap equation provided in Fig 3.2.1. The solution for a quark of flavor $q = u, d, s$ take the form

$$S_q(k) = \frac{\not{k} + M_q}{k^2 + M_q^2 + i\epsilon}, \tag{3.2.3}$$

where M_q denotes the dressed (constituent) quark mass.

Putting the quark condensate formula in Eq. (3.2.2) into the gap equation in Eq. (3.2.1) and evaluating it using proper-time regularization scheme, it then gives

$$\begin{aligned} M_q &= m_q - 2G_\pi\langle\bar{\psi}\psi\rangle \\ &= m_q + \frac{3M_qG_\pi}{\pi^2}\int_{\frac{1}{(\Lambda_{\mathrm{UV}})^2}}^{\frac{1}{(\Lambda_{\mathrm{IR}})^2}} \frac{d\tau}{\tau^2}e^{-\tau(M_q^2)}, \end{aligned} \tag{3.2.4}$$

where the quark condensate [8] in Eq. (3.2.2) becomes,

$$\langle\bar{\psi}\psi\rangle = -\frac{3M_q}{2\pi^2}\int_{\frac{1}{(\Lambda_{\mathrm{UV}})^2}}^{\frac{1}{(\Lambda_{\mathrm{IR}})^2}} \frac{d\tau}{\tau^2}e^{-\tau(M_q^2)}. \tag{3.2.5}$$

Clearly Eq. (3.2.4) shows that there is a trivial solution when $G_\pi = 0$ [9], but a non-perturbative solution also exists at large G_π. By setting $m_q \sim 0$ (chiral limit), the Lagrangian respects the chiral symmetry $SU(3)_{\mathrm{L}} \otimes SU(3)_{\mathrm{R}}$ and it produces a gap of $\Delta E = 2M_q$ in the spectrum of quark [39]. In the chiral limit, the constituent quark mass has non-trivial solution where $M \neq 0$ provided $G_\pi > G_{\mathrm{critical}}$. This is clearly shown in Fig. 3.2.2. This corresponds to DCSB and the Nambu-Goldstone phase [10].

[7] The effective coupling, G_π, is the same in different phases and temperature and quark chemical potential independent.

[8] From Eq. (3.2.4), the quark condensate can be also written as $\langle\bar{\psi}\psi\rangle = -\dfrac{M_q - m_q}{2G_\pi}$.

[9] One finds that $m_\pi = 0$ when $m_q = 0$. This corresponds with the Goldstone theorem.

[10] The Nambu-Goldstone phase occurs when the chiral symmetry has been dynamically broken.

In addition, when $m_q = 0$, the critical coupling has a form,

$$G_{\text{critical}} = \frac{\pi^2}{3(\Lambda_{\text{UV}}^2 - \Lambda_{\text{IR}}^2)}, \tag{3.2.6}$$

with Λ_{UV} and Λ_{IR} denote ultraviolet and infrared cutoffs, respectively. From Eq. (3.2.1), we also see clearly that when $M \neq m_q$ then $\langle\bar{\psi}\psi\rangle \neq 0$. This indicates that the dynamical mass generation is also associated with the generation of a non-zero chiral condensate.

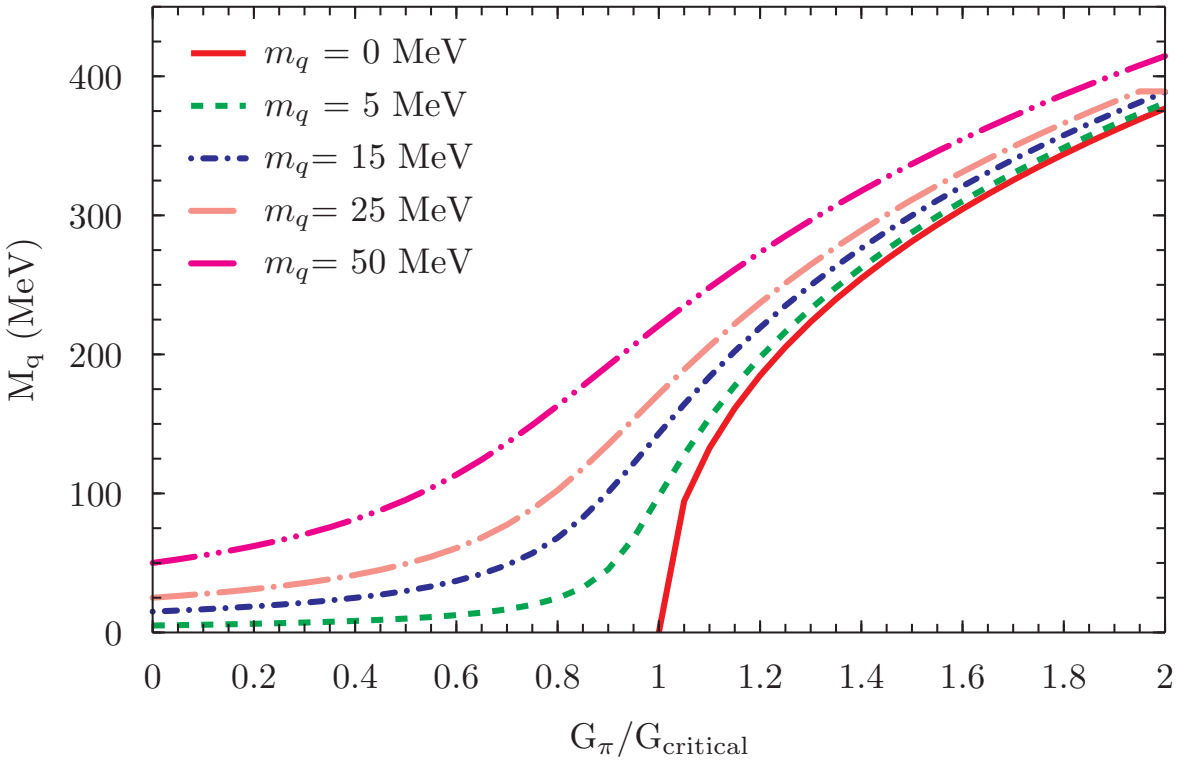

Figure 3.2.2: Dynamical quark mass generation (M_q) as a function of $\frac{G_\pi}{G_{\text{critical}}}$. The dynamical quark mass was computed using the NJL model with the ultraviolet cut-off $\Lambda_{\text{UV}} = 0.645$ GeV and infra-red cut-off, $\Lambda_{\text{IR}} = 0.240$ GeV. A full parameter set used can be found in Section 4.3.

Figure. 3.2.2 also shows that, in the chiral limit, the chiral condensate are zero ($\langle\bar{\psi}\psi\rangle = 0$) when $G_\pi < G_{\text{critical}}$. This is known as the Wigner-Weyl phase. As explained in Chapter 2, chiral symmetry and its dynamical breaking play a key role in low energy QCD. We have demonstrated that the NJL model provides a clear mechanism for the chiral symmetry breaking.

3.3 Proper-Time Regularization Scheme

As mentioned earlier, the NJL model is non-renormalizable and not confining. Hence some regularization procedure must be used to avoid divergences. There are several possible regularization schemes available in the market for solving the divergent problem.

They are Euclidean-4 momentum [52], Pauli-Villars regularization [71] and recently a Gaussian in Euclidean space. In this thesis, we choose to employ the PTR [23–25, 30–32, 34–38, 41, 43, 44, 47–57, 78, 159, 160] by taking the ultraviolet (UV) and infrared (IR) cutoffs into account. The ultraviolet cutoff is very important to obtain finite solutions. This PTR is chosen to regulate the divergences arising from loop integrals in order to obtain finite values of the physical quantities via ultraviolet cutoff. Additionally, PTR is especially interesting because if one also introduces an infra-red cut-off, Λ_{IR}, it simulates quark confinement by eliminating on-shell quark propagation, while respecting chiral symmetry. As a result it has been widely used. The PTR scheme is formally expressed by

$$\begin{aligned}\frac{1}{X^{\mathrm{n}}} &= \frac{1}{(\mathrm{n}-1)!}\int_0^\infty d\tau\tau^{\mathrm{n}-1}e^{-\tau X} \\ &\to \frac{1}{(\mathrm{n}-1)!}\int_{\frac{1}{(\Lambda_{\mathrm{UV}})^2}}^{\frac{1}{(\Lambda_{\mathrm{IR}})^2}} d\tau\tau^{\mathrm{n}-1}e^{-\tau X},\end{aligned} \tag{3.3.1}$$

here X^{n} denotes an energy denominator obtained after introducing Feynman parameters and performing a Wick rotation to rotate the loop integral to Euclidean space. This is a function of quark momentum. Technically we only need an ultraviolet cutoff, Λ_{UV}, to render the theory finite. However, in quark bound states we also include the infrared cutoff, Λ_{IR}, which has the effect of eliminating nonphysical quark thresholds for the decay of hadrons into free quarks. In this work, we choose $\Lambda_{\mathrm{IR}} = 0.240$ GeV [48, 159] as an input parameter. This must be chosen to reflect the confinement scale of QCD. [11] Notice that none of the results found here are especially sensitive to this choice.

3.4 Bethe-Salpeter Equation for Mesons

As mentioned in Section 2.3 that quarks and gluons are confined within hadrons, therefore we should deal with the bound states theory [12]. In the past, several studies have been made to calculate the bound state of composite particles [21, 22, 161–164]. At that time, the energy level of the bound state systems of two particles was calculated via a quantized field. Thus, the result would be used as an input to Schrodinger equation or Dirac equation. However this method has treated in non-relativistic region (atom level). Therefore, it faces a difficulty of a relativistic interactions and singular forces. To overcome this problem, Dancoff [165] has been proposed a method using a field theory to solve a Schrodinger equation for one field. However, this method has a problem once we want to include higher approximations. Later on, Bethe and Salpeter [161, 164] proposed a two body wave function equation in the covariant form. Therefore, this equation is free from divergences as in the S-matrix theory. This method is well known as the BSE. In the BSE, the Feynman two body kernel of the scattering

[11] The confinement scale in QCD is of the order of $\Lambda_{QCD} \sim 0.300$GeV.

[12] Bound states emerge as poles in n point Green's functions. In our case, mesons poses the poles in the 4-point Green functions, $\langle 0 \mid q_1 q_1 \bar{q}_2 \bar{q}_2 \mid 0 \rangle$.

can be re-written as an integral equation [159, 161, 164]. For the aim of this thesis, we treat a meson as a bound state via BSE in the NJL framework.

In the NJL model, a meson is described as a quark-antiquark bound state with the meson properties determined by the BSE [159, 161, 164]. In the BSE, the quark-antiquark interaction in the bound state is summed to all orders corresponding to an infinite series of ladder diagram and it becomes an infinite series of bubble graphs in the NJL model. The mesons considered here – π, K, ρ and ω – are realized in the NJL model as quark–antiquark bound states whose properties are governed by the BSE. The interaction between the quark-antiquark pair in the BSE is illustrated in Fig. 3.4.1

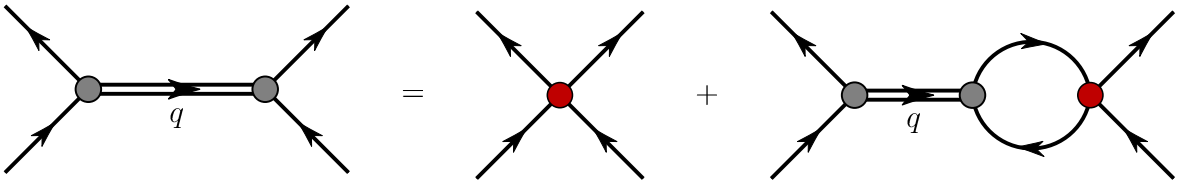

Figure 3.4.1: Illustration of the BSE describing the interaction between a quark-antiquark pair in bound state.

The scattering amplitude T of the quark-antiquark interaction is then expressed as

$$T(q) = \mathcal{K} + \int \frac{d^4k}{(2\pi)^4} \mathcal{K}\mathcal{S}(k+q)T(q)\mathcal{S}(k), \tag{3.4.1}$$

where q is the total momentum of the two body system, $\mathcal{K}$ is the quark-antiquark interaction kernel and the indices denote Dirac, isospin and color degrees of freedom. $T(q)$ is the 4-point quark-antiquark scattering amplitude and $\mathcal{S}(k+q)$ stands for a two body dressed propagator.

The elementary quark-antiquark interaction kernel, $\mathcal{K}$ derived from Eq. (3.4.1), can be formally take the form

$$\begin{aligned}\mathcal{K}_{\alpha\beta,\gamma\delta} &= \sum_{\Omega} \mathcal{K}_{\Omega}\, \Omega_{\gamma\delta}\, \bar{\Omega}_{\alpha\beta} \\ &= 2i\, G_\pi \left[(\lambda_a)_{\gamma\delta}\, (\lambda_a)_{\alpha\beta} + (\lambda_a\gamma_5)_{\gamma\delta}\, (\lambda_a\gamma_5)_{\alpha\beta}\right] \\ &- 2i\, G_\rho \left[(\lambda_a\gamma^\mu)_{\gamma\delta}\, (\lambda_a\, \gamma_\mu)_{\alpha\beta} + (\lambda_a\, \gamma^\mu\gamma_5)_{\gamma\delta}\, (\lambda_a\gamma_\mu\gamma_5)_{\alpha\beta}\right], \end{aligned} \tag{3.4.2}$$

where the indices represent Dirac, colour and isospin. Note, in this work we assume that $m_u = m_d = m$, and with the Lagrangian of Eq. (3.1.6) the ρ and ω mesons are mass degenerate, differing only in their flavour structure. The kernel is constructed based on the three flavor NJL Lagrangian in Eq. (3.1.6) and the definitions of the variables used here are the same with the variable in Lagrangian. The BSE solutions for the pion, kaon, ρ, ω and ϕ are, respectively, given by

$$T_\pi(q)_{\alpha\beta,\gamma\delta} = [\gamma_5 T_i]_{\alpha\beta}\, t_\pi(q)\, [\gamma_5 T_j]_{\gamma\delta}\,, \tag{3.4.3}$$

$$T_{\rm K}(q)_{\alpha\beta,\gamma\delta} = [\gamma_5 T_i]_{\alpha\beta}\, t_K(q)\, [\gamma_5 T_j]_{\gamma\delta}\,, \tag{3.4.4}$$

$$T_\rho(q)_{\alpha\beta,\gamma\delta} = [\gamma_\mu T_i]_{\alpha\beta}\, t_\rho^{\mu\nu}(q)\, [\gamma_\nu T_j]_{\gamma\delta}\,, \tag{3.4.5}$$

$$T_\omega(q)_{\alpha\beta,\gamma\delta} = [\gamma_\mu T_i]_{\alpha\beta}\, t_\omega^{\mu\nu}(q)\, [\gamma_\nu T_j]_{\gamma\delta}\,, \tag{3.4.6}$$

$$T_\phi(q)_{\alpha\beta,\gamma\delta} = [\gamma_\mu T_i]_{\alpha\beta}\, t_\omega^{\mu\nu}(q)\, [\gamma_\nu T_j]_{\gamma\delta}\,, \tag{3.4.7}$$

where T_i and $T_j = \lambda_3$ for the π^0 and $T_i = \frac{1}{\sqrt{2}}(\lambda_1 \pm i\lambda_2)$ and $T_j = \frac{1}{\sqrt{2}}(\lambda_1 \mp i\lambda_2)$ for creating a π^+ or π^-. Then the $K^\pm$ require $T_i = \frac{1}{\sqrt{2}}(\lambda_4 \pm i\lambda_5)$ and $T_j = \frac{1}{\sqrt{2}}(\lambda_4 \mp i\lambda_5)$. The reduced t- matrices, t_π, t_K, $t_\rho^{\mu\nu}$ and $t_\omega^{\mu\nu}$, in these channels take the form

$$t_\pi(q) = \frac{-2iG_\pi}{1 + 2G_\pi \Pi_\pi(q^2)}, \tag{3.4.8}$$

$$t_{\rm K}(q) = \frac{-2iG_\pi}{1 + 2G_\pi \Pi_{\rm K}(q^2)}, \tag{3.4.9}$$

$$t_\rho^{\mu\nu}(q) = \frac{-2iG_\rho}{1 + 2G_\rho \Pi_{vv}(q^2)} \left(g^{\mu\nu} + 2G_\rho \Pi_{vv}(q^2) \frac{q^\mu q^\nu}{q^2} \right), \tag{3.4.10}$$

$$t_\omega^{\mu\nu}(q) = \frac{-2iG_\omega}{1 + 2G_\omega \Pi_{vv}(q^2)} \left(g^{\mu\nu} + 2G_\omega \Pi_{vv}(q^2) \frac{q^\mu q^\nu}{q^2} \right), \tag{3.4.11}$$

$$t_\phi^{\mu\nu}(q) = \frac{-2iG_\phi}{1 + 2G_\phi \Pi_{vv}(q^2)} \left(g^{\mu\nu} + 2G_\phi \Pi_{vv}(q^2) \frac{q^\mu q^\nu}{q^2} \right), \tag{3.4.12}$$

where the bubble diagrams appearing for the pion, $\Pi_\pi(q^2)$, kaon, $\Pi_{\rm K}(q^2)$, ρ and ω as well as ϕ, $\Pi_{vv}(q^2)$ read:

$$\Pi_\pi(q^2)\delta_{ij} = 2iN_C \int \frac{d^4k}{(2\pi)^4} Tr_D \left[\gamma_5 T_i S_l(k) \gamma_5 T_j S_l(k+q)\right], \tag{3.4.13}$$

$$\Pi_{\rm K}(q^2)\delta_{ij} = 2iN_C \int \frac{d^4k}{(2\pi)^4} Tr_D \left[\gamma_5 T_i S_l(k) \gamma_5 T_j S_s(k+q)\right], \tag{3.4.14}$$

$$\Pi_{vv}^{ab}(q^2) \left(g^{\mu\nu} - \frac{q^\mu q^\nu}{q^2} \right) = 2iN_C \int \frac{d^4k}{(2\pi)^4} Tr_D \left[\gamma^\mu S_a(k) \gamma^\nu S_b(k+q)\right], \tag{3.4.15}$$

where $\Pi_\rho = \Pi_\omega = \Pi_{vv}^{ll}$ and $\Pi_\phi = \Pi_{vv}^{ss}$ and the trace is over Dirac indices only. The subscripts l and s denote the flavor indices for the light and strange quarks, respectively. The polarization insertion (bubble graph) Feynman diagram is illustrated in Fig. 3.4.2.

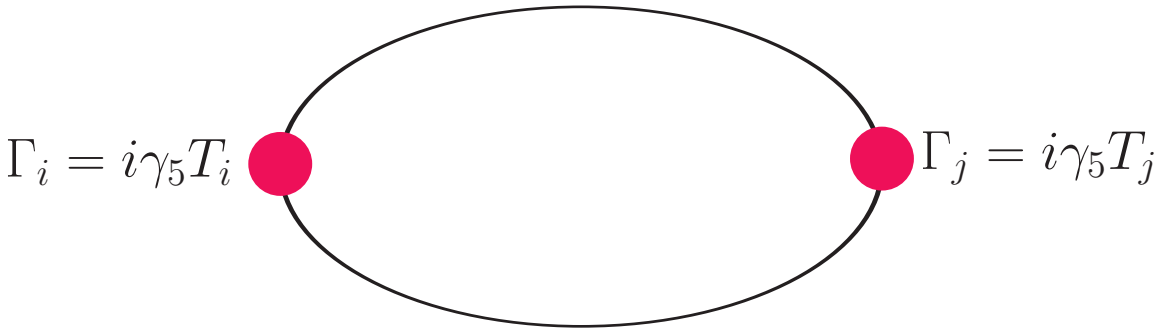

Figure 3.4.2: The diagrammatic representation of the polarization insertion (bubble graph) in the pseudoscalar channel.

Thus the bubble graph of the pion, kaon and vector meson, respectively, in Eq. (3.4.13) in the proper-time regularization scheme can be read as

$$\Pi_\pi(q^2) = -\frac{N_C N_F}{4\pi^2}\int_{\frac{1}{(\Lambda_{\rm UV})^2}}^{\frac{1}{(\Lambda_{\rm UV})^2}} \frac{d\tau}{\tau^2} e^{-\tau M^2} - \frac{N_C N_F k^2}{8\pi^2}\int_0^1 dx \int_{\frac{1}{(\Lambda_{\rm UV})^2}}^{\frac{1}{(\Lambda_{\rm UV})^2}} \frac{d\tau}{\tau} e^{-\tau(k^2(x^2-x)+M^2)}, \tag{3.4.16}$$

$$\Pi_{\rm K}(q^2) = -\frac{N_C}{2\pi^2}\int_0^1 dx \int_{\frac{1}{(\Lambda_{\rm UV})^2}}^{\frac{1}{(\Lambda_{\rm UV})^2}} \frac{d\tau}{\tau^2} e^{-\tau k^2(x^2-x)+xM_2^2-(x-1)M_1^2} \times \left[1+\tau\left[2k^2(x-x^2)-xM_2+(x-1)M_1+M_2M_1\right]\right], \tag{3.4.17}$$

$$\Pi_{\rm vv}(q^2) = -\frac{N_C q^2}{\pi^2}\int_0^1 dx \int_{\frac{1}{(\Lambda_{\rm UV})^2}}^{\frac{1}{(\Lambda_{\rm UV})^2}} \frac{d\tau}{\tau} e^{-\tau(q^2(x^2-x)+M^2)}\left[x(1-x)\right], \tag{3.4.18}$$

where N_F, N_C, $\Lambda_{\rm UV}$ and $\Lambda_{\rm IR}$ denote the number of flavor, number of color, UV cut-off and IR cut-off, respectively and $q^2 = -Q^2$.

3.5 Meson Properties in the NJL model

In this section we present meson properties in the NJL model. They are pseudoscalar meson quark-antiquark coupling, pseudoscalar meson masses, pseudoscalar meson decay constant and GMOR relation for kaon and pion in the NJL model. A descriptions of each meson properties are delivered in the section below.

3.5.1 Meson Quark-Antiquark Coupling

The momentum derivative of the pseudoscalar bubble graph (polarization insertion) function in Eq. (3.4.13) yields a quark meson coupling constant, $g_{\pi\bar{q}q}$ for the pion and $g_{K\bar{q}q}$ for the kaon as well as other mesons. These are determined from the pole in the quark- antiquark T-matrix in Eq. (3.4.8). Further details of the derivation of the meson quark-antiquark coupling can be found in Appendix A.12. Comparing to the expansion result of the general form of the T-matrix near a bound state pole,

$$g^{-2}_{\pi\bar{\rm q}{\rm q}} = -\left(\frac{\partial\Pi_\pi(q^2)}{\partial q^2}\right)|_{q^2=m_\pi^2}, \tag{3.5.1}$$

$$g^{-2}_{{\rm K}\bar{\rm q}{\rm q}} = -\left(\frac{\partial\Pi_{\rm K}(q^2)}{\partial q^2}\right)|_{q^2=m_K^2}, \tag{3.5.2}$$

$$g^{-2}_{\rho,\omega\bar{\rm q}{\rm q}} = -\left(\frac{\partial\Pi_{vv}(q^2)}{\partial q^2}\right)|_{q^2=m_{\rho,\omega}^2}, \tag{3.5.3}$$

In the PTR scheme [13], the meson quark-antiquark coupling constant are obtained as

$$g^{-2}_{\pi\bar{q}q} = \frac{N_C N_F}{8\pi^2}\int_0^1 dx \int_{\frac{1}{(\Lambda_{\rm UV})^2}}^{\frac{1}{(\Lambda_{\rm UV})^2}} d\tau e^{-\tau(k^2(x^2-x)+M^2)}\left[\frac{1}{\tau}-k^2(x^2-x)\right], \tag{3.5.4}$$

[13] We apply a Feynman parameterization and Wick rotation before performing a PTR scheme.

$$g^{-2}_{K\bar{q}q} = \frac{N_C}{2\pi^2}\int_0^1 dx \int_{\frac{1}{(\Lambda_{\rm UV})^2}}^{\frac{1}{(\Lambda_{\rm UV})^2}} \frac{d\tau}{\tau} e^{-\tau(k^2(x^2-x)+xM_2^2-(x-1)M_1^2)} \times \left[3-\tau\left[2k^2(x-x^2)-xM_2^2+(x-1)M_1^2+M_1M_2\right]\right], \quad (3.5.5)$$

$$g^{-2}_{\rho,\omega\bar{q}q} = \frac{N_C}{2\pi^2}\int_0^1 dx \int_{\frac{1}{(\Lambda_{\rm UV})^2}}^{\frac{1}{(\Lambda_{\rm UV})^2}} d\tau x(1-x) e^{-\tau(M^2_{\rm vv}(x^2-x)+M^2)}\left[\frac{1}{\tau}-M^2_{\rm vv}(x^2-x)\right], \quad (3.5.6)$$

where $M_{\rm vv}$ stands for vector meson masses (ρ, ω, and ϕ). These meson quark-antiquark coupling constants are essential input for evaluating the form factor and parton distribution function and other observables in the next chapters.

3.5.2 Meson Masses

The meson masses are calculated from the pole in the t-matrix. From the Eq. (3.4.8) the masses of the pseudoscalar meson (π^+, K^+) and vector mesons (ρ, ω) are respectively given as

$$1+2G_\pi\Pi_\pi(k^2=m_\pi^2)=0, \quad (3.5.7)$$

$$1+2G_\pi\Pi_K(k^2=m_K^2)=0, \quad (3.5.8)$$

$$1+2G_\rho\Pi_{vv}(k^2=m_\rho^2)=0, \quad (3.5.9)$$

$$1+2G_\omega\Pi_{vv}(k^2=m_\omega^2)=0, \quad (3.5.10)$$

where m_π, m_K, m_ρ and m_ω are, respectively, the masses of the π, K, ρ and ω. By putting the bubble diagram in Eq (3.4.16) and the dressed quark masses in Eq. (3.2.4) (see Appendix A.11 and A.13), the kaon and pion masses are then expressed as

$$m^2_{\pi^+} = -\left[\frac{m}{M}\right]\frac{1}{8iG_\pi N_C \mathscr{I}^\pi_{21}(k^2)}, \quad (3.5.11)$$

$$m^2_{K^+} = -\left[\frac{m_s}{M_s}+\frac{m_u}{M_u}\right]\frac{1}{16iG_\pi N_C \mathscr{I}^K_{21}(k^2)} + (M_s-M_u)^2, \quad (3.5.12)$$

where m_{π^+} and m_{K^+} denote pion and kaon masses, respectively. The quantities $\mathscr{I}^\pi_{21}(k^2)$ and $\mathscr{I}^K_{21}(k^2)$ take the form

$$\mathscr{I}^\pi_{21}(k^2) = \int\frac{d^4p}{(2\pi)^4}\int_0^1 \frac{1}{[p^2+k^2(x-x^2)-xM_d^2+(x-1)M_u^2]^2}, \quad (3.5.13)$$

$$\mathscr{I}^K_{21}(k^2) = \int\frac{d^4p}{(2\pi)^4}\int_0^1 \frac{1}{[p^2+k^2(x-x^2)-xM_s^2+(x-1)M_u^2]^2}, \quad (3.5.14)$$

here M_u, M_s, and M_d are the constituent quark masses of the up, strange and down quarks, respectively. These expressions are obtained after we apply the Feynman parameterization for two propagators.

The final expression for $\mathscr{I}^\pi_{21}(k^2)$ and $\mathscr{I}^K_{21}(k^2)$ in Eq. (3.5.13), after performing the proper time regularization in Eq. (3.5.13), are obtained as

$$\mathscr{I}^\pi_{21}(k^2) = \frac{i}{16\pi^2}\int_0^1 dx \int_{\frac{1}{\Lambda^2_{\rm UV}}}^{\frac{1}{\Lambda^2_{\rm IR}}}\frac{d\tau}{\tau} e^{-\tau(k^2(x^2-x)+xM_d^2-(x-1)M_u^2)}, \quad (3.5.15)$$

$$\mathscr{I}_{21}^{K}(k^2) = \frac{i}{16\pi^2}\int_0^1 dx \int_{\frac{1}{\Lambda_{\rm UV}^2}}^{\frac{1}{\Lambda_{\rm IR}^2}} \frac{d\tau}{\tau} e^{-\tau(k^2(x^2-x)+xM_s^2-(x-1)M_u^2)}, \tag{3.5.16}$$

where $k^2 = m_\pi^2$ for the pion and $k^2 = m_K^2$ for the kaon. From Eq. (3.5.11) we see that the kaon and pion masses will vanish in the chiral limit, that is $m_q \to 0$, not $M \to 0$, where M is the constituent quark mass.

3.6 Meson Decay Constant

Beside the bubble graph and pion and kaon masses, other important observable, which can be measured in experiment is the pseudoscalar meson decay constants, $f_{\mathscr{M}}$, where $\mathscr{M}$ is the pseudoscalar meson (for the kaon and pion). Based on Feynman diagram in Fig. 3.6.1, the pseudoscalar meson decay constant can be defined through the matrix element,

$$\langle 0 \mid \bar{\psi}\gamma_\mu\gamma_5\frac{1}{2}\tau_a \mid \pi_b(q)\rangle = i f_{\mathscr{M}} q_\mu \delta_{ab}, \tag{3.6.1}$$

where the π_b denotes a pion with isospin b. In the NJL model, the pion decay constant f_π also can be illustrated in Fig. 3.6.1.

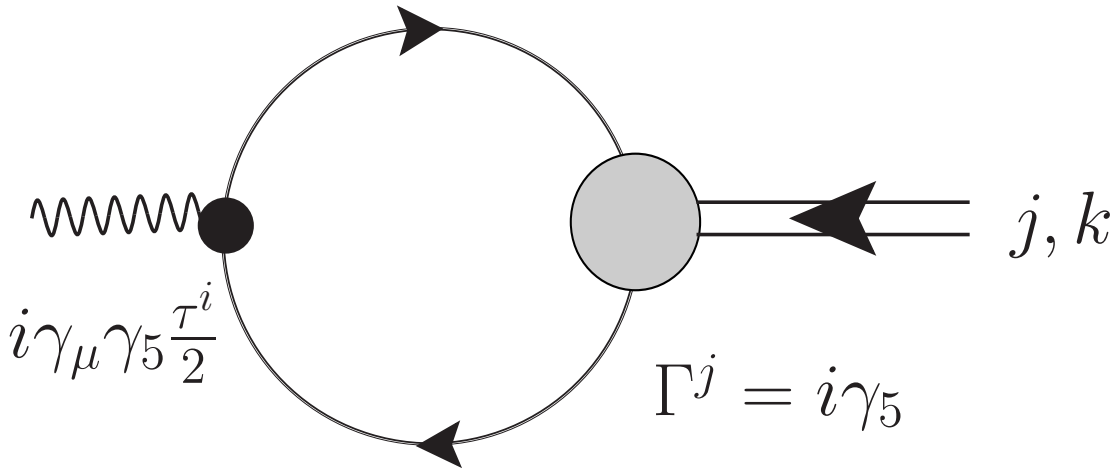

Figure 3.6.1: Diagram representing the pseudoscalar meson ($K$and π) decay in the NJL model. The two lines with arrow is a pseudoscalar meson and the bold line is an external axial-vector field.

The pseudoscalar meson decay constant in Eq. (3.6.1) is analytically evaluated becomes

$$ik_\mu f_{\mathscr{M}} = -N_C g_{\mathscr{M}q\bar{q}} \int \frac{d^4p}{(2\pi)^4} Tr\left[\gamma_\mu\gamma_5 S(p+\frac{k}{2})\gamma_5 S(p-\frac{k}{2}\right], \tag{3.6.2}$$

For the sake of simplicity, we now evaluated the pion decay and kaon decay, separately. Then performing the Feynman paramterization, Wick rotation and PTR scheme

to Eq. (3.6.2), the pion decay constant can be rewritten as

$$f_\pi = \frac{N_C g_{\pi q\bar{q}} M}{4\pi^2} \int_0^1 dx \int_{\frac{1}{(\Lambda_{\rm UV})^2}}^{\frac{1}{(\Lambda_{\rm IR})^2}} \frac{d\tau}{\tau} e^{-\tau(k^2(x^2-x)+M^2)}, \tag{3.6.3}$$

where $k^2 = m_\pi^2$, $g_{\pi q\bar{q}}$ denotes a quark-pion coupling constant, which is defined in Eq. (3.5.1). Similarly for the kaon decay constant, we find

$$f_K = \frac{N_C g_{Kq\bar{q}}}{4\pi^2} \left[(1-x)M_2 + xM_1\right] \int_0^1 dx \int_{\frac{1}{(\Lambda_{\rm UV})^2}}^{\frac{1}{(\Lambda_{\rm IR})^2}} \frac{d\tau}{\tau} e^{-\tau(k^2(x^2-x)+xM_2^2-(x-1)M_1^2)}, \tag{3.6.4}$$

$$\tag{3.6.5}$$

where $k^2 = m_K^2$ and the quark-kaon coupling constant is defined in Eq. (3.5.1).

Using the gap equation in Eq. (3.2.4) and pion and kaon mass conditions in Eq. (3.5.11), it gives a following expression,

$$f_\pi^2 m_\pi^2 \approx -m_q \langle \bar{\psi}\psi \rangle \tag{3.6.6}$$

$$f_K^2 m_K^2 \approx -m_q \langle \bar{\psi}\psi \rangle. \tag{3.6.7}$$

With this result, the first order approximation to the GMOR [117] current algebra relation can be obtained as

$$f_\pi^2 m_\pi^2 = -\frac{1}{2}\left(m_u + m_d\right)\langle \bar{u}u + \bar{d}d \rangle \tag{3.6.8}$$

$$f_K^2 m_K^2 = -\frac{1}{2}\left(m_u + m_s\right)\langle \bar{u}u + \bar{s}s \rangle, \tag{3.6.9}$$

where m_u, m_d and m_s are up, down and strange current (bare) quark masses, respectively. In physics interpretation, this result explicitly shows that the chiral symmetry is not destroyed by the PTR scheme to the NJL model.

3.7 Summary

In this chapter we have presented a brief introduction to the NJL model, including the Lagrangian, dynamical quark mass and gap equation, PTR scheme and the BSE yielding a bound state of the quark-antiquark pair in the kaon. We have already shown that the NJL model can be used to describe the kaon and pion in terms of quark degrees of freedom. The NJL model exhibits DCSB in vacuum have been demonstrated. The DCSB gives rise to dynamically generated dressed quark masses.

After introducing the BSE formulation, we derived the meson properties in the NJL model. They are pseudoscalar meson quark-anti-quark coupling, pseudoscalar meson masses, pseudoscalar decay constant and GMOR relation for the kaon and pion in the NJL model. Later on these meson properties will be used to compute the kaon form factor and parton distribution functions in Chapters 4 and 5, respectively.

4

Elastic Form Factors

The electromagnetic form factors of the pseudoscalar mesons (K and π) provide important and useful information concerning their internal structure [166]. Additionally, in perturbative QCD (pQCD) theory, the electromagnetic form factor at high Q^2 provides information to test the validity of pQCD. Extensively, the electromagnetic form factors of the pion [167–182] and nucleon [32, 33, 48–50, 54–56, 58, 63–65, 72, 73, 95, 96, 181] have been well studied experimentally or theoretically, using several different approaches. In contrast, there are only few studies of the kaon electromagnetic form factor [78, 100, 155].

From the experimental point of view, the availability of the kaon electromagnetic form factor data in the space-like region ($\mathrm{Q}^2 < 0$) is considerably rare. The kaon electromagnetic data is only measured at very low energies around $\mathrm{Q}^2 \leq 0.2\ \mathrm{GeV}^2$ [183]. This is linked to unavailability of the meson as a target in the laboratory. Meanwhile, there is more the experimental data for the time-like region ($\mathrm{Q}^2 > 0$), available up to several GeV^2, but they suffer from somewhat large uncertainties. However, because we restrict our work to the space-like region, we do not discuss this point further in this thesis. In theoretical studies, as mentioned earlier, there are just a few studies of the kaon electromagnetic form factors in the space-like region [184–191]. With this limitation in mind, it is not possible to decide which theoretical model approaches can be used to describe the kaon electromagnetic form factor well. Therefore, more studies are required to have more complete information about the kaon internal structure. The NJL model is relatively straightforward to calculate and typically yields results comparable to more sophisticated approaches such as DSE model and Lattice QCD. In such cases, the kaon form factor result in the NJL model can be used as a guidance for future kaon experiments, lattice QCD studies or more other sophisticated model approaches.

In this work, we therefore study the kaon electromagnetic form factor in the space-like region in the NJL model. This provides a direct insight into the spatial charge distribution and currents in the kaon. It would be fascinating to see the behavior

of each flavour of the quark sector form factors of the kaon and pion in the NJL model. The electromagnetic form factor is a favorable observable, beside the parton distribution function, for studying the internal structure of elementary particles. The most important reason for studying the form factor of the quark-antiquark bound state is to test the particular quark model and to explore the low energy behaviour of QCD. We also focus on the structure of the kaon with a particular interest in the effects of the larger mass of the strange quark. At present, a detailed understanding of pion and kaon structure is hampered by the rather small sample of experimental data [221, 227]. It is known that u_{K^+} is somewhat softer than u_{π^+} in the large-x valence region, which we will show is a natural consequence of the larger mass of the spectator strange quark in the K^+ (see Chapter 5). While at the present time one does not know the separate flavor contributions to the kaon elastic form factor, one may hope that it will prove possible to measure them in future. Given the phenomenological importance of the DYWR, it is certainly of considerable theoretical interest to compare the flavor dependence of the large-x PDFs with the corresponding large-Q^2 behaviour of the separate flavor contributions to the elastic form factor.

In this chapter, we present our calculation of the K-meson form factor as well as its quark sector form factor using the SU(3) NJL model, which was introduced in Chapter 3, with a PTR scheme [23–25, 30–32, 34–38, 41, 43, 44, 47–57] to simulate the effect of quark confinement. The separate contributions of each flavour quark sector form factor to the total elastic form factor of the kaon will be explored with and without the effect of dressing at the quark-photon vertex. Later on, the ratio of the quark sector form factors in the kaon in particular and pion are investigated. A comparison our model prediction with existing experimental data is presented. Throughout this work, more deep knowledge and information concerning the behavior of each flavour quark contribution within the kaon and pion will be revealed. Moreover, in our calculation, we calculate the kaon form factor with both bare quarks and dressed quarks by modifying the dressed quark-photon vertex. The dressed quark-photon vertex poses the interaction of a virtual photon with a nonpoint-like constituent quark, which is adopted from Ref. [192] [1]. This makes a significant change in the kaon and pion form factor needed, in order to agree well with experimental data. We therefore select this method in our calculation. Our kaon form factor calculation without and with a dressed quark in the NJL model with a PTR scheme will be presented in the section below.

4.1 Pseudoscalar Meson Form Factor

In this section we describe an electromagnetic interaction of the kaon and pion. In order to determine the electromagnetic current of the kaon and pion, we couple the electromagnetic field to the quark field via minimal substitution: $i\partial\!\!\!/ \to i\partial\!\!\!/ - \hat{Q}A_\mu\gamma^\mu$ in the three flavor NJL model Lagrangian in Eq. (3.1.6), where A_μ is electromagnetic field vector potential, e is the positron charge and $\hat{Q} = \mathrm{diag}\,[e_u, e_d, e_s] = \dfrac{e}{2}\left(\lambda_3 + \dfrac{1}{\sqrt{3}}\lambda_8\right)$ is the quark charge operator, where e_q are the quark charges. Here λ_3 and λ_8 are the

[1] The quark-photon vertex in the NJL model is given by the solution to an inhomogeneous Bethe-Salpeter equation (BSE).

usual Gell-Mann matrices in flavor space. The electromagnetic current for the kaon K^+ and pion π^+ are formally expressed in the matrix element reads

$$J^{\mu}_{\alpha}(p,p') = \langle \alpha(p') \mid \mathcal{J}^{\mu}(0) \mid \alpha(p) \rangle = (p^{\mu} + p'^{\mu}) F_{\alpha}(Q^2), \qquad \alpha = \pi, K, \tag{4.1.1}$$

where p and p' denote the incoming and outgoing four momenta of the pseudoscalar mesons, $q^2 = (p-p')^2$ or $q^2 \equiv -\mathrm{Q}^2$, where Q^2 is four momentum transfer of virtual photon. $\mathcal{J}^{\mu}(0)$ is the electromagnetic current, $\mid \alpha(k) \rangle$ [2] stands for the full bound state of the kaon (mesons) and $F_{\alpha}(Q^2)$ is the kaon or pion elastic form factor. The electromagnetic vector current of the total kaon and pion in the NJL model are denoted by $\mathcal{J}^{\mu}_{K}(p,p')$ and $\mathcal{J}^{\mu}_{\pi}(p,p')$, respectively. We will evaluate both electromagnetic currents using the NJL model in the section below.

4.2 Kaon Form Factor with Bare Quark

In this section we derive a kaon form factor with the bare quark (pointlike case). The quark-photon vertex for a bare quark is given by

$$\Lambda^{\mu(bare)}_{\gamma q}(p,p') = \frac{1}{2}\left(\lambda_3 + \frac{1}{\sqrt{3}}\lambda_8\right)\gamma^{\mu}, \tag{4.2.1}$$

where λ_3 and λ_8 denote SU(3) generators, which are defined in Appendix A.2. For the pion case [3], the quark-photon vertex for the bare quark can be projected onto flavor sectors, it then gives $\left(e_u\frac{1+\tau_3}{2} + e_d\frac{1-\tau_3}{2}\right)$, where e_u and e_d are the up and down quark charges, respectively.

Using the quark-photon vertex for the bare quark in Eq. (4.2.1), the electromagnetic form factor of the kaon and pion can be derived from Fig. 4.2.1. As we know that in QCD the valence quarks of the kaon (pion) consist of the up (up) and anti-strange (anti-down) quark. Therefore, only two Feynman diagrams contribute to the meson electromagnetic form factor [4]. One diagram, the photon couples to the quark and another diagram, the photon couples to the anti-quark, as provided in Fig. 4.2.1. Thus, the full meson form factor in the NJL model is given by the two Feynman diagrams as depicted in Fig 4.2.1. Based upon the Feynman diagrams in Fig. 4.2.1, the full expression for the matrix element of the electromagnetic current of the kaon, with the bare quark-photon vertex in Eq.(4.2.1), can be written as

$$J^{\mu}_{u/K^+}(p,p') = -g^2_{Kq\bar{q}}\int \frac{d^4p}{(2\pi)^4}\,(\gamma_5 T_j)_{\lambda'\epsilon'}\left[iS_u(p'+k)\Theta^{\mu}iS_u(p+k)\right]_{\epsilon'\epsilon}(\gamma_5 T_i)_{\lambda\epsilon}\,iS_s(k)_{\lambda\lambda'}, \tag{4.2.2}$$

[2] The quantity $\langle \alpha(p') \mid \mathcal{J}^{\mu}(0) \mid \alpha(p) \rangle$ is the meson-photon vertex. The calculation of the hadronic part is unknown due to the non-perturbative dynamics.

[3] For the pion case, $M_u = M_d$ in the SU(2) isospin symmetry limit.

[4] Note that in this form factor calculation, we consider the quark as a pointlike particle (without dressing). The quark without dressing is also called a bare quark and its kaon form factor is denoted by $F_K(Q^2)$, whereas the kaon form factor with quark dressing is symbolized by $F^{bse}_K(Q^2)$.

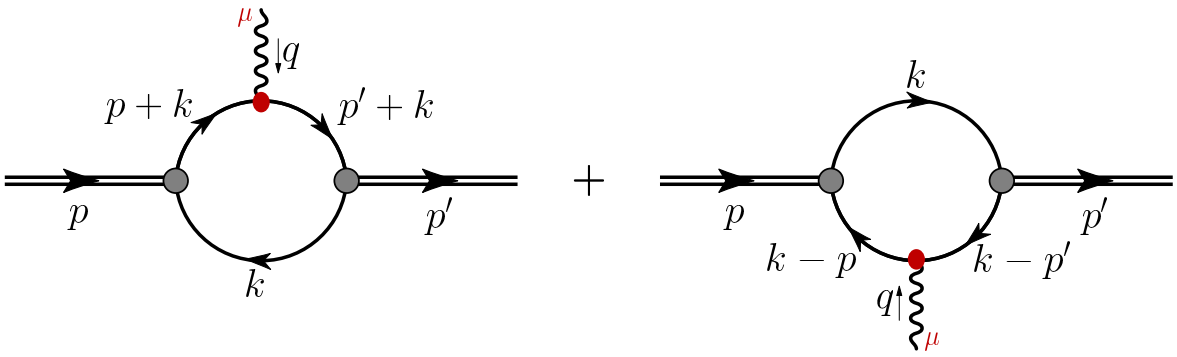

Figure 4.2.1: Diagrammatic representation of the electromagnetic form factor of the kaon and pion. The Feynman diagram for the valence quark is on the left hand side and for the valence anti-quark is on the right hand side. The operator insertion, Θ^μ is $\frac{1}{2}e\left(\frac{\lambda_8}{\sqrt{3}}+\lambda_3\right)\gamma^\mu$.

$$J^\mu_{s/K^+}(p,p') = -g^2_{Kq\bar{q}}\int\frac{d^4p}{(2\pi)^4}\left(\gamma_5 T_j\right)_{\lambda'\epsilon'} iS_u(k)_{\epsilon'\epsilon}\left(\gamma_5 T_i\right)_{\lambda\epsilon}\left[iS_s(k-p)\Theta^\mu iS_s(k-p')\right]_{\lambda\lambda'}, \tag{4.2.3}$$

where T_j, T_i are the isospin operators of the kaon, respectively. The flavor matrices for the kaon in the SU(3) NJL model is $T_i = T_j = \frac{(\lambda_4 \pm i\lambda_5)}{\sqrt{2}}$, where λ_4 and λ_5 are the SU(3) generators, respectively. The minus sign is from the closed fermion loop. For the pion case, the flavor matrices from Bethe-Salpeter vertices is defined as $T_i = T_j = \frac{(\lambda_1 \pm i\lambda_2)}{\sqrt{2}}$.

Rearranging the indices in Eq. (4.2.2) and putting the operator insertion [5] into Eq. (4.2.2), one has the form

$$\begin{aligned} J^\mu_{K^+}(k,k') &= J^\mu_{u/K^+}(p,p') + J^\mu_{s/K^+}(p,p') \\ &= e_u\Lambda^\mu_{u/K^+}(p,p') + e_s\Lambda^\mu_{s/K^+}(-p,-p'), \end{aligned} \tag{4.2.4}$$

where e_u and e_s are, respectively, up and anti-strange quark charges. Then the form factors $\Lambda^\mu_{u/K^+}(p,p')$ and $\Lambda^\mu_{s/K^+}(-p,-p')$, (a full derivation of the $\Lambda^\mu_u(p,p')$ and $\Lambda^\mu_s(-p,-p')$ will summarized in Appendix A.14), are obtained by

$$\Lambda^\mu_{u/K^+}(p,p') = 2iN_C g^2_{K\bar{q}q}\int\frac{d^4p}{(2\pi)^4} Tr\left[\gamma_5 S_u(k+p')\gamma^\mu S_u(k+p)\gamma_5 S_s(k)\right], \tag{4.2.5}$$

$$\Lambda^\mu_{s/K^+}(-p,-p') = 2iN_C g^2_{K\bar{q}q}\int\frac{d^4p}{(2\pi)^4} Tr\left[\gamma_5 S_s(k-p)\gamma^\mu S_s(k-p')\gamma_5 S_u(k)\right], \tag{4.2.6}$$

where the trace is over Dirac, color and flavour indices and the *minus* sign in the second line indicates the anti-quark momentum and $N_C = 3$ denotes the number of

[5] The operator insertion can be also written as $\left[\left(\frac{1}{6}+\frac{\tau_3}{2}\right)e_u + e_s\right]\gamma^\mu$, where τ_3 denotes a Pauli matrix.

colors. $S_u(p)$ and $S_s(p)$ are the dressed up and anti-strange quark propagators. In the flavour space the quark propagator reads $S(p) = \text{diag}[S_u(p), S_d(p), S_s(p)]$. Note that the first line in Eq. (4.2.5) relates to the left diagram in Fig. 4.2.1 and the second line in Eq. (4.2.5) relates to the right diagram in Fig. 4.2.1. Similarly, a derivation of the pion form factor can be easily obtained by replacing the s quark with a d quark and the kaon quark-antiquark coupling constant $g_{K\bar{q}q}$ with the pion quark-antiquark coupling constant $g_{\pi\bar{q}q}$.

We will focus on the quark sector and total form factors for π^+, K^+ and K^0. Upon inspection of Eqs. (4.2.5) and (4.2.6) we have

$$\Lambda^{\mu}_{u/K^+}(p, p') \propto \Lambda^{\mu}_{s/K^+}(-p, -p'), \tag{4.2.7}$$

where the constant of proportionally is the ratio of the struck quark charges.

For the form factors, we find the expression for the meson form factors which can be composed into a sum over the quark charges multiplied by quark sector form factors :

$$F^{(\text{bare})}_{\pi^+}(Q^2) = e_u F^u_{\pi}(Q^2) - e_d F^d_{\pi}(Q^2) = (e_u - e_d)\, F^u_{\pi}(Q^2), \tag{4.2.8}$$

$$F^{(\text{bare})}_{K^+}(Q^2) = e_u F^u_{K}(Q^2) - e_s F^s_{K}(Q^2), \tag{4.2.9}$$

$$F^{(\text{bare})}_{K^0}(Q^2) = e_d F^u_{K}(Q^2) - e_s F^s_{K}(Q^2), \tag{4.2.10}$$

here $F^u_{\pi^+,K^+}(Q^2)$ [6] is the up quark sector form factor, which contributes to the total pion and kaon electromagnetic form factor, $F^d_{\pi^+}(Q^2)$ is the anti-down quark sector form factor, which contributes to the pion electromagnetic form factor and $F^s_{K^+}(Q^2)$ denotes the anti-strange quark sector form factor, which gives a contribution to kaon form factor. The quark sector form factors $F^i_{\alpha}(Q^2)$ represent the contribution of the current quarks of flavor i [7] to total pseudoscalar meson form factor, $F_{\alpha}(Q^2)$, where the subscript α denotes a pseudoscalar meson. Note that $F^u_{\pi^+}(Q^2) = F^d_{\pi^+}(Q^2)$, so that the pion form factor only has a single quark sector form factor contribution.

After performing a Feynman parameterization, a Wick rotation and a PTR scheme to each quark sector form factor in Eq. (4.2.8), the expression for the quark sector form factor of the pion is given by

$$\begin{aligned} F^u_{\pi^+}(Q^2) = {} & \frac{N_C g^2_{\pi q\bar{q}}}{4\pi^2} \int_0^1 dx \int_{\frac{1}{(\Lambda_{\text{UV}})^2}}^{\frac{1}{(\Lambda_{\text{IR}})^2}} \frac{d\tau}{\tau} e^{-\tau(-Q^2(x^2-x)+M_u^2)} \\ & + \frac{N_C g^2_{\pi q\bar{q}}}{4\pi^2} \int_0^1 dx \int_0^{1-x} dz \int_{\frac{1}{(\Lambda_{\text{UV}})^2}}^{\frac{1}{(\Lambda_{\text{IR}})^2}} d\tau \\ & \times e^{-\tau(k^2[(x+z)^2-(x+z)]+xzQ^2+M_d^2(1-x-z)+M_u^2(x+z))} \\ & \times [k^2(x+z) + (M_u - M_d)^2(x+z) - 2M_d^2 + 2M_d M_u]. \end{aligned} \tag{4.2.11}$$

[6] From Eqs. (4.2.4) and (4.2.8), we obtain that $F^u_{K^+}(Q^2) = \Lambda^{\mu}_{u/K^+}(k, k')$. Similarly, this can also be applied to other quark sector form factors.

[7] The up quark charge $e_u = \frac{2}{3}$, the down quark charge $e_d = -\frac{1}{3}$ and the strange quark charge, $e_s = -\frac{1}{3}$.

Here N_C denotes the number of colors and M_u and M_d are up and down dynamical quark masses as defined in Eq. (3.2.1). In the pion case we assume that $M_u = M_d$, corresponding to the SU(2) isospin symmetry. Therefore we only introduce a single up quark sector form factor. The quark sector form factor of the kaon then has the form

$$\begin{aligned} F^u_{K^+}(Q^2) = & \frac{N_C g^2_{Kq\bar{q}}}{4\pi^2}\int_0^1 dx \int_{\frac{1}{(\Lambda_{\rm UV})^2}}^{\frac{1}{(\Lambda_{\rm IR})^2}} \frac{d\tau}{\tau} e^{-\tau(-Q^2(x^2-x)+M_u^2)} \\ & + \frac{N_C g^2_{Kq\bar{q}}}{4\pi^2}\int_0^1 dx \int_0^{1-x} dz \int_{\frac{1}{(\Lambda_{\rm UV})^2}}^{\frac{1}{(\Lambda_{\rm IR})^2}} d\tau \\ & \times e^{-\tau(k^2[(x+z)^2-(x+z)]+xzQ^2+M_s^2(1-x-z)+M_u^2(x+z))} \\ & \times [k^2(x+z)+(M_u-M_s)^2(x+z)-2M_s^2+2M_sM_u], \end{aligned} \tag{4.2.12}$$

$$\begin{aligned} F^s_{K^+}(Q^2) = & \frac{N_C g^2_{Kq\bar{q}}}{4\pi^2}\int_0^1 dx \int_{\frac{1}{(\Lambda_{\rm UV})^2}}^{\frac{1}{(\Lambda_{\rm IR})^2}} \frac{d\tau}{\tau} e^{-\tau(-Q^2(x^2-x)+M_s^2)} \\ & + \frac{N_C g^2_{Kq\bar{q}}}{4\pi^2}\int_0^1 dx \int_0^{1-x} dz \int_{\frac{1}{(\Lambda_{\rm UV})^2}}^{\frac{1}{(\Lambda_{\rm IR})^2}} d\tau \\ & \times e^{-\tau(k^2[(x+z)^2-(x+z)]+xzQ^2+M_u^2(1-x-z)+M_s^2(x+z))} \\ & \times [k^2(x+z)+(M_s-M_u)^2(x+z)-2M_u^2+2M_uM_s], \end{aligned} \tag{4.2.13}$$

where $M_u \neq M_s$ for the kaon. The normalization of the quark sector form factors in Eqs. (4.2.11), (4.2.12) and (4.2.13) are straightforwardly evaluated by taking $Q^2 = 0$, giving $F_{\pi^+,K^+}(Q^2=0) = 1$.

These results are denoted as "bare" because the quark-photon vertex is elementary the result, that is, $\Lambda^{\mu(\rm bare)}_{\gamma q} = \hat{Q}\,\gamma^\mu$. Note, these expressions automatically satisfy charge conservation. The quark-sector form factors for a hadron α are defined by

$$F_\alpha(Q^2) = \sum_q e_q F^q_\alpha = e_u\, F^u_\alpha(Q^2) + e_d\, F^d_\alpha(Q^2) + e_s\, F^s_\alpha(Q^2) + \ldots \tag{4.2.14}$$

Therefore the "bare" pseudoscalar meson quark-sector form factors are there easily read off from Eqs. (4.2.8)-(4.2.10). The form factor in this form, as in Eq. (4.2.8), is very useful for investigating the CSV, to which we will apply this quark sector form factor later in Chapter 6.

4.3 Results for the Kaon Form Factor with Bare Quark

In this section we discuss the results for the kaon form factors as well as pion form factors. Firstly, the parameters, G_π, $\Lambda_{\rm UV}$, M_s, m_u and m_s in the NJL model must be determined in order to compute the kaon and pion form factors. As already explained, we fix $\Lambda_{\rm IR}$= 0.240 GeV. The constituent light quark mass is M_q= 0.4 GeV. The

physical pion and kaon masses are respectively, $m_\pi = 0.14$ GeV and $m_K = 0.495$ GeV, f_K= 0.097 GeV and f_π=0.093 GeV. By fixing the parameters using these values, we obtain $\Lambda_{\rm UV}$= 645 MeV, G_π= 19.04 GeV^{-2}, M_s = 0.611 GeV, and m_s = 0.356 GeV. Then we obtain the coupling constants $g_{\pi\bar{q}q} = 4.23$ and $g_{K\bar{q}q} = 4.57$, which are used in Eq. (3.5.4) to compute the kaon form factor as well as the pion form factor. Using the physical mass of the ρ meson, $m_\rho = 0.770$ GeV, we obtained $G_\rho = 11.04$ GeV^{-2} and we also obtained $m_\phi = 1.057$ GeV. The numerical results for the kaon and pion form factors without (bare quark) and with vector mesons (ρ, ω, ϕ) are given below. The values of the parameters of our NJL model are summarized in Table 4.3.1.

Table 4.3.1: The values of the parameters of the NJL model used in this calculation [159] and their experimental values. The units of the parameters (powers of GeV) are seen in the text.

Parameters	Our NJL calculation	Experiment
f_K	0.097	0.113 ± 0.001
m_K	0.495	0.4937
f_π	0.093	0.0924 ± 0.001
m_π	0.14	0.1385
M_q	0.4	-
Λ_{IR}	0.240	-
Λ_{UV}	0.645	-
G_π	19.04	-
M_s	0.611	-
m_s	0.356	-
$g_{Kq\bar{q}}$	4.57	-
$g_{\pi q\bar{q}}$	4.23	-
m_ρ	0.770	-
m_ω	0.782	-
G_ρ	11.045	-
G_ω	10.414	-
m_ϕ	1.057	-

After fixing the free parameters in the NJL model, we use them to determine the kaon form factor with bare quark (and with dressed quark later). We firstly begin to compute the total kaon form factor with the bare quark in Eq. (4.2.8) and the quark sector form factors of the kaon in Eqs. (4.2.11), (4.2.12) and (4.2.13). Note that the quark sector form factors are determined without the quark charges, as in Eq. (4.2.8). Our results for the kaon form factor with bare quark and its quark sector form factors are depicted in Fig. 4.3.1. The bare kaon form factor and its quark sector form factors are calculated over the range four momentum squared, $Q^2 = 0 - 6$ GeV^2. Figure 4.3.1 exhibits a dramatic difference between the up quark sector form factor, $F_K^u(Q^2)$ and the anti-strange quark sector form factor, $F_K^s(Q^2)$. The latter becomes much larger as Q^2 increases. To see the behavior of the quark sector form factors at large Q^2, we plot the quark sector form factors of the kaon over the range $Q^2 = 0 - 20$ GeV^2 in Fig. 4.3.2. This shows that the up quark sector form factor decreases faster than the anti-strange quark sector form factor. This is expectedly because the $M_s > M_u$, where M_s and M_u are the dressed anti-strange and up quark masses, respectively. This indication clearly seen in Fig. 4.3.3 and 4.3.4.

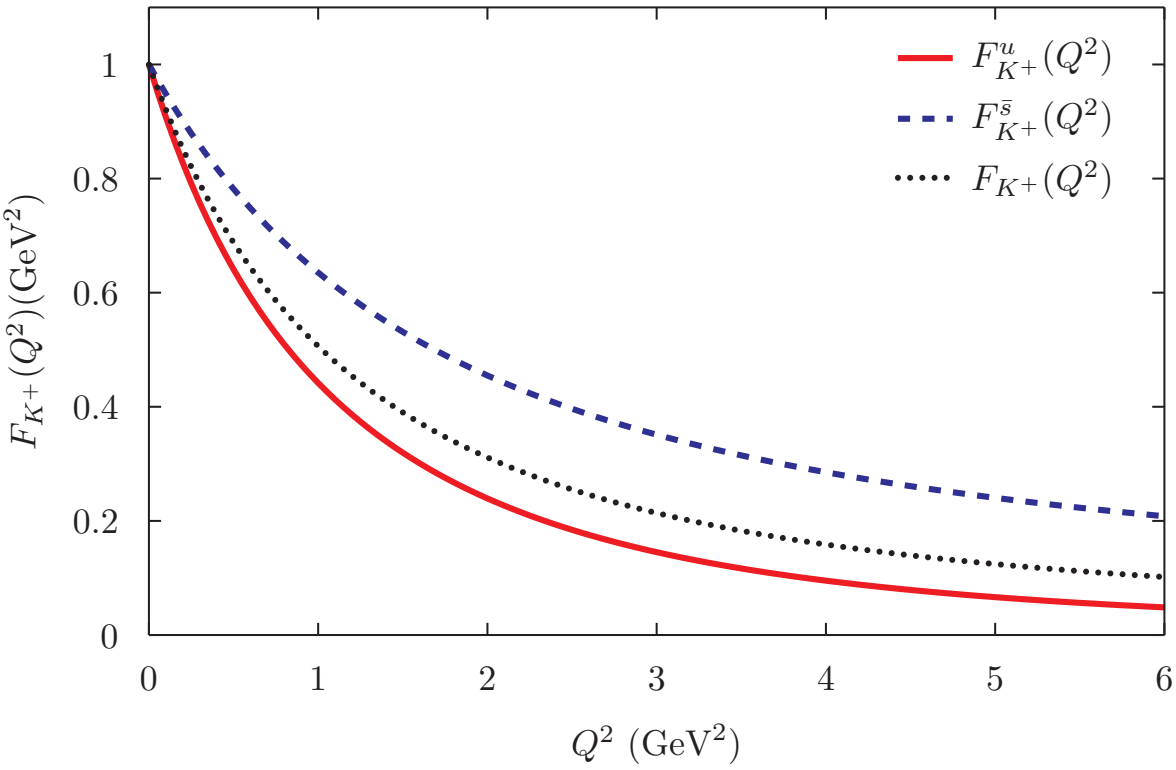

Figure 4.3.1: The form factor of the kaon with bare quarks and its quark sector form factors are provided over the range $Q^2 = 0$ - 6 GeV^2. The up quark sector form factor of the kaon (red solid line), the anti-strange quark sector form factor (blue dashed line) and the total kaon form factor (black dotted line).

The anti-strange quark sector form factor $Q^2\ F_K^s(Q^2)$ grows with increasing Q^2. In contrast the up quark sector form factor of the kaon multiplied by Q^2, $Q^2\ F_K^u(Q^2)$, decreases with increasing Q^2. This clearly indicates that the anti-strange quark sector

form factor has a larger contribution than the up quark sector form factor to the total bare kaon form factor at both small and large Q^2.

Our total kaon form factor with a bare quark is compared to the available experimental data from Ref. [183] and to the empirical monopole function,

$$F_K^{\text{empirical}}(Q^2) = \frac{1}{1+\frac{Q^2}{m_\rho^2}}, \tag{4.3.1}$$

where m_ρ stand for ρ mass, in Fig. 4.3.5. This shows that our kaon form factor prediction, which is represented by the black solid line, is larger than experimental data [183] and the empirical monopole. This indicates that our kaon form factor with a bare quark is in disagreement with the experimental data in Ref. [183] and the phenomenological monopole with $m_\rho^2 = 0.61\text{GeV}^2$. It shows that our kaon form factor with a bare quark is larger than others. This is because we treat the quark as a pointlike particle. While this is expected to be a good approximation at large Q^2, the empirical monopole (VMD) prediction shows remarkable agreement with existing experimental data [183]. In other words, our NJL model does not give a good description of the existing data. Hence, next, we will improve our calculation by considering a dressed quark in Section 4.5.

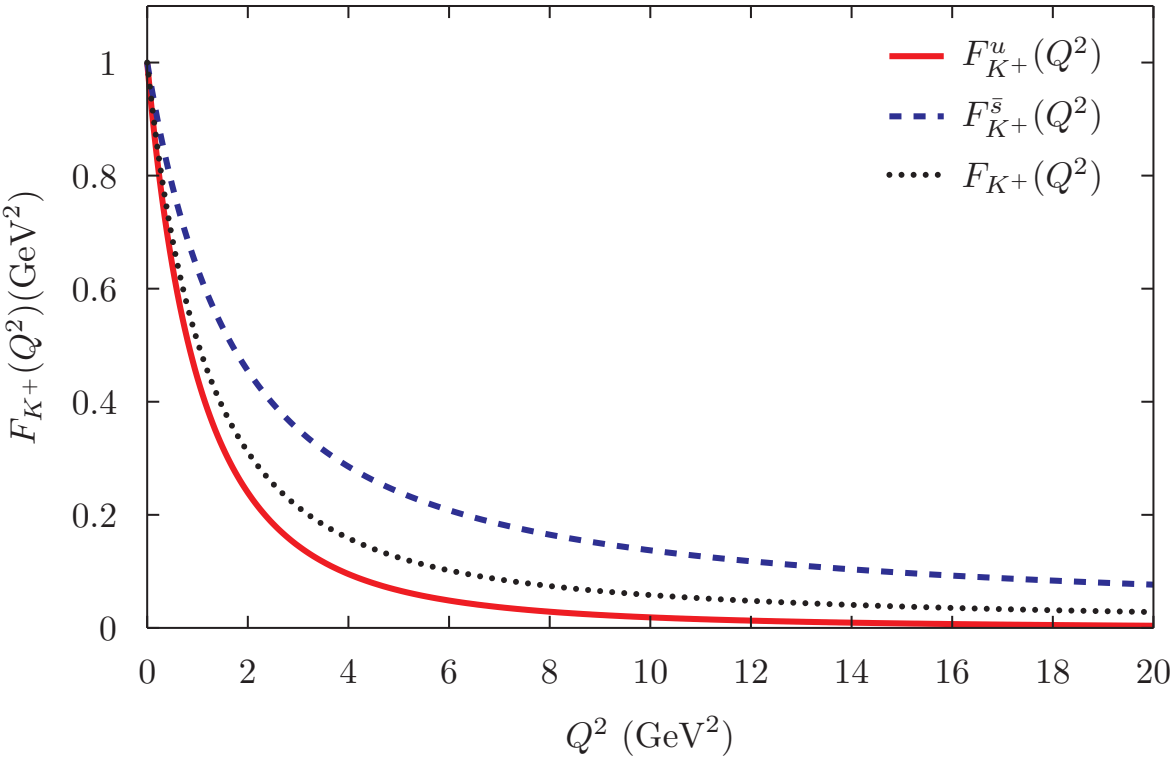

Figure 4.3.2: As in Fig 4.3.1 but the kaon form factors with bare quarks are shown over the range $Q^2 = 0 - 20$ GeV^2.

Next, our numerical result for the pion form factor with bare quarks and its quark sector form factors is illustrated in Fig. 4.3.6. The parameter set used in this calculation

is the same as for the kaon calculation in Table 4.3.1. Figure 4.3.6 indicates that the up quark sector form factor of the pion is identical to the anti-down quark sector form factor, as pointed out in Eq. (4.2.8). The pion form factor with bare quarks decreases rapidly with increasing Q^2. This is caused by the pion form factor being small at large Q^2. In addition, we provide the pion quark form factor and the quark sector form factors of the pion at large Q^2, over the range 0 - 20 GeV^2 in Fig. 4.3.7. This figure is very useful to observe the behavior of the pion form factor at large Q^2 or in the asymptotic region. Then, we compare our pion form factor calculation to the experimental data from Refs. [167, 168, 177] and the empirical monopole [178] with $m_\rho^2 = 0.775$ GeV^2. Similar to the kaon form factor with bare quarks result, the pion form factor with bare quarks result is not consistent with the existing experimental data [167, 168, 177] or the phenomenological monopole [178]. This difference is clearly seen in Figs. 4.3.8, 4.3.9, and 4.3.10, where, in the both figures, the pion form factor with bare quarks multiplied by Q^2 is plotted as a function of Q^2. Figure. 4.3.10 indicates that our NJL prediction tends to decrease in the larger Q^2 region and shows relatively the same trend as the monopole prediction at around $Q^2 = 6$ GeV^2. Overall, it seems that our form factor of the pion with bare quarks does not agree well with either the experimental data [167, 168, 177] or the phenomenological monopole [178]. Then, we will develop our result with the form factor of the pion by modifying the quark-photon vertex to include a dressed quark-photon vertex in Section 4.5.

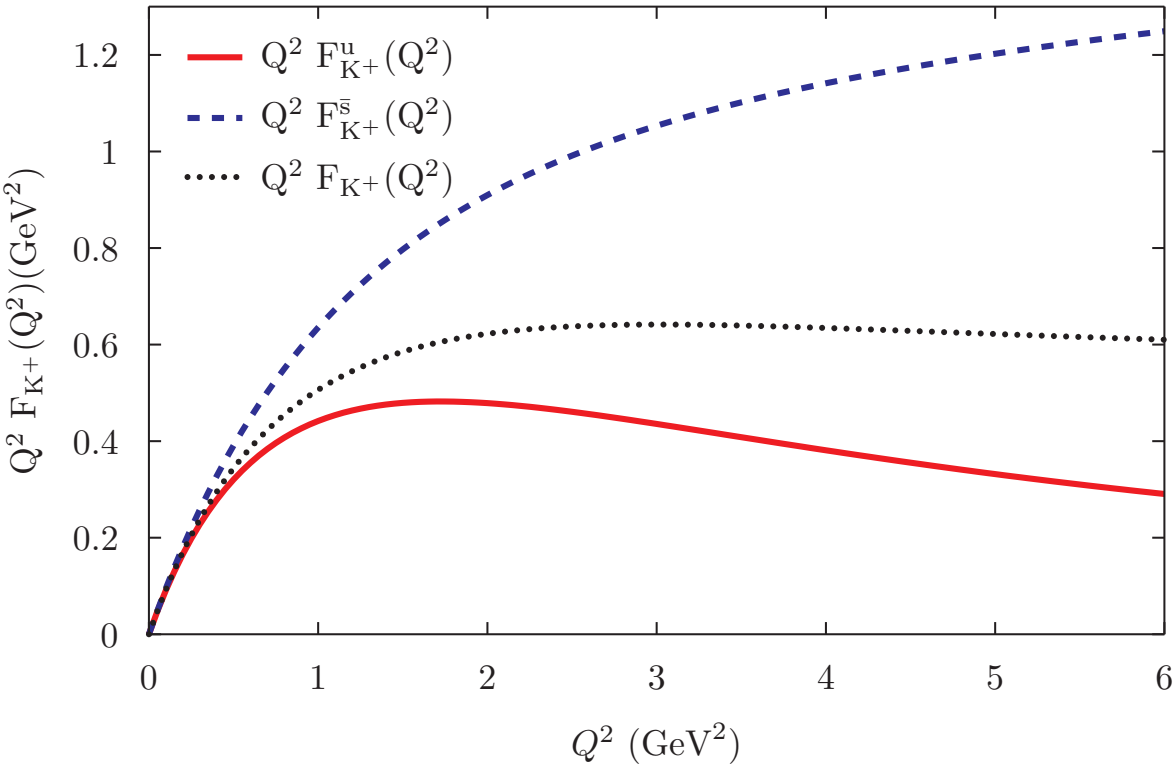

Figure 4.3.3: As in Fig. 4.3.1 but the form factor of the kaon with bare quarks and its quark sector form factors multiplied by Q^2 are shown over the range $Q^2 = 0 - 6$ GeV^2.

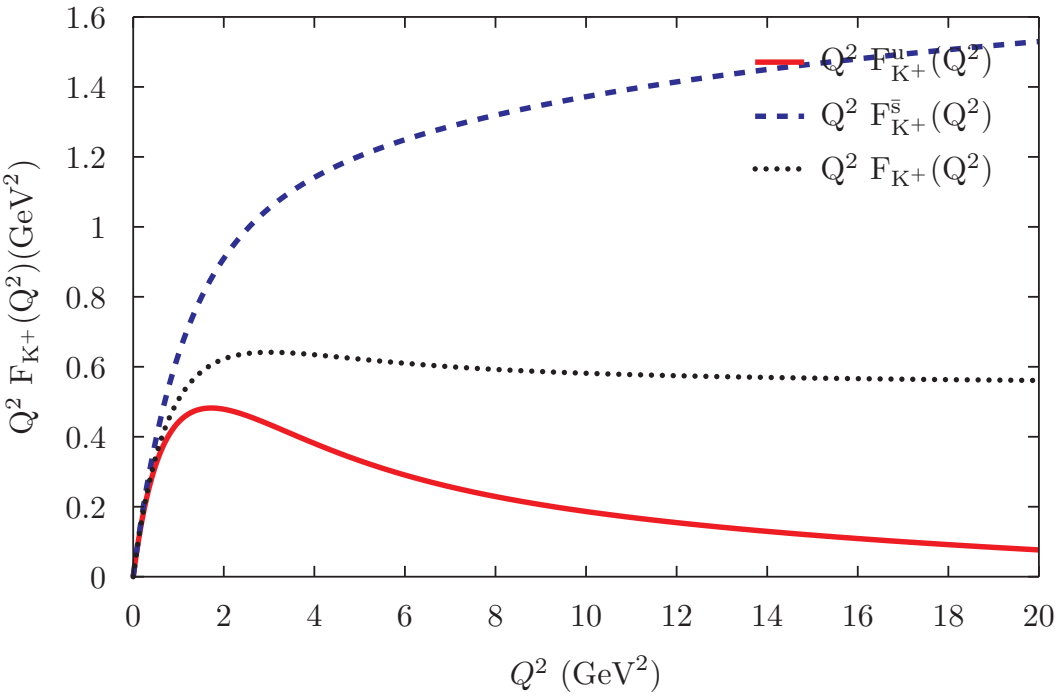

Figure 4.3.4: As in Fig. 4.3.3, but the bare form factor of the kaon and its quark sector form factors multiplied by Q^2 are shown over the range $Q^2 = 0 - 20$ GeV^2.

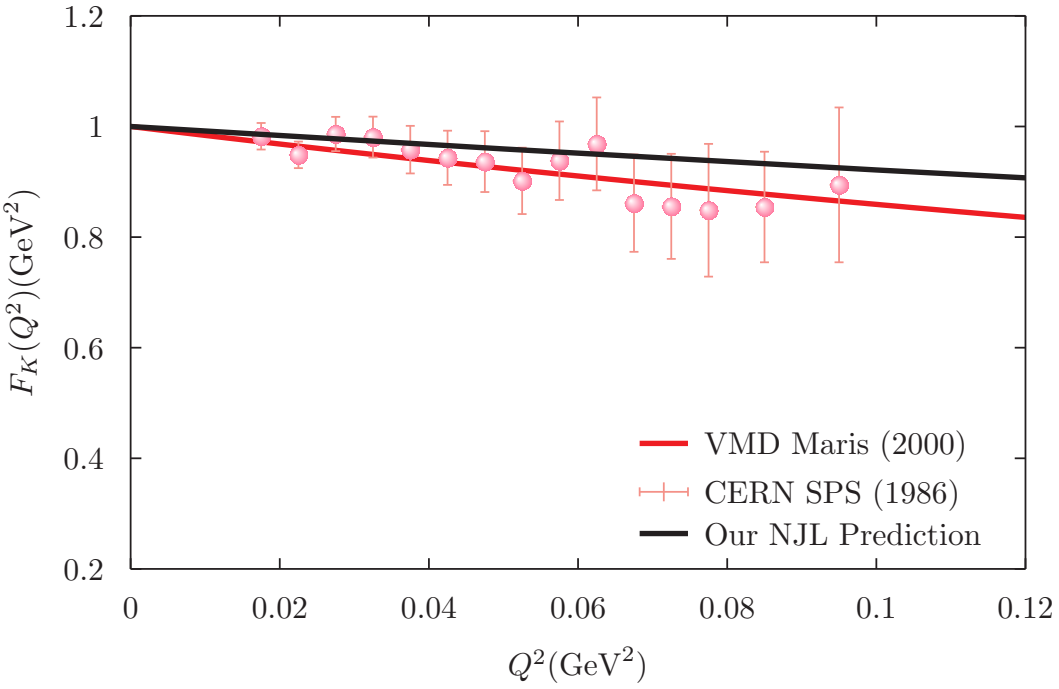

Figure 4.3.5: The form factor of the kaon with bare quarks compared to available experimental data [183] (salmon dotted line) and VMD prediction (red-solid-line). Our NJL model is represented by the black solid line.

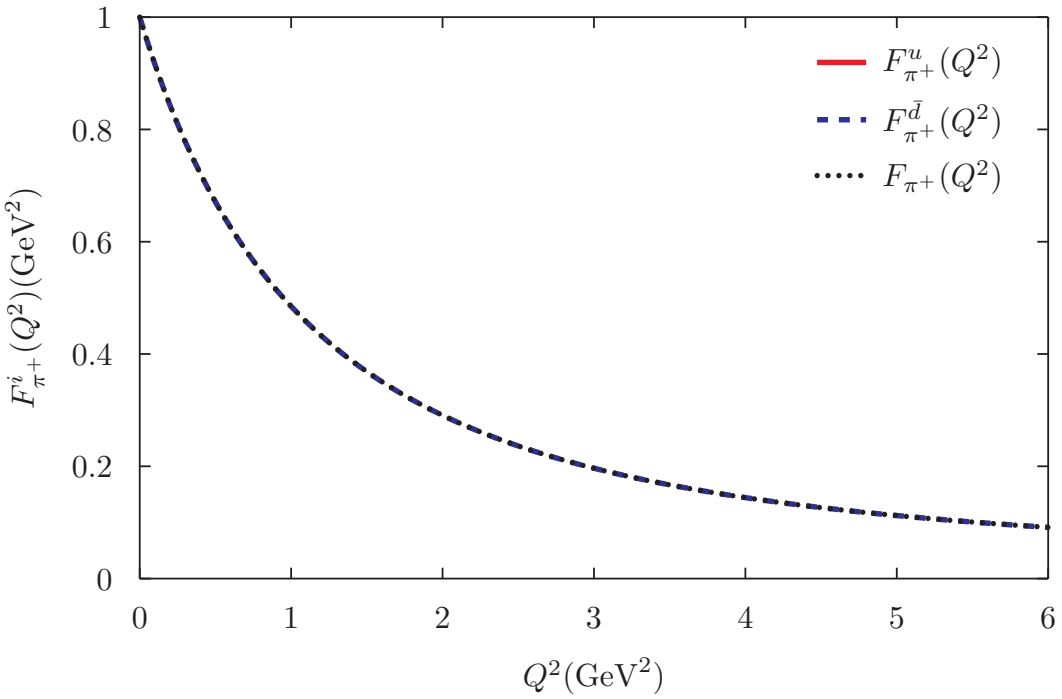

Figure 4.3.6: As in Fig 4.3.1 but for pion form factor and its quark sector form factors.

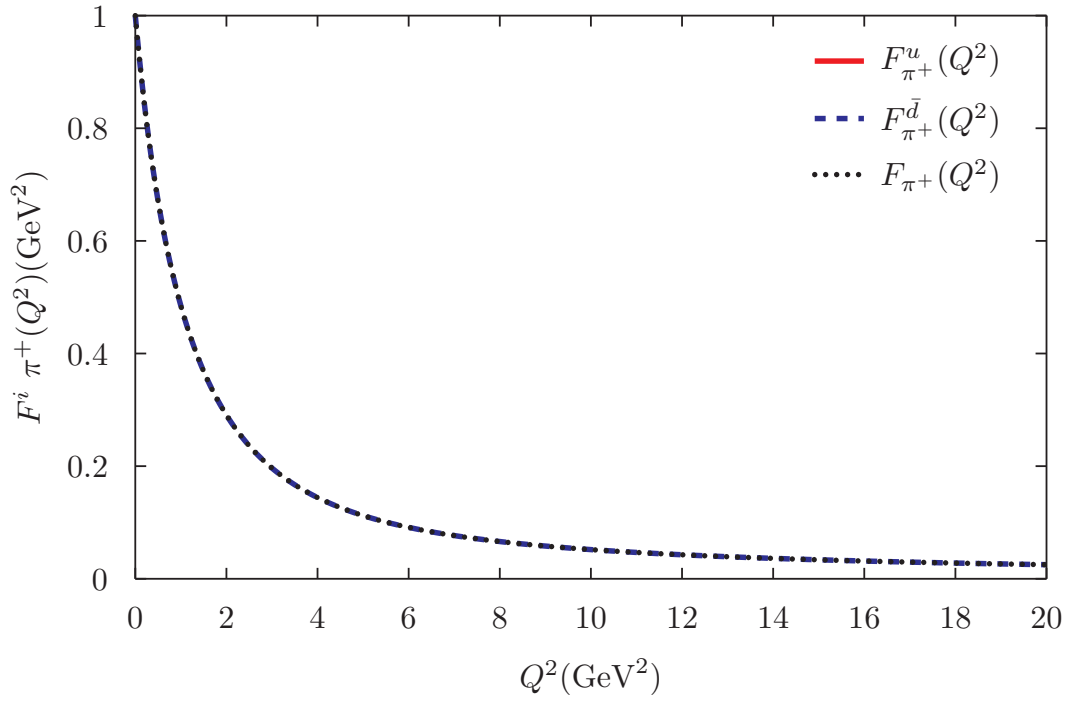

Figure 4.3.7: As in Fig 4.3.6 but for large Q^2.

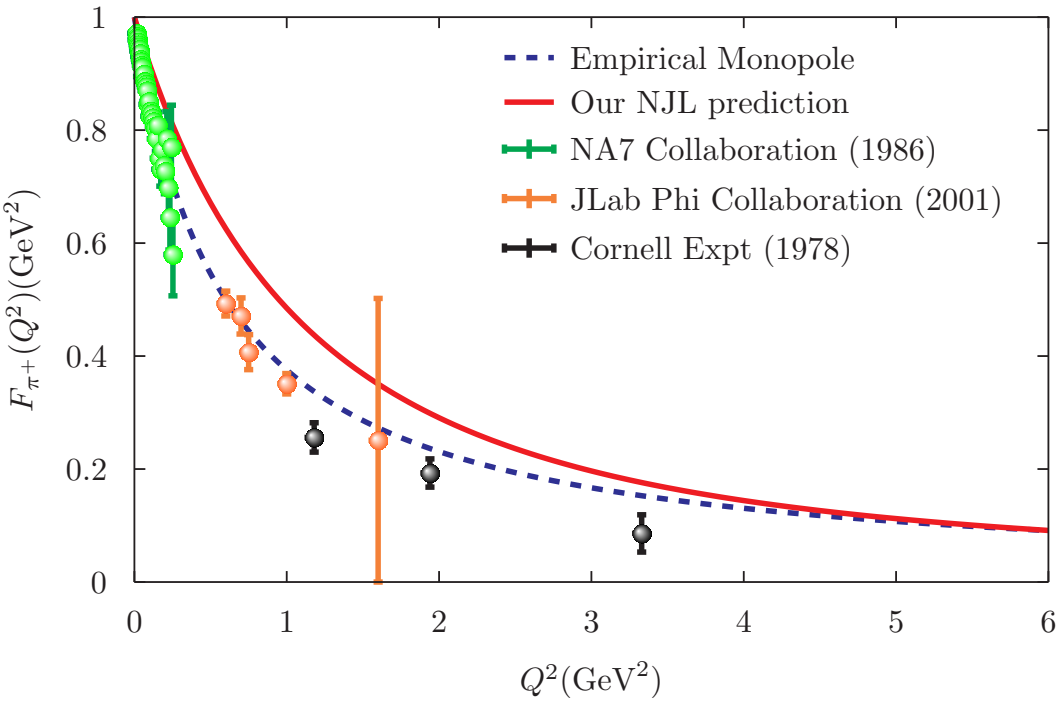

Figure 4.3.8: The bare form factor of the pion compared to existing experimental data [167, 168, 177] and empirical monopole (VMD).

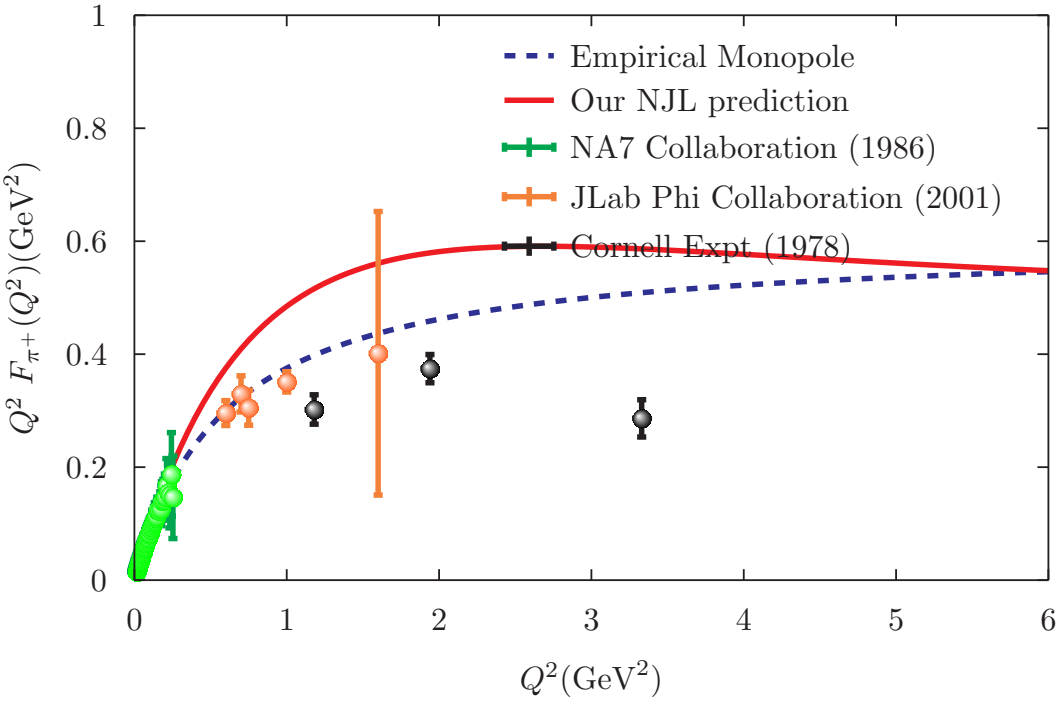

Figure 4.3.9: As in Fig. 4.3.8 but for large Q^2, up to 6 GeV^2 and plot $Q^2 F_\pi(Q^2)$ as a function of Q^2. The experimental data are from Refs. [167, 168, 177].

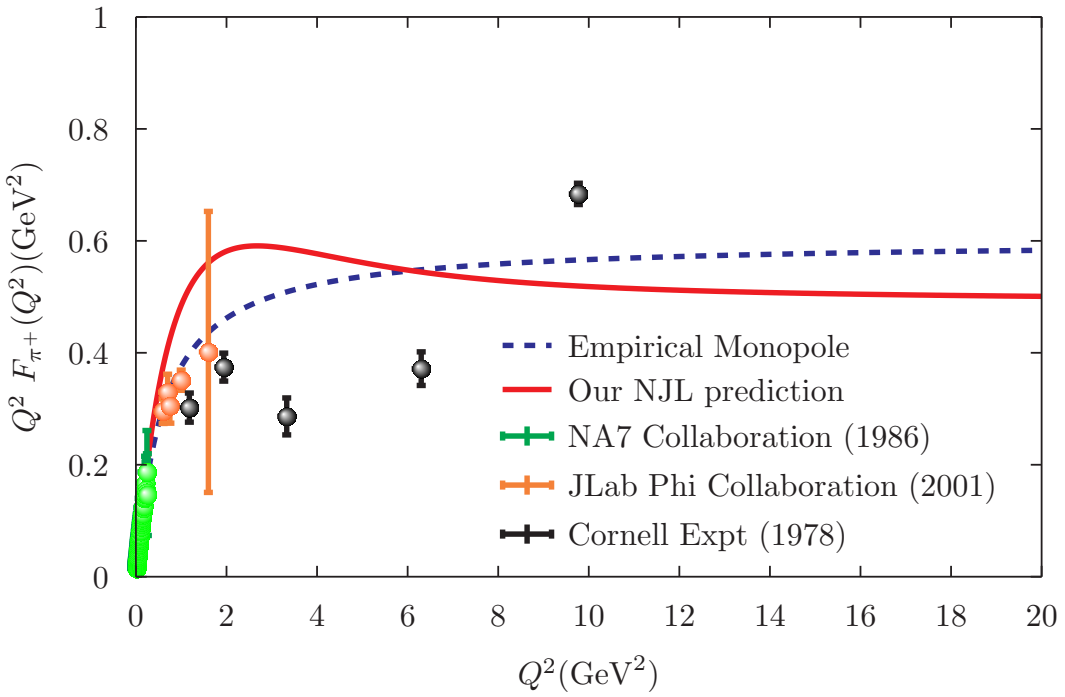

Figure 4.3.10: As in Fig. 4.3.9 but for larger Q^2, up to 20 GeV^2. The available experimental data are taken from Refs. [167, 168, 177].

4.4 Quark Photon Vertex

Before we discuss the results for the kaon form factor with a dressed quark-photon vertex in Section 4.5, the modification of the quark photon vertex, which includes the dressed quark, is presented. In Section 4.3, we have computed the kaon and pion form factors using the quark-photon vertex for the bare (pointlike) quark. As a result, we found that the kaon and pion form factors did not quantitatively agree well with the kaon [183] and pion experimental data [167, 168, 177]. Therefore, here, we improve our previous result of the kaon and pion form factors by means of the quark-photon vertex modified consistently. The quark-photon vertex in the NJL model is given by solving an inhomogeneous BSE self-consistently. The diagrammatic representation of the quark-photon vertex – including vector mesons automatically – is illustrated in Fig. 4.4.1.

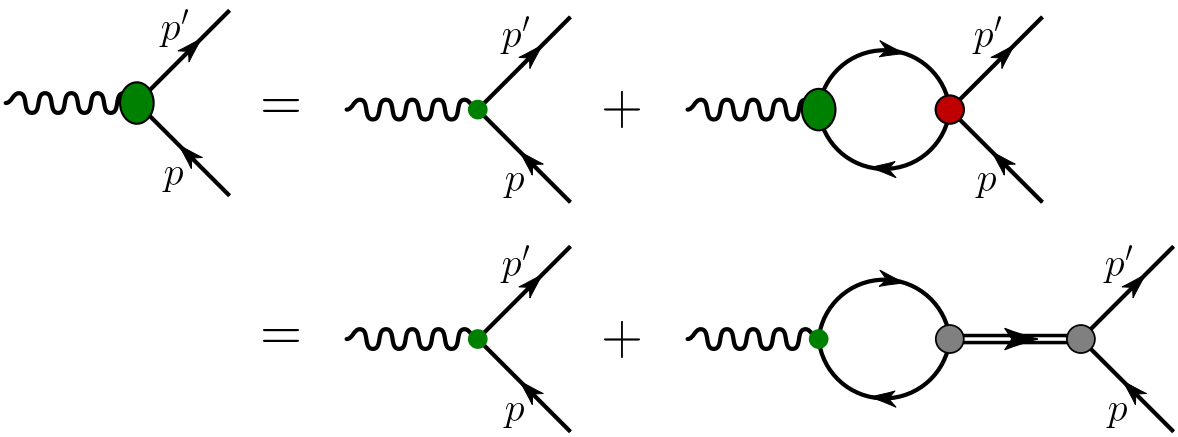

Figure 4.4.1: The quark-photon vertex including the vector meson intermediate states automatically. The large shaded is the solution of the inhomogeneous BSE, which represents the quark-photon vertex. The small dotted is the inhomogeneous driving term, the shaded circle is the interaction kernel of $q\bar{q}$ in the NJL model in Eq. 3.4.2, for which only ρ and ω intermediate states (interaction channels) contribute.

The large oval denotes the quark-photon vertex $\Lambda^{\mu}_{\gamma Q}(p',p)$. The kernel of the four-fermion interaction is given in Eq. (3.4.2), that is $K_{\alpha\beta,\gamma\delta} = -2iG_{\omega}(\gamma_{\mu})_{\alpha\beta}(\gamma^{\mu})_{\gamma\delta} - 2iG_{\rho}(\gamma_{\mu}\tau)_{\alpha\beta}(\gamma^{\mu}\tau)_{\gamma\delta}$. This quark-photon vertex automatically combines the pole structure of the vertex corresponding to the vector mesons of the homogeneous BSE. Using this method, the bare quark-photon vertex in Eq. 4.2.1, which has an isoscalar and an isovector component, is generally expressed as

$$\begin{aligned}\Lambda^{\mu}_{\gamma Q}(p',p) &= \frac{1}{6}\Lambda^{\mu}_{\omega}(p',p) + \frac{\tau_3}{2}\Lambda^{\mu}_{\rho}(p',p) \\ &= \frac{(1+\tau_3)}{2}\Lambda^{\mu}_{U}(p',p) + \frac{(1-\tau_3)}{2}\Lambda^{\mu}_{D}(p',p),\end{aligned} \tag{4.4.1}$$

where the subscripts U, D denote the dressed up and down quarks, respectively. The second line in Eq. (4.4.1) shows that the quark-photon vertex is separated into flavor sectors assigned by dressed quarks.

In general, the quark-photon vertex has 4 longitudinal and 8 transverse components (with respect to the photon momentum) [8]. By following the expression of the standard NJL $\bar{q}q$ kernel interaction, which is only momentum transfer dependent, the contributions to the quark-photon vertex in Eq. (4.4.1) from the NJL BSE have the form

$$\Lambda^{(BSE)\mu}_{\omega}(q) = \gamma^{\mu} + \left(\gamma^{\mu} - \frac{q^{\mu}\not{q}}{q^2}\right)\hat{F}_{1\omega}(q^2) + \frac{i\sigma^{\mu\nu}q_{\nu}}{2M}F_{2\omega}(q^2), \tag{4.4.2}$$

$$\Lambda^{(BSE)\mu}_{\rho}(q) = \gamma^{\mu} + \left(\gamma^{\mu} - \frac{q^{\mu}\not{q}}{q^2}\right)\hat{F}_{1\rho}(q^2) + \frac{i\sigma^{\mu\nu}q_{\nu}}{2M}F_{2\rho}(q^2). \tag{4.4.3}$$

[8] There are 12 Lorentz structures in total, where each Lorentz structure is a scalar function of the three variables, namely, q^2, p'^2 and p^2, respectively.

The forms in Eqs. (4.4.2) and (4.4.3) satisfy the Ward-Takahashi identity (WTI), which takes the form

$$q_\mu \Lambda^\mu_{\gamma Q}(p',p) = \left(\frac{1}{6}+\frac{\tau_3}{2}\right)\left[S^{-1}(p') - S^{-1}(p)\right], \tag{4.4.4}$$

where $S^{-1}(p')$ is a quark propagator, which was defined in Eq. (3.5.4). This is demanded by U(1) vector gauge invariance.

Using the current conservation, the terms contain $\frac{q^\mu \not{q}}{q^2}$ in Eqs. (4.4.2) and (4.4.3) cannot contribute to the hadron form factors. Then the final effective vertex can be written as

$$\Lambda_i^{(bse)\mu}(q) = \gamma^\mu F_{1i}(q^2) + \frac{i\sigma^{\mu\nu}q_\nu}{2M}F_{2i}(q^2), \tag{4.4.5}$$

with $i = \omega, \rho$ and $F_{1i}(q^2) = 1 + \hat{F}_{1i}(q^2)$. The vertex $F_{1\omega}(q^2) = 1 = F_{1\rho}$ and $F_{2\omega}(q^2) = 0 = F_{2\rho}(q^2)$ for the pointlike quark. Note that the quark interaction in the NJL model not only generates dynamically a dressed quark mass, but also generates nontrivial dressed quark form factors.

The inhomogeneous BSE for the quark-photon vertex, as illustrated in Fig. 4.4.1, can be formally defined by

$$\Lambda^\mu_{\gamma Q}(p',p) = \gamma^\mu \hat{Q} + \sum_\Omega iK_\omega \Omega \int \frac{d^4k}{(2\pi)^4} Tr\left[\bar{\Omega} S(k+q)\Lambda^\mu_{\gamma Q}(p',p)S(k)\right], \tag{4.4.6}$$

where $\hat{Q}$ is the quark charge operator, as defined in Eq. (4.2.1). The interaction kernel in the second term is defined in Eq. (3.4.2) and the quark-photon vertex is given in Eq. (4.4.1), (4.4.2) and (4.4.3). This implies that the interaction channel contributes only isovector-vector and isoscalar-vector terms, as pointed out earlier. By solving the inhomogeneous BSE self-consistently with the electromagnetic current in Eq. (4.4.3), the dressed quark form factors are obtained :

$$F_{1i}(q^2) = \frac{1}{1+2G_i\Pi_{vv}(q^2)}, \qquad F_{2i}(q^2) = 0, \tag{4.4.7}$$

where $i = \omega, \rho$. Then the dressed U and D quarks, which are given by BSE, take the form

$$F_{1Q}^{(bse)}(Q^2) = \frac{1}{6}F_{1\omega}(Q^2) \pm \frac{1}{2}F_{1\rho}(Q^2), \tag{4.4.8}$$

where the plus sign stands for the dressed U quark and the superscript bse indicates that the form factors are taken from the BSE. In Section 4.5, we will evaluate the kaon and pion form factors with dressed quarks using this procedure.

4.5 Kaon Form Factor With Dressed Quark

In this section, we develop the kaon form factor results in Eq. (4.2.8) with the modification of the quark-photon vertex in Eq. (4.4.8) incorporating the dressed quark,

which automatically includes the vector meson intermediate states such as ρ, ω and ϕ as illustrated in Fig. (4.4.1). As discussed earlier in Section 4.4, the vector mesons are accommodated by separating an isoscalar and an isovector component in the quark-photon vertex. Recalling again here, the modification of the quark-photon vertex in Eq. 4.4.1, is expressed as

$$\Lambda^{\mu}_{\gamma Q}(p',p) = \frac{1}{6}\Lambda^{\mu}_{\omega}(p',p) + \frac{\tau_3}{2}\Lambda^{\mu}_{\rho}(p',p), \tag{4.5.1}$$

where $\Lambda^{\mu}_{\omega}(p',p)$, $\Lambda^{\mu}_{\rho}(p,p')$ are the vertex functions from the NJL BSE.

From the expression of the three flavor NJL Lagrangian in Eq. (3.1.6), only the isovector-vector interaction, $-2iG_{\rho}\left(\gamma_{\mu}\mathbf{t}\right)_{\alpha\beta}\left(\gamma_{\mu}\mathbf{t}\right)_{\gamma\delta}$ and the isoscalar-vector interaction, $-2iG_{\omega}\left(\gamma_{\mu}\right)_{\alpha\beta}\left(\gamma_{\mu}\right)_{\gamma\delta}$ terms have a role. However there is no G_{ϕ} coupling constant in the SU(3) NJL Lagrangian in Eq. (3.1.6), so one should simply use either G_{ω} or G_{ρ} coupling constants. In order to properly include the ϕ vector meson in the calculation, one should generalize the SU(3) NJL Lagrangian to SU(3) flavor and work with SU(3) flavor matrices in the Bethe-Salpeter (BS) vertices and the charge operator, $\hat{Q}$.

In the SU(3) NJL, the ϕ has flavor singlet and octet pieces and therefore in principle the ϕ should be a weighted average of the G_{ω} and G_{ρ} coupling constants, however since they are very similar, we simply multiplied the strange quark contributions by the dressed quark form factor, $F_{1\phi}(q^2)$, as we determine in Eq. (4.5.5). After a simple derivation, the effective vertex functions in the NJL BSE model, which satisfy the WTI, are then expressed as

$$\Lambda^{(bse)\mu}_{\omega}(q) = \gamma^{\mu}F_{1\omega}(q^2) + \frac{i\sigma^{\mu\nu}q_{\nu}}{2M}F_{2\omega}(q^2), \tag{4.5.2}$$

$$\Lambda^{(bse)\mu}_{\rho}(q) = \gamma^{\mu}F_{1\rho}(q^2) + \frac{i\sigma^{\mu\nu}q_{\nu}}{2M}F_{2\rho}(q^2), \tag{4.5.3}$$

$$\Lambda^{(bse)\mu}_{\phi}(q) = \gamma^{\mu}F_{1\phi}(q^2) + \frac{i\sigma^{\mu\nu}q_{\nu}}{2M}F_{2\phi}(q^2), \tag{4.5.4}$$

where the ρ and ω mesons contribute to the up and down quark form factors and the ϕ meson contribute to the strange quark form factor. The expression for the dressed quark form factors, $F_{1i}(q^2)$ and $F_{2i}(q^2)$ in Eq. (4.5.2), which automatically contain the vector mesons, can be defined as

$$F_{1i}(q^2) = \frac{1}{1 + 2G_i\Pi_{vv}(q^2)} \qquad\qquad F_{2i}(q^2) = 0, \tag{4.5.5}$$

where $i = \omega, \rho, \phi$. Based upon the reduced t-matrix, the $F_{1\omega}$, $F_{1\rho}$ and $F_{1\phi}$ possess a pole at $q^2 = m_{\omega}^2$, $q^2 = m_{\rho}^2$ and $q^2 = m_{\phi}^2$, respectively. The G_i is the coupling constant of the $i(= \rho, \omega, \phi)$ vector mesons, and $\Pi_{vv}(q^2)$ is the bubble graph in the ρ, ω and ϕ channels, which is defined in Eq. (3.4.13). Note that the NJL BSE does not have a Pauli form factor for the dressed quark because they do not include the tensor-tensor 4-fermion interaction. The dressed up, anti-down and anti-strange quark form factors are depicted in Fig. 4.6.1.

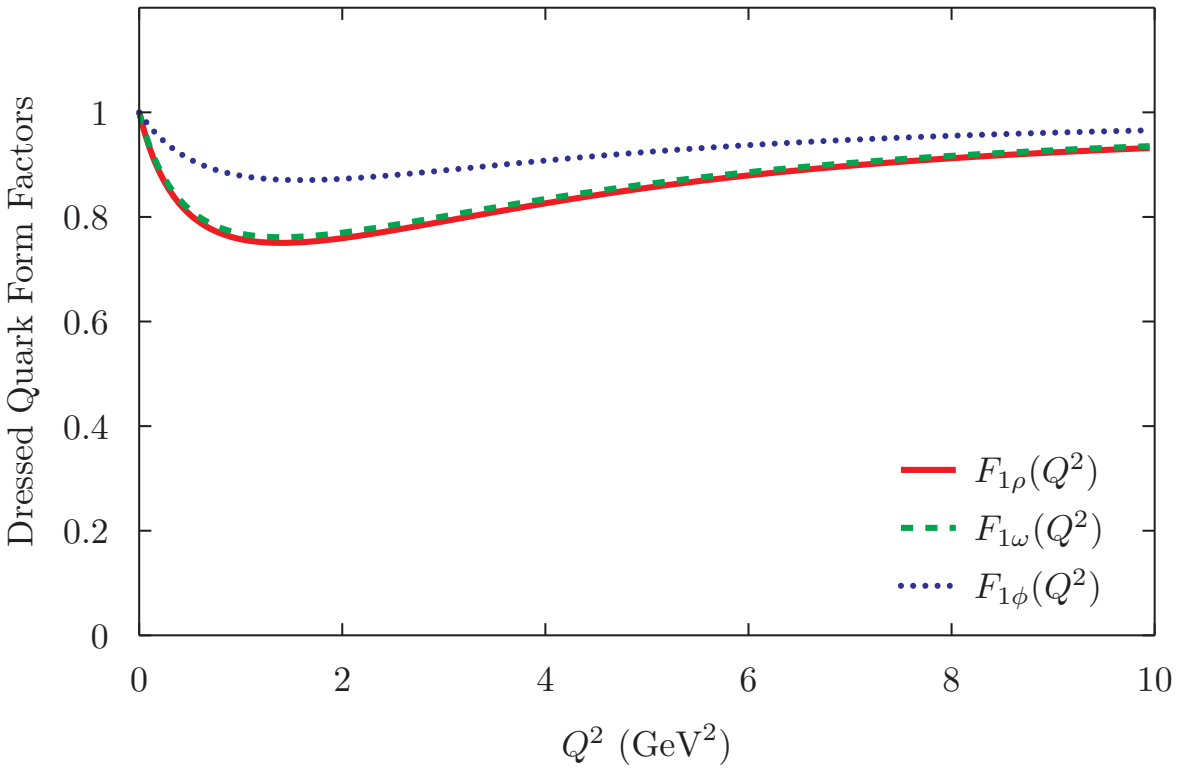

Figure 4.5.1: The dressed up, anti-down and anti-strange quark form factors. These are obtained from the inhomogeneous BSE associated with the electromagnetic current.

The expression for the bubble graph in Eq. (4.5.5), after applying the Feynman parameterization and PTR scheme, has the form

$$\Pi_{vv}(q^2) = -\frac{N_C}{\pi^2} q^2 \int_0^1 dx \int_{\frac{1}{(\Lambda_{\rm UV})^2}}^{\frac{1}{(\Lambda_{\rm IR})^2}} \frac{d\tau}{\tau} e^{-\tau(q^2(x^2-x)+M^2)}[x-x^2]. \tag{4.5.6}$$

Where the subscript vv denotes the vector meson intermediate states (ρ, ω and ϕ). For the ϕ vector meson intermediate state, we set $M = M_s$, which is constituent strange quark mass, because we assume that ϕ decays into ss quark states.

Therefore, with the NJL Lagrangian of Eq. (3.1.6) there is no flavour mixing in the dressed quark form factors, in analogy with the dressed quark masses. The dressed quark form factors are illustrated in Fig. 4.6.1. In the limit $Q^2 \to \infty$ these form factors reduce to the elementary quark charges, as must be the case in QCD because of asymptotic freedom. For small Q^2 these results are similar to vector meson dominance, where the dressed u and d quarks are dressed by ρ and ω mesons and the dressed s quark by the ϕ meson. Note, the denominators in Eqs. (4.5.7)- (4.5.9) are the same as the pole condition obtained by solving the Bethe-Salpeter in the ρ, ω or ϕ channels. Therefore the dressed u and d quark form factors have poles at $Q^2 = -m_\rho^2 = -m_\omega^2$, and the dressed s quark form factor has a pole at $Q^2 = -m_\phi^2$.

Thus, the dressed quark form factors for the u, d and s which calculated from BSE

reads:

$$F_{1U}^{(bse)}(Q^2) = \frac{1}{6}F_{1\omega}(Q^2) + \frac{1}{2}F_{1\rho}(Q^2), \tag{4.5.7}$$

$$F_{1D}^{(bse)}(Q^2) = \frac{1}{6}F_{1\omega}(Q^2) - \frac{1}{2}F_{1\rho}(Q^2), \tag{4.5.8}$$

$$F_{1S}^{(bse)}(Q^2) = -\frac{1}{3}F_{1\phi}(Q^2), \tag{4.5.9}$$

where the superscript (bse) indicates that the quark form factors are computed from the BSE. By following the form of the form factor in Eq. (4.2.8), the dressed quark form factors in Eq. (4.5.7) can be decomposed into the dressed quark sector form factors, that is

$$F_{1U}^{(bse)}(Q^2) = e_u F_{1U}^{u}(Q^2) - e_d F_{1U}^{d}(Q^2), \tag{4.5.10}$$

$$F_{1D}^{(bse)}(Q^2) = e_u F_{1D}^{u}(Q^2) - e_d F_{1D}^{d}(Q^2), \tag{4.5.11}$$

$$F_{1S}^{(bse)}(Q^2) = -e_s F_{1S}^{s}, \tag{4.5.12}$$

where $F_{1U}^{u}(Q^2)$, $F_{1D}^{d}(Q^2)$ and $F_{1S}^{s}(Q^2)$ are the dressed up, down and strange quark sector form factor.

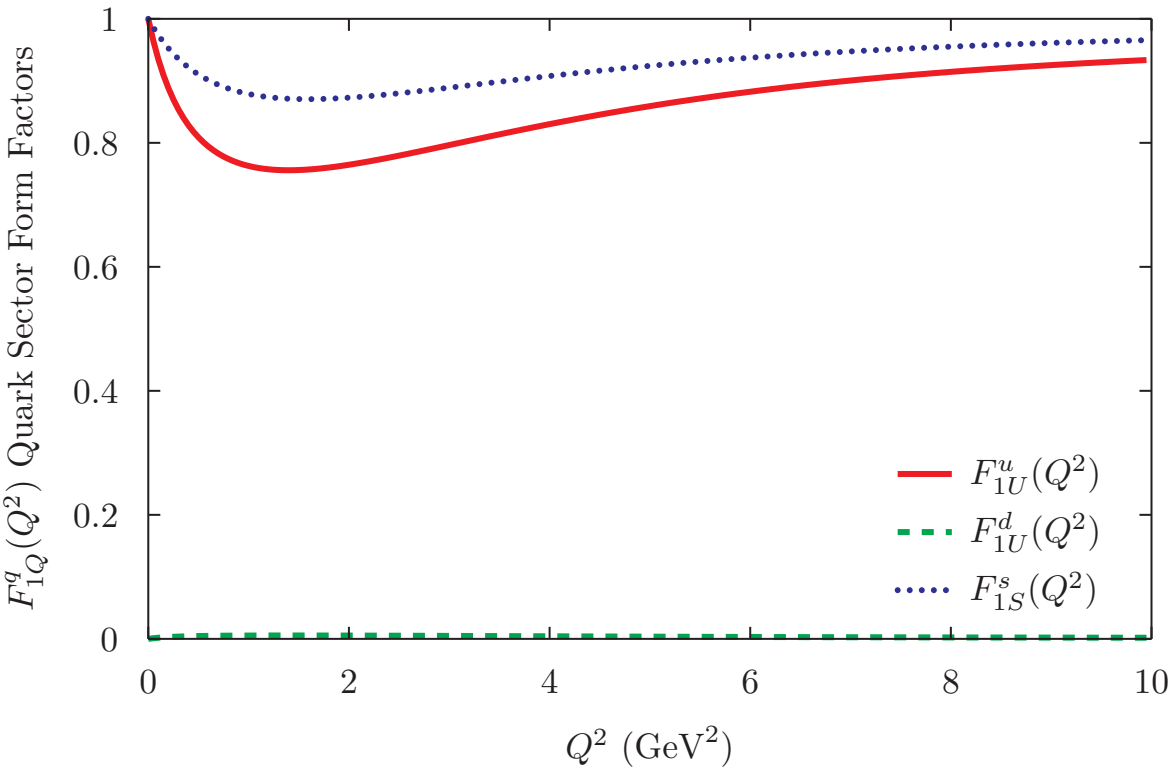

Figure 4.5.2: The dressed up, anti-down and anti-strange quark Dirac form factors in Eq. (4.5.13) separated into quark sector. The red solid line is the up quark sector (u) of the dressed up quark (U), the blue dotted line represents the strange quark sector (s) of the dressed strange quark (S) and the green dashed line is the down quark sector (d) of the dressed up quark (U).

These quark sector form factors in Eq. (4.5.10) are defined as

$$F^u_{1U}(Q^2) = \frac{1}{2}\left[F_{1\omega}(Q^2) + F_{1\rho}(Q^2)\right], \tag{4.5.13}$$

$$F^d_{1U}(Q^2) = \frac{1}{2}\left[F_{1\omega}(Q^2) - F_{1\rho}(Q^2)\right], \tag{4.5.14}$$

$$F^u_{1D}(Q^2) = \frac{1}{2}\left[F_{1\omega}(Q^2) - F_{1\rho}(Q^2)\right], \tag{4.5.15}$$

$$F^d_{1D}(Q^2) = \frac{1}{2}\left[F_{1\omega}(Q^2) + F_{1\rho}(Q^2)\right], \tag{4.5.16}$$

$$F^s_{1S}(Q^2) = F_{1\phi}(Q^2). \tag{4.5.17}$$

The dressed quark BSE form factors are given in Eq. (4.5.5). The results satisfy the SU(2) charge symmetry, where $F^u_{1D}(Q^2) = F^d_{1U}(Q^2)$ and $F^d_{1D}(Q^2) = F^u_{1U}(Q^2)$. The plot of the dressed quark sectors in Eq. (4.5.13) are depicted in Fig. 4.5.2.

Finally, by considering the dressed quark BSE form factors in Eq. (4.5.7), one automatically includes the vector mesons (ρ, ω and ϕ) intermediate states in Fig. 4.4.1. The total kaon form factor with dressed quarks in Eq. (4.2.8) can be compactly written as

$$F_K(Q^2) = [F_{1U}(Q^2) f^{us}_K(Q^2) - F_{1S}(Q^2) f^{su}_K(Q^2)] + [F_{2U}(Q^2) - F_{2S}(Q^2)] f^T_K(Q^2), \tag{4.5.18}$$

with $Q^2 = -q^2$ is the four momentum transfer of the virtual photon and the expression for the $f^{us}_K(Q^2)$ and $f^{su}_K(Q^2)$ are defined

$$\begin{aligned} f^{us}_K(Q^2) = {} & \frac{N_C g^2_{Kq\bar{q}}}{4\pi^2} \int_0^1 dx \int_{\frac{1}{(\Lambda_{UV})^2}}^{\frac{1}{(\Lambda_{IR})^2}} \frac{d\tau}{\tau} e^{-\tau(q^2(x^2-x)+M_1^2)} \\ & + \frac{N_C g^2_{Kq\bar{q}}}{4\pi^2} \int_0^1 dx \int_0^{1-x} dz \int_{\frac{1}{(\Lambda_{UV})^2}}^{\frac{1}{(\Lambda_{IR})^2}} d\tau e^{-\tau(k^2[(x+z)^2-(x+z)]-xzq^2+M_2^2(1-x-z)+M_1^2(x+z))} \\ & \times [k^2(x+z) + (M_1 - M_2)^2(x+z) - 2M_2^2 + 2M_2 M_1], \end{aligned} \tag{4.5.19}$$

$$\begin{aligned} f^{su}_K(Q^2) = {} & \frac{N_C g^2_{Kq\bar{q}}}{4\pi^2} \int_0^1 dx \int_{\frac{1}{(\Lambda_{UV})^2}}^{\frac{1}{(\Lambda_{IR})^2}} \frac{d\tau}{\tau} e^{-\tau(q^2(x^2-x)+M_2^2)} \\ & + \frac{N_C g^2_{Kq\bar{q}}}{4\pi^2} \int_0^1 dx \int_0^{1-x} dz \int_{\frac{1}{(\Lambda_{UV})^2}}^{\frac{1}{(\Lambda_{IR})^2}} d\tau e^{-\tau(k^2[(x+z)^2-(x+z)]-xzq^2+M_1^2(1-x-z)+M_2^2(x+z))} \\ & \times [k^2(x+z) + (M_2 - M_1)^2(x+z) - 2M_1^2 + 2M_1 M_2], \end{aligned} \tag{4.5.20}$$

where, in our work, we take $M_1 = M_u$ and $M_2 = M_s$ which stand for the constituent up and anti-strange quark masses, respectively and $f^{us}_K(Q^2)$ is the vector kaon body form factor, where the first superscript indicates the struck quark and the second the spectator, as depicted in Fig. 4.2.1. Similarly, the total pion form factor with dressed quarks has the form

$$F_\pi(Q^2) = [F_{1U}(Q^2) - F_{1D}(Q^2)] f_\pi^{ud}(Q^2) + [F_{2U}(Q^2) - F_{2D}(Q^2)] f_\pi^T(Q^2), \quad (4.5.21)$$

here $f_\pi^{ud}(Q^2) = f_\pi^{du}(Q^2)$ is the vector pion body form factors, as depicted in Fig. 4.2.1. The $f_\pi^{ud}(Q^2)$ term in Eq. (4.5.21) is defined :

$$\begin{aligned} f_\pi^{ud}(Q^2) = & \frac{N_C g_{\pi q\bar{q}}^2}{4\pi^2} \int_0^1 dx \int_{\frac{1}{(\Lambda_{UV})^2}}^{\frac{1}{(\Lambda_{IR})^2}} \frac{d\tau}{\tau} e^{-\tau(q^2(x^2-x)+M_1^2)} \\ & + \frac{N_C g_{\pi q\bar{q}}^2}{4\pi^2} \int_0^1 dx \int_0^{1-x} dz \int_{\frac{1}{(\Lambda_{UV})^2}}^{\frac{1}{(\Lambda_{IR})^2}} d\tau e^{-\tau(k^2[(x+z)^2-(x+z)]-xzq^2+M_2^2(1-x-z)+M_1^2(x+z))} \\ & \times [k^2(x+z) + (M_1 - M_2)^2(x+z) - 2M_2^2 + 2M_2 M_1]. \end{aligned} \quad (4.5.22)$$

For simplicity, the kaon and pion form factors in Eqs. (4.5.18) and (4.5.21) are decomposed into their corresponding quark sector form factors, it has the form

$$F_K(Q^2) = e_u F_K^u(Q^2) - e_s F_K^s(Q^2), \quad (4.5.23)$$
$$F_\pi(Q^2) = e_u F_\pi^u(Q^2) - e_d F_\pi^d(Q^2), \quad (4.5.24)$$

where $F_K^u(Q^2), F_K^s(Q^2)$ and $F_\pi^d(Q^2)$ denote the up, anti-strange and anti-down quark sector form factors, respectively. They are defined as

$$F_\pi^u(Q^2) = \left[\frac{1}{4} F_{1\omega}(Q^2) + \frac{3}{4} F_{1\rho}(Q^2)\right] f_\pi^{ud}(Q^2), \quad (4.5.25)$$
$$F_\pi^d(Q^2) = \left[\frac{1}{4} F_{1\omega}(Q^2) + \frac{3}{4} F_{1\rho}(Q^2)\right] f_\pi^{du}(Q^2), \quad (4.5.26)$$
$$F_K^u(Q^2) = \left[\frac{1}{4} F_{1\omega}(Q^2) + \frac{3}{4} F_{1\rho}(Q^2)\right] f_K^{us}(Q^2), \quad (4.5.27)$$
$$F_K^s(Q^2) = \left[F_{1\phi}(Q^2)\right] f_K^{su}(Q^2), \quad (4.5.28)$$

with $F_{1\omega}(Q^2)$, $F_{1\rho}(Q^2)$ and $F_{1\phi}(Q^2)$ defined in Eq. (4.4.7). For the sake of simplicity, we treat the $G_\omega = G_\rho$ in this work. This is because the m_ω is not given by the G_ω term. In fact, the ω-mass, m_ω is given by a combination of G_ρ and G_ω [9], whereas the ρ-mass is determined by G_ρ. By setting $G_\omega = G_\rho$, the quark sector form factors in Eq. (4.5.25) has the form

$$F_\pi^u(Q^2) = \left[F_{1\rho}(Q^2)\right] f_\pi^{ud}(Q^2), \quad (4.5.29)$$
$$F_\pi^d(Q^2) = \left[F_{1\rho}(Q^2)\right] f_\pi^{du}(Q^2), \quad (4.5.30)$$
$$F_K^u(Q^2) = \left[F_{1\rho}(Q^2)\right] f_K^{us}(Q^2), \quad (4.5.31)$$
$$F_K^s(Q^2) = \left[F_{1\phi}(Q^2)\right] f_K^{su}(Q^2). \quad (4.5.32)$$

[9] The ϕ mass is also likely determined by G_ρ and G_ω and in principle there is a complicated in the VMD equations.

4.6 Results for the Kaon Form Factor with Dressed Quarks

In this section, we discuss our numerical results of the development of the kaon and pion form factor including the vector mesons correlations in the NJL model. The parameters used are the same as the parameters used in Section 4.3 and Table 4.3.1. In our calculation, we include the dressing of the quark-photon vertex, as explained in the previous section. The dressed up and anti-down quark BSE form factor results are depicted in Fig. 4.6.1. For the up and down BSE quark form factors, our result is consistent with the result in Ref. [192]. However, in this thesis, we extend our calculation for the dressed anti-strange quark BSE form factor. Our results on the dressed anti-strange quark BSE form factor is also shown in Fig 4.6.1.

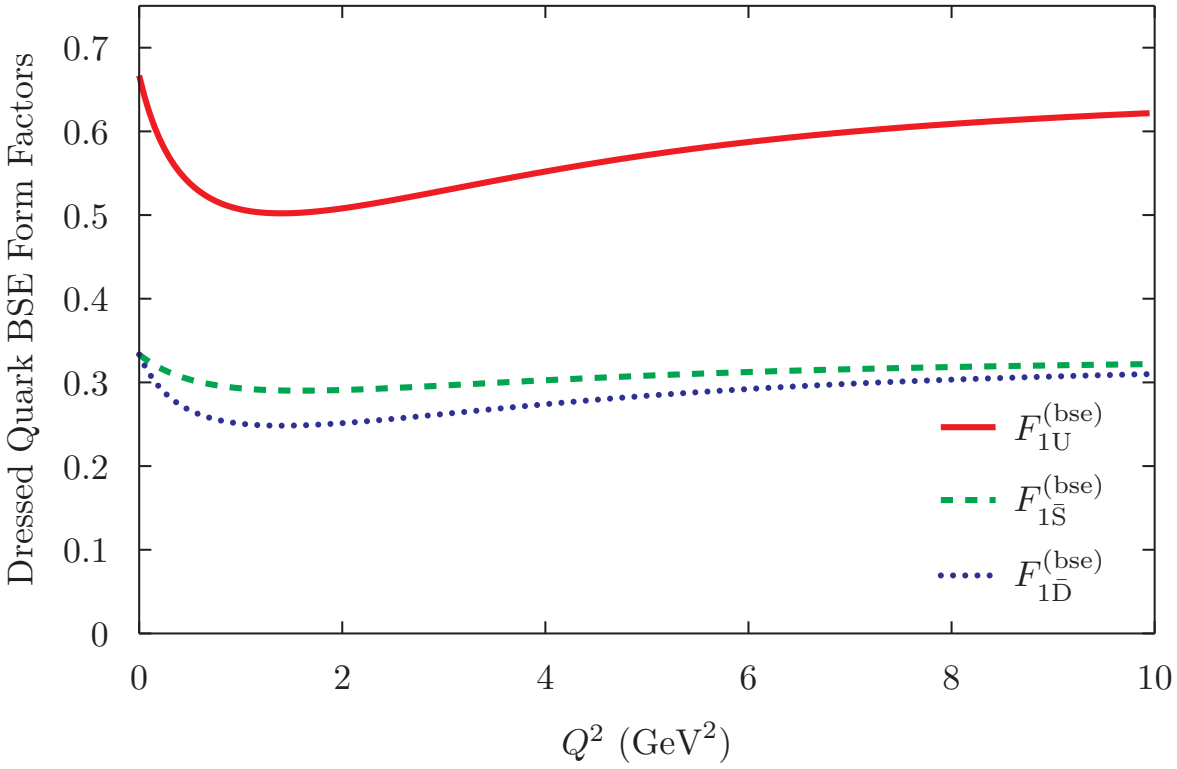

Figure 4.6.1: Dressed BSE quark form factors. The dressed up quark BSE form factor (red solid line), the dressed anti-down quark BSE form factor (blue dotted line) and the dressed anti-strange quark BSE form factor (green dashed line) are shown. The bse superscript stands for the quark form factors obtained from the BSE. The U, D, S subscripts denote the dressed quark BSE form factors.

Figure 4.6.1 shows that the up quark BSE form factor increases smoothly with increasing Q^2 above about 1 GeV^2. In addition, the anti-down quark BSE from factor has a similar trend as the up quark BSE form factor, but they are different in magnitude. The anti-strange quark BSE form factor almost has the same trend as the anti-down quark BSE form factor but the magnitude of the anti-strange quark BSE form factor is a bit larger than the anti-down quark BSE form factor. This indicates that these quark

BSE form factors give a sizable contribution to the kaon and pion form factors. This is because the quark BSE form factors do not drop to zero as the transfer four momentum goes to infinity, $Q^2 \to \infty$. Figure. 4.6.1 also shows that the quark BSE form factors behave as the bare current quark at large Q^2. This is given by $F_{1U}^{(bse)}(Q^2) = e_u, F_{1D}^{(bse)} = e_d$ and $F_{1S}^{(bse)} = e_s$ at infinite Q^2. In other words, this indicates that the virtual photon interacts with a bare current quark at large Q^2. Our result is consistent with the QCD based on asymptotic freedom and the result in Ref. [192].

Figure 4.6.2 displays the numerical results for the kaon form factor with a dressed quark BSE form factor. We clearly observe the different contributions of the valence quark sector form factors of the kaon to the total kaon form factor. The figure is plotted over the range $Q^2 = 0$ - 6 GeV^2. The valence quark contribution to the kaon form factor arising from the anti-strange quark sector form factor $F_{K^+}^s(Q^2)$ is dominant over the up quark sector form factor, $F_{K^+}^u(Q^2)$ over the whole Q^2 region. The difference is clearly seen in Figs. 4.6.3 and 4.6.4, where the figures are plotted at larger Q^2. Later on, a comparison with the existing experimental data [183] is depicted in Fig. 4.6.5.

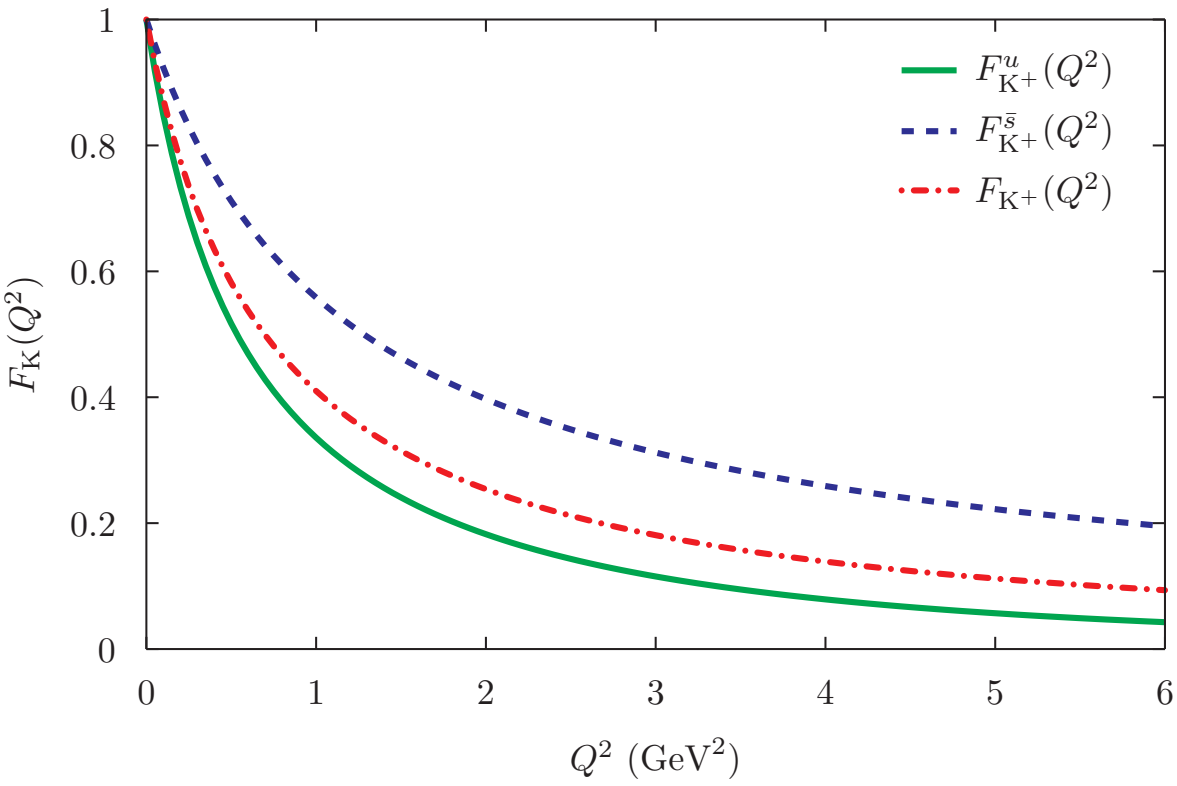

Figure 4.6.2: The total kaon form factor, $F_{K^+}(Q^2)$ and its quark sector form factors. The up quark sector form factor of the kaon (green solid line), $F_{K^+}^u(Q^2)$, the anti-strange quark sector form factor of the kaon (blue dashed line), $F_{K^+}^s(Q^2)$, and the total kaon form factor (red dot-dashed line) are provided.

Moreover, we plot the anti-strange and up quark sector form factors in the kaon multiplied by Q^2, $Q^2 F_{K^+}^{u,s}(Q^2)$, as a function of Q^2, in order to identify for any significant difference between them. Our result, depicted in Fig. 4.6.3, demonstrates a dramatic

difference between the anti-strange and up quark sector form factors over the range $Q^2 = 0$ - 6 GeV^2. We also show the kaon form factor multiplied by Q^2, $Q^2 F_{K^+}(Q^2)$, as a function of Q^2, up to virtual squared four momentum transfer, $Q^2 = 20$ GeV^2 in Fig. 4.6.4. Figures. 4.6.3 and 4.6.4 show that the anti-strange quark sector form factor of the kaon with the dressed quark is larger than the up quark sector form factor of the kaon with the dressed quark over the whole Q^2 region. Again, this indicates that the anti-strange quark gives a larger contribution than the up quark to the total kaon form factor. Comparison with our previous results on the kaon form factor with bare quark in Section 4.3, our current results on the kaon form factor with the dressed quark and its quark sector form factors is softer, as expected. Furthermore, Figs. 4.6.3 and 4.6.4 is shown in anticipation of future experimental measurements from JLab and COMPASS.

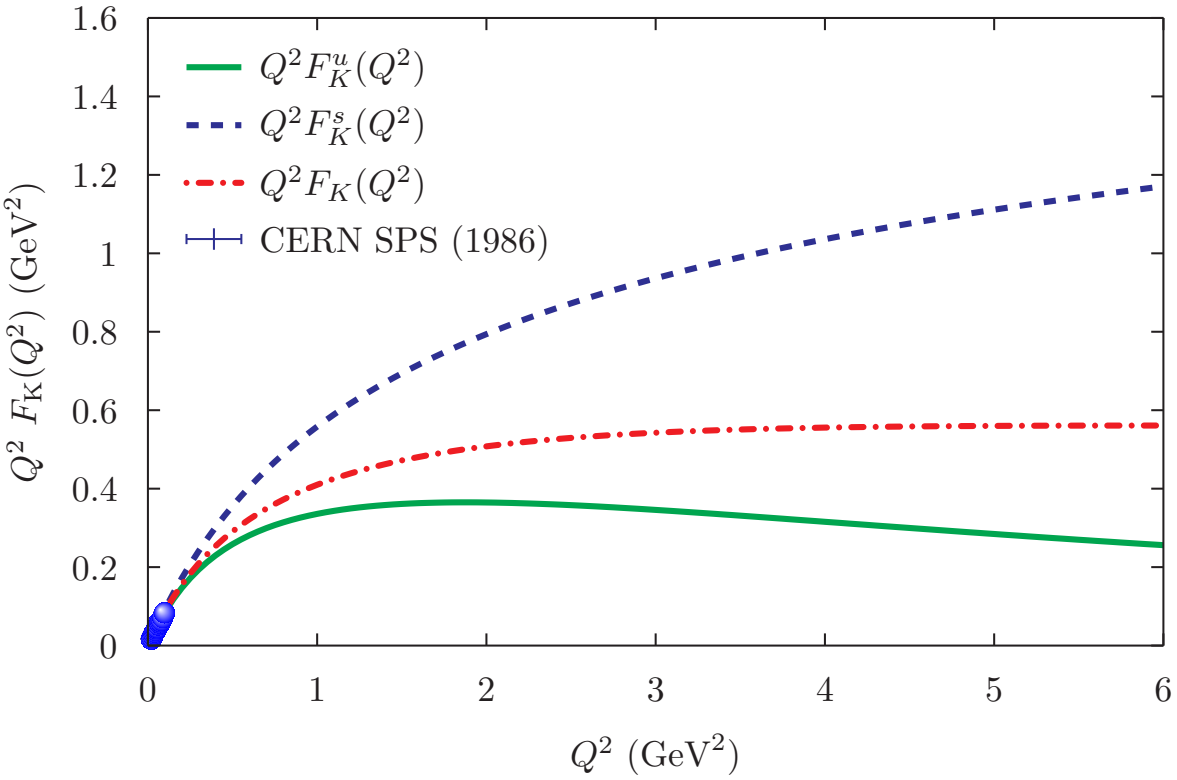

Figure 4.6.3: As in Fig. 4.6.2, but for the $Q^2 F^i_{K^+}(Q^2)$ (where i are quark flavors) is shown up to $Q^2 = 6$ GeV^2.

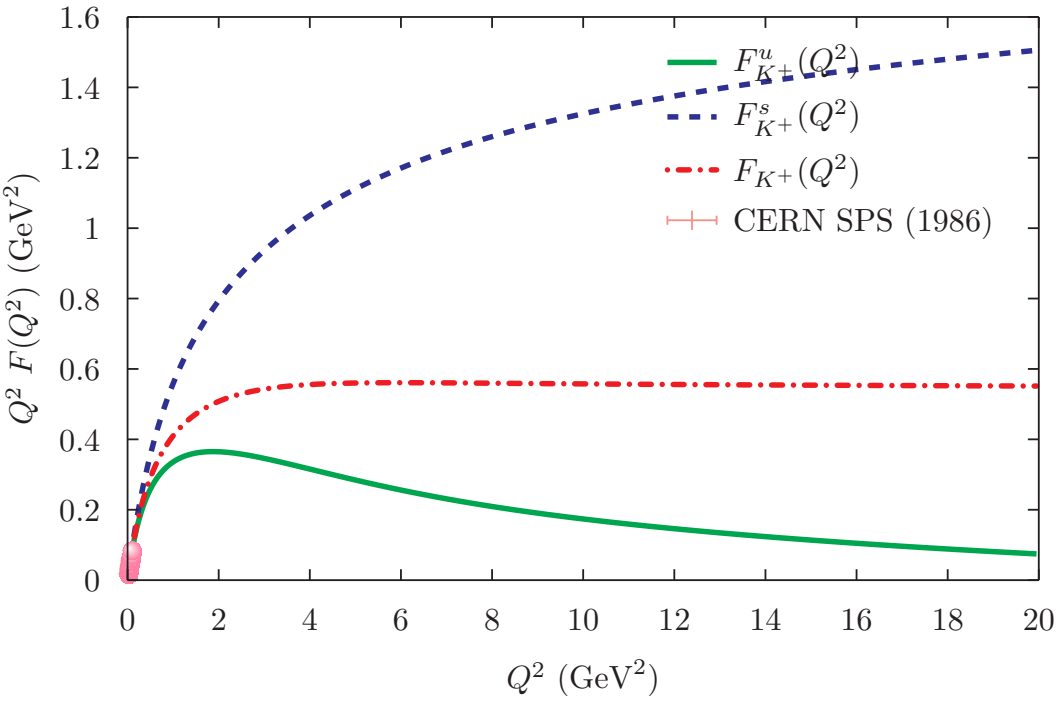

Figure 4.6.4: As in Fig. 4.6.3, but for $Q^2 F^i_{K^+}(Q^2)$ is shown up to $Q^2 = 20$ GeV^2, where $i =$ u, s.

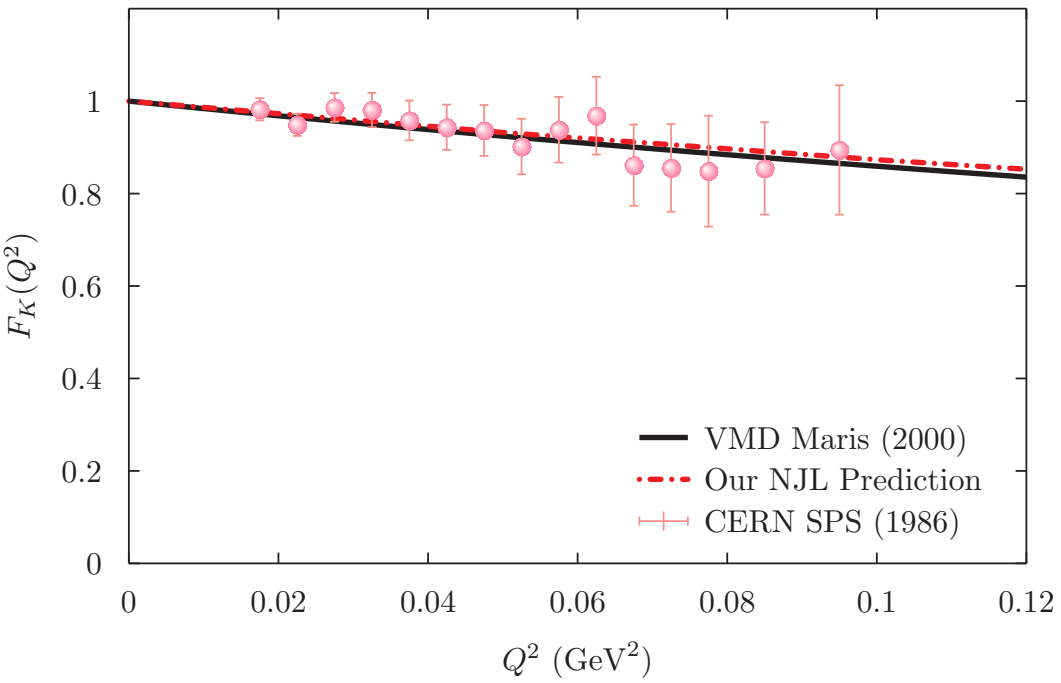

Figure 4.6.5: The total form factor of the kaon, $F_K(Q^2)$ is compared to experimental data [183] up to $Q^2 = 0.12$ GeV^2.

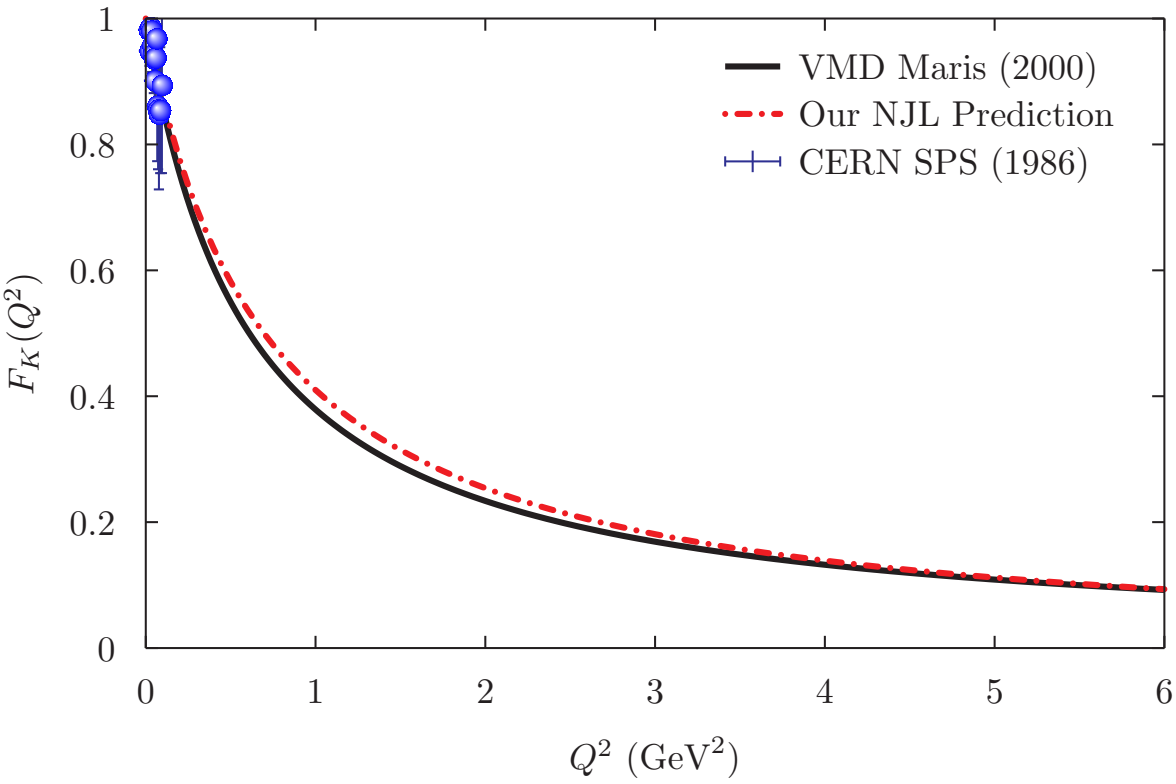

Figure 4.6.6: The total kaon form factor, $F_K(Q^2)$ compared to experimental data and the empirical monopole (VMD) up to $Q^2 = 6$ GeV^2.

Figure 4.6.4 illustrates the quark sector form factor contributions to the total form factor of the kaon over the range $Q^2 = 0$ - 20 GeV^2. Again, the result clearly shows that the anti-strange quark sector form factor reveals a very significant contribution to the total kaon form factor. This is expected due to the higher mass of the anti-strange quark. Thus, we compare our total kaon form factor multiplied by Q^2 with the existing experimental data [183] in Fig. 4.6.7.

In Fig. 4.6.5, we provide a comparison between our kaon form factor result, the available experimental data [183] and the empirical monopole (VMD). The result is compared to available experimental data over the range $Q^2 = 0$ - 0.12 GeV^2. This shows the vector meson dominance model prediction (VMD) (black solid line), our model calculation prediction (red dot-dashed line) and the existing experimental data [183] (blue-point). Our result shows remarkable agreement with the experimental data [183] and the empirical monopole (VMD). Unfortunately, there is as yet no data with which we can compare at larger momentum transfer, Q^2. It will therefore be very interesting and promising to compare our model prediction with experimental data for large Q^2 in the future.

In Fig.4.6.6 our kaon from factor calculation is qualitatively compared with the vector meson dominance (VMD) prediction with m_ρ^2= 0.61 GeV^2, where m_ρ is the mass of the ρ meson, at higher momentum transfer up to 6 GeV^2. We show the VMD prediction (black solid line), our prediction for the kaon form factor (red dot-dashed line) and the existing experimental data [183] (blue point). Our result agrees well with

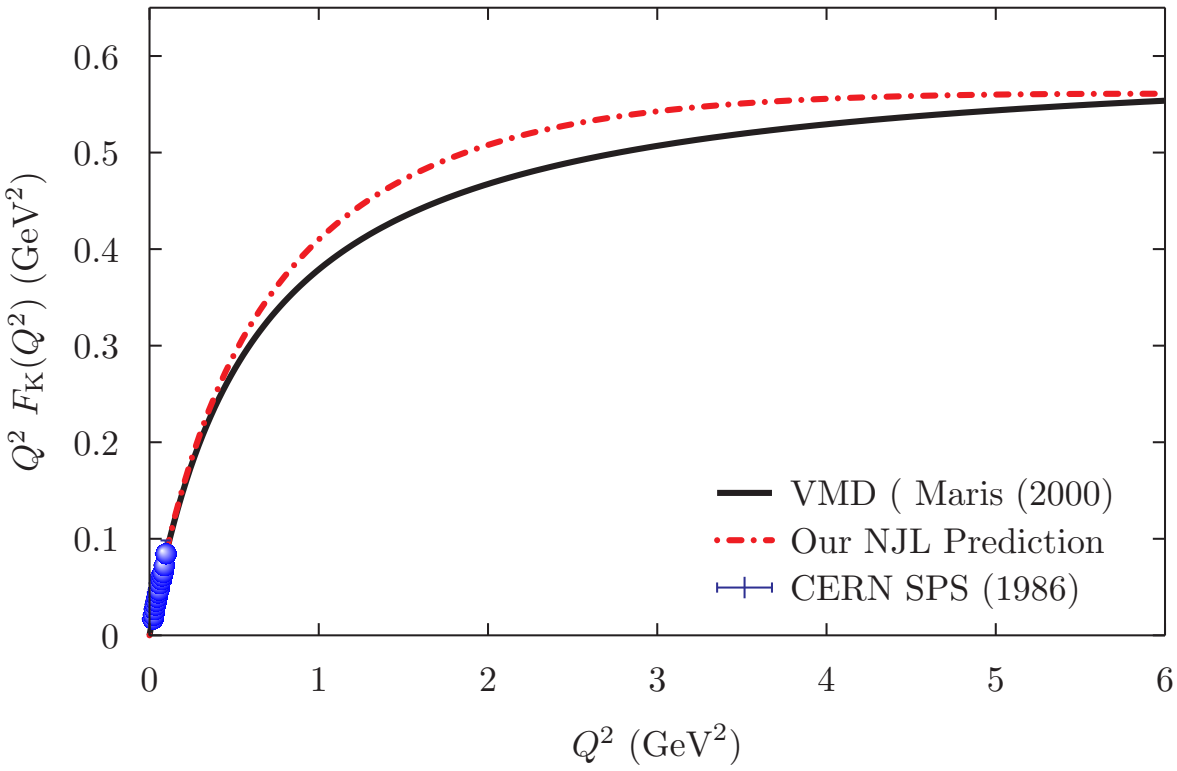

Figure 4.6.7: As in Fig. 4.6.6, but for $Q^2 F_K(Q^2)$.

the VMD result.

Then, in Fig. 4.6.7, we show the kaon form factor multiplied by the momentum transfer, Q^2, $Q^2 F_{K^+}(Q^2)$, in order to illustrate a significant difference between our prediction and the VMD model. The VMD model prediction (black solid line) is shown along with our NJL model prediction for the kaon form factor (red dot-dashed line) and the existing experimental data [183] (blue point). As in Fig. 4.6.3, multiplication by Q^2 is very helpful if one is interested in flavor differences.

Next, we display the result of the pion form factor in Fig. 4.6.8. The pion form factor is straightforwardly computed from the kaon form factor formula by taking $M_s \to M_d = M_u = M_q$, where M_q is the (dressed) constituent quark mass.

Figure 4.6.8 displays our pion form factor in comparison with both the experimental data [167, 168, 176, 177] and the empirical monopole (VMD) model with $m_\rho = 0.775$ GeV [178]. We show the empirical monopole (VMD) prediction [178] (black solid line), the Dyson-Schwinger equation rainbow ladder truncation (DSE-RLT) prediction [178] (green dashed line), the total pion form factor, $F_{\pi^+}(Q^2)$ (red dot-dashed line) and the experimental data – Volmer et al. [167] (salmon point), Amendolia et al. [168] (orange point), Huber et al. [176] (magenta point), and Bebek et al. [177] (blue point). Our pion electromagnetic form factor calculation is consistent with the experimental data [167, 168, 176, 177]. Next, we show the result of the form factor of the pion multiplied by Q^2 in Fig. 4.6.9.

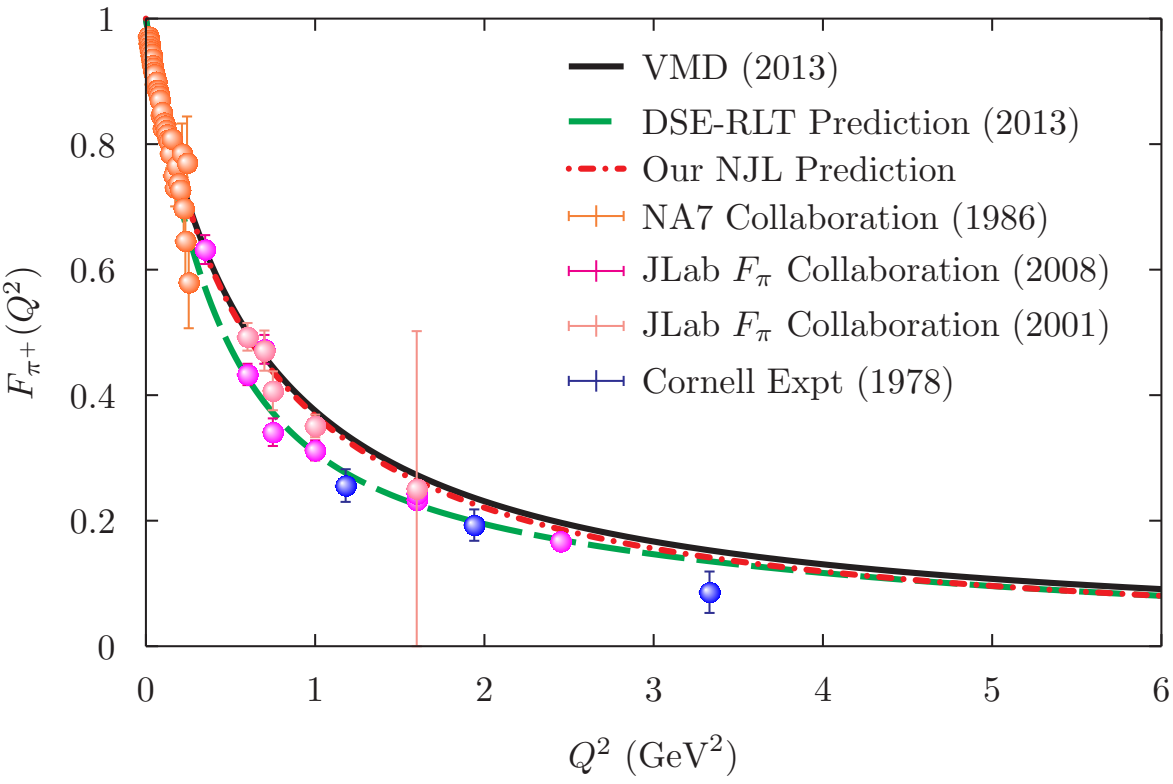

Figure 4.6.8: The pion form factor, $F_\pi(Q^2)$, is compared to the existing experimental data [167, 168, 176, 177].

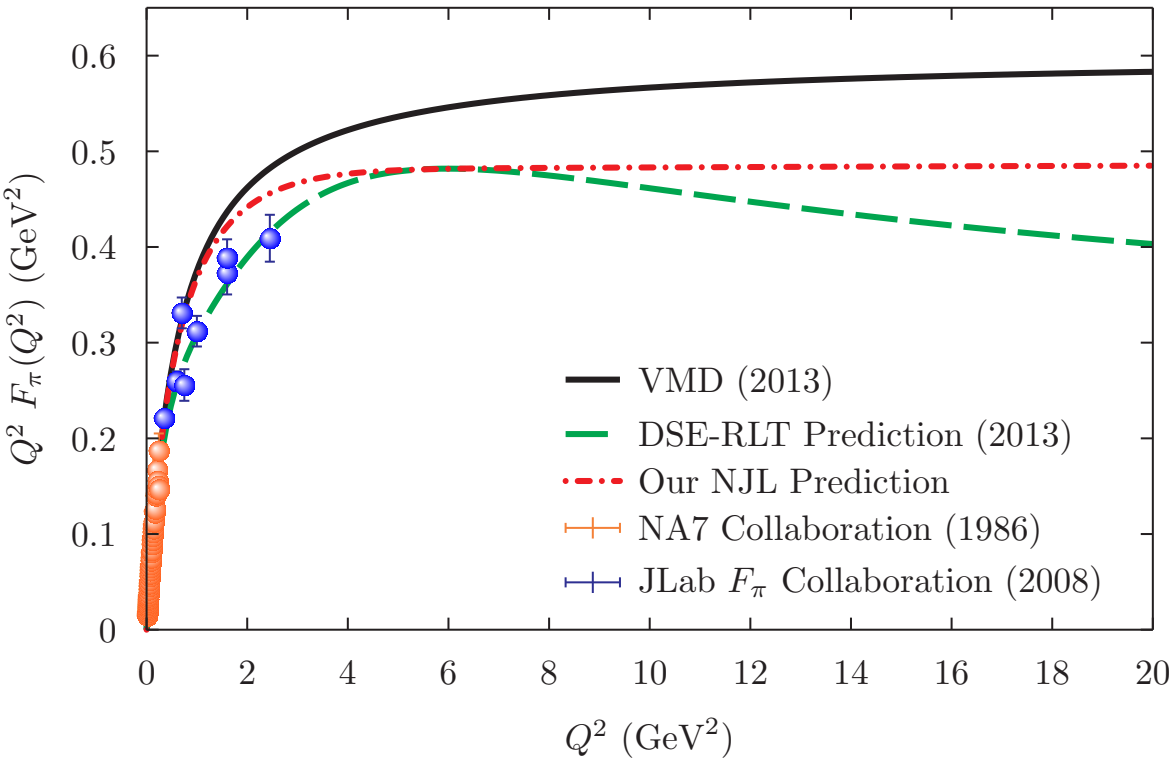

Figure 4.6.9: Total pion form factor with dressed quark multiplied by Q^2, $Q^2F_\pi(Q^2)$.

Figure 4.6.9 exhibits our numerical calculation on the pion electromagnetic form factor with the dressed quark multiplied by Q^2 at large momentum transfer squared, up to $Q^2 = 20$ GeV^2. The empirical monopole (VMD) prediction [178] is the black solid line, the DSE-RLT model prediction [178], our NJL model prediction is the red dot-dashed line and the experimental data are the orange [168] and blue points [176]. This explicitly shows that the pion form factor multiplied by Q^2 is more or less constant (flat) over the whole momentum transfer squared region, starting at around $Q^2 = 2$ GeV^2. However, our pion form factor result has $\frac{1}{Q^2}$ behaviour, as pQCD prediction at large Q^2. Moreover, that the total pion form factor multiplied by the squared four momentum transfer, Q^2, is compared to the existing experimental data [168, 176], is depicted in Fig. 4.6.10. Compared to the kaon result in Fig. 4.6.7, our pion form factor with dressed quark multiplied by the squared four momentum transfer shows a good agreement with existing experimental data [168, 176] and empirical monopole (VMD) prediction [178] at lower Q^2. In addition, our results shows that the Dyson Schwinger equation rainbow-ladder truncation and our NJL model have similar predictions at around $Q^2 = 6$ GeV^2, as clearly indicated in Fig. 4.6.10.

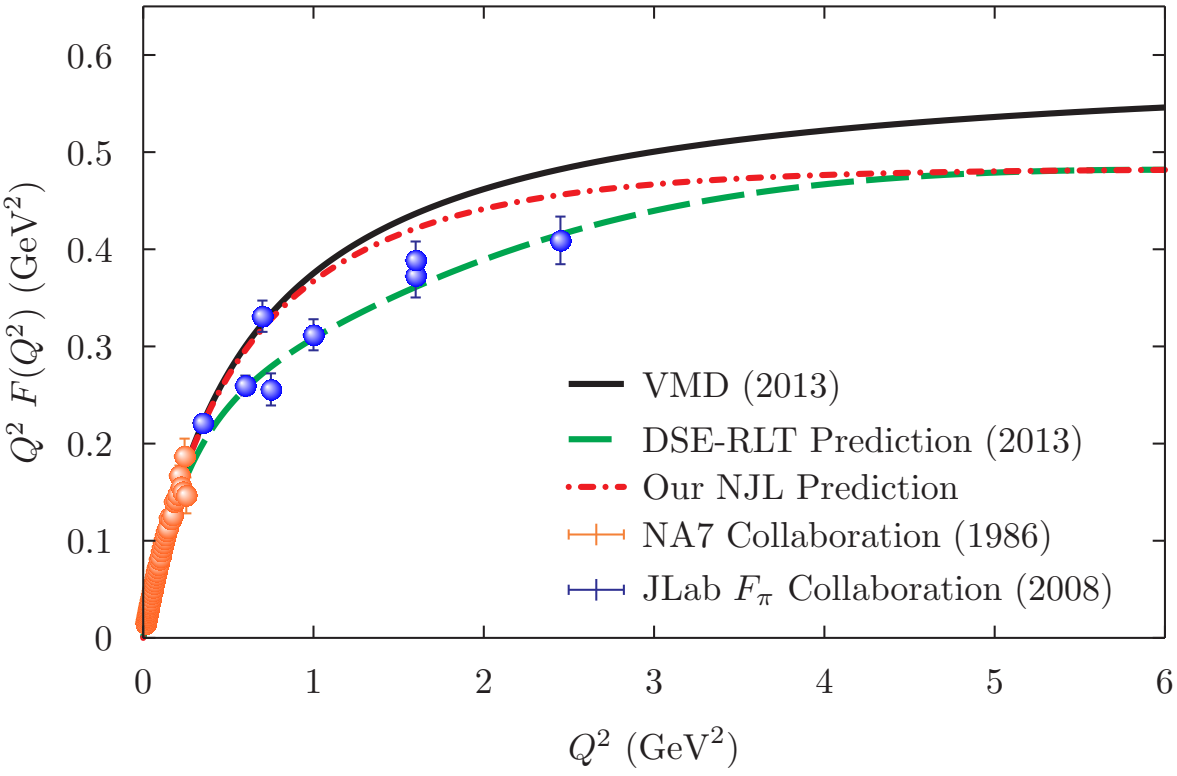

Figure 4.6.10: Total pion form factor multiplied by Q^2, $Q^2F_\pi(Q^2)$, is compared to existing experimental data [168, 176], empirical monopole [178] and DSE-RLT prediction [178]. We show the empirical monopole prediction using m_ρ [178] (black solid line), the total pion form factor multiplied by Q^2, $Q^2F_{\pi^+}(Q^2)$ (red dot-dashed line) and the existing experimental data of Amendolia et al. [168] (orange point) and Huber et al. [176] (blue point).

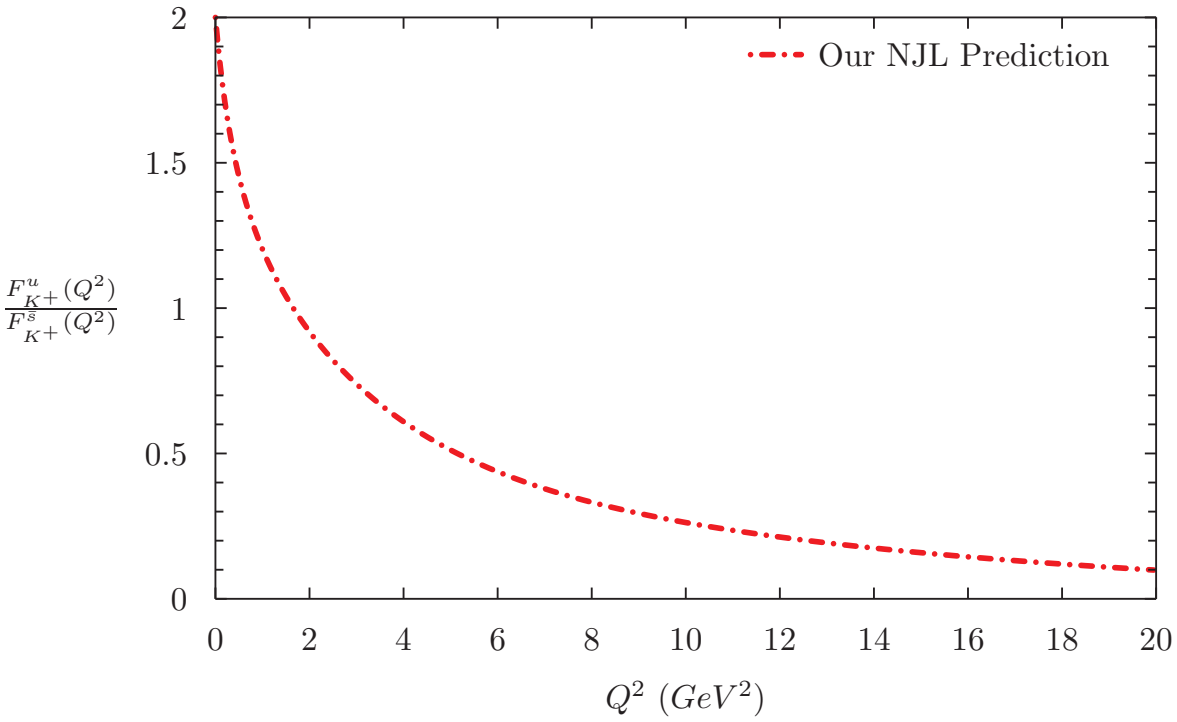

Figure 4.6.11: Ratio of the up quark sector form factor of the kaon, $F^u_{K^+}(Q^2)$ to the anti-strange quark sector form factor of the kaon, $F^s_{K^+}(Q^2)$ as a function of Q^2.

Figure. 4.6.11 shows the ratio of the up quark sector form factor to the anti-strange quark sector form factor of the kaon up to $Q^2 = 20$ GeV^2, in order to understand the sensitivity of the local hadronic environment of the valence quark contribution in the kaon. The ratio of the up and anti-strange quark sector form factors in the charged kaon decreases rapidly with increasing squared four momentum transfer, Q^2. This means the valence up quark distribution is much smaller than the valence anti-strange quark distribution in the kaon. Therefore, the up quark distribution is suppressed by the anti-strange quark distribution in the kaon as the squared four momentum transfer increases.

Similarly, in order to investigate the effect of the hadronic environment on the up quark sector form factor of the kaon compared to the up quark sector form factor of the pion, we show the ratio between them in Fig. 4.6.12. Clearly, the effect of the heavy spectator is to dramatically reduce the up quark sector form factor at larger Q^2.

Moreover, the ratio of the anti-strange sector quark form factor of the kaon to the anti-down quark sector form factor of the pion is investigated. The result of this ratio is depicted in Fig. 4.6.13.

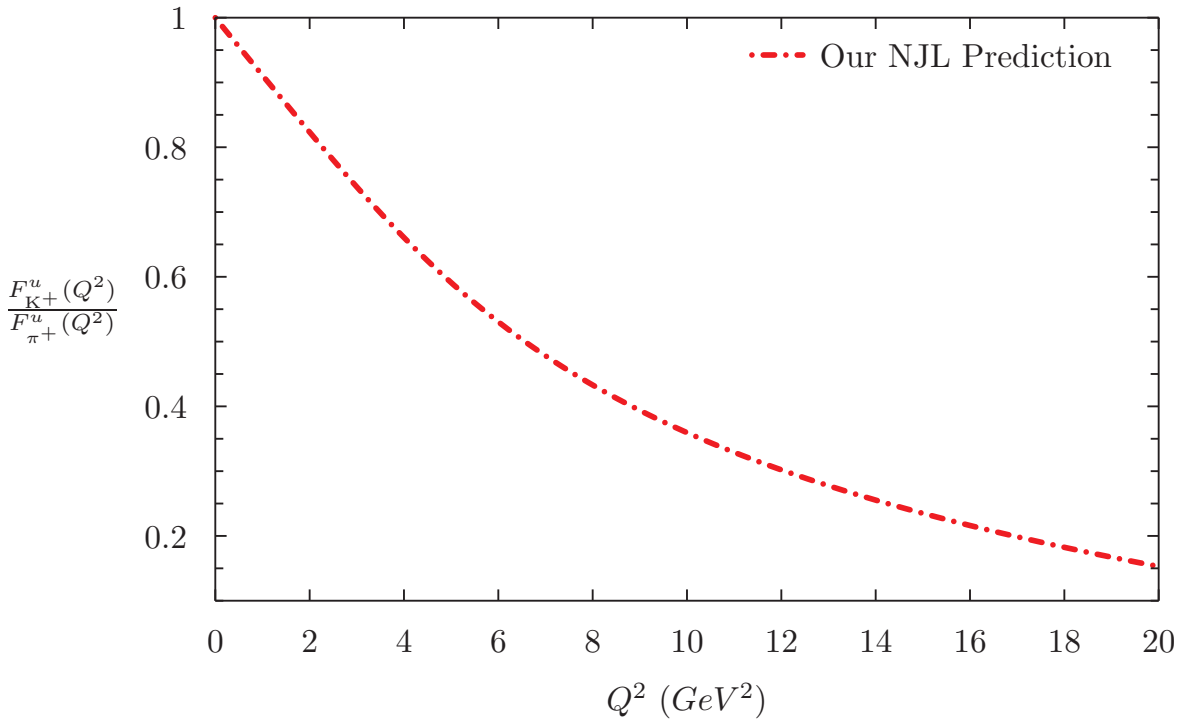

Figure 4.6.12: Ratio of the up quark sector form factor of the kaon to the up quark sector form factor of the pion, $\frac{F^u_{K^+}(Q^2)}{F^u_{\pi^+}(Q^2)}$ as a function of Q^2.

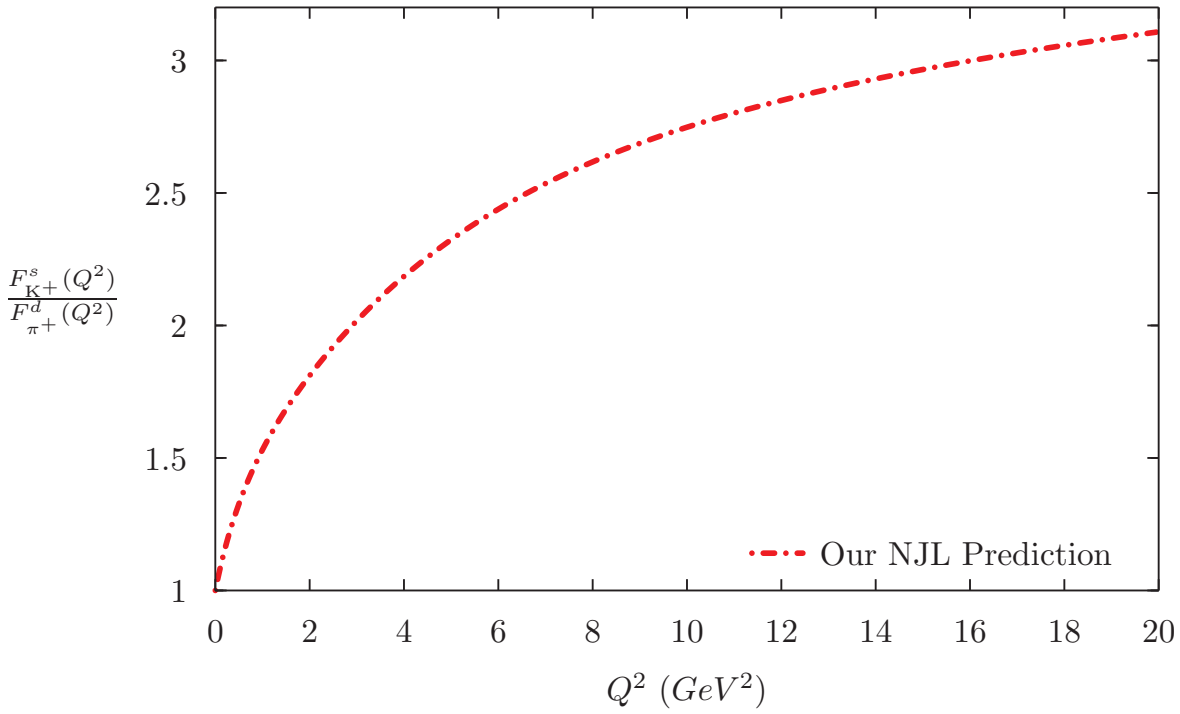

Figure 4.6.13: Ratio of the anti-strange quark sector form factor of the kaon to the anti-down quark sector form factor of the pion, $\frac{F^s_{K^+}(Q^2)}{F^{\bar{d}}_{\pi^+}(Q^2)}$ as a function of Q^2.

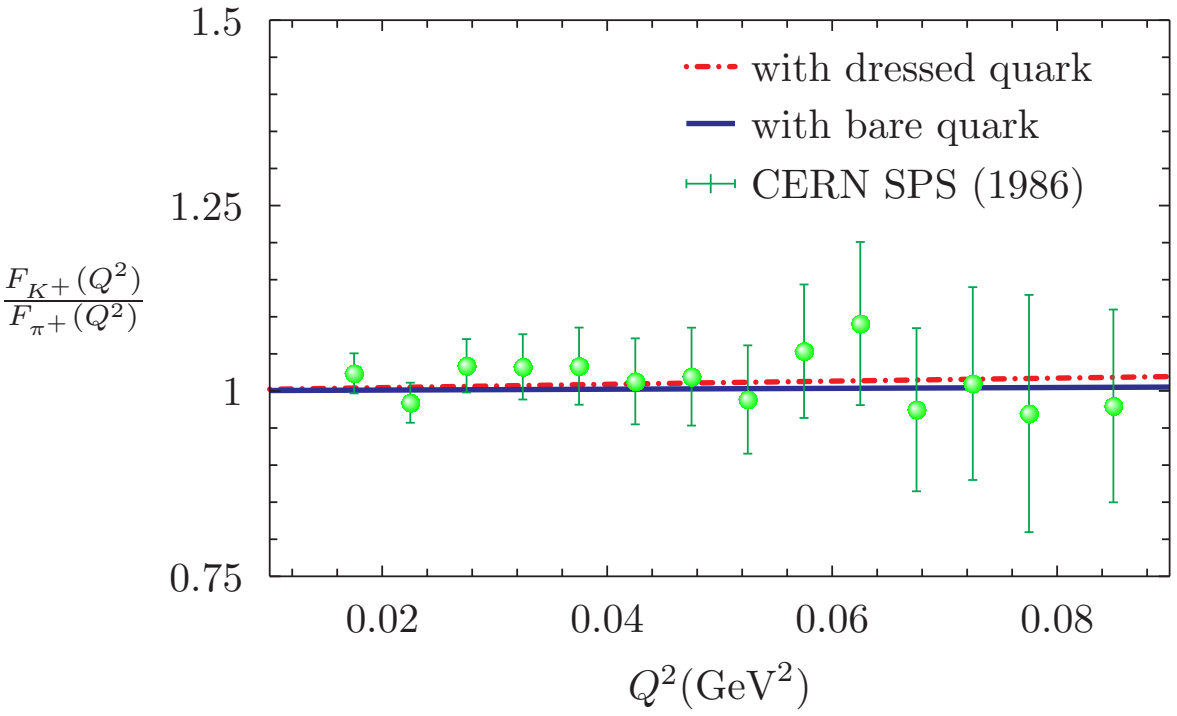

Figure 4.6.14: Ratio of the total kaon form factor to the total pion form factor including the vector mesons (red dot-dashed line) and without the vector mesons – bare (blue dashed line) is shown up to $Q^2 = 0.09$ GeV^2.

Figure 4.6.13 shows clearly that the ratio of the anti-strange quark form factor of the kaon to the anti-down quark form factor of the pion increases dramatically with increasing the squared four momentum transfer. This reveals that the anti-strange quark sector form factor in the kaon has a sizable contribution compared to the anti-down quark sector form factor in the pion. Consequently, the total kaon form factor is larger than the total pion form factor, as illustrated in Figs. 4.6.14 and 4.6.15.

Comparison with the existing experimental data of Ref. [183] for the ratio of the kaon and pion form factor with or without the dressed quark up to $Q^2 = 0.09$ GeV^2 is illustrated in Fig. 4.6.14. Our NJL prediction for the ratio of the kaon and pion form factors is in remarkable agreement with data [183], at small Q^2. Our NJL prediction for large Q^2 is depicted in Fig. 4.6.15.

The ratio of the total kaon form factor to the total pion form factor with and without dressed quarks is illustrated in Fig. 4.6.15. There is a significant difference arising from the dressing over the whole range of Q^2. Additionally, Figure. 4.6.15 clearly indicates that the vector mesons make a significant contribution to the form factors.

4.7 Kaon Form Factor with Pion Cloud

In this section we discuss the kaon form factor with pion cloud. Several authors argued that the pion cloud give a sizeable contribution to the charge radius, which approximately $10 - 15\%$ [193–196]. More details of the pion cloud effects can be found in

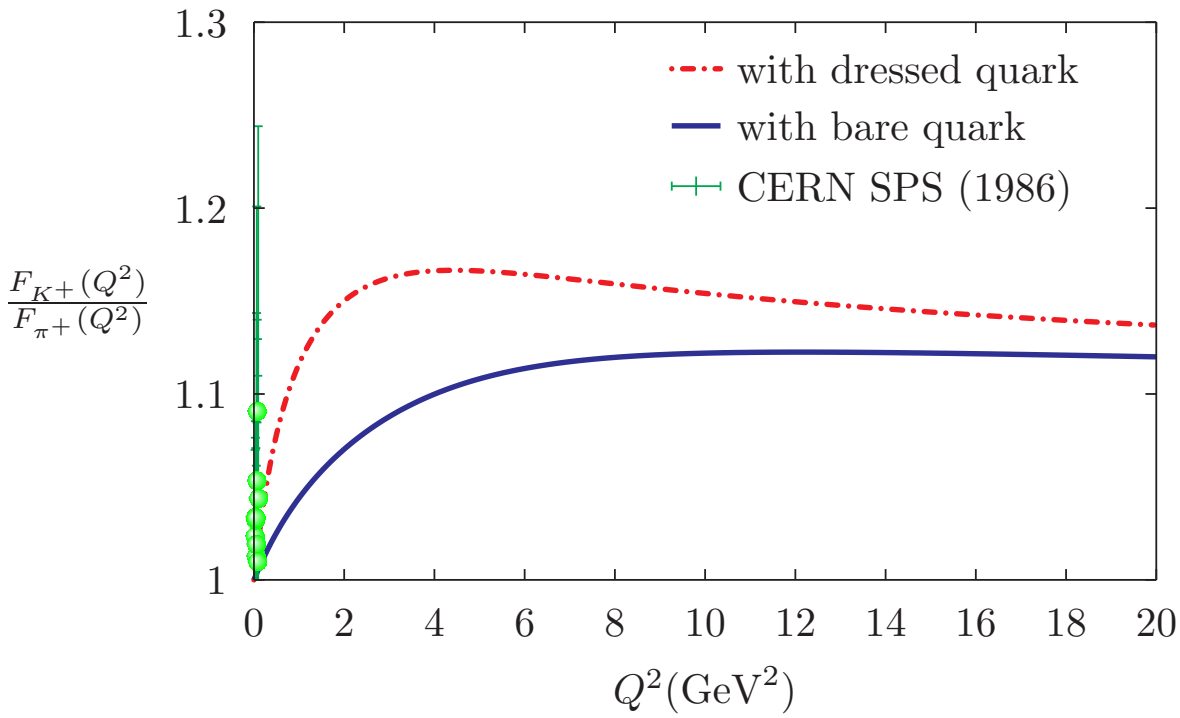

Figure 4.6.15: Ratio of the total kaon form factor to the total pion form factor including the vector meson (red dot-dashed line) and without vector meson – bare (blue dashed line) is shown up to $Q^2 = 20$ GeV^2.

Ref. [31, 197–199, 231, 232]. With this reason, we compute the kaon and pion form factor with dressed quark (vmd) plus the pion cloud (pc). The corrections is treated as a perturbation to the dressed quark BSE form factors. To include the pion cloud, the quark-photon vertex in Eq. (4.2.1) is modified, as in Eq. (4.4.1). It then has the form

$$\Lambda^{\mu}_{\gamma Q}(p',p) = \frac{(1+\tau_3)}{2}\Lambda^{\mu}_{U}(p',p) + \frac{(1-\tau_3)}{2}\Lambda^{\mu}_{D}(p',p), \tag{4.7.1}$$

where $\Lambda^{\mu}_{U}(p',p)$ and $\Lambda^{\mu}_{D}(p',p)$ are the dressed quark sector currents. They then have a form

$$\Lambda^{\mu}_{U}(p',p) = \gamma^{\mu}F_{1U}(Q^2) + \frac{i\sigma^{\mu\nu}q_{\nu}}{2M}F_{2U}(Q^2), \tag{4.7.2}$$

$$\Lambda^{\mu}_{D}(p',p) = \gamma^{\mu}F_{1D}(Q^2) + \frac{i\sigma^{\mu\nu}q_{\nu}}{2M}F_{2D}(Q^2), \tag{4.7.3}$$

where the dressed quark form factors (the pion cloud plus vmd) reads

$$F_{1U}(Q^2) = Z\left[\frac{1}{6}F_{1\omega}(Q^2) + \frac{1}{2}F_{1\rho}(Q^2)\right] + \left[F_{1\omega}(Q^2) - F_{1\rho}(Q^2)\right]f_1^{(q)} + F_{1\rho}(Q^2)f_1^{(\pi)}, \tag{4.7.4}$$

$$F_{1D}(Q^2) = Z\left[\frac{1}{6}F_{1\omega}(Q^2) - \frac{1}{2}F_{1\rho}(Q^2)\right] + \left[F_{1\omega}(Q^2) + F_{1\rho}(Q^2)\right]f_1^{(q)} - F_{1\rho}(Q^2)f_1^{(\pi)}, \tag{4.7.5}$$

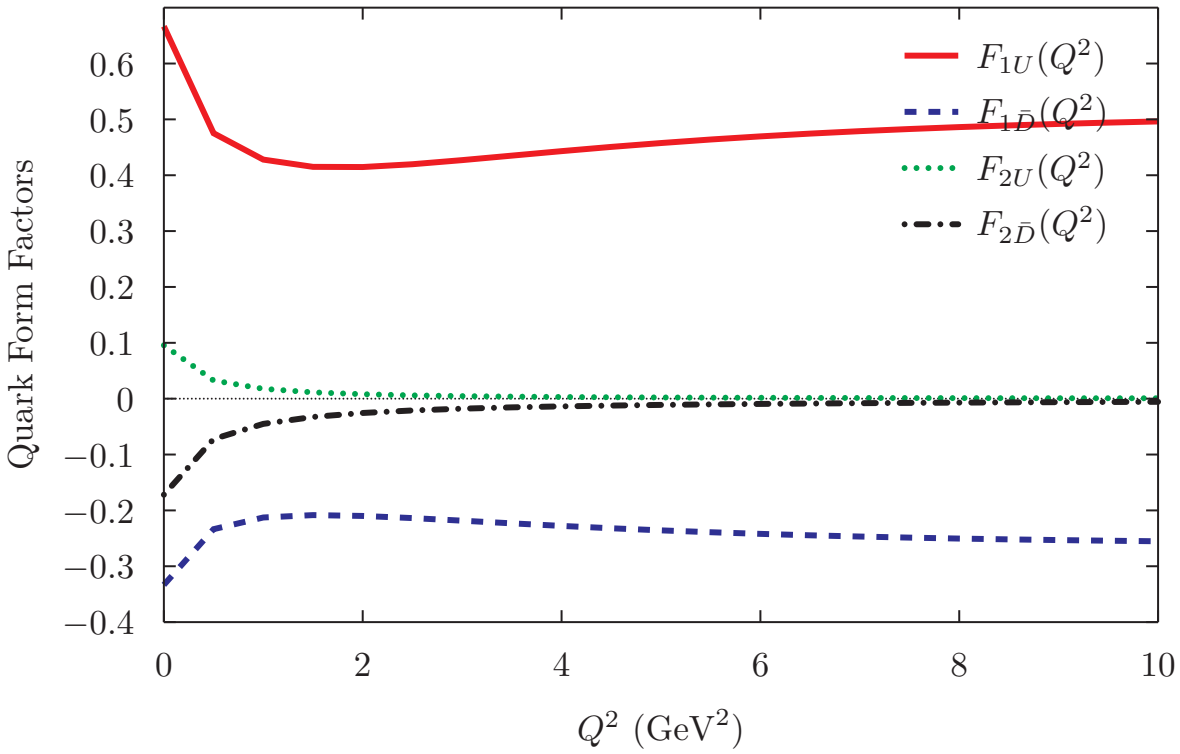

Figure 4.7.1: Dressed up and anti-down quark form factors including the pion loop corrections.

$$F_{2U}(Q^2) = \left[F_{1\omega}(Q^2) - F_{1\rho}(Q^2)\right] f_2^{(q)} + F_{1\rho}(Q^2) f_2^{(\pi)}, \tag{4.7.6}$$

$$F_{2D}(Q^2) = \left[F_{1\omega}(Q^2) + F_{1\rho}(Q^2)\right] f_2^{(q)} - F_{1\rho}(Q^2) f_2^{(\pi)}. \tag{4.7.7}$$

The body form factors, $f_1^{(q)}, f_1^{(\pi)}, f_2^{(q)}$ and $f_2^{(\pi)}$, are depicted in Fig. 4.7.2. The subscript q and π denote that the photon hits the quark in the second diagram and the pion in the third diagram, respectively. The subscripts of 1 and 2 denote, respectively, second and third diagram in Fig. 4.7.2. The dressed quark form factors are illustrated in Fig. 4.7.1. This shows that the result is consistent with the result in Ref. [192].

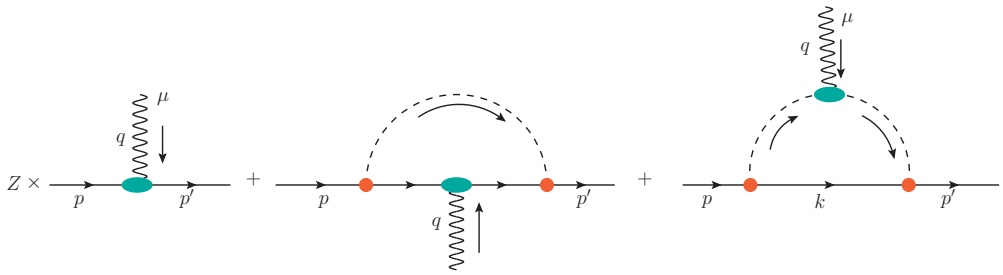

Figure 4.7.2: Pion cloud contribution to the quark photon vertex. The quark wave function renormalization factor Z represents the probability of striking a dressed quark without a pion cloud. The second and third diagrams, where the photon couples to the dressed quarks are represented a quark-photon vertex (shaded oval).

Setting $F_{1\omega}(Q^2) = 1$ and $F_{1\rho}(Q^2) = 1$ in Eq. (4.7.4), the dressed quark form factors including only the pion cloud, is easily obtained as

$$F_{1U}^{(\pi)}(Q^2) = Ze_u + f_1^{(\pi)}, \tag{4.7.8}$$

$$F_{1D}^{(\pi)}(Q^2) = Ze_d + 2f_1^{(q)} - f_1^{(\pi)}, \tag{4.7.9}$$

$$F_{2U}^{(\pi)}(Q^2) = f_2^{(\pi)}, \tag{4.7.10}$$

$$F_{2D}^{(\pi)}(Q^2) = 2f_2^{(q)} - f_2^{(\pi)}, \tag{4.7.11}$$

where the superscript π denotes the pion cloud contribution.

By evaluating the second and third diagrams in Fig. 4.7.2, we can extract the body form factors $f_1^{(q)}, f_1^{(\pi)}, f_2^{(q)}$ and $f_2^{(\pi)}$. After applying the Gordon decomposition identity $(p'^{\mu} + p^{\mu}) = 2M\gamma^{\mu} - i\sigma^{\mu\nu}q_{\nu}$ to the quark-photon vertex expression, we obtain

$$\begin{aligned} f_1^{(q)}(Q^2) = {} & \frac{g_\pi^2}{32\pi^2}\int_0^1 dx \int_{-x}^{x} dy \int d\tau \frac{1}{\tau} e^{-\tau(x^2M^2 + \frac{1}{4}(x^2-y^2)Q^2 + (1-x)m_\pi^2)} \\ & + \frac{g_\pi^2}{32\pi^2}\int_0^1 dx \int_{-x}^{x} dy \int_{\frac{1}{\Lambda_{UV}^2}}^{\infty} \frac{d\tau}{2}[2x(x-1)M^2 - x\frac{Q^2}{4} - \frac{1}{\tau}] \\ & \times e^{-\tau(x^2M^2 + \frac{1}{4}(x^2-y^2)Q^2 + (1-x)m_\pi^2)}, \end{aligned} \tag{4.7.12}$$

$$f_2^{(q)}(Q^2) = \frac{-g_\pi^2 M^2}{16\pi^2}\int_0^1 dx \int_{-x}^{x} dy \int_{\frac{1}{\Lambda_{UV}^2}}^{\infty} d\tau [x^2] e^{-\tau(x^2M^2 + \frac{1}{4}(x^2-y^2)Q^2 + (1-x)m_\pi^2)}, \tag{4.7.13}$$

and the third diagram has a form

$$\begin{aligned} f_1^{(\pi)}(Q^2) = {} & F_\pi^{(bare)}(Q^2)\frac{g_\pi^2}{16\pi^2}\int_0^1 dx \int_{-x}^{x} dy \int d\tau e^{-\tau((x-1)^2M^2 + \frac{1}{4}(x^2-y^2)Q^2 + xm_\pi^2)} \\ & \times [\frac{1}{\tau} - 2M^2(1-x)^2], \end{aligned} \tag{4.7.14}$$

$$f_2^{(\pi)}(Q^2) = F_\pi^{(bare)}(Q^2)\frac{g_\pi^2 M^2}{8\pi^2}\int_0^1 dx \int_{-x}^{x} dy \int d\tau e^{-\tau((x-1)^2M^2 + \frac{1}{4}(x^2-y^2)Q^2 + xm_\pi^2)}[(1-x)^2]. \tag{4.7.15}$$

The result of the dressed quark body form factors in Eqs. 4.7.12 and (4.7.15) including the pion loop is illustrated in Fig. 4.7.3

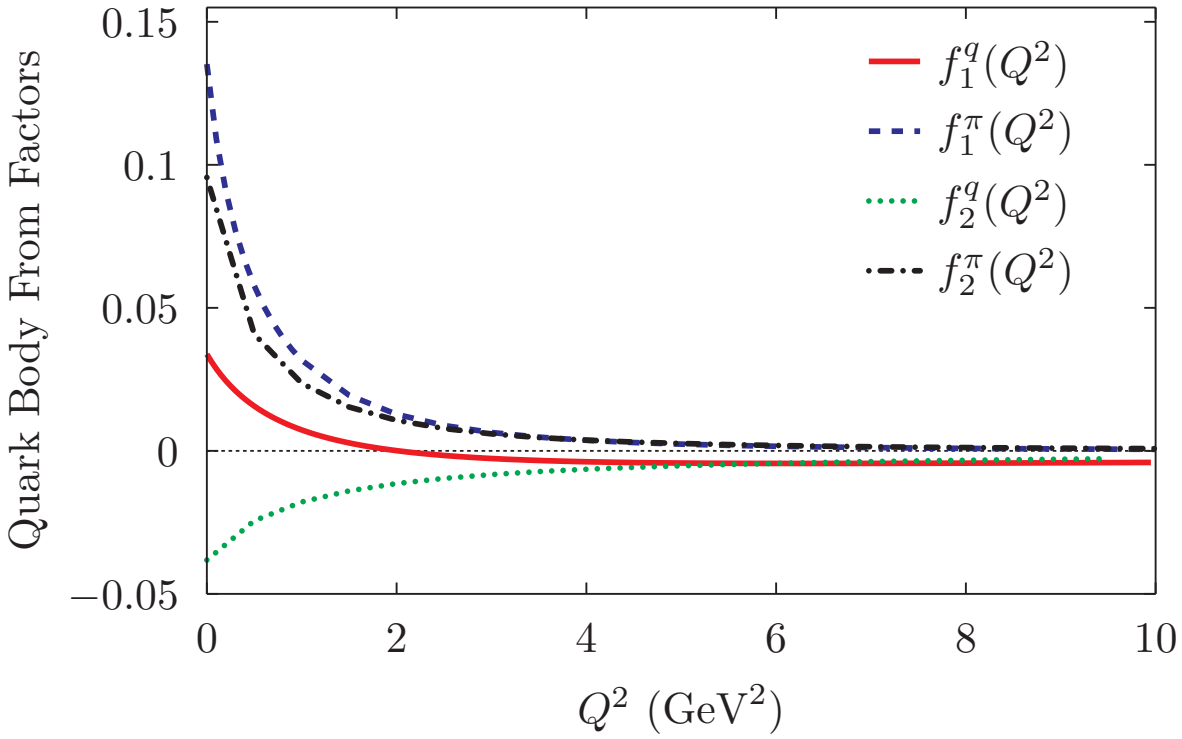

Figure 4.7.3: Dressed quark body form factors associated with the pion loop correction. $f_1^q(Q^2)$ and $f_2^q(Q^2)$ are come from the second diagram in Fig. 4.7.2 and $f_1^{(\pi)}(Q^2)$ and $f_2^{(\pi)}(Q^2)$ are from the third diagram.

Our result of the dressed quark body form factors including the pion cloud in Fig. 4.7.3 is consistent with the result in Ref. [192]. Then, this result is extended to calculate the kaon form factor including the dressed quarks and pion cloud, which is the first calculation of the kaon form factor by using this method. Finally, our new result for the kaon form factor is presented in Section 4.8. On the other hand, the dressed quark propagator receives an additional self-energy correction, Z in Eq. (4.7.4), which is shown in Fig. 4.7.4.

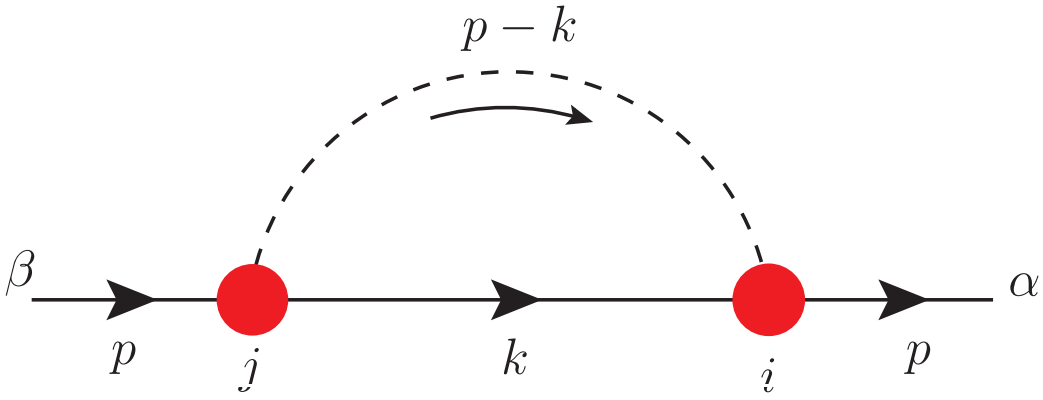

Figure 4.7.4: Pion cloud contribution to the dressed quark self-energy. The pion couples to the dressed quarks via $\gamma_5\tau_i$ and the pion t-matrix is approximated by its pole form.

The pion loop shifts the dressed quark mass by a constant, giving the quark propagator in the form

$$\tilde{S}(k) = ZS(k), \tag{4.7.16}$$

$$Z = \left[1 + \frac{\partial\Sigma(p)}{\partial \not{p}}\right]_{\not{p}=M}, \tag{4.7.17}$$

where $\Sigma(p)$ stands for the dressed quark self-energy with the pion cloud contribution, which is depicted in Fig. 4.7.4. From Fig. 4.7.4, the dressed quark self-energy with the pion cloud is

$$\Sigma(p) = 3ig_{\pi qq}^2 \int \frac{d^4k}{(2\pi)^4} i\mathcal{D}_\pi(p-k)\gamma_5 iS_l(k)\gamma_5, \tag{4.7.18}$$

where the propagator of the pion and fermions can be defined as

$$\mathcal{D}_\pi(p-k) = \frac{1}{[(p-k)^2 - m_\pi^2 + i\epsilon]}, \tag{4.7.19}$$

$$S_l(k) = \frac{\not{k} + M}{[k^2 - M^2 + i\epsilon]}, \tag{4.7.20}$$

where m_π and M are the pion mass and the constituent quark mass, respectively. In the PTR scheme, it can be defined as

$$\Sigma(k) = \frac{3g_{\pi qq}^2}{16\pi^2}\int_0^1 d\alpha(M - \alpha\not{p}) \int_0^\infty \frac{d\tau}{\tau} e^{-\tau((\alpha^2-\alpha)p^2 + \alpha m_\pi^2 + (1-\alpha)M^2)}. \tag{4.7.21}$$

Using the self-energy in Eq. (4.7.21), we straightforwardly evaluate the wave function renormalization Z, in Eq. (4.7.16). It then gives

$$Z = \left[1 + \frac{3g_{\pi qq}^2}{8\pi^2}\int_0^1 d\alpha \int_{\frac{1}{\Lambda_{\rm UV}^2}}^\infty d\tau \left((\alpha^2-\alpha)(\alpha-1)M^2 - \frac{\alpha}{2\tau}\right) e^{-\tau((\alpha^2-\alpha)p^2 + \alpha m_\pi^2 + (1-\alpha)M^2)}\right], \tag{4.7.22}$$

By plugging the quark-photon vertex in Eq. (4.7.1) into Eq. (4.2.2), evaluating them and comparing with the current electromagnetic form factor in Eq. (4.1.1), the pion form factor including pion cloud is written as

$$F_\pi(Q^2) = \left[F_{1U}(Q^2) - F_{1D}(Q^2)\right] f_\pi^V(Q^2) + \left[F_{2U}(Q^2) - F_{2D}(Q^2)\right] f_\pi^T(Q^2), \quad (4.7.23)$$

Similarly, the kaon form factor has the form

$$F_K(Q^2) = \left[F_{1U}(Q^2) - F_{1S}(Q^2)\right] f_K^V(Q^2) + \left[F_{2U}(Q^2) - F_{2S}(Q^2)\right] f_K^T(Q^2), \quad (4.7.24)$$

where the body factors of the kaon f_K^V and f_K^T (see full derivation in Appendix **??**) can be defined as

$$f_K^V(Q^2) = F_K^{(\text{bare})}(Q^2), \quad (4.7.25)$$

$$f_K^T(Q^2) = \frac{3g_{Kq\bar{q}}^2}{16\pi^2 M_u} Q^2 \int_0^1 dx \int_{-x}^{x} dy \int_{\frac{1}{\Lambda_{\text{UV}}^2}}^{\frac{1}{\Lambda_{\text{IR}}^2}} d\tau \left[(1-x)M_s + xM_u\right] \times e^{-\tau(xM_u^2 + (1-x)(M_s - xm_K)^2 + \frac{Q^2}{4}(x^2 - y^2))}, \quad (4.7.26)$$

where $F_K(Q^2)$ is given in Eq. 4.2.8 [10] and the body form factors for the pion $f_\pi^V(Q^2)$ and $f_\pi^T(Q^2)$ are defined

$$f_\pi^V(Q^2) = F_\pi^{(\text{bare})}(Q^2), \quad (4.7.27)$$

$$f_\pi^T(Q^2) = \frac{3g_{\pi q\bar{q}}^2}{16\pi^2 M_u} Q^2 \int_0^1 dx \int_{-x}^{x} dy \int_{\frac{1}{\Lambda_{\text{UV}}^2}}^{\frac{1}{\Lambda_{\text{IR}}^2}} d\tau \left[(1-x)M_d + xM_u\right] \times e^{-\tau(xM_u^2 + (1-x)(M_d - xm_\pi)^2 + \frac{Q^2}{4}(x^2 - y^2))}, \quad (4.7.28)$$

where $F_\pi(Q^2)$ is defined in Eq. 4.2.8.

4.8 Results for the Pion Form Factor with Pion Cloud

In this section our numerical results for the pion form factor including the pion cloud are discussed. Our first numerical results for the pion form factor with the pion cloud is shown in Figs. 4.8.1. Figure 4.8.1 provides the pion form factor with the pion cloud over the range $Q^2 = 0$ -10 GeV^2. This shows that the solid red lines represents the pion form factor including pion cloud (pc) and vector mesons (vmd), the pion form factor with the bare quark is represented by the black dotted lines and the pion form factor including only vector mesons is labeled by the blue dashed dotted lines.

[10] The vector part of the body form factors of the kaon equals to the bare form factor of the kaon. Similarly, this applies for the pion case.

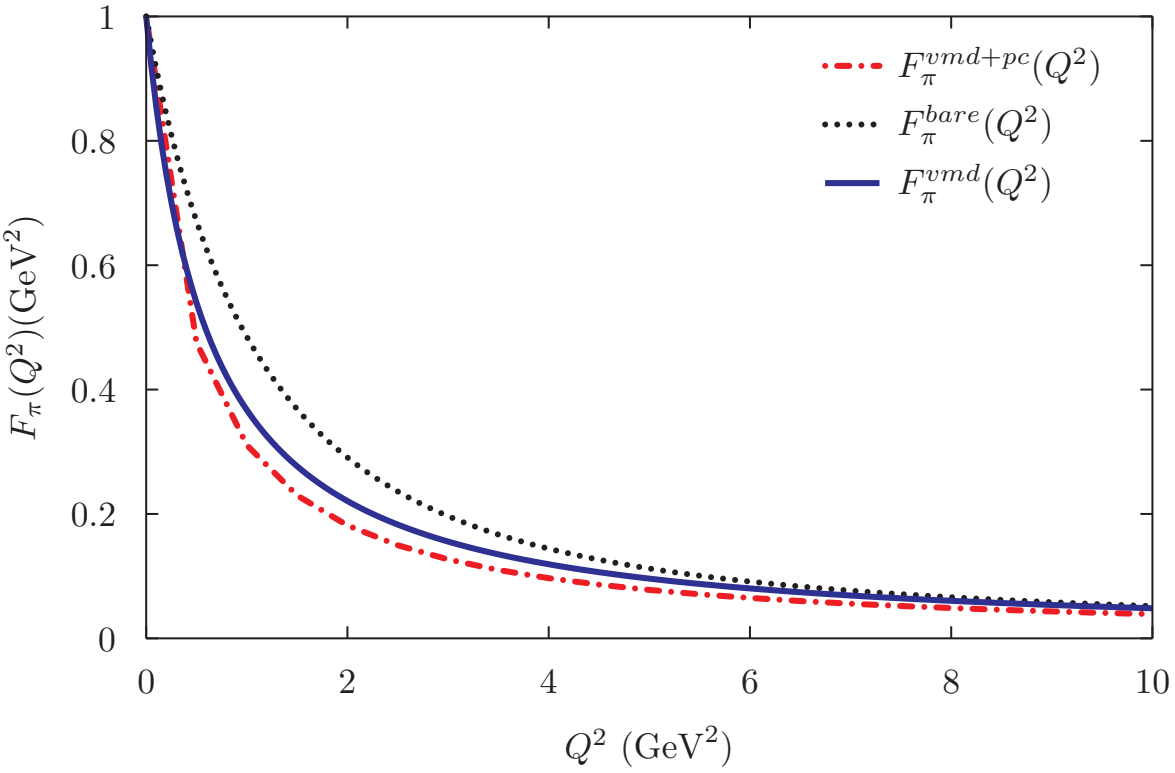

Figure 4.8.1: The pion form factors with pion cloud.

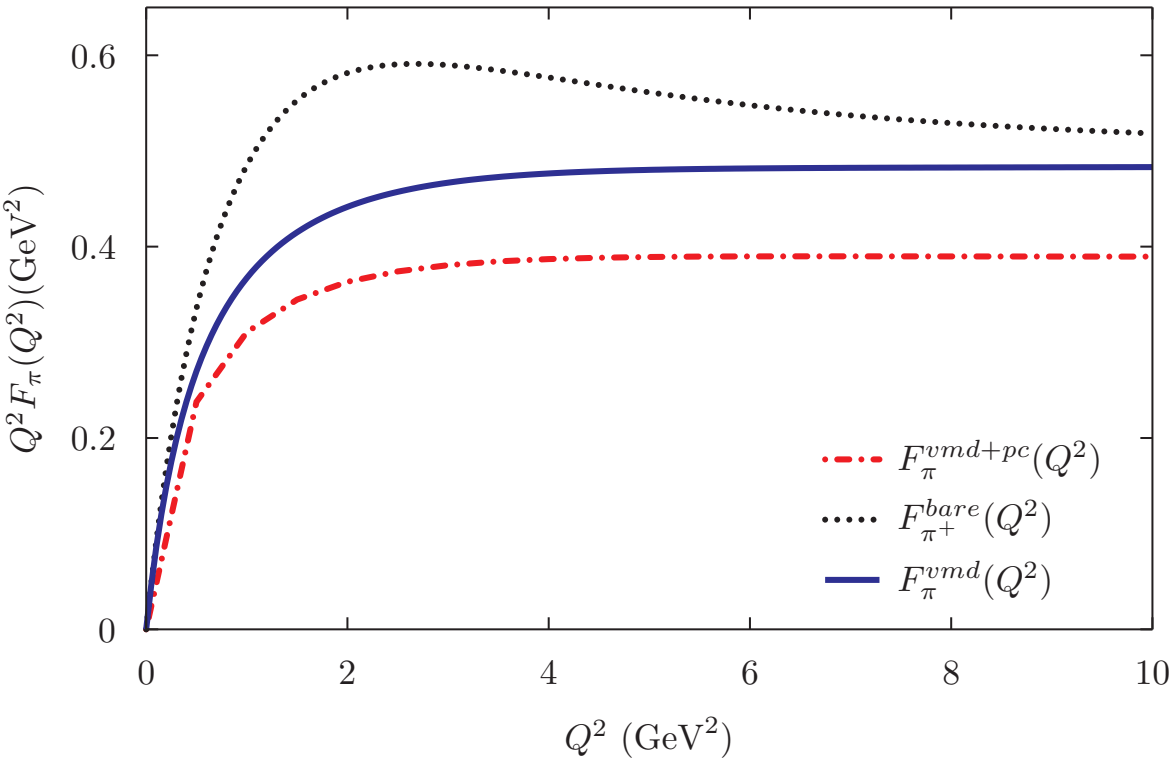

Figure 4.8.2: As in Fig. 4.8.1 but the pion form factor is multiplied with Q^2.

This clearly indicates the pion form factor, $F_\pi^{vmd+pc}(Q^2)$ is softer than other pion form factors ($F_\pi^{vmd}(Q^2)$ and $F_\pi^{bare}(Q^2)$). The pion form factors multiplied by Q^2 are given in Fig. 4.8.2. At large Q^2 the pion form factors plateau, where we find that $Q^2F_\pi^{vmd+pc} \to 0.39$, $Q^2F_\pi^{vmd}(Q^2) \to 0.48$ and $Q^2F_\pi^{bare}(Q^2) \to 0.52$. Thus, a comparison between our pion form factor results, the existing experimental data [168, 176], the empirical monopole (VMD) [178] and the DSE-RLT result of Ref. [178] is depicted in Fig. 4.8.3. This shows that our pion form factor result, $F_\pi^{vmd+pc}(Q^2)$ agree well with the DSE-RLT result [178] and the existing experimental data [176]. Similarly as in Fig. 4.8.2, we provide the pion form factor result multiplied by Q^2 comparing to the existing experimental data [168, 176, 177] in Fig. 4.8.4. Surprisingly, we find that our pion form factor result, $Q^2F_\pi^{vmd+pc}(Q^2)$ is softer than the DSE-RLT result [178]. Our model prediction is in excellent agreement with the DSE-RLT prediction as well as the existing experimental data. From Fig. 4.8.4, our pion form factor result is consistent with the perturbative QCD prediction [200–202]

$$Q^2F_\pi(Q^2) \to 16\pi f_\pi^2 \alpha_S(Q^2), \tag{4.8.1}$$

where f_π denotes the pion decay constant and $\alpha_S(Q^2)$ is the running coupling constant. A complete discussion for the meson form factor in large Q^2 will be presented in Section 4.9.

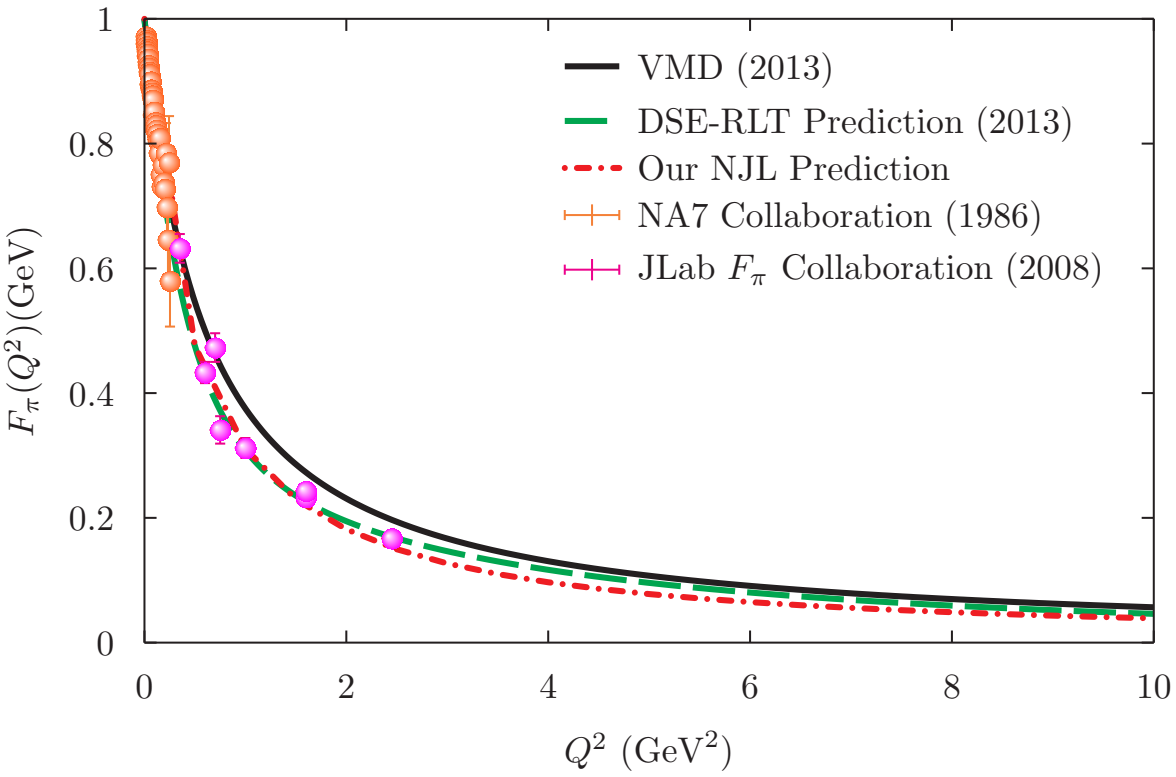

Figure 4.8.3: As in Fig. 4.8.1 but the form factor is compared to the existing experimental data [168, 176, 177].

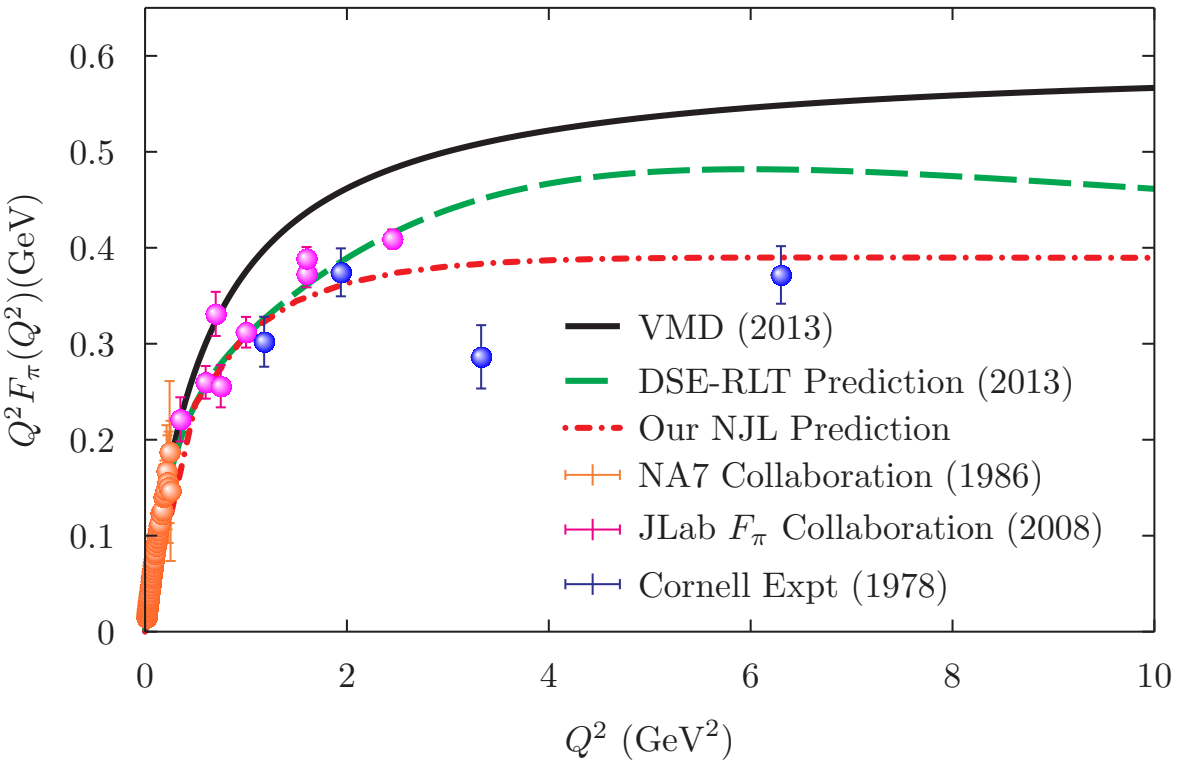

Figure 4.8.4: As in Fig. 4.8.3 but the pion form factor is multiplied with Q^2. The pion form factor data is from Refs. [168, 176, 177].

Here we recall the expression of the kaon and pion form factor Eq. (4.2.8), they have the form

$$F_K(Q^2) = e_u F_K^u(Q^2) - e_s F_K^s(Q^2), \tag{4.8.2}$$
$$F_\pi(Q^2) = e_u F_\pi^u(Q^2) - e_d F_\pi^d(Q^2). \tag{4.8.3}$$

From Eq. (4.8.2), the charge radius of the kaon and pion are defined by relation

$$\frac{dF_K(Q^2)}{dQ^2}\,|_{Q^2=0} = -\frac{1}{6}\langle r^2\rangle_K, \tag{4.8.4}$$
$$\frac{dF_\pi(Q^2)}{dQ^2}\,|_{Q^2=0} = -\frac{1}{6}\langle r^2\rangle_\pi, \tag{4.8.5}$$

Thus, the charge radius square of the quark sector form factors of the kaon are defined as

$$\frac{F_K^u(Q^2)}{F_K^u(0)} = 1 - \frac{1}{6}Q^2\langle r^2\rangle_{u/K}, \tag{4.8.6}$$
$$\frac{F_K^s(Q^2)}{F_K^s(0)} = 1 - \frac{1}{6}Q^2\langle r^2\rangle_{s/K}, \tag{4.8.7}$$

Similarly for the pion, the charge radius square of the quark sector form factors have the form

$$\frac{F_\pi^u(Q^2)}{F_\pi^u(0)} = 1 - \frac{1}{6}Q^2\langle r^2\rangle_{u/\pi}, \tag{4.8.8}$$

$$\frac{F_\pi^d(Q^2)}{F_\pi^d(0)} = 1 - \frac{1}{6}Q^2\langle r^2\rangle_{d/\pi}, \tag{4.8.9}$$

Finally, the total charge radius square of the kaon an pion (see Appendix A.17) can be written as

$$\langle r^2\rangle_K = \frac{2}{3}\langle r^2\rangle_{u/K} + \frac{1}{3}\langle r^2\rangle_{s/K}, \tag{4.8.10}$$

$$\langle r^2\rangle_\pi = \frac{2}{3}\langle r^2\rangle_{u/\pi} + \frac{1}{3}\langle r^2\rangle_{d/\pi}. \tag{4.8.11}$$

Using Eqs. (4.8.4) we compute the charge radius squared of the kaon and pion as well as their quark sector form factors. Our numerical results for the charge radius squared are summarized in Table 4.8.1 and Table 4.8.2.

Table 4.8.1: A charge radius squared of the kaon and the pion and their quark sector charge radius with bare quarks.

Particle	$\langle r^2\rangle_{u/\pi,u/K}$ (fm^2)	$\langle r^2\rangle_{d/\pi,s/K}$ (fm^2)	$\langle r^2\rangle$ (fm^2)	$\langle r\rangle$ (fm)	$\frac{\langle r\rangle_\pi}{\langle r\rangle_K}$
Pion (u d)	0.21	0.21	0.21	0.46	1.02
Kaon (u s)	0.24	0.13	0.20	0.45	

Table 4.8.2: A charge radius squared of the kaon and the pion and their quark sector charge radius including the vector mesons (dressed quark).

Particle	$\langle r^2\rangle_{u/\pi,u/K}$ (fm^2)	$\langle r^2\rangle_{d/\pi,s/K}$ (fm^2)	$\langle r^2\rangle$ (fm^2)	$\langle r\rangle$ (fm)	$\frac{\langle r\rangle_\pi}{\langle r\rangle_K}$
Pion (u d)	0.39	0.39	0.39	0.62	1.07
Kaon (u s)	0.42	0.19	0.34	0.59	

We find that the pion charge radius with dressed quark is approximately 6 % smaller than the experimental value, $r^{exp} = 0.663 \pm 0.006\ fm$ [168, 169]. Our kaon mean square charge radius and the experimental value, $\langle r_K^2\rangle = 0.34 \pm 0.05\ fm^2$ [183] are found to be very similar. Our difference between the charge pion and kaon mean square radii is consistent with the experimental value, $\langle r_\pi^2\rangle - \langle r_K^2\rangle = 0.10 \pm 0.045\ fm^2$ [183].

4.9 Kaon Form Factor at Large Q^2

In this section we discuss the investigation of the asymptotic behaviour of the electromagnetic form factor of the kaon and pion. At large Q^2, the strong interaction can be expanded in terms of $\alpha_S(Q^2)$. This is the so-called as pQCD [202–205]. The lowest

order contribution to kaon form factor is described by the interaction of a single gluon between two quarks and the momentum dependence of the hard gluon propagator is obtained proportionally to $\frac{1}{Q^2}$ at large Q^2. With the same procedure, the meson form factor at large Q^2 has the correct form $F_{K/\pi}(Q^2 \to \infty) \sim \frac{1}{Q^2}$ scaling. This scaling result is consistent with quark counting rules predictions [206–211].

Based upon the factorized pQCD scheme [206, 208, 209], the asymptotic prediction for the kaon and pion form factor in the space-like region has the form

$$F_K(Q^2) \to \frac{8\pi\alpha_S(Q^2)f_K^2}{Q^2}, \tag{4.9.1}$$

$$F_\pi(Q^2) \to \frac{8\pi\alpha_S(Q^2)f_\pi^2}{Q^2}. \tag{4.9.2}$$

Therefore the kaon-to-pion form factor ratio in the asymptotic pQCD [206, 208, 209] can be straightforwardly written as

$$\frac{F_K(Q^2)}{F_\pi(Q^2)} = \frac{f_K^2}{f_\pi^2} = 1.49 \pm 0.03. \tag{4.9.3}$$

Using the PDG values, $f_K = 159.8 \pm 1.5$ MeV and $f_\pi = 130.7 \pm 0.4$ MeV. While the kaon-to-pion form factor ratio using the Chernyak and Zhitnitsky (CZ) distribution amplitude [211] has the form

$$\frac{F_K(Q^2)}{F_\pi(Q^2)} = \frac{f_K^2}{f_\pi^2}\frac{I_K}{I_\pi} = 0.99 \pm 0.02, \tag{4.9.4}$$

with $\frac{I_K}{I_\pi} = 2/3$ comes from the CZ distribution amplitude for the pion and kaon [211].

Based on the kaon form factor multiplied by Q^2, our results for the kaon form factor and its quark sector form factor in the asymptotic region are obtained

$$Q^2F_K^{(vmd)}(Q^2) \to 0.55 \tag{4.9.5}$$

$$Q^2F_K^{u}(Q^2) \to 0.07 \tag{4.9.6}$$

$$Q^2F_K^{s}(Q^2) \to 1.5. \tag{4.9.7}$$

Similarly our numerical results for the pion form factor at large Q^2 are found that

$$Q^2F_\pi^{(vmd)}(Q^2) \to 0.48 \tag{4.9.8}$$

$$Q^2F_\pi^{(vmd+pc)}(Q^2) \to 0.39 \tag{4.9.9}$$

$$Q^2F_\pi^{(bare)}(Q^2) \to 0.52. \tag{4.9.10}$$

Using the kaon form factor and pion form factor at large Q^2, we compute the ratio, $\frac{F_K(Q^2)}{F_\pi(Q^2)} \sim 1.15$.

4.10 Conclusion

The kaon and pion form factors has been computed in the NJL model with help of the proper time regularization scheme. In our calculation, we systematically investigated the kaon and pion form factors starting from the kaon and pion form factors with bare quarks, the kaon and pion form factors with the dressed quark (vmd) and the pion form factor with the pion cloud. Our kaon form factor with bare quarks result is in disagreement with the existing experimental data [183], as indicated in Fig. 4.3.5. The larger contribution of the quark sector form factor of the kaon to total kaon form factor arises from the valence s-quark, which has heavier mass than u-quark mass. Similarly, the pion form factor also underestimates the existing experimental data and VMD result. This is clearly indicated in Fig. 4.3.9, where the pion form factor is multiplied by Q^2.

Later on, for improving our previous result of the bare kaon form factor, we developed our model by modifying the quark-photon vertex into an isoscalar and isovector components, as pointed out in Eq. (4.4.1). By applying this quark-photon vertex, our kaon form factor result has an excellent agreement with the existing experimental data as well as the empirical monopole (VMD) result in the low Q^2. Unfortunately, there is as yet no data with which we can compare at larger Q^2. However, our kaon form factor result will be very interesting and promising to compare with experimental data for large Q^2 in the future. Similarly, our pion also yields an excellent agreement with the existing experimental data and VMD result, as illustrated in Fig. 4.6.8. In this point, the pion form factor, $F_\pi(Q^2)$, is compared to existing experimental data [167, 168, 176, 177]. In addition, our form factor of the pion result is consistent with the DSE-RLT result. This indicates that our NJL model has a similar prediction at around $Q^2 = 6$ GeV^2, as shown in Fig. 4.6.10.

Moreover we also calculated the ratio of the total kaon form factor to the total pion form factor including the dressed quark and without vector meson – bare quarks. Comparing our results to CERN SPS data at lower Q^2, the ratio of our numerical result has remarkably agreement with that existing experimental data.

Furthermore, the kaon and pion form factor with the pion cloud have been calculated. Some authors argued that the pion cloud gives a sizable contribution to the charge radius, which approximately $10-15\%$ [193, 194]. More details of the pion cloud effects can be found in Ref. [31, 197, 231, 232]. With this argument in mind, we compute the pion form factor with the dressed quark (vmd) plus the pion cloud (pc). Our numerical result shows an excellent agreement with the DSE-RLT result [178] as well as the existing experimental data [168, 176, 177]. Our pion form factor with dressed quark (vmd) plus the pion cloud is softer than the VMD result, as shown in Figs. 4.8.3 and 4.8.4, where the pion form factor multiplied with Q^2.

At large Q^2 (in the asymptotic region), the pion form factor plateau, where we find as illustrated in Fig. 4.8.4:

$$Q^2 F_\pi^{vmd+pc}(Q^2) \to 0.39, \tag{4.10.1}$$

$$Q^2 F_\pi^{vmd}(Q^2) \to 0.48, \tag{4.10.2}$$

$$Q^2 F_\pi^{bare}(Q^2) \to 0.52. \tag{4.10.3}$$

This indicates that in the large Q^2 (in the asymptotic region) our numerical results are consistent with the factorized pQCD prediction [200–202]. The perturbative QCD predicts that the pion form factor behaves as $Q^2 F_\pi(Q^2) \rightarrow$ constant (flat), where constant $= 8\pi f_\pi^2 \alpha_S(Q^2)$, where f_π is the pion decay constant and $\alpha_S(Q^2$ is the one-loop running coupling constant of QCD.

5
Quark Distributions

The valence quark distribution is a basic nonperturbative ingredient for QCD based on hard scattering processes. The quark distribution can be extracted by analyzing inclusive processes, as discussed in Chapter 2. The study of parton distribution functions in terms of the effective QCD theories [212] has been quite successfully used to understand the nonperturbative internal structure of the kaon and pion, which play an important role in the low energy QCD. The approaches used include the NJL model with the sharp Euclidean cutoff [85, 86], NJL model with the Pauli-Villars regularization [87, 88], the soliton bag model [90, 90, 91], the statistical model [100, 101], the gauge invariant non-local chiral quark model [213, 214], the Dyson Schwinger equation (DSE) [215] and the meson cloud model [216, 217]. Moreover, the valence quark distribution observable has been used to investigate the internal structure of the nucleon using a wide variety of theoretical models, from the MIT bag model [218, 219], to the chiral soliton model [220], the NJL model [56] and the BSE approach [83, 84].

In recent years, a review of the valence quark distribution of the pion was done by Holt and Roberts in Ref. [221]. In that letter, they argued that our understanding of the internal structure of the kaon and pion is still not satisfactory. This includes especially the behavior of the valence quark at large-x, as also pointed out in Ref. [215], and in the valence quark region [221], which is at $x \geq 0.4$. Therefore, they suggested measuring the valence quark distribution of the mesons and nucleons at large-x at JLAB, FNAL, CERN, J-PARC and GSI using the Drell-Yan (DY) interactions in order to provide new data. This new data is very important to extract information of the hadron structure and has a great potential to resolve the problem in the large-x, as well as to discriminate among different theoretical model calculations [90, 159, 213–222, 228, 229]. In addition, a measurement of the parton distribution of the pion at future electron-ion collider (EIC) is very promising to resolve the problem of the meson structure, as pointed out earlier. Recently, there have been a few measurements of the valence quark distribution of the pion [222, 223, 225, 226], whereas for the kaon, we only have existing experimental data in Ref [227], which was measured 25 years ago.

This implies that the valence quark distribution of the kaon, in particular, is not really well understood, because of the restricted experimental data .

On the theoretical side, the valence PDFs, which involves the calculation of the non-perturbative structure of the kaon and pion, have been performed within the light cone (LC) or light front (LF) framework [80, 229, 230]. The structure functions of the π^-, K^- and ρ mesons have also been studied within the SU(3)$_f$ NJL model using a sharp momentum cutoff [85, 86]. They found that at a low energy scale ($Q^2 = Q_0^2 = 0.25$ GeV^2), characteristic of a valence dominated quark model, the peak of the quark distribution of the pion appears at $x \sim 0.6$. They argued that their result is consistent with the pion wave function result calculated in the light cone framework [230]. Additionally, they found that at a low momentum scale the anti-strange quark carries a larger fraction of the kaon momentum than the light up (down) quarks. They also suggested that the ratio of the up quark distribution in the kaon, $u_K(x)$, to that in the pion, $u_{\pi^+}(x)$, at $Q^2 = 20$ GeV^2, could be understood by taking $\dfrac{u_K(x \sim 1)}{u_\pi(x \sim 1)} \sim \left(\dfrac{M_u}{M_s}\right)^2 \sim 0.5$ at a low momentum scale [85, 86].

The structure function of the pion, kaon and eta mesons have also been investigated in the SU(3) NJL model using the Pauli-Villars (PV) regularization [87, 88]. There the meson was taken to be a deeply bound $q\bar{q}$ state and a fully covariant description of the pseudoscalar meson was constructed. They found that the effect of the finite pion mass correction was negligible, while the effect of the finite kaon mass correction was approximately 10 %. They also compared the evolved valence quark distribution of the pion with the existing experimental data [87, 88]. Recent work on the valence quark distribution of the pion and kaon was performed using the DSE model. For the ratio of the up quark distributions of the kaon and pion at around $x \sim 1$, they found $\dfrac{u_K(x \sim 1)}{u_\pi(x \sim 1)} \sim \dfrac{f_\pi^2}{f_K^2}\left(\dfrac{M_u}{M_s}\right)^4 \sim 0.3$. They argued that the ratio shows a strong environmental dependence of the up quark distributions in the large x [215]. However, their model prediction was not in good agreement with the experimental data [227], in particular at large x ($x \to 1$). This problem remains unresolved. In their letter, they suggested that more data was needed in order to clarify the behavior of the valence quark distribution at high-x, as pointed out in Ref. [279]. More comprehensive reviews of the structure functions of the kaon and that of the pion can be found in Refs. [215, 221]

In this chapter, with this in mind, we investigate the structure of the kaon in particular by evaluating the valence quark distributions (PDF) within the three flavors NJL model, using proper-time regularization. This simulates the effect of confinement, as explained in Chapter 3 and is a Poincaré covariant quantum field theory, which preserves many properties of QCD in the low energy region. We also explain how we extract the PDF from its moments. Then, we show that the PDF in the NJL model satisfies the number and momentum sum rules, which guarantee conservation of the charge and momentum, respectively. Next, our evolution result of the valence quark distribution of the kaon and pion using the DGLAP equation [234], as discussed earlier in Section 2.11, are presented. This then give us access to compare our kaon and

pion PDF results to experimental data. The DGLAP evolution [234] will generate the perturbative, extrinsic sea of the quark-antiquark pairs and gluons, at large Q^2, as given in Eq. (2.11.5). Then, our numerical results for the valence quark distribution of the kaon and the pion are presented in Sections 5.1 and 5.3, respectively.

5.1 Quark Distributions of the Kaon

In this section, we determine the valence quark of the kaon and pion in the NJL model. The twist-2 the quark distribution in the kaon and pion are formally defined by

$$q_\alpha(x) = p^+ \int \frac{d\xi^-}{2\pi} e^{ixp^+\xi^-} \langle \alpha \mid \bar{\psi}_q(0)\gamma^+\psi_q\left(\xi^-\right) \mid \alpha\rangle_c, \tag{5.1.1}$$

where q stands for the quark flavour, c denotes a connected matrix element, meaning the vacuum transitions of the $\langle 0 \mid J_\mu J_\nu \mid 0\rangle\langle P \mid P\rangle$ do not contribute to the valence quark distribution, and $\langle\alpha \mid$ denotes the pseudoscalar meson (kaon or the pion) and $x = \dfrac{k^+}{p^+}$ is the Bjorken scaling variable, whee p^+ is the plus-component of the hadron momentum and k^+ is the plus-component of the struck quark momentum. Further, $Q^2 = -q^2$ denotes the four momentum transfer of virtual photon and P is the momentum of the target. Note that the gluons are frozen out in the valence dominated NJL model and therefore the gauge link factor in Eq. (5.1.1) is unity.

The valence quark distribution functions of the pion or kaon are given by the two Feynman diagrams in Fig. 5.1.1, where the operator insertion is given by

$$\Theta = \gamma^+\delta\left(x - \frac{k^+}{p^+}\right)\hat{P}_q, \tag{5.1.2}$$

and $\hat{P}_q$ is the projection operator for quarks of flavour q:

$$\hat{P}_{u/d} = \frac{1}{2}\left(\frac{2}{3}\,\mathbb{1} \pm \lambda_3 + \frac{1}{\sqrt{3}}\,\lambda_8\right) \tag{5.1.3}$$

$$\hat{P}_s = \frac{1}{3}\,\mathbb{1} - \frac{1}{\sqrt{3}}\,\lambda_8. \tag{5.1.4}$$

Using the relation $\bar{q}(x) = -q(-x)$ the valence quark and anti-quark distributions in the pion of kaon are evaluated. Following the kaon form factor derivation, the valence quark distribution has two Feynman diagrams, which contribute to the kaon and pion parton distribution functions. These come from the quark and antiquark contributions as illustrated in Fig. 5.1.1.

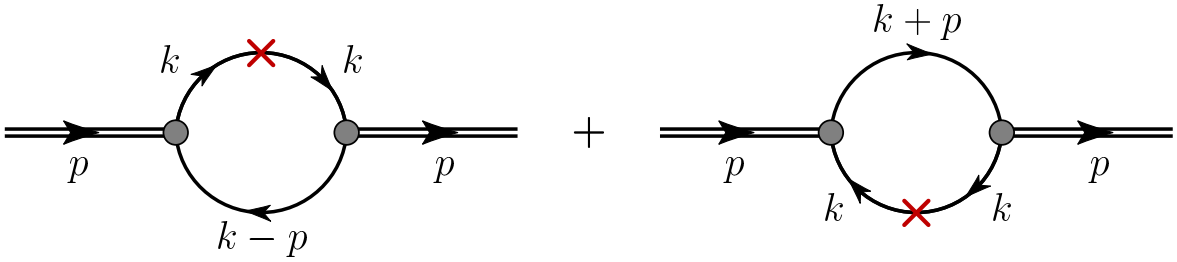

Figure 5.1.1: The Feynman diagrams for the valence quark distributions in the kaon. The red cross denotes the operator insertion, which is given by $\gamma^+\delta\left(x-\frac{k^+}{p^+}\right)\frac{1}{2}(\mathbb{1}\pm\lambda_3+\frac{1}{\sqrt{3}}\lambda_8)$, where the plus sign is for the up quark projection and the minus sign denotes the anti-down quark projection.

Based upon the Feynman diagrams in Fig. 5.1.1, the valence quark and antiquark distributions in the kaon can be straightforwardly defined as

$$q_K(x)=\frac{ig^2_{K\bar{q}q}}{k_-}\int\frac{d^4q}{(2\pi)^4}\delta\left(x-\frac{q_-}{k_-}\right)Tr\left[\gamma_5 S_1(q)\gamma^+ S_1(q)\gamma_5 S_2(q+k)\right], \tag{5.1.5}$$

$$\bar{q}_K(x)=\frac{ig^2_{K\bar{q}q}}{k_-}\int\frac{d^4q}{(2\pi)^4}\delta\left(x-\frac{q_-}{k_-}\right)Tr\left[\gamma_5 S_2(q)\gamma^+ S_2(q)\gamma_5 S_1(q+k)\right], \tag{5.1.6}$$

where $q(x)$, $\bar{q}(x)$ are, respectively, the valence quark and antiquark distributions. $g_{K\bar{q}q}$ is the kaon quark-antiquark coupling constant, which is defined in Eq. (3.5.1).

We then employ the Ward Identities $S_1(q)\gamma^+S_1(q)=-\frac{\partial S_1(q)}{\partial q^-}$ to Eq. (5.1.5) and perform an integration by parts. This yields the expression for the quark and antiquark distributions, that is

$$q_K(x)=-2iN_C g^2_{K\bar{q}q}\frac{\partial}{\partial p^2}\int\frac{d^4q}{(2\pi)^4}\left(x-\frac{q_-}{k_-}\right)Tr\left[\gamma_5 S_1(q)\gamma_5 S_2(q-k)\right], \tag{5.1.7}$$

$$\bar{q}_K(x)=-2iN_C g^2_{K\bar{q}q}\frac{\partial}{\partial p^2}\int\frac{d^4q}{(2\pi)^4}\left(x-\frac{q_-}{k_-}\right)Tr\left[\gamma_5 S_2(q)\gamma_5 S_1(q+k)\right], \tag{5.1.8}$$

In our calculation, the valence quark and antiquark distributions are evaluated via the moments of the PDFs. This provides the symmetric combination of the parton and anti-parton distribution functions for the first moment and the anti-symmetric combination for the second moment. In brief, the moments of the PDFs are introduced as

$$\mathcal{A}_{\rm n}=\langle x^{n-1}q_K(x)\rangle=\int_0^1 dx x^{n-1}q_K(x), \tag{5.1.9}$$

with $q_K(x)$ the valence quark distributions of the kaon and $n=1,2,\cdots$ is an integer, which is the order of the moment. In order to extract the PDF of the kaon, we evaluate

the valence quark distributions in Eq. (5.1.7) via moments by plugging the valence quark distribution into Eq. (5.1.9). Next, we perform a Feynman parameterization, a Wick rotation and a PTR scheme, respectively, the final expression of the valence quark distribution in the kaon is obtained as (A full derivation of the kaon parton distribution can be found in Appendix A.16)

$$q_K(x) = \frac{N_C g_{K\bar{q}q}^2}{4\pi^2} \int_{\frac{1}{\Lambda_{\rm UV}^2}}^{\frac{1}{\Lambda_{\rm IR}^2}} d\tau \frac{1}{\tau} e^{-\tau(k^2(x^2-x)+xM_2^2-M_1^2(x-1))} \times \left[1+\tau\left[k^2\left(x-x^2\right)-\left(x-x^2\right)\left(M_2-M_1\right)^2\right]\right] \tag{5.1.10}$$

$$\bar{q}_K(x) = \frac{N_C g_{K\bar{q}q}^2}{4\pi^2} \int_{\frac{1}{\Lambda_{\rm UV}^2}}^{\frac{1}{\Lambda_{\rm IR}^2}} d\tau \frac{1}{\tau} e^{-\tau(k^2(x^2-x)+xM_1^2-M_2^2(x-1))} \times \left[1+\tau\left[k^2\left(x-x^2\right)-\left(x-x^2\right)\left(M_1-M_2\right)^2\right]\right], \tag{5.1.11}$$

where M_1, M_2 are the constituent quark masses of the quark and antiquark, respectively and N_C denotes the number of colors. For the pion case, $M_1 = M_2 = M$, where M is the constituent quark mass. Note that the formula in Eq. (5.1.10) is written in general form, so it can be used easily for the different cases of the pseudoscalar mesons and the valence quark distribution formulation is $q_v(x) = q(x) - \bar{q}(x)$.

The valence quark distributions for the kaon are very important to satisfy the baryon number conservation [1] and momentum conservation. This guarantees the validity of the baryon number and momentum sum rules. The expression of the baryon number sum rules is defined as

$$\int_0^1 dx\ u_v^K(x) = 1 = \int_0^1 dx\ \bar{s}_v^K(x), \tag{5.1.12}$$

with $u_v^K(x) = [u_K(x) - \bar{u}_K(x)]$ [2] and $\bar{s}_v^K(x) = [\bar{s}_K(x) - s_K(x)]$ [3]. The subscript v denotes a valence quark. This also guarantees that the positively charged kaon only has a u- quark and an $\bar{s}$- quark.

The momentum sum rules can be formulated as

$$\int_0^1 dx\ x\left[u_v^{K^+}(x) + \bar{s}_v^{K^+}(x)\right] = 1, \tag{5.1.13}$$

where the $u_v^K(x)$ and $\bar{s}_v^K(x)$ are the valence up- and anti-strange quark distributions, respectively. Note that the strange quark distribution in the kaon is assumed negligeble in this calculation. This is because in the NJL model we do not consider the sea-quarks and gluons, only the valence quarks. In perturbative QCD, the sea quarks can be produced by gluons, which is decay quarks and anti-quarks. Therefore, the virtual strange quark may be expected to produced by QCD evolution, which means it is not zero at higher Q^2. Analogous results hold for the remaining kaons and the pions.

[1] The baryon number conservation is equivalent to charge conservation

[2] $u_v^{K^+}(x, Q_0^2) = \bar{u}_v^{K^-}(x, Q_0^2)$.

[3] $\bar{s}_v^{K^+}(x, Q_0^2) = s_v^{K^-}(x, Q_0^2)$.

5.2 Results for Quark Distributions of the Kaon

In this section, we discuss our numerical results for the PDFs of the kaon. The numerical result are computed with the use of the NJL model parameter sets, as given in Section 4.3. The valence up and anti-strange quark distributions are computed using Eqs. (5.1.10), (5.1.12) and (5.1.13). The initial model scale of the NJL model must be determined. As discussed in Section 2.11, the initial scale of the NJL model for parton distribution function in our calculation is chosen to be, Q_0^2= 0.16 GeV^2 [231–233]. Any valence dominated quark model must match QCD at a low scale, where we know that the valence quarks dominate empirically. Then, after the initial model is determined, the valence quark distributions are evolved to higher Q^2 with the help of the DGLAP equation [234] in order to compare with the experimental data from the Drell-Yan reaction as well as the empirical parameterizations.

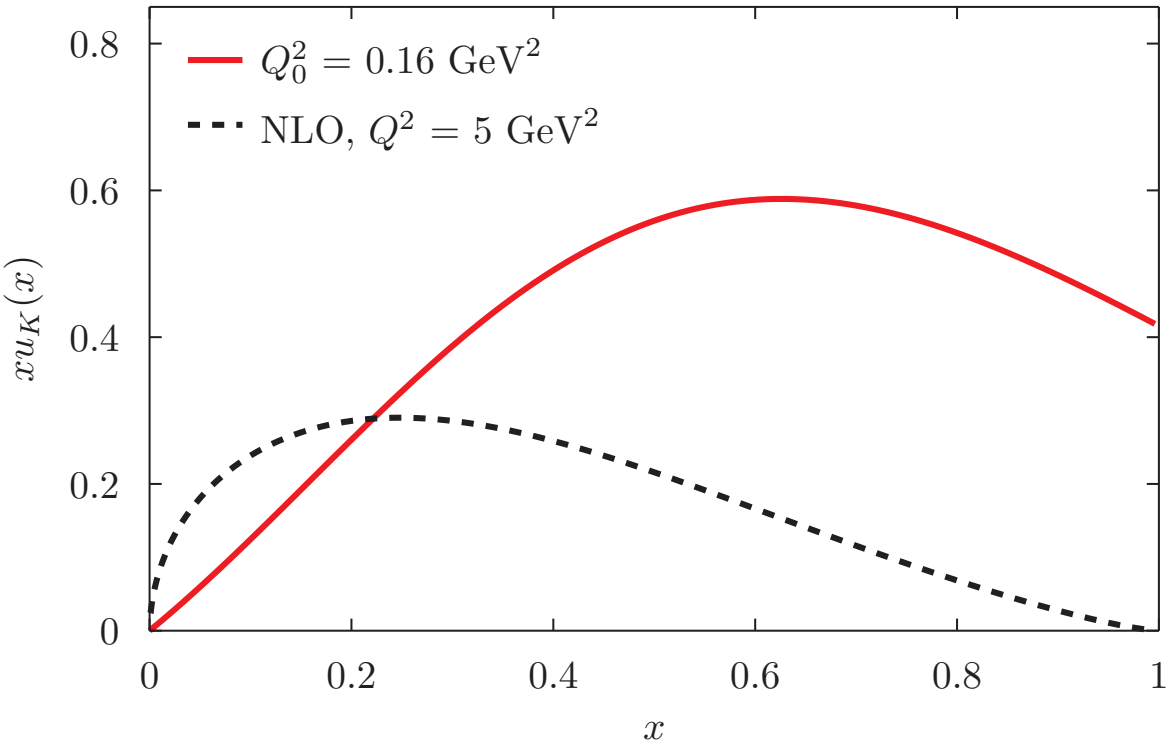

Figure 5.2.1: The valence up quark distribution of the kaon K^+. The valence up quark distributions of the kaon at the NJL model scale, $Q_0^2 = 0.16$ GeV^2 (red solid line) and the valence up quark distribution of the kaon evolved up to NLO to the scale, $Q^2 = 5$ GeV^2 (black dashed line).

Figure. 5.2.1 shows the valence up quark distribution computed at the NJL model scale, $Q_0^2 = 0.16$ GeV^2. Then, this is evolved at NLO using DGLAP equation [234] to a scale, $Q^2 = 5$ GeV^2. Clearly, we found that the distribution peak for the evolved up quark distribution is at around $x \sim 0.2$. This evolved distribution decreases smoothly with increasing x, where x denotes the Bjorken variable. The average momentum fraction carried by the valence quarks in the kaon at the NJL model scale, $Q_0^2 = 0.16$

GeV^2, based upon the momentum sum rules in Eq. 5.1.13 is written as

$$\int_0^1 dx\, x \left[u_v^K(x, Q_0^2) + \bar{s}_v^K(x, Q_0^2)\right] = [0.42 + 0.58] = 1. \tag{5.2.1}$$

Here Q_0^2 is the NJL model momentum scale. This indicates that all the momentum of the kaon is carried by the kaon's valence quarks. In other words, the momentum is conserved at the NJL model scale at the model scale, Q_0^2. In Eq. (5.2.1), this reveals that the valence anti-strange quark carries more momentum than the valence up quark in the kaon, which agrees with DSE-RL analysis in Ref. [215]. A logarithm of the average momentum fraction carried by the valence u-quark in the kaon for the various Q^2 as a function of the moments is depicted in Fig. 5.2.2 and the average momentum carried by valence u quark in the kaon for the various moments as a function of the Q^2 is displayed in Fig. 5.2.3.

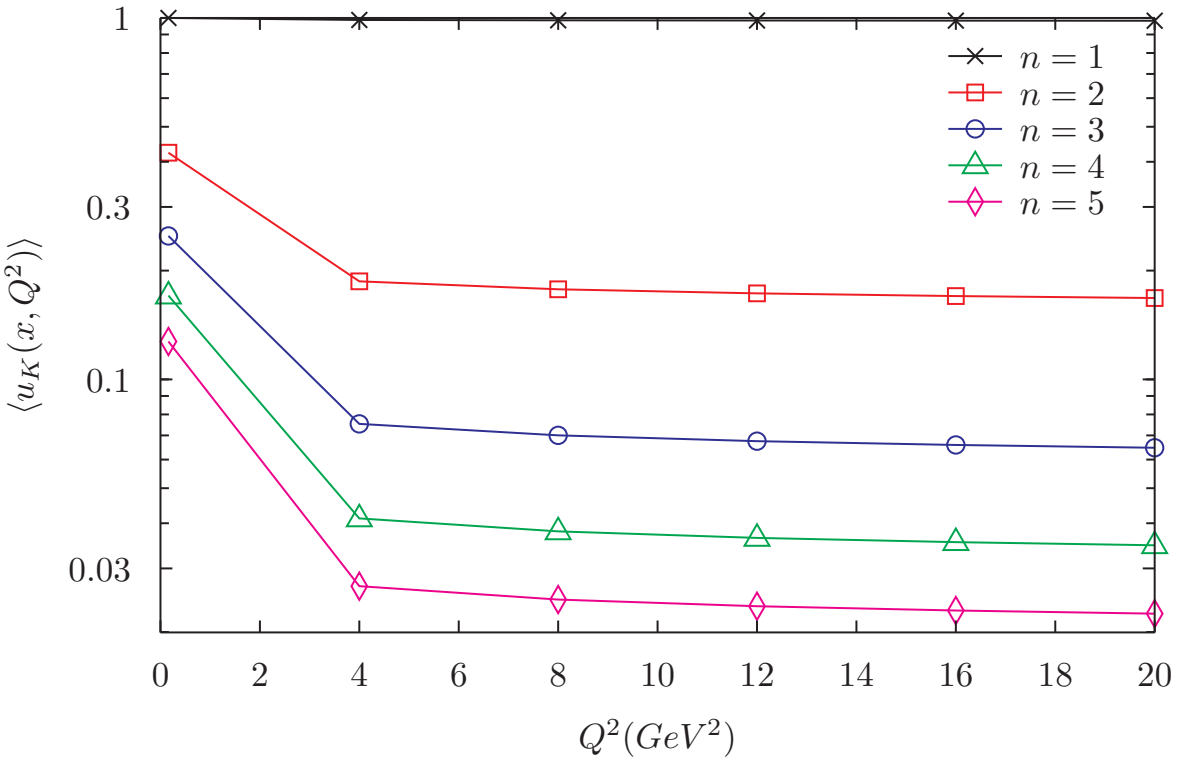

Figure 5.2.2: The average momentum of the valence up quark as a function of the Q^2, for the various moments PDF.

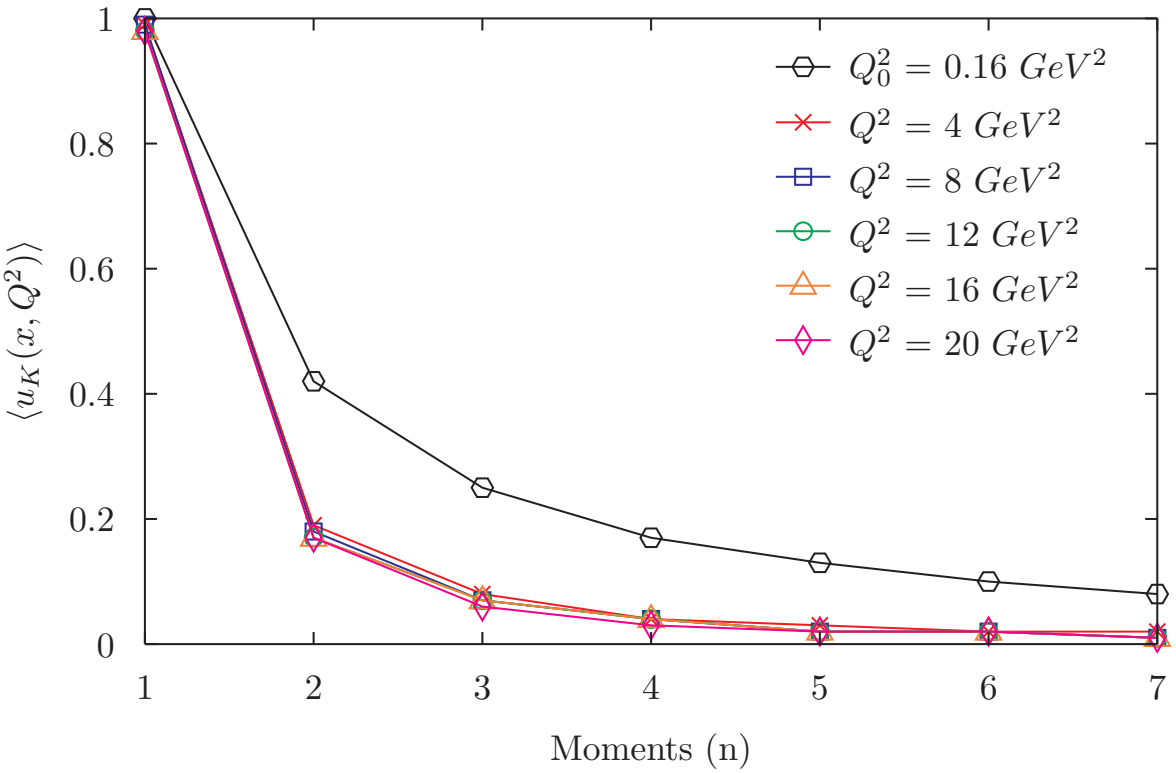

Figure 5.2.3: As in Fig. 5.2.2, but as function of the moments PDF, for the various Q^2.

Figure 5.2.3 shows that the average momentum carried by the valence u quark in the kaon decrease with increasing the moments (n), but is almost constant for the various Q^2. The moments of the distribution of the valence quark u for the various Q^2, which are calculated using the NJL model with proper-time regularization scheme, are summarized in Table 5.2.1.

Table 5.2.1: The moments of the kaon valence up quark distribution at the NJL model scale, $Q_0^2 = 0.16$ GeV^2 (second column) and after evolved up to the NLO at the various scale, $Q^2 = 4$,8 ,12 ,16 ,20 GeV^2 (third column, respectively), where n denotes moments.

n	u_v^K (x, 0.16)	u_v^K (x, 4)	u_v^K (x, 8)	u_v^K (x, 12)	u_v^K (x, 16)	u_v^K (x, 20)
1	1.00	0.99	0.99	0.98	0.98	0.98
2	0.42	0.19	0.18	0.17	0.17	0.17
3	0.25	0.08	0.07	0.07	0.07	0.06
4	0.17	0.04	0.04	0.04	0.04	0.04
5	0.13	0.03	0.02	0.02	0.02	0.02

Table 5.2.2: The moments of the kaon valence anti-strange distribution at the NJL model scale, $Q_0^2 = 0.16$ GeV^2 (second column) and after evolved at NLO at the various scale, $Q^2 = 4$,8 ,12 ,16 ,20 GeV^2 (third column, respectively), where n denotes moments.

n	$\bar{s}_v^K$ (x, 0.16)	$\bar{s}_v^K$ (x, 4)	$\bar{s}_v^K$ (x, 8)	$\bar{s}_v^K$ (x,12)	$\bar{s}_v^K$ (x,16)	$\bar{s}_v^K$ (x,20)
1	1.0	1.02	1.02	1.02	1.02	1.02
2	0.58	0.27	0.26	0.25	0.25	0.24
3	0.40	0.13	0.12	0.12	0.12	0.11
4	0.31	0.08	0.08	0.07	0.07	0.07
5	0.25	0.06	0.05	0.05	0.05	0.05

Similarly, using the same procedure as in the u-quark, the logarithm of the average momentum of the valence $\bar{s}$-quark in the kaon is calculated for the various of the Q^2 as a function of the moments, which is depicted in Fig. 5.2.4 and the average momentum of the valence $\bar{s}$-quark in the kaon for the various of the moments as a function of the Q^2, is illustrated in Fig. 5.2.5. A summary of the average momentum of the $\bar{s}$ for the various Q^2 and moments can be found in Table 5.2.2.

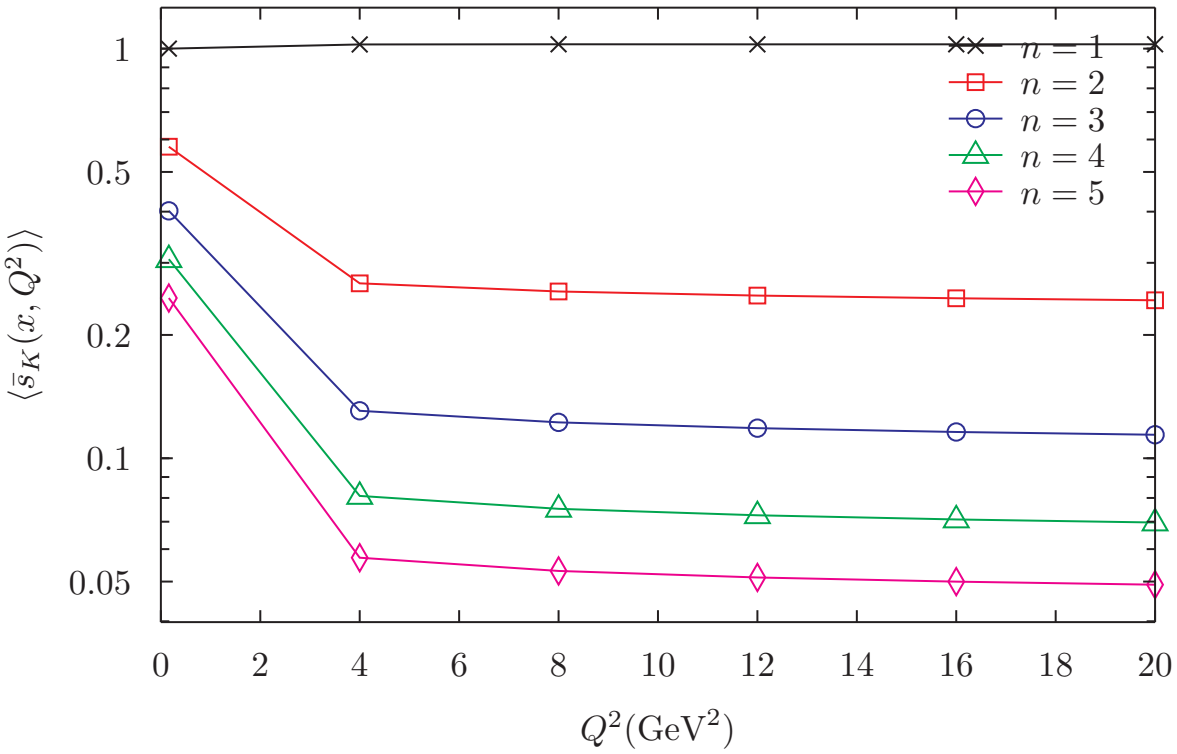

Figure 5.2.4: The average momentum of the valence anti-strange quark as a function of the Q^2, for the various moments PDF.

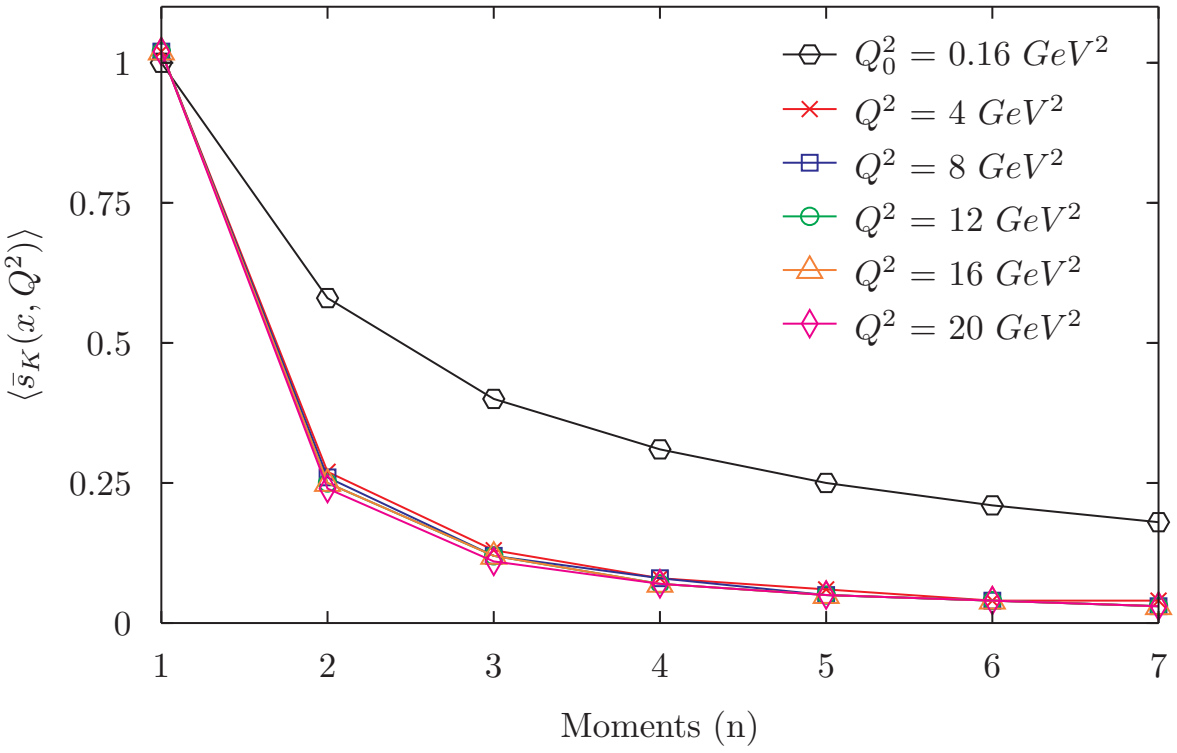

Figure 5.2.5: As in Fig. 5.2.4, but as function of the moments PDF, for the various Q^2.

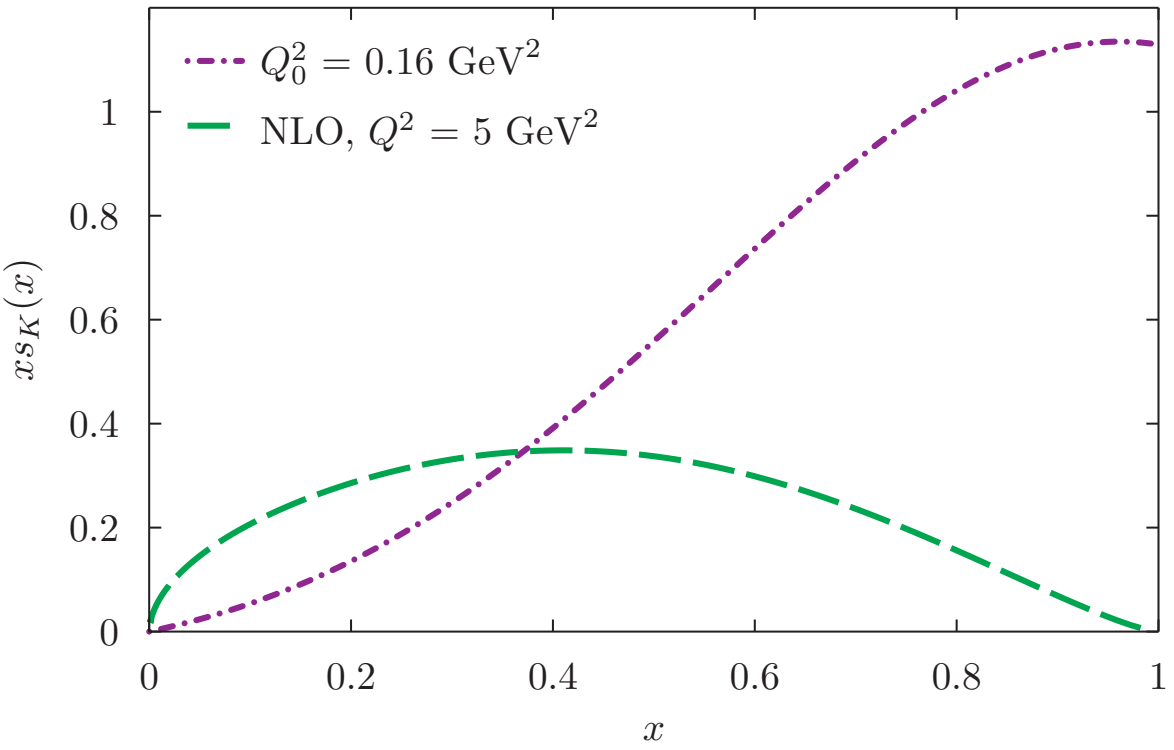

Figure 5.2.6: The valence anti-strange quark distribution of the kaon K^+. The valence anti-strange quark distributions of the kaon at the NJL model scale, $Q_0^2 = 0.16$ GeV^2 (plum dashed dot line) and the valence up quark distribution of the kaon evolved up at NLO to a scale, $Q^2 = 5$ GeV^2 (green dashed line).

In Fig. 5.2.6 we display our result for the valence anti-strange quark distribution, at the NJL model scale, $Q_0^2 = 0.16$ GeV^2. Then, we also show the anti-strange quark distribution evolved at NLO to a scale, $Q^2 = 5$ GeV^2. Figure 5.2.6 indicates that the evolved anti-strange quark distribution has a peak over the range $x = 0$- 0.45 and it then decreases at $x > 0.45$. If we compare the result of the up quark distribution in Fig. 5.2.1 to the result of the anti-strange quark distribution, this shows that the up quark distribution decreases faster than the anti strange quark distribution. This is expected due to the mass of the strange quark is heavier than the light quarks such as the up and down quarks. Also, Figure 5.2.6 shows that the valence anti-strange quark distribution has a peak at around $x \sim 0.45$ at $Q^2 = 5$ GeV^2.

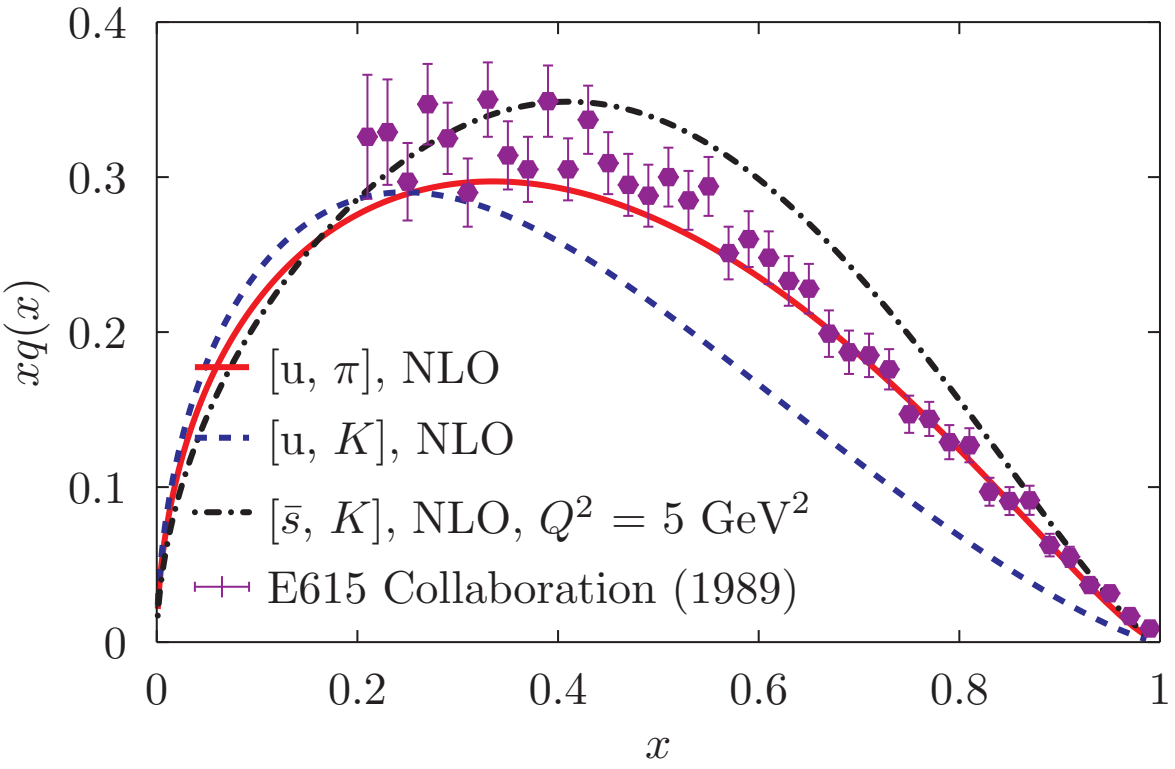

Figure 5.2.7: The valence quark distributions of the kaon and pion at NLO are compared to experimental data. We show the valence up quark distribution of the kaon (blue dashed line), the valence anti-strange quark distributions of the kaon (black dashed dot line) and the valence up quark distribution of the pion (red solid line). The experimental data are taken from Ref. [227] (plum point).

In Fig. 5.2.7 we show a comparison of our results for the valence quark distribution in the kaon and pion to the experimental data [227]. This clearly shows the evolved valence up quark distributions of the pion has a remarkable agreement with this experimental data. In contrast, the valence u-quark distribution of the kaon decreases faster than other valence quark distributions. This indicates that the valence u-quark of the pion carries larger momentum than the valence u-quark of the kaon over the range $x = 0.2$ - 1.0. This result is consistent with previous model analyses [85, 86, 215]. In addition, this difference is obviously seen in Fig. 5.2.9. Moreover, Figure 5.2.7 also shows that the valence anti-strange quark distribution gives the highest contribution to the kaon distribution at large x. This indicates that the heavy strange quark carries a larger fraction of the kaon momentum than that of the light quarks, as explained earlier. This is also consistent with other model calculation predictions [85, 86, 215]. However, the experiment data does not cover the valence quark distribution in the low x region, which is still a problem up to now. This is because the structure function in this region are dominated by sea quarks and gluons. To include the sea quarks and gluons, we must include the higher Fock states in our model [216–219].

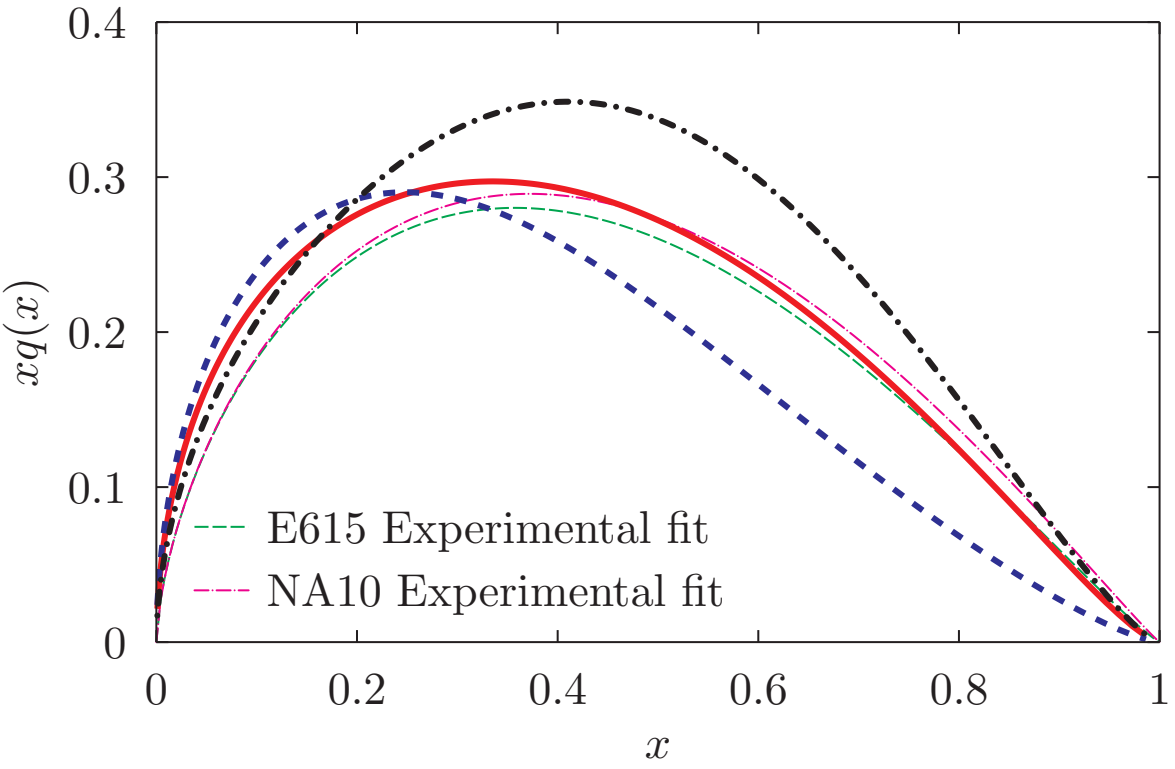

Figure 5.2.8: As in Fig. 5.2.7, but compared to the E615 and NA10 experimental fit [228].

In Fig. 5.2.8 we show a comparison of the valence u-quark distribution of the pion and the valence u-quark and $\bar{s}$- quark distributions of the kaon and the experimental fit in Ref. [228]. We show the valence up quark distribution of the kaon (blue dashed line), the valence anti-strange quark distributions of the kaon (black dashed dotted line) and the valence up quark distribution of the pion (red solid line). The parameterization of the experimental fit has the form

$$xV_\pi = A_v x^\alpha [1-x]^\beta, \tag{5.2.2}$$

where A_v was determined in terms of α and β. For the E615 experimental fit, the values of $A_v = 0.9 \pm 0.3$, $\alpha = 0.64 \pm 0.03$, $\beta = 1.15 \pm 0.02$ were chosen, whereas for the NA10 experimental fit, the values were $A_v = 0.9 \pm 0.3$, $\alpha = 0.64 \pm 0.03$, $\beta = 1.08 \pm 0.02$. More details about these parameters can be found in Ref. [228]. Note that these parameter sets have been compared to the parton distribution at $Q^2 = 5$ GeV^2, as done in this work. Figure 5.2.8 shows that the valence u-quark distribution of the pion shows good agreement with both experimental fit models [228], in particular at large x.

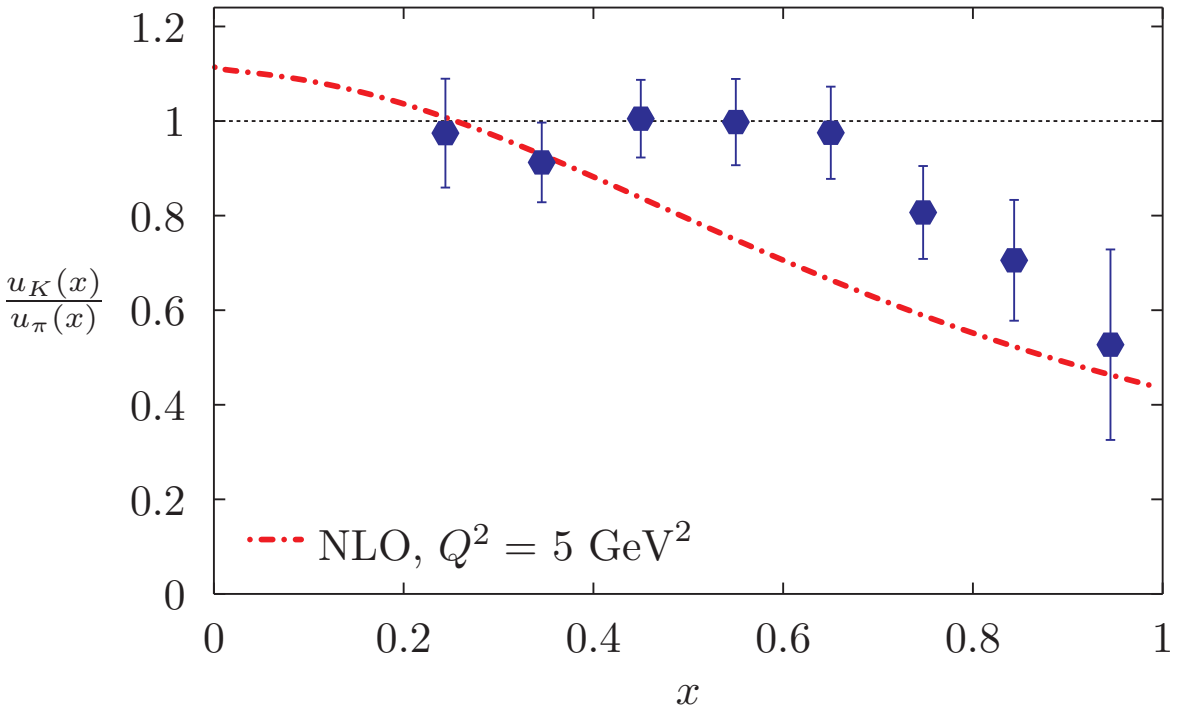

Figure 5.2.9: Ratio of the valence up quark distribution of the kaon to that of the pion, after evolving at NLO to a scale, $Q^2 = 5$ GeV^2 (red dashed dotted line). This ratio is compared to the Drell-Yan experimental data in Ref. [225, 226]. The data is taken from dimuon sample events with invariant mass $4.1 < M < 8.5$ GeV.

In Fig. 5.2.9 we show the ratio of the up quark parton distributions of the kaon to that of the pion, after evolving at NLO to a scale, $Q^2 = 5$ GeV^2. The ratio of the up quark distribution of the kaon to the pion decreases with increasing x. This indicates that the valence up quark distribution of the kaon is lower than the valence up quark distribution of the pion, in contrast with the form factor result, given in Section 4, where the up quark form factor in the kaon is larger than form factor in the pion. In addition, this ratio indicates that the anti-strange quark carries a higher kaon momentum fraction than the up quark. Moreover, our ratio prediction, in Fig. 5.2.9, provides the ratio of the valence up quark distribution of the kaon to the pion at $x \sim 1$, $\frac{u_K(x \sim 1)}{u_\pi(x \sim 1)} \sim$ approximately 0.4. In comparing our result with the experimental data, which is taken from the Drell-Yan experiment in Ref. [225, 226], our result is in good agreement with the available data [225, 226].

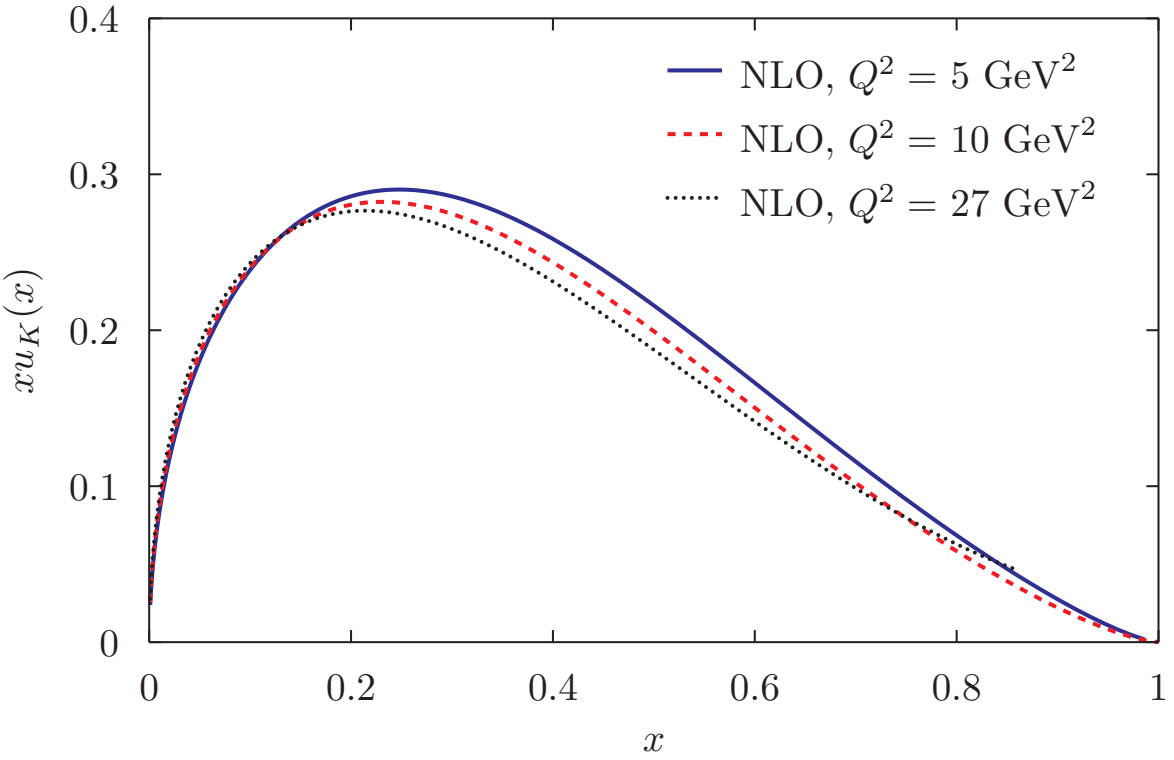

Figure 5.2.10: The valence up quark distribution of the kaon, after evolving at NLO to a scale, $Q^2 = 5$ GeV^2 (red dashed dotted line), 10 GeV^2 and 27 GeV^2.

In Fig. 5.2.10 we display the valence u-quark distribution of the kaon for various $Q^2 = 5$, 10, 27 GeV^2, respectively. The valence u-quark distribution of the kaon, evolved at NLO to a scale $Q^2 = 5$, 10 and 27 GeV^2 are represented by the blue solid line, red dashed line and black dotted line, respectively. Clearly, this shows that the valence u-quark distributions of the kaon decrease above $x \sim 0.15$ with increasing Q^2 evolution. However their shapes look quite similar.

Similarly, Figure 5.2.11 shows the anti-strange quark distribution of the kaon for various Q^2, as in Fig. 5.2.10. The evolved anti-strange quark distribution at NLO to a scale $Q^2 = 5$ GeV^2 has a different distribution, which is quite larger than the others. The evolved anti-strange quark distribution at NLO at a scale $Q^2 = 10$ GeV^2 has the same shape as that of the anti-strange quark distribution at a scale $Q^2 = 27$ GeV^2 . This is very important, since we want to compare our model to experiment in the future, at large Q^2. Also, this may be important to see the behavior of the valence quark distribution at large Q^2.

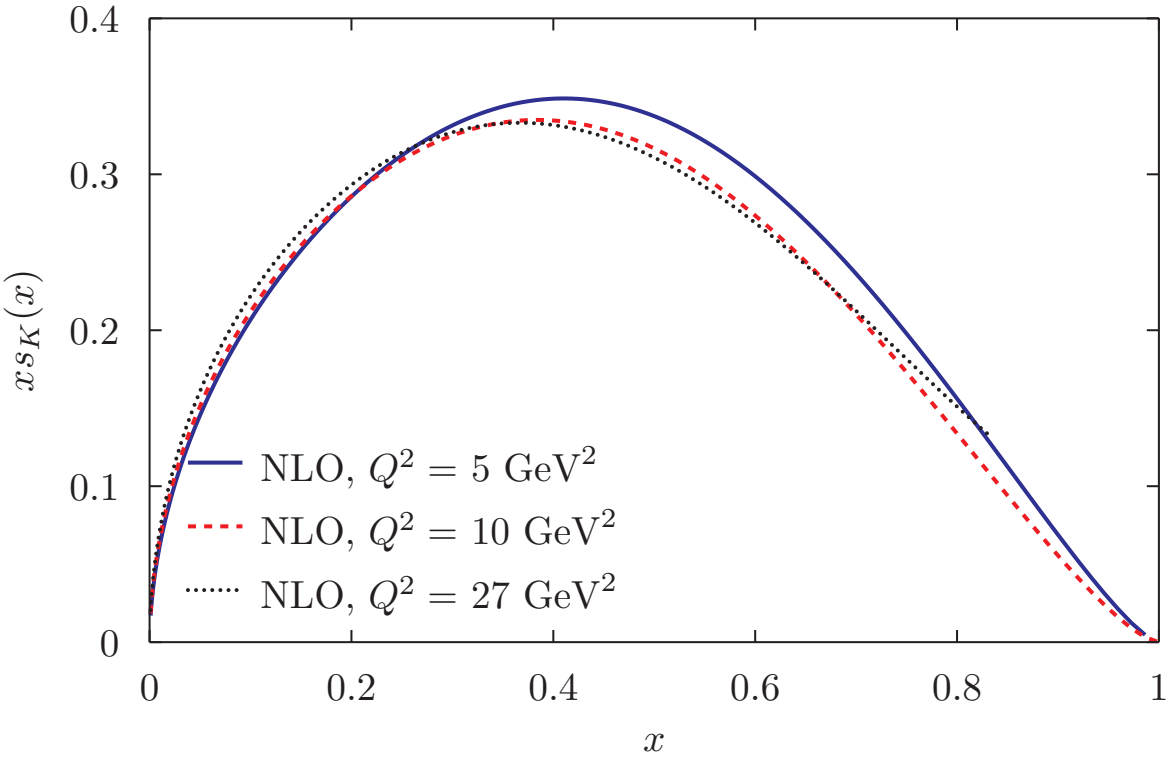

Figure 5.2.11: As in Fig. 5.2.10, but for the valence anti-strange quark distribution of the kaon.

5.3 Quark Distributions of the Pion

In this section we present the derivation of the valence quark distributions of the pion, particularly for positively charge pion π^+, in the NJL model with the help of the proper-time regularization scheme. The derivation is similar to the kaon case. However in the pion case, we consider isospin symmetry, $M_u = M_d = M$, as pointed out in Section 5.2. Consequently, the relation between the valence up-quark distributions of the pion $u_\pi(x)[\equiv q_\pi(x)]$ and the valence anti-down quark distributions $\bar{d}_\pi(x)[\equiv \bar{q}_\pi(x)]$ in Eq. (5.1.10) is $u_\pi(x) = \bar{d}_\pi(x)$. In fact, we only derive one quark distribution.

With this in mind, following the same procedure as for the kaon, the quark distribution of the pion is evaluated based on the Feynman diagram in Fig. 5.1.1, that is

$$q_\pi(x) = \frac{ig^2_{\pi\bar{q}q}}{k_-}\int \frac{d^4q}{(2\pi)^4}\delta\left(x - \frac{q_-}{k_-}\right) Tr\left[\gamma_5 S(q)\gamma^+ S(q)\gamma_5 S(q+k)\right], \tag{5.3.1}$$

$$\bar{q}_\pi(x) = \frac{ig^2_{\pi\bar{q}q}}{k_-}\int \frac{d^4q}{(2\pi)^4}\delta\left(x - \frac{q_-}{k_-}\right) Tr\left[\gamma_5 S(q)\gamma^+ S(q)\gamma_5 S(q+k)\right], \tag{5.3.2}$$

where the $q_\pi(x)$ denotes the valence quark distribution of the pion and $\bar{q}_\pi(x)$ is the valence anti-quark distribution of the pion. The spin independent anti-quark distributions are obtained from the quark distributions in the negative x domain [231, 232],

via the symmetry relation, $\bar{q}(x) = -q(-x)$. The isospin factor in Eq. (5.3.1) has been evaluated $\frac{1}{2}(1 + \tau_q\tau_\pi) = 1$.

Using Ward-Takahashi identity and integrating by parts, Eq. (5.3.1) can be simplified. It then has a form

$$q_\pi(x) = -2iN_C g^2_{\pi\bar{q}q}\frac{\partial}{\partial p^2}\int\frac{d^4q}{(2\pi)^4}\left(x - \frac{q_-}{k_-}\right)Tr\left[\gamma_5 S(q)\gamma_5 S(q-k)\right], \tag{5.3.3}$$

$$\bar{q}_\pi(x) = -2iN_C g^2_{\pi\bar{q}q}\frac{\partial}{\partial p^2}\int\frac{d^4q}{(2\pi)^4}\left(x - \frac{q_-}{k_-}\right)Tr\left[\gamma_5 S(q)\gamma_5 S(q+k)\right], \tag{5.3.4}$$

Note that the $q_\pi(x)$ has support between $0 \leq x \leq 1$ and therefore $\bar{q}_\pi$ has support between $-1 \leq x \leq 0$.

Next, substituting the quark propagators to Eq. (5.3.3), employing the Feynman parameterization, Wick rotation and PTR scheme, one obtains

$$q_\pi(x) = \frac{N_C g^2_{\pi\bar{q}q}}{4\pi^2}\int_0^1 dx\int_{\frac{1}{(\Lambda_{\rm UV})^2}}^{\frac{1}{(\Lambda_{\rm IR})^2}} d\tau\left[\frac{1}{\tau} - x(1-x)m_\pi^2\right]e^{-\tau(x(x-1)m_\pi^2 + M^2)}, \tag{5.3.5}$$

where the formula of the quark distribution of the pion is similar as the anti-quark distribution of the pion, $q_\pi(x) = \bar{q}_\pi(x)$, therefore we do not repeat again the $\bar{q}_\pi(x)$ in Eq. (5.3.5).

The quark and anti-quark distribution of the pion should satisfy the baryon number and momentum conservation, as in Section 5.2. The baryon number sum rules is written as

$$\int_0^1 dx\ u_v^\pi(x) = 1 = \int_0^1 dx\ \bar{d}_v^\pi(x), \tag{5.3.6}$$

where $u_v^\pi(x) = [u_\pi(x) - \bar{u}_\pi(x)]$ and $\bar{d}_v^\pi(x) = [\bar{d}_\pi(x) - d_\pi(x)]$. Here $u_\pi(x)$, $\bar{u}_\pi$, $\bar{d}_\pi(x)$ and $d_\pi(x)$ are the up quark, anti-up quark, anti-down quark and down quark distributions of the pion, respectively. However, $\bar{u}_\pi(x) = 0$ and $d_\pi(x) = 0$. This is because they do not contain the valence quarks of the pion. These sum rules ensure that the π^+ contains one and only one up valence quark and anti-down valence quark.

For the momentum sum rules, the expression can be written as

$$\int_0^1 dx\ x\left[u_v^{\pi^+}(x) + \bar{d}_v^{\pi^+}(x)\right] = 1. \tag{5.3.7}$$

5.4 Results for Quark Distributions of the Pion

In this section, our numerical results of the valence quark distribution of the pion are discussed. The valence quark distribution of the pion in Eq. (5.3.5) are computed using the parameter sets in the NJL model. The valence quark distribution of the pion ought to satisfy the baryon number and momentum sum rules. In order to compare to experimental data, we evolute the valence quark distribution of the pion using the DGLAP [234].

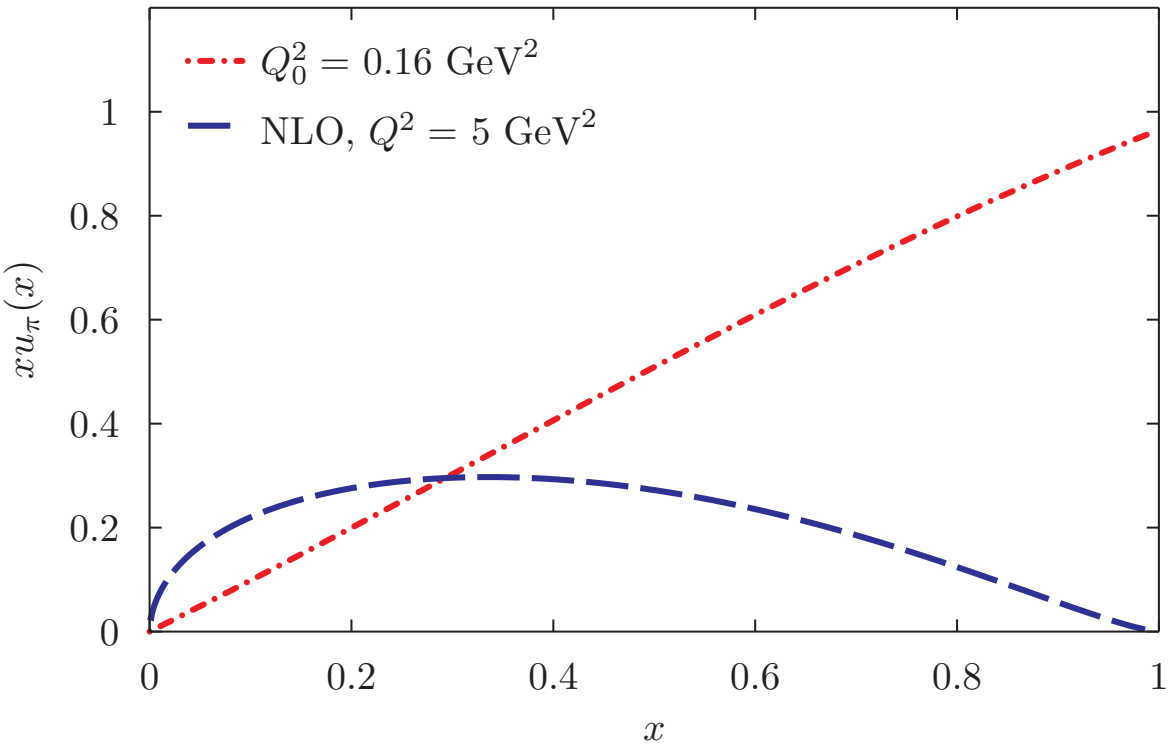

Figure 5.4.1: The valence up quark distribution of the pion. The valence up quark distributions of the pion at the NJL model scale, $Q_0^2 = 0.16$ GeV^2 (red dashed dotted line) and the valence up quark distribution of the pion evolved at NLO to a scale, $Q^2 = 5$ GeV^2 (blue dashed line).

In Fig. 5.4.1 we display our numerical result for the u- quark distribution of the pion at the NJL model scale, $Q_0^2 = 0.16$ GeV^2 and after evolution at NLO to a scale, with the help of the DGLAP [234], $Q^2 = 5$ GeV^2. We see the evolved valence up quark distribution decreases smoothly with increasing above $x \sim 0.3$. The peak of the evolved valence quark distribution is approximately around $x \sim 0.25$. Then the average momentum carried by u-quark in the pion for the various Q^2 as a function of the moments is depicted in Fig. 5.4.3 and for the various moments as a function of the Q^2 is illustrated in Fig. 5.4.4. We also summarize the n^{th} moments of the valence u-quark in the pion in Table 5.4.1.

Figure 5.4.2 shows the valence anti-down quark distribution of the pion which is identical to that of the up quark distribution in the pion, both at the NJL model scale, $Q_0^2 = 0.16$ GeV^2 or at evolved to a scale $Q^2 = 5$ GeV^2. This is because of isospin symmetry, where the constituent quark masses , $M_u = M_d = M$, as pointed out earlier. The valence anti-down quark distributions of the pion at the NJL model scale, $Q_0^2 = 0.16$ GeV^2 (black dashed dotted line) and the valence anti-down quark distribution of the pion evolved at NLO to a scale, $Q^2 = 5$ GeV^2 (red dashed line).

Table 5.4.1: The moments of the pion valence u-quark distribution at the NJL model scale, $Q_0^2 = 0.16$ GeV^2 (second column) and after evolving at NLO to the various scale, $Q^2 = 4$,8 ,12 ,16 ,20 GeV^2 (third column, respectively), where n denotes moments.

n	u_v^π (x, 0.16)	u_v^π (x, 4)	u_v^π (x, 8)	u_v^π (x,12)	u_v^π (x,16)	u_v^π (x, 20)
1	1.00	1.01	1.01	1.01	1.01	1.01
2	0.50	0.23	0.22	0.22	0.21	0.21
3	0.33	0.11	0.10	0.10	0.10	0.10
4	0.25	0.07	0.06	0.06	0.06	0.06
5	0.20	0.05	0.044	0.04	0.04	0.04

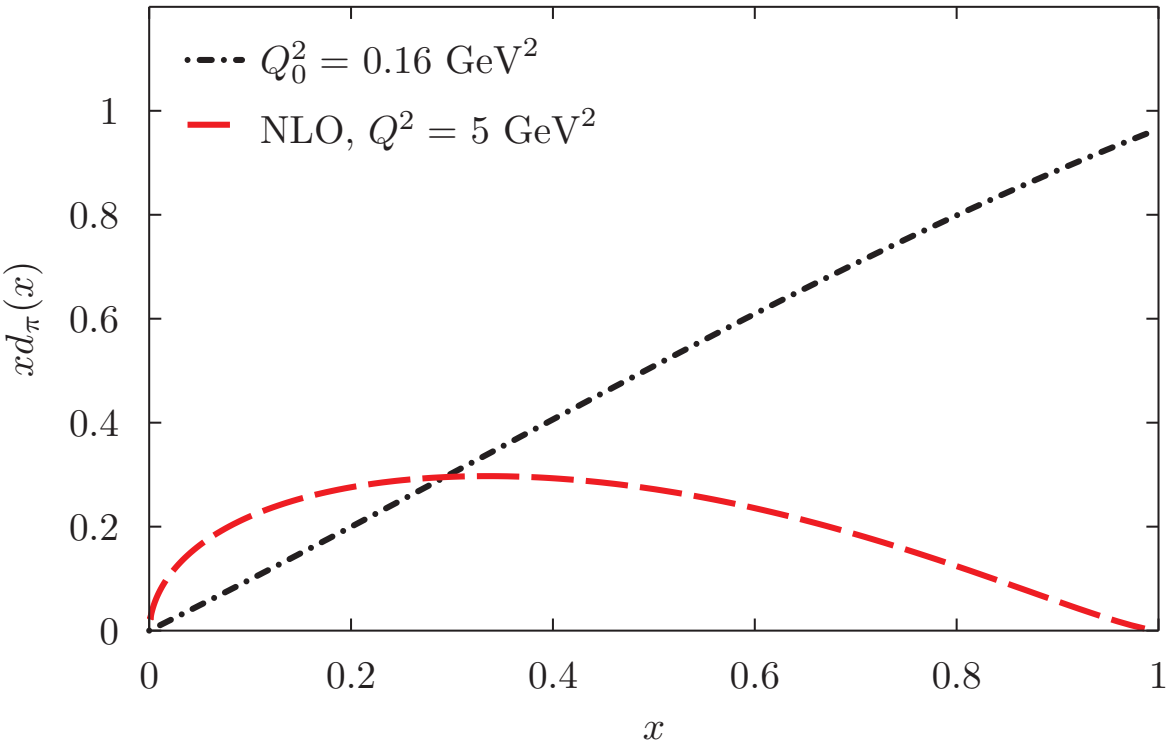

Figure 5.4.2: The valence anti-down quark distribution of the pion.

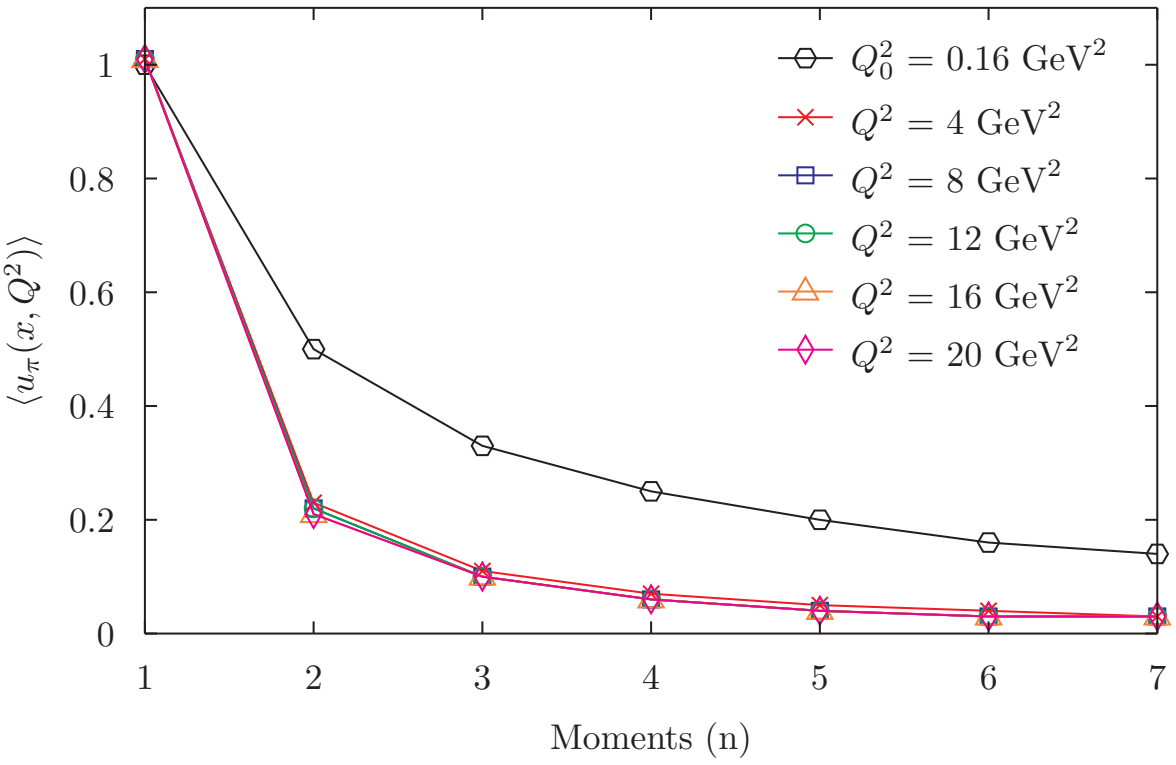

Figure 5.4.3: The average momentum of the valence u-quark distribution of the pion for the various Q^2 as a function of the moments.

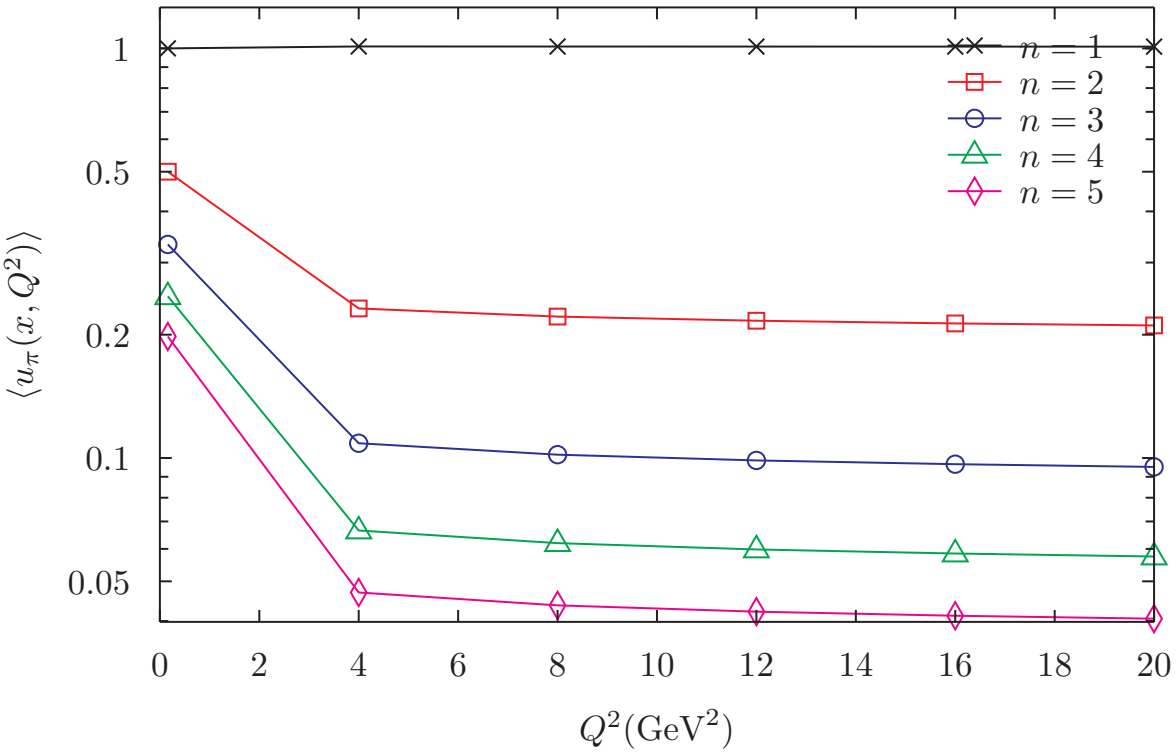

Figure 5.4.4: As in Fig. 5.4.3, but for the various moments as a function of the Q^2.

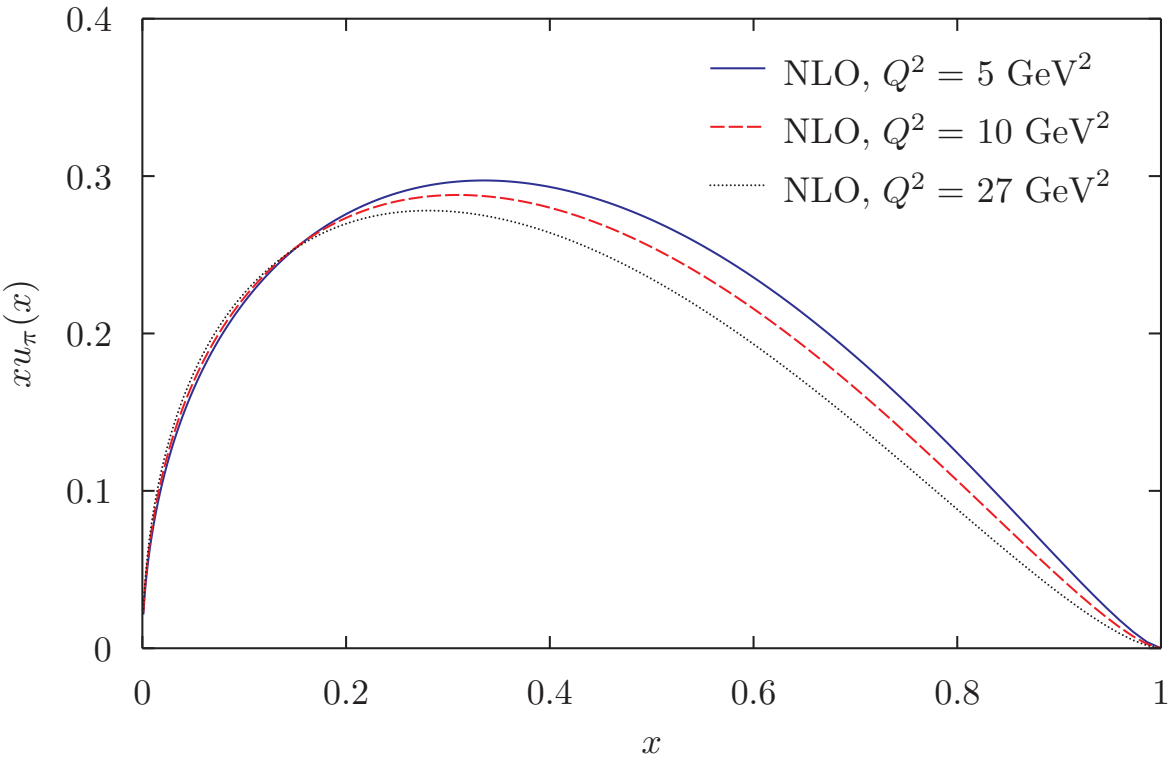

Figure 5.4.5: The valence up quark distribution of the pion, after evolving at NLO to a scale, $Q^2 = 5$ GeV^2 (red dashed dotted line), 10 GeV^2 and 27 GeV^2.

Figure 5.4.3 shows that the average momentum of the valence u-quark decreases with increasing the moments, which is similar trend as in kaon. Finally, we calculate the first two moments of the momentum distribution function of the valence u-quark of the pion using the NJL model with help of the PTR scheme at a evolution scale $Q^2 =$ 4 GeV^2, $2\langle x\rangle_\pi \sim 0.46$ and the second moment, $2\langle x^2\rangle_\pi \sim 0.22$. Our NJL prediction is consistent with predictions of the previous analyses in the various models such as Aicher *et al*. in Ref. [235] has a first moment, $2\langle x\rangle_\pi = 0.55$ and the second moment, $2\langle x^2\rangle_\pi = 0.18$, at a scale $Q^2 = 4$ GeV^2, Sutton *et al*. in Ref. [228] has a first moment, $2\langle x\rangle_\pi = 0.40 \pm 0.02$ and the second moment, $2\langle x^2\rangle_\pi = 0.16 \pm 0.01$, at a scale $Q^2 =$ 4 GeV^2 and Lattice calculation in Ref. [236] has a first moment, $2\langle x\rangle_\pi = 0.46 \pm 0.07$ and the second moment, $2\langle x^2\rangle_\pi = 0.18 \pm 0.05$, at a scale $Q^2 = 49$ GeV^2.

In Fig. 5.4.5 we display the valence u-quark distribution of the pion for the various $Q^2 = 5$, 10, 27 GeV^2, respectively, as in kaon. The valence u-quark distribution of the pion, evolved at NLO, with help of the DGLAP [234], to a scale $Q^2 =$ (5, 10 and 27) GeV^2, are represented by the blue solid line, red dashed line and black dotted line, respectively. This shows that the valence u-quark distributions of the pion decrease with increasing Q^2 evolution above $x \sim 0.25$. In addition, we shows the anti-down quark distribution of the pion for the various Q^2 in Fig. 5.4.6. This indicates that the evolved anti-down quark distribution is identical to the evolved up quark distribution of the pion at all Q^2.

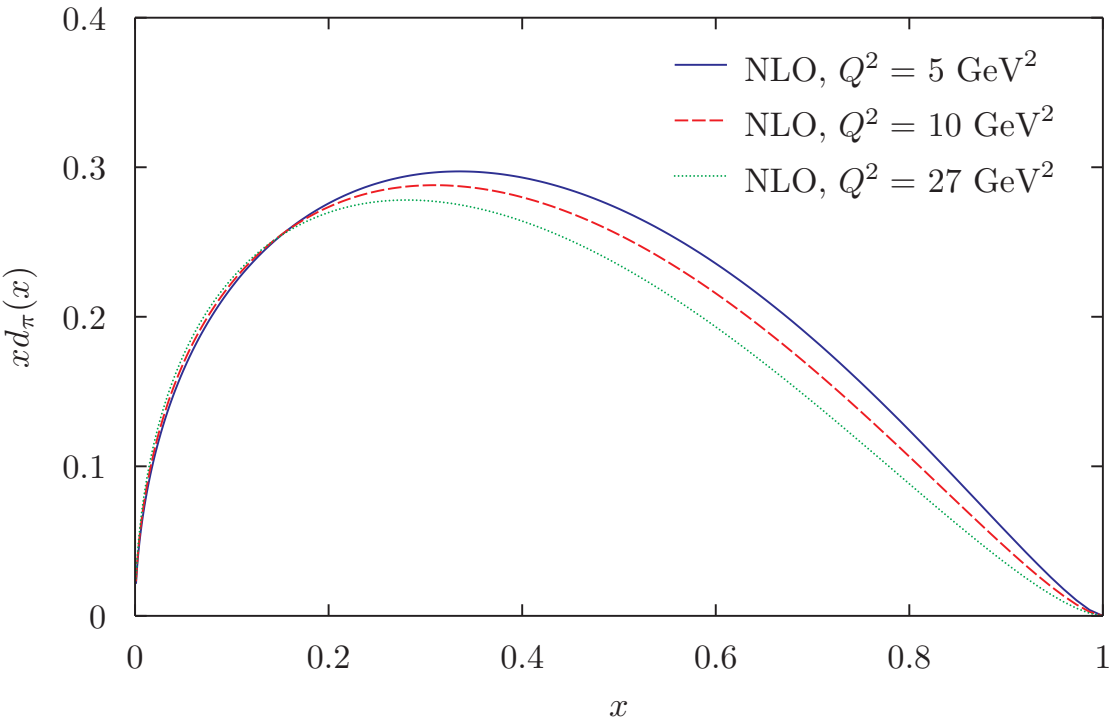

Figure 5.4.6: As in Fig. 5.4.5, but for the valence anti-down quark distribution of the pion.

5.5 Quark Distributions at Large-x

In this section we discuss the valence quark distributions of the kaon and pion at large -x and their relation with the form factor at large Q^2. The limit x $\to$ 1 corresponds to elastic scattering from the target and as such it it natural to expect correspondence between form factors and PDFs in this limit. Such correspondence was first considered by Drell and Yan [237] and West [238] [4], finding relation:

$$F(Q^2) \sim \frac{1}{Q^{2n}}, \quad Q^2 >> \Lambda_{QCD} \qquad \Longleftrightarrow \qquad q(x) \sim (1-x)^{2n-1}, \quad x \to 1, \tag{5.5.1}$$

where n is related to the number of valence constituents in the hadron.

The valence u-quark distributions of the pion, the valence u-quark distributions of the kaon and the valence $\bar{s}$-quark distributions of the kaon has the form

$$u_\pi(x) = \frac{3}{4\pi^2} g^2_{\pi qq} \int \frac{d\tau}{\tau} e^{-\tau(-k^2(x-x^2)+M^2)} \left[1 + k^2\tau(x-x^2))\right], \tag{5.5.2}$$

where $k^2 = m_\pi^2$.

$$u_K(x,k^2) = \frac{N_C g^2_{Kqq}}{4\pi^2} \int d\tau \frac{1}{\tau} e^{-\tau(k^2(x^2-x)+xM_2^2-M_1^2(x-1))}$$

[4] Later it is well known as the Drell-Yan West relation.

$$\times \left[1+\tau\left[k^2(x-x^2)-(x-x^2)(M_2-M_1)^2\right]\right]. \tag{5.5.3}$$

$$\bar{s}_K(x,k^2) = \frac{N_C g_{Kqq}^2}{4\pi^2}\int d\tau \frac{1}{\tau} e^{-\tau(k^2(x^2-x)+xM_1^2-M_2^2(x-1))} \times \left[1+\tau\left[k^2(x-x^2)-(x-x^2)(M_1-M_2)^2\right]\right], \tag{5.5.4}$$

where $k^2 = m_K^2$. These equations satisfy the baryon number and momentum sum rules, as explained in the previous section. Our numerical results for the valence quark distributions at large x will be discussed in Section 5.6.

5.6 Results for Quark Distributions at large-x

In this section we discuss our complementary result for the kaon and pion PDF at large x. Through the parton distribution functions of the kaon and pion in Eqs. (5.5.2)-(5.5.4), we numerically evaluate the PDF of the kaon at $x \to 1$ for large -x. We note that the valence quark distribution in the low energy scale has no physical meaning at this model scale, since the valence quark distribution at the low energy scale consider non-negligeble contributions from all twist operator. However we just show our result for the valence quark distributions within the kaon at the model scale, $Q_0^2 = 0.16\ GeV^2$:

$$u_{K^+}(x \to 1) = 0.4, \tag{5.6.1}$$

$$\bar{s}_{K^+}(x \to 1) = 1.13, \tag{5.6.2}$$

similarly for the pion case, we obtain

$$u_{\pi^+}(x \to 1) = \bar{d}_{\pi^+}(x \to 1) = 1. \tag{5.6.3}$$

Our results for the valence quark distributions of the kaon for varying Q^2 will be shown in Table 5.6.1. We then compute the ratio between the valence u-quark distributions of the kaon and pion at large x ($x \to 1$), one obtains

$$\frac{u_{K^+}(x\sim 1)}{u_{\pi^+}(x\sim 1)} = 0.4. \tag{5.6.4}$$

On the contrary, the Dyson-Schwinger equation rainbow-ladder (DSE-RL) prediction in Ref. [215] gives

$$\frac{u_{K^+}(x\sim 1)}{u_{\pi^+}(x\sim 1)} = \frac{f_\pi}{f_K}\left(\frac{M_u}{M_s}\right)^4 = 0.3, \tag{5.6.5}$$

and at low momentum scale the NJL model result using the sharp cutoff in Ref. [85, 86] yields the ratio,

$$\frac{u_{K^+}(x\sim 1)}{u_{\pi^+}(x\sim 1)} = \left(\frac{M_u}{M_s}\right)^2 = 0.5. \tag{5.6.6}$$

Table 5.6.1: The valence quark distributions of the kaon and pion at large x for varying Q^2.

Q^2 (GeV^2)	$u_{K^+}(x\to 1)$	$\bar{s}_{K^+}(x\to 1)$	$u_{\pi^+}(x\to 1)$	$\frac{u_{K^+}(x\to 1)}{u_{\pi^+}(x\to 1)}$	$\frac{\bar{s}_{K^+}(x\to 1)}{\bar{d}_{\pi^+}(x\to 1)}$
Q_0^2=0.16 GeV^2	0.4	1.13	1.00	0.4	1.18
4	0.002	0.0054	0.0046	0.4	1.17
8	0.001	0.0036	0.0031	0.3	1.16
12	0.001	0.0029	0.0025	0.4	1.16
16	0.00098	0.0026	0.0022	0.4	1.18
20	0.00088	0.0023	0.00198	0.4	1.16
10^2	0.00047	0.0012	0.0011	0.4	1.09
10^4	0.00013	0.00036	0.00030	0.4	1.20
10^6	0.000057	0.00015	0.00013	0.4	1.15

Using the DYWR [237–240], we attempt to understand the behavior of the valence quark distributions at large x and large Q^2. To achieve our goal, we simply calculate the valence quark distributions of the kaon and pion and evolve them with the help of the DGLAP at a scale $Q^2 = \left(4, 8, 12, 16, 20, 10^2, 10^4, 10^6\right)$ GeV^2. After evolving the valence quark distributions, we numerically compute the valence quark distribution at large x for each Q^2. Our numerical results are summarized in Table 5.6.1. We find $\frac{u_K(x)}{u_\pi(x)} \sim 0.4$ as $x \to 1$, in good agreement with existing data from Ref. [225].

5.7 Drell Yan West Relation

In this section we calculate the valence quark distribution at large x and Q^2 via DYWR. By using the values of the valence quark distribution at large x for each the squared four momentum transfer in Table 5.7.1, we extract the n parameter which shows the number of constituent quark inside kaon or pion. Based upon DWYR in Eq. (5.5.1), the scaling behaviour of the kaon and pion PDF and the logarithm of them, as x approximate to one, for the pion is written as

$$u_\pi(x) = \bar{d}_\pi(x) \sim (1-x)^{2n-1} \sim (1-x)^{\beta_{u_\pi}} \tag{5.7.1}$$

$$\ln[u_\pi(x)] = (\beta_{u_\pi}) \ln[(1-x)], \tag{5.7.2}$$

where $\beta_{u_\pi} = 2n-1$ is taken for simple calculation and similarly for the kaon can be expressed

$$u_K(x) \sim (1-x)^{\beta_{u_K}} \tag{5.7.3}$$

Table 5.7.1: The values of n of the valence quark distribution of the kaon and pion. The values of β are extracted using Eqs. (5.7.1) - (5.7.3). Using a relation between β and n, which is defined as $\beta_{u_\pi} = 2n_{u_\pi} - 1$, we can determine $n_{u\pi}$. The values of β parameter is obtained from the fitting procedure.

Q^2 (GeV^2)	β_{u_π}	n_{u_π}	β_{u_K}	n_{u_K}	β_{s_K}	n_{s_k}
4	1.299	1.2	1.400	1.2	1.330	1.2
8	1.390	1.2	1.488	1.2	1.420	1.2
12	1.437	1.2	1.532	1.3	1.466	1.2
16	1.468	1.2	1.562	1.3	1.497	1.2
20	1.490	1.2	1.584	1.3	1.519	1.2
10^2	1.631	1.3	1.720	1.4	1.659	1.3
10^4	1.908	1.4	1.989	1.5	1.934	1.5
10^6	2.097	1.5	2.173	1.6	2.121	1.5
Q_0^2=0.16 GeV^2	0.0027	0.5	0.0018	0.5	0.015	0.5

$$\bar{s}_K(x) \sim (1-x)^{\beta_{u_{\bar{s}}}} \tag{5.7.4}$$
$$\ln[u_K(x)] = (\beta_{u_K}) \ln[(1-x)] \tag{5.7.5}$$
$$\ln[\bar{s}_K(x)] = (\beta_{\bar{s}_K}) \ln[(1-x)]. \tag{5.7.6}$$

Now we extract the n [5] parameter in Eq. (5.7.1). The values of the $\beta_{u\pi}$ and $n_{u\pi}$ is found in Table 5.7.1.

Using almost the same procedure, we can extract the power scaling of the kaon and pion form factors in Eq. (5.5.1). We firstly recall the general formula for the pseudoscalar form factor in the asymptotic region, it has the form

$$F_P(Q^2) = \frac{1}{Q^{2n}}. \tag{5.7.7}$$

By applying the logarithm in the both sides in Eq. (5.7.7), one obtains

$$\ln[F_P(Q^2)] = -n \ln[Q^2], \tag{5.7.8}$$

where P denotes pseudoscalar mesons. We then calculate the logarithm of the kaon and pion form factors, one then obtains

$$\ln[F_u^{K^+}(Q^2)] = \ln[\frac{0.52 e_u}{Q^2}] = \ln[\frac{0.345}{Q^2}] = \ln[0.345] - \ln[Q^2] \tag{5.7.9}$$

[5] $\beta_{u\pi} = 2n_{u\pi} - 1$ stand for the extracted paramater (constant) from the valence u-quark distributions of the pion at larger -x and $n_{u\pi}$ can be also determined.

$$\ln[F_{\bar{s}}^{K^+}(Q^2)] = \ln[\frac{0.23e_s}{Q^2}] = \ln[0.08] - \ln[Q^2]. \tag{5.7.10}$$

We then extract the n for the kaon form factor by comparing the general form factor in Eq. (5.7.8) and our form factor calculation results in Eq. (5.7.9). This clearly indicates that $n \sim 1$ for the up and strange quarks in the kaon. A summary of results can be found in Table 5.7.2.

Similarly for the pion, one obtains

$$\begin{aligned} \ln[F_u^{\pi^+}(Q^2)] &= \ln[0.45e_u] - \ln[Q^2] = \ln[0.3] - \ln[Q^2], \\ \ln[F_{\bar{d}}^{\pi^+}(Q^2)] &= \ln[0.45e_d] - \ln[Q^2] = \ln[0.15] - \ln[Q^2], \end{aligned} \tag{5.7.11}$$

A result summary of the power scaling for the pion form factor is provided in Table 5.7.2.

Table 5.7.2: The n values for the kaon and pion form factor.

particle	$n_{F_u^\pi}$	$n_{F_{\bar{d}}^\pi}$	n_π	$n_{F_u^K}$	$n_{F_{\bar{s}}^K}$	n_K
Pion (u $\bar{d}$)	1	1	1			
Kaon (u $\bar{s}$)				1	1	1

Overall, we find that the valence quark distributions of the kaon and pion behave as $q_\pi \sim (1-x)^1$ after DGLAP evolution to various Q^2, as shown in Table 5.7.1. In addition, the kaon and pion form factors at large -Q^2 have a form $F_P(Q^2) \sim \frac{1}{Q^2}$.

5.8 Conclusion

The valence quark distributions of the kaon and pion have been computed. Our numerical result for the positively charged kaon is shown in Fig. 5.2.1. We found that the distribution peak for the evolved up quark distributions is at around $x \sim 0.2$. The average momentum fraction carried by the valence quarks in the kaon at the NJL model scale, $Q_0^2 = 0.16$ GeV^2:

$$\int_0^1 dx x \left[u_v^K(x, Q_0^2) + \bar{s}_v^K(x, Q_0^2)\right] = 0.42 + 0.58 = 1. \tag{5.8.1}$$

This means at the model scale, Q_0^2, all the momentum of the positively charged kaon are carried by the kaon's valence quarks. This result is consistent with the DSE-RL result [215]. The average momentum of the valence u-and $\bar{s}$-quarks of the kaon are summarized in Table 5.2.1 and 5.2.2.

Thus, the valence quarks in the kaon and pion are compared to the available experimental data [227]. The u-quark distribution in the pion has a good agreement with the data [227]. In addition, the u-quark distribution also agrees well with the E615 and NA10 experiment fit models [228].

We compared our ratio prediction, $\frac{u_K(x)}{u_\pi(x)}$, after evolving at NLO to a scale, $Q^2 = 5$ GeV^2 to the existing data, as illustrated in Fig. 5.2.9. Our result has a good agreement with the existing data [225]. At $x \sim 1$, the ratio, $\frac{u_K(x)}{u_\pi(x)}$, is approximately 0.4.

Finally, we find that the valence quark distributions of the kaon and pion behave as $q_\pi \sim (1-x)^1$ after DGLAP evolution to various Q^2, as shown in Table 5.7.1. In addition, the kaon and pion form factors at large -Q^2 have a form $F_P(Q^2) \sim \frac{1}{Q^2}$.

6

Charge Symmetry Violation

In the preceding chapters the form factors and parton distribution functions of the kaon and the pion have been discussed. In those calculations we considered that the non-strange quarks to satisfy charge symmetry [1], which implies $m_u = m_d$, and hence $M_u = M_d$ as in Refs. [241–244]. However, these non-strange quarks actually have slightly different masses in nature [244–246], where $m_u \neq m_d$, and hence $M_u \neq M_d$ [241–246]. This is because at the partonic level, charge symmetry is broken spontaneously, but it is hidden by DCSB. This intrinsic quark mass difference leads to the so-called charge symmetry violation (CSV) [2]. For instance, the quark mass differences can be found in the Particle Data Group (PDG) [16] and several previous analyses in chiral perturbation theory (ChPT) [247, 248], that is, the light quark masses of the m_u = 2.3 ± 0.7 (0.5) MeV and m_d = 4.8 ± 0.7 (0.3) MeV and the ratio of the u- and the d-quark masses, namely $\frac{m_u}{m_d}$ = 0.38 - 0.58 and $\frac{m_s}{m_d}$ = 17 - 22 [16]. Consequently, this u-d quark mass difference has an implications for the isospin breaking in the masses of the composite particles (mass splitting) such as the proton and neutron masses, the negatively charge pion and the neutral pion masses and the negatively charge kaon and the neutral kaon masses. Experimentally, the value of the mass differences of the octet baryons are $m_p - m_n$ = -1.29 MeV, $m_{\Sigma^0} - m_{\Sigma^-}$ = - 4.81 ± 0.04 MeV, $m_{\Sigma^+} - m_{\Sigma^-}$ = - 8.08 ± 0.08 MeV, and $m_{\Xi^0} - m_{\Xi^-}$ = - 6.50 ± 0.25 MeV, and the value of the quark mass differences of the kaons and pions are, respectively, $\Delta m_\pi = m_{\pi^\pm} - m_{\pi^0}$ = 4.5936 ± 0.0005 MeV and $\Delta m_K = m_{K^\pm} - m_{K^0}$ = - 3.995 ± 0.0034 MeV [249, 250]. Aside from its implications for the mass splitting of different particles, as mentioned

[1] Charge symmetry is related to the invariance of the QCD Hamiltonian invariance under a 180^o rotation about the 2-axis in isospace corresponding to the interchange of u and d quarks and also protons and neutrons. At the partonic level, charge symmetry implies the equality of different parton distribution functions: $u^p(x,Q^2) = d^n(x,Q^2), \quad d^p(x,Q^2) = u^n(x,Q^2)$. There is an analogous relation for anti-quark PDF.

[2] In some references, CSV is also called as charge symmetry breaking (CSB).

earlier, the CSV in parton distribution functions also plays a significant role in order to determine a precision tests of the weak interaction in the Standard model [251]. An understanding of CSV is required to explain the discrepancy between the predicted and measured binding energy differences of mirror nuclei, which is well known as the Okamoto-Nolen-Schiffer anomaly [252, 253, 255] and to reduce the 3σ deviation from the standard model found in the NuTeV measurement [256].

From point of view of QCD, CSV arises due to the quark mass differences between non-strange quarks as well as an electromagnetic interaction among the non-strange quarks [257–260]. However, an electromagnetic interaction has a minor contribution at higher energies and is less well known. It is expected that the contribution of the electromagnetic force with coupling constant, $\alpha_{EM} = \frac{1}{137}$, on masses are at the 1 % level or smaller, as mentioned in Ref. [261], therefore it is very difficult to measure. Recently, with a fully dynamical simulation of QED+QCD technique, the QCDSF-UKQCD collaboration observed the pseudo-scalar meson masses to study the effect of CSV is due to QCD, arising from the u-d quark mass difference and the effect of CSV is due to QED, arising from the different charges of the light quarks [261]. They found that the effect of the electromagnetic interaction is very small in the pions because the quarks are very light, however it is much larger in the kaons because the strange quark mass is heavier. Therefore, the non-strange quark mass differences become an interesting feature of the QCD view of CSV. In addition, CSV is an important background in the extraction of the strange vector form factor of the nucleon [262]. In the past, some theoretical and phenomenological calculations have been performed on the nucleon electromagnetic form factors [262] and parton distribution function (PDF) [263–269]. Also, another investigation on the nuclear CSV has been performed by Coon et al. [265]. In their letter, they suggested a connection between the CSV at low energy in nuclear [3] and particle physics.

At this stage there is very little in the way of a quantitative determination of the extent of CSV. Definitive experiments are certainly needed. Several attempts to measure CSV have been performed. One previous measurement result indicated that the experimental limit of CSV in PDFs was around, approximately, 5-10 % [266, 267]. Knowledge of the extent of CSV is critical to test physics beyond the standard model [267] and to find a new physics beyond standard model. A recent work on CSV has been investigated on the spin independent and dependent parton distribution functions of the nucleon [268]. They found that the chiral corrections are qualitatively more significant for the spin-independent moments and its effect to the spin dependent CSV moments are quite small. Therefore, our work, in this thesis, is certainly relevant to the exploration of the CSV effect on PDF and the electromagnetic form factor of the pseudoscalar mesons. The results of this work are very useful to provide the additional contributions of CSV in the kaon and pion PDF to the Drell-Yan ratio. Note that the largest contribution arises from the differences between $\bar{d}$-quark in the positively charged pion (π^+) and the u-quark in the negatively charged pion (π^-), as explained in Ref. [264].

[3]The parton distribution functions obey the chiral symmetry at nuclear physics energy scale. This is because the CSV effects are extremely small in this energy scale.

In this chapter, we explore and investigate the CSV effect in the parton spin-independent distribution functions and form factors of the pseudoscalar mesons in the NJL model, with the help of the proper-time regularization scheme. They provide valuable insight into the nuclear environment sensitivity of the quark distributions inside the kaon or pion. In this work, we focus on CSV arising from the light constituent quark mass differences, which is represented by $\delta M = M_u - M_d$. This is because the isospin symmetry breaking through the current quark masses is not usually observed in hadronic physics but through the constituent quark masses. The light quark mass difference contribution is expected, approximately, one percent of any typical energy scale of QCD. Next, here, we define the expression for the average constituent quark mass, $M = \frac{1}{2}(M_u + M_d)$, where M_u and M_d denote the constituent masses of the up and anti-down quarks, respectively. Using the gap equation of the NJL model, we numerically obtain the constituent quark mass, $M = 0.4$ GeV, which is used in this work. With this expression of M, the constituent masses of the up and anti-down quarks in the pion are formulated as

$$M_u = M - \delta M, \tag{6.0.1}$$

$$M_d = M + \delta M, \tag{6.0.2}$$

where δM [4] denotes the light quark mass difference and more details can be found in Refs. [257–259, 267]. Thus, we explore the effect of the light quark mass difference on the u-quark sector form factor of the pion, $F_u^\pi(Q^2)$ in Eq. (4.2.8) and the d-quark sector form factor of the pion, $F_d^\pi(Q^2)$ in Eq. (4.2.8), respectively, by plugging the new masses of the light quarks, $M \to M_u$ and $M \to M_d$, in Eq. (6.0.1). Similarly, for the kaon, we only consider the non-strange valence quark changing. We then investigate the light quark mass difference effect in the kaon PDF and FF by evaluating their ratio and differences. Note that, in the kaon case, the down and up quarks come from the different kaons, namely, K^0 and K^+. We emphasize that we will observe CSV effect in the kaon parton distribution functions in Eqs. (5.1.10) and (5.3.5), as pointed out earlier. The constituent quark masses with δM are then utilized as the input to the form factors and parton distribution functions. In our form factor calculation, we ignore the charge of the quarks in order to purely see CSV effect in the form factors. Our formalism and numerical results will be discussed in the next section.

6.1 Charge Symmetry Violation in Form Factors

In this section charge symmetry violation on the quark sector form factor of the kaons and pions is discussed. To investigate effect of the quark mass difference δM in the kaon and pion quark sector form factors, we recall the expression of the quark sector form factors in Eq. (4.2.8) for quark sector form factors and Eq. (4.2.12) and (4.2.13)

[4] The values of δM are chosen based on the current $u - d$ mass difference and therefore the values of δM ought to be (0.0033, 0.0050, 0.010) GeV, since those values are more realistic.

for the quark sector form factors for the kaon in Section 4.2, respectively, that is

$$\begin{aligned}
F^u_{\pi^+}(Q^2) = & \frac{N_C g_{\pi q\bar{q}^2}}{4\pi^2}\int_0^1 dx \int_{\frac{1}{(\Lambda_{\rm UV})^2}}^{\frac{1}{(\Lambda_{\rm IR})^2}} \frac{d\tau}{\tau} e^{-\tau(-Q^2(x^2-x)+M_u^2)} \\
& + \frac{N_C g^2_{\pi q\bar{q}}}{4\pi^2}\int_0^1 dx \int_0^{1-x} dz \int_{\frac{1}{(\Lambda_{\rm UV})^2}}^{\frac{1}{(\Lambda_{\rm IR})^2}} d\tau \\
& \times e^{-\tau(k^2[(x+z)^2-(x+z)]+xzQ^2+M_d^2(1-x-z)+M_u^2(x+z))} \\
& \times [k^2(x+z)+(M_u-M_d)^2(x+z)-2M_d^2+2M_dM_u], \qquad (6.1.1)
\end{aligned}$$

$$\begin{aligned}
F^d_{\pi^+}(Q^2) = & \frac{N_C g_{\pi q\bar{q}^2}}{4\pi^2}\int_0^1 dx \int_{\frac{1}{(\Lambda_{\rm UV})^2}}^{\frac{1}{(\Lambda_{\rm IR})^2}} \frac{d\tau}{\tau} e^{-\tau(-Q^2(x^2-x)+M_d^2)} \\
& + \frac{N_C g^2_{\pi q\bar{q}}}{4\pi^2}\int_0^1 dx \int_0^{1-x} dz \int_{\frac{1}{(\Lambda_{\rm UV})^2}}^{\frac{1}{(\Lambda_{\rm IR})^2}} d\tau \\
& \times e^{-\tau(k^2[(x+z)^2-(x+z)]+xzQ^2+M_u^2(1-x-z)+M_d^2(x+z))} \\
& \times [k^2(x+z)+(M_d-M_u)^2(x+z)-2M_u^2+2M_uM_d], \qquad (6.1.2)
\end{aligned}$$

$$\begin{aligned}
F^u_{K^+}(Q^2) = & \frac{N_C g^2_{Kq\bar{q}}}{4\pi^2}\int_0^1 dx \int_{\frac{1}{(\Lambda_{\rm UV})^2}}^{\frac{1}{(\Lambda_{\rm IR})^2}} \frac{d\tau}{\tau} e^{-\tau(-Q^2(x^2-x)+M_u^2)} \\
& + \frac{N_C g^2_{Kq\bar{q}}}{4\pi^2}\int_0^1 dx \int_0^{1-x} dz \int_{\frac{1}{(\Lambda_{\rm UV})^2}}^{\frac{1}{(\Lambda_{\rm IR})^2}} d\tau \\
& \times e^{-\tau(k^2[(x+z)^2-(x+z)]+xzQ^2+M_s^2(1-x-z)+M_u^2(x+z))} \\
& \times [k^2(x+z)+(M_u-M_s)^2(x+z)-2M_s^2+2M_sM_u], \qquad (6.1.3)
\end{aligned}$$

$$\begin{aligned}
F^s_{K^+}(Q^2) = & \frac{N_C g^2_{Kq\bar{q}}}{4\pi^2}\int_0^1 dx \int_{\frac{1}{(\Lambda_{\rm UV})^2}}^{\frac{1}{(\Lambda_{\rm IR})^2}} \frac{d\tau}{\tau} e^{-\tau(-Q^2(x^2-x)+M_s^2)} \\
& + \frac{N_C g^2_{Kq\bar{q}}}{4\pi^2}\int_0^1 dx \int_0^{1-x} dz \int_{\frac{1}{(\Lambda_{\rm UV})^2}}^{\frac{1}{(\Lambda_{\rm IR})^2}} d\tau \\
& \times e^{-\tau(k^2[(x+z)^2-(x+z)]+xzQ^2+M_u^2(1-x-z)+M_s^2(x+z))} \\
& \times [k^2(x+z)+(M_s-M_u)^2(x+z)-2M_u^2+2M_uM_s]. \qquad (6.1.4)
\end{aligned}$$

Clearly, $F^u_{\pi^+}(Q^2) \neq F^d_{\pi^+}(Q^2)$, because of the constituent u-d quark mass differences. The constituent u quark mass is denoted by $M_u = M - \delta M$ and the constituent d-quark mass is denoted by $M_d = M + \delta M$. Our numerical results for the CSV on the quark sector form factors within the kaon and pion will be discussed in Section 6.2.

6.2 Results for the Charge Symmetry Violation in the Pion Form Factor

In this section our numerical results for the ratio of the u quark sector form factor to $\bar{d}$ quark sector form factor in the pion ($\pi^+ = u\bar{d}$), $\frac{F_\pi^u(Q^2)}{F_\pi^{\bar{d}}(Q^2)}$ as a function of the virtual four momentum transfer are discussed. Note that the u and $\bar{d}$ quark charges are not considered in the calculation in order to observe purely the quark mass difference effect, as pointed out earlier. The full parameter sets of the NJL model used in this calculation can be found in Section 4.3 and our previous paper [159]. The numerical results will give information not only on the direct effect of the quark mass but also the influence of the nuclear environment inside the pion. This information is also very useful if we want to extend to the more complex systems such as the proton, neutron and octet baryon.

With these new definitions of M_u and M_d, we fix $\delta M = 0.000$ GeV, $\delta M = 0.0033$ GeV, $\delta M = 0.0050$ GeV and $\delta M = 0.010$ GeV, respectively. Next, we employ the new values of the M_u and M_d as an input to the form factors in Eq. (6.1.1). Our numerical results on the ratio of the u-quark sector form factor to $\bar{d}$-quark sector form factor in the pion, which is composed by the valence quark $\pi^+ = u\bar{d}$, $\frac{F_\pi^u(Q^2)}{F_\pi^{\bar{d}}(Q^2)}$ as a function of the virtual squared four momentum transfer Q^2 is depicted in Fig. 6.2.1. A summary of the new values of the M_u and M_d, their ratio and their effect on the pion mass is shown in Table. 6.2.1.

Later on, we also investigate the quark mass differences in the quark sector form factors of the different kaons in Section 6.2.1. In this thesis, we extract the quark mass differences from the $K^0 - K^+$ mass differences to determine the value of the CSV. We know that the neutral kaon consists of the d and $\bar{s}$ quarks and the positively charged kaon consists of the u and $\bar{s}$ quarks, at the parton level. Since we intend to determine the value of the u-d quark mass differences from the kaon mass difference K^0 - K^+, then we commonly consider that the $\bar{s}$-quark is as a spectator, so it can be subtracted out from the kaon mass difference. With this in mind, for instance, let us consider the neutral kaon mass $m_{K^0} = 497.67$ MeV and the positively charged kaon $m_{K^+} = 493.68$ MeV, the value of the quark mass difference, which is determined from the kaon mass differences, is qualitatively obtained by means of $m_{K^0}(497.67)$ - $m_{K^+}(493.68) \sim M_d$ - $M_u = 3.99$ MeV. The various values of the quark mass difference used in the quark sector form factors analysis are based on this M_d - M_u value. Our numerical results for the CSV effects on the quark sector form factors within the kaon are given in the next section below.

Table 6.2.1: The values of the up and anti-down quark masses and pion mass m_π by taking the constituent up and anti-down quark masses, $M_u = M - \delta M$ and $M_d = M - \delta M$, respectively. In this work, we set the constituent quark mass $M = 0.40$ GeV, which is computed using the NJL model. The model parameters used in this calculation are $\Lambda_{UV} = 0.645$ GeV, $m_q = 0.0164$ GeV, $g_{\pi q\bar{q}} = 4.23$, and $f_\pi = 0.093$ GeV [159]. All units are in GeV and $\delta M = M_d - M_u$.

M_u	M_d	δM	$\frac{m_u}{m_d}$	m_π^2	m_u	m_d
0.400	0.400	0.000	1.00	0.0196	0.016	0.016
0.3967	0.4033	0.0033	0.57	0.0196	0.012	0.020
0.395	0.405	0.005	0.42	0.0197	0.0096	0.023
0.390	0.410	0.010	0.10	0.0198	0.0030	0.030

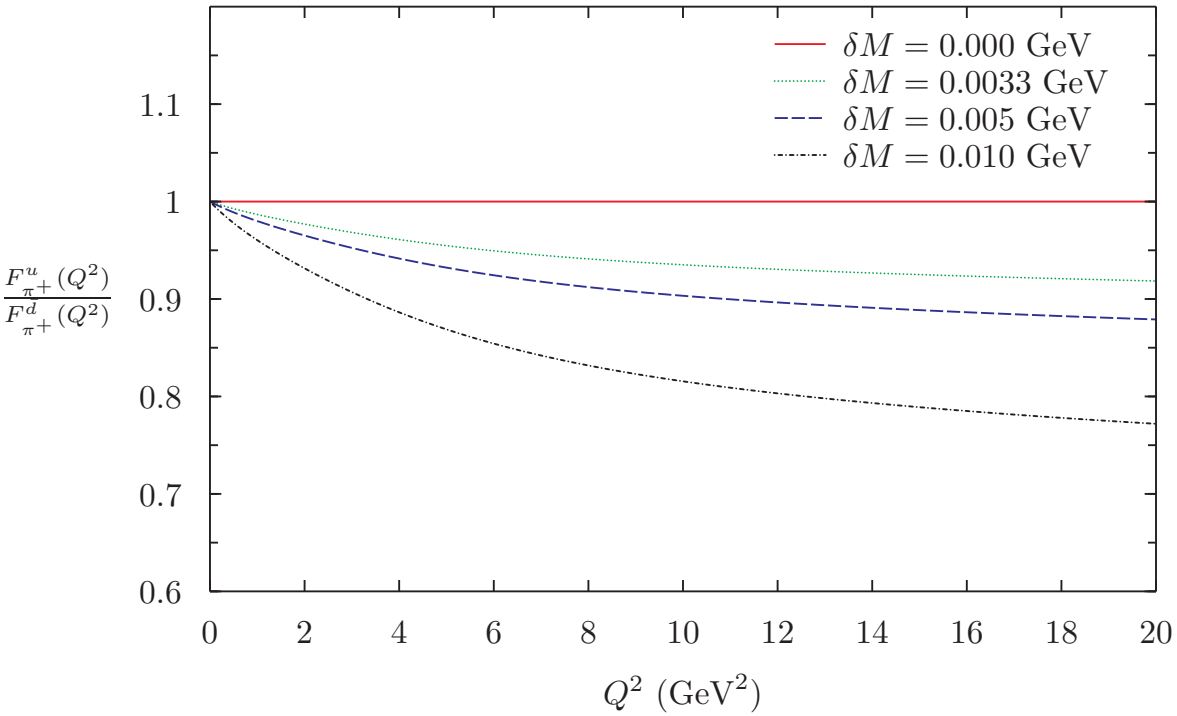

Figure 6.2.1: Ratio of the up quark sector form factor to anti-down quark sector form factor in the pion for the various δM as a function of the virtual squared four momentum transfer Q^2.

In Fig. 6.2.1 we display that the ratio of the u-and d-quark sector form factors, $\frac{F^u_\pi(Q^2)}{F^{\bar{d}}_\pi(Q^2)}$, for the various values of δM, as a function of Q^2. The ratios are calculated

for the $\delta M = 0.000$ GeV [5] (red solid line), $\delta M = 0.0033$ GeV (green dotted line), $\delta M = 0.0050$ GeV (blue dashed line) and $\delta M = 0.010$ GeV (black dot-dashed line), respectively. This clearly shows that the $\frac{F_\pi^u(Q^2)}{F_\pi^{\bar{d}}(Q^2)}$ decreases with increasing Q^2 and δM. This indicates that the distribution of the down quark in the pion is larger than the up quark distribution, as the value of the δM increases. In Fig. 6.2.2 we show the change in the individual quark contribution, $F_{\pi^+}^u(Q^2)$, as M_u decreases, whereas in contrast Fig. 6.2.3 shows $F_{\pi^+}^{\bar{d}}(Q^2)$, as M_d increases. By multiplying the individual quark sector form factors by Q^2, we emphasize the corresponding effects at higher Q^2 in Figs. 6.2.4 and 6.2.5.

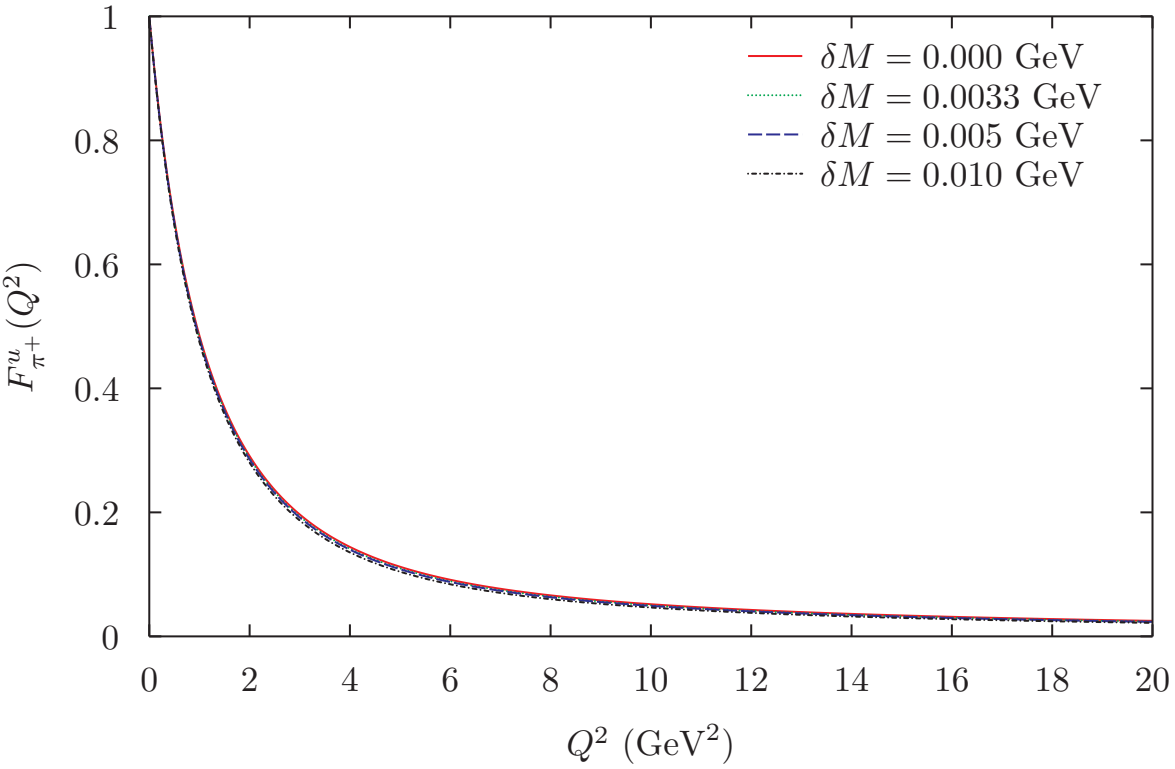

Figure 6.2.2: The up quark sector form factor of the pion for the various δM as a function of the virtual squared four momentum transfer, Q^2.

[5] The $\delta M = 0.000$ means that $M_u = M_d$, which implies charge symmetry.

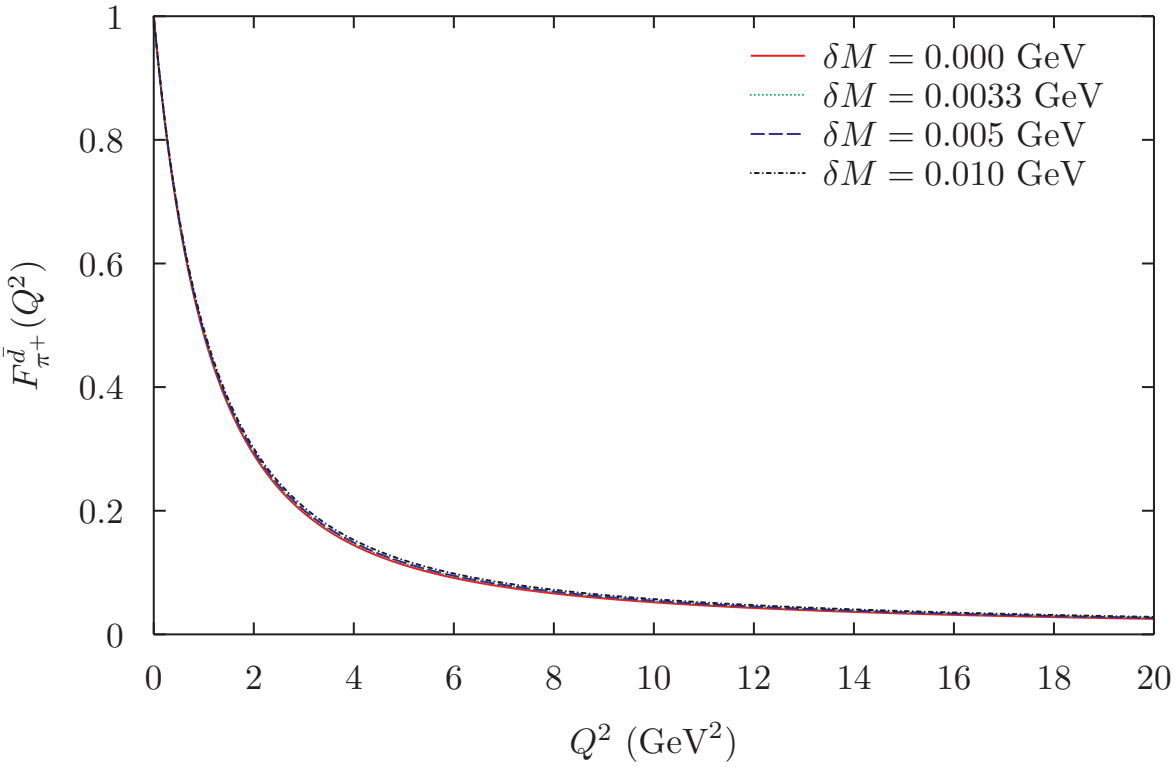

Figure 6.2.3: As in Fig. 6.2.2, but for the anti-down quark sector form factor.

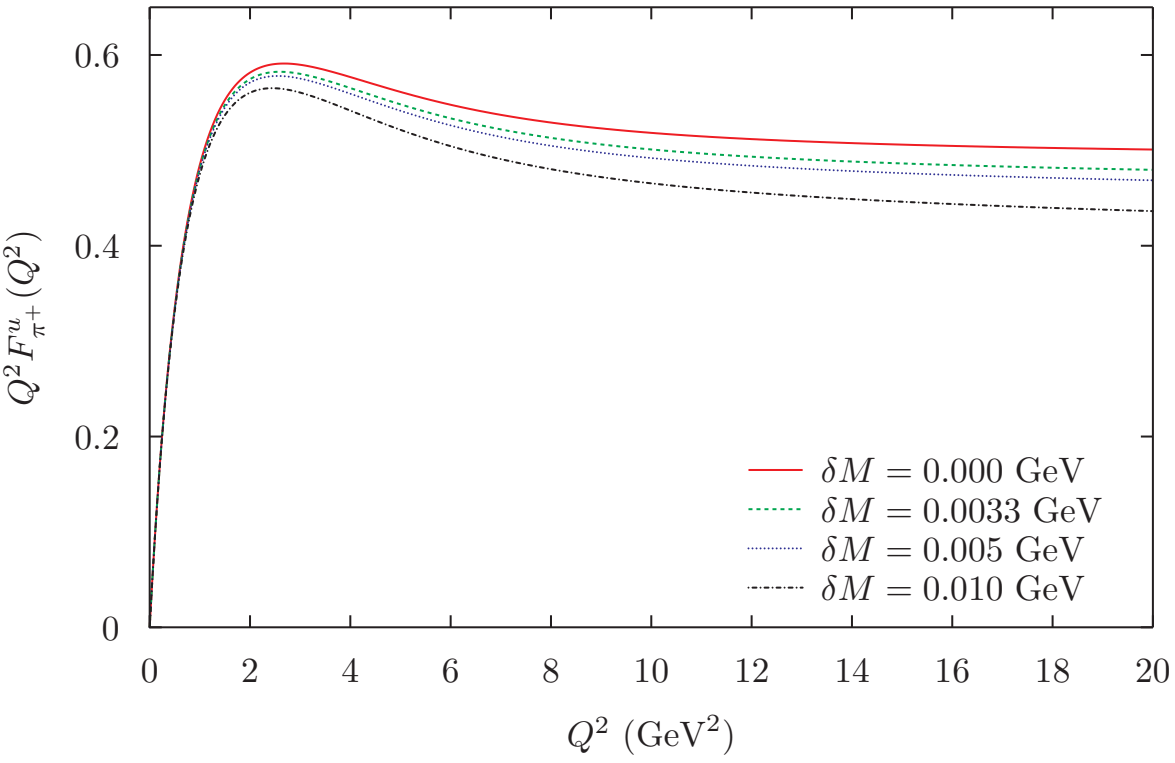

Figure 6.2.4: The up-quark sector form factor of the pion multiplied by Q^2 for the various δM as a function of the virtual squared four momentum transfer Q^2.

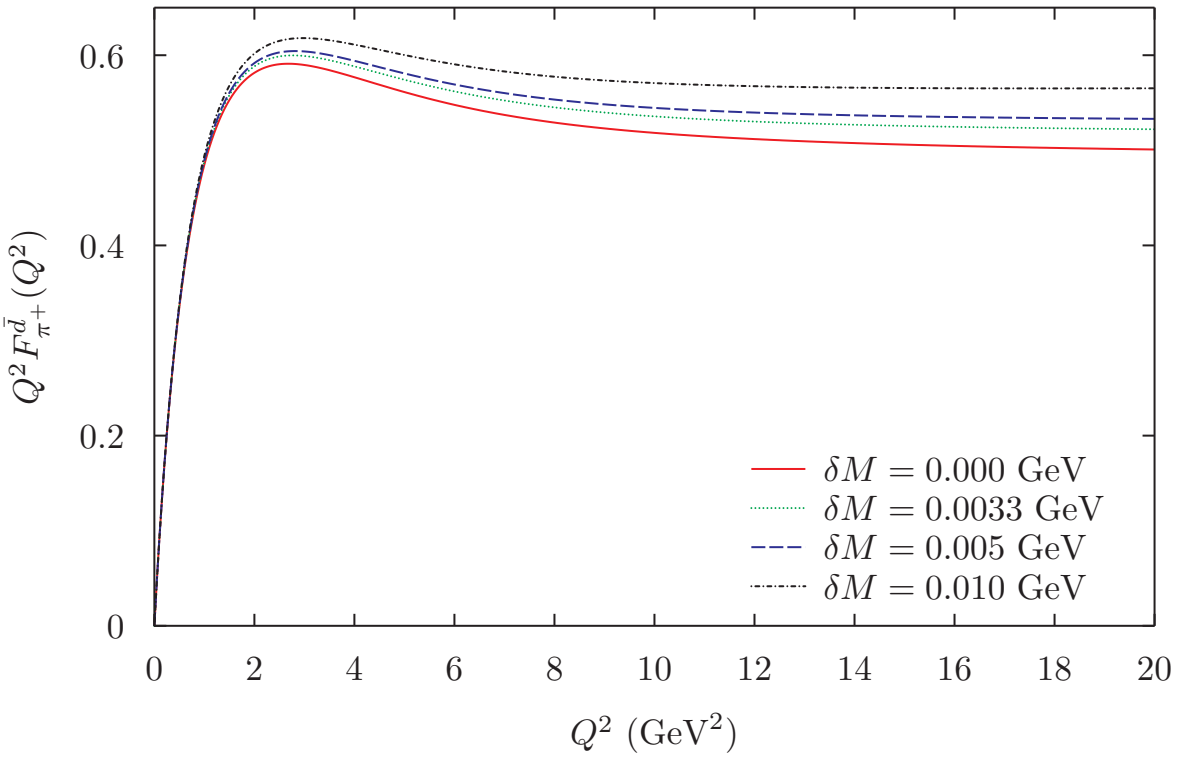

Figure 6.2.5: As in Fig. 6.2.4, but for the anti-down quark sector form factor of the pion.

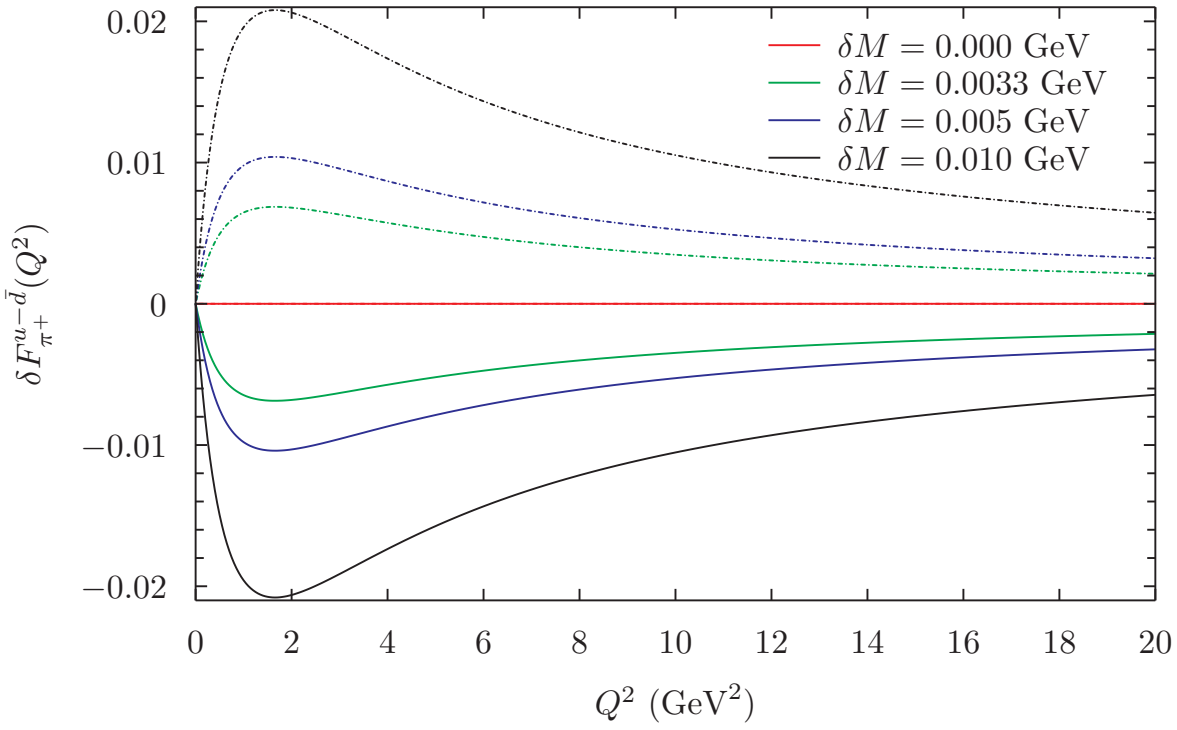

Figure 6.2.6: As in Fig. 6.2.4, but for $\delta F^{u-\bar{d}}_{\pi^+}(Q^2) = F^{u}_{\pi^+}(Q^2) - F^{\bar{d}}_{\pi^+}(Q^2)$ (solid line) and $\delta F^{\bar{d}-u}_{\pi^+}(Q^2) = F^{\bar{d}}_{\pi^+}(Q^2) - F^{u}_{\pi^+}(Q^2)$ (dashed line).

Figure 6.2.6 shows our numerical results for the difference $\delta F_{\pi^+}^{u-\bar{d}}(Q^2) = F_{\pi^+}^{u}(Q^2) - F_{\pi^+}^{\bar{d}}(Q^2)$ (solid line) and $\delta F_{\pi^+}^{\bar{d}-u}(Q^2) = F_{\pi^+}^{\bar{d}}(Q^2) - F_{\pi^+}^{u}(Q^2)$ (dashed line) as a function of Q^2. Explicitly, the quark sector form factor differences, $\delta F_{\pi^+}^{u-\bar{d}}(Q^2)$ within the pion grows with increasing quark mass differences, δM and Q^2. Their differences, $\delta F_{\pi^+}^{u-\bar{d}}(Q^2)$ and $\delta F_{\pi^+}^{\bar{d}-u}(Q^2)$, have opposite sign, but they are the same in magnitude. Then the relation between both can be written as $\delta F_{\pi^+}^{u-\bar{d}}(Q^2) = -\delta F_{\pi^+}^{\bar{d}-u}(Q^2)$. This also means $F_{\pi^+}^{u}(Q^2) < F_{\pi^+}^{\bar{d}}(Q^2)$, since the constituent u-quark mass is smaller than constituent $\bar{d}$-quark mass. Overall, this qualitatively indicates that the quark sector form factors are very sensitive to the quark mass differences δM. In other words, this result confirms that CSV has a quite significant effect to the quark sector form factors in the pion.

6.2.1 Kaon Form Factor

Next, we discuss our numerical results for the CSV effect on the quark sector form factors within the kaons. Using a similar procedure to the pion case, the u-d quark mass difference (CSV) effect on the quark sector form factors within the different types of kaon are calculated using Eqs. (6.1.3) and (6.1.4). In this calculation, we emphasize that the u-quark comes from the positively charged kaon (K^+) and the $\bar{d}$-quark comes from the neutral kaon (K^0), as pointed out earlier. Our numerical results for the quark sector form factors of different kaons are shown in Figs. 6.2.7.

In Fig. 6.2.7, we display our result for the ratio of the up quark sector form factor in the kaon plus ($K^+ = [u, \bar{s}]$) to the down quark form factor sector in the kaon neutral ($K^0 = [d, \bar{s}]$). Similar procedure to the pion case, the quark sector form factors do not include the quark charges in the calculation.

Based on Dashen's theorem, the electromagnetic effects for positively charged mesons, namely K^+ and π^+ are the same in magnitude, whereas neutral mesons such as K^0 and π^0 disappear [272]. However, the electromagntic effect is not easy to handle in particular for the kaon. Therefore, we just consider the quark mass difference, without the electromagnetic effects, in this section. The ratio are calculated for the $\delta M = 0.000$ GeV (red solid line), $\delta M = 0.0033$ GeV (green dotted line), $\delta M = 0.0050$ GeV (blue dashed line) and $\delta M = 0.010$ GeV (black dot-dashed line), respectively. This shows that the ratios, $\dfrac{F_{\mathrm{K}^+}^{u}(Q^2)}{F_{\mathrm{K}^0}^{d}(Q^2)}$, for the various the quark mass differences δM, explicitly decrease with increasing non-strange quark mass differences, δM and Q^2.

The analysis of the CSV effect for the ratio of the individual quark form factors of the kaons can be seen in Figs. 6.2.8 and 6.2.9. We plot the ratio of the valence quark form factors for the positively charged kaon K^+ and neutral kaon K^0, respectively. These figures are very useful to clearly see the behavior of the individual u- and $\bar{s}$-quark sector form factors in the K^+ and of the individual d- and $\bar{s}$-quark sector form factors within the K^0 by varying the quark mass differences and also to explain the ratio in Fig. 6.2.7 clearly. Figure 6.2.8 indicates that the u-quark sector form factor in K^+ decreases with increasing δM and Q^2, as illustrated in Fig. 6.2.10. This result confirms that, in the K^+ the u-quark sector form factor is suppressed approximately 10 % of the s-quark sector form factor. In particular, we concentrate on the u and d-quarks sector form factors, rather than the s-quark in the K^+ and K^0, respectively.

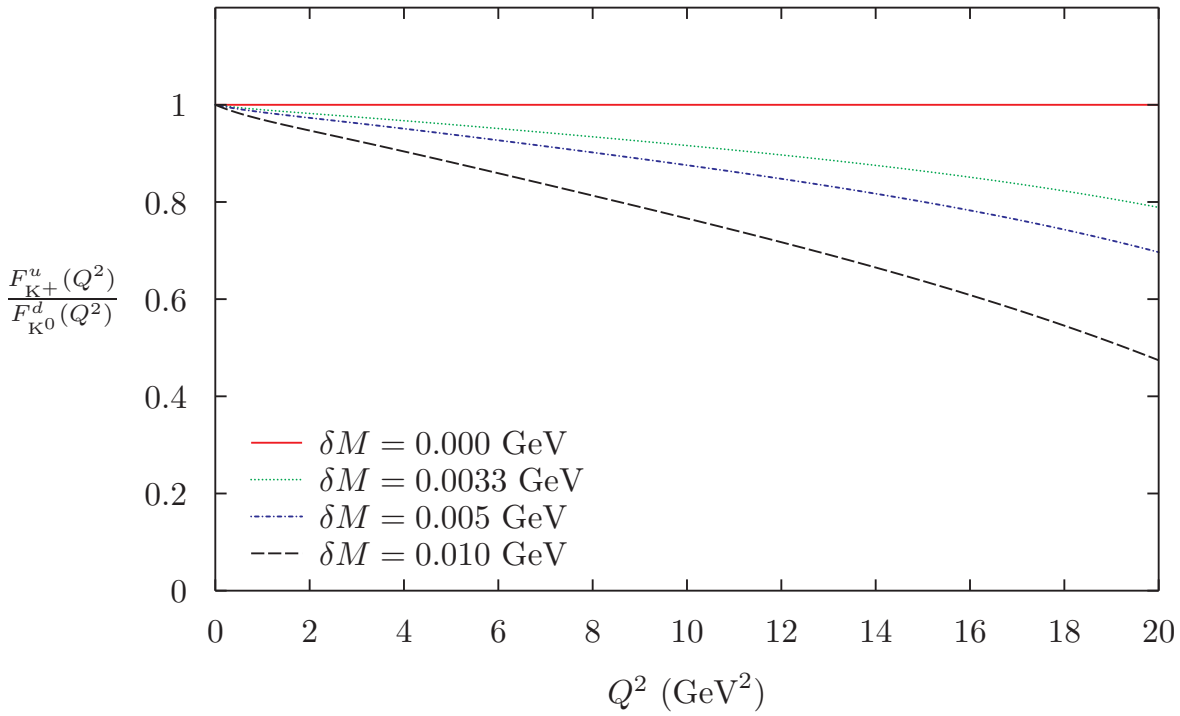

Figure 6.2.7: Ratio of the up quark sector form factor in the kaon plus (K^+) to the down quark sector form factor in the kaon neutral (K^0) as a function of the virtual squared four momentum transfer Q^2.

Later on, we show the effect of CSV in $F^s_{K^+}(Q^2)$ and $F^s_{K^0}(Q^2)$ in order to give a full description of the CSV effect in the kaon. Figure 6.2.10 shows the CSV has a sizable effect on the u-quark sector form factor in the K^+, as explained earlier. On the contrary, the CSV effect on $F^s_{K^+}(Q^2)$ changes only a little bit with varying δM. The $\bar{s}$-quark sector form factor in the K^+ increases with increasing δM, as shown in Fig. 6.2.11.

We then explore the quark sector form factor of the internal structure of the K^0 for the various δM. To explore the behavior of the valence quark within the K^0, we plot the ratio of and individual quark sector form factor as a function of δM and and Q^2 in Figs. 6.2.9, 6.2.12 and 6.2.13. Figure 6.2.9 shows that the ratio of $\frac{F^d_{K^0}(Q^2)}{F^s_{K^0}(Q^2)}$ increases with increasing δM, but decreases with increasing Q^2. This means that the $F^d_{K^0}(Q^2)$ is larger than the $F^s_{K^0}(Q^2)$ for the various δM. This is more clearly seen from the individual quark sector form factors in the K^0 in Figs. 6.2.12 and 6.2.13. Note that the d-quark sector form factor of the K^0 is the same in magnitude as the u-quark sector form factor in the K^+, whereas the $\bar{s}$-quark sector form factor of the K^0 is the same magnitude as the $\bar{s}$-quark form factor in the K^+. This indicates that the d-quark sector form factor within the K^0 increases with increasing the δM and decreases with decreasing Q^2. The tendency of the d-quark sector form factor in the K^0 and u-quark sector form factor in the K^+ are different and have reverse sign. For the strange quark in the K^0, the $F^s_{K^0}(Q^2)$ decreases with increasing δM. This indicates that the $\bar{s}$ quark sector form factor in the K^0 is suppressed by the d-quark sector form factor in the K^0.

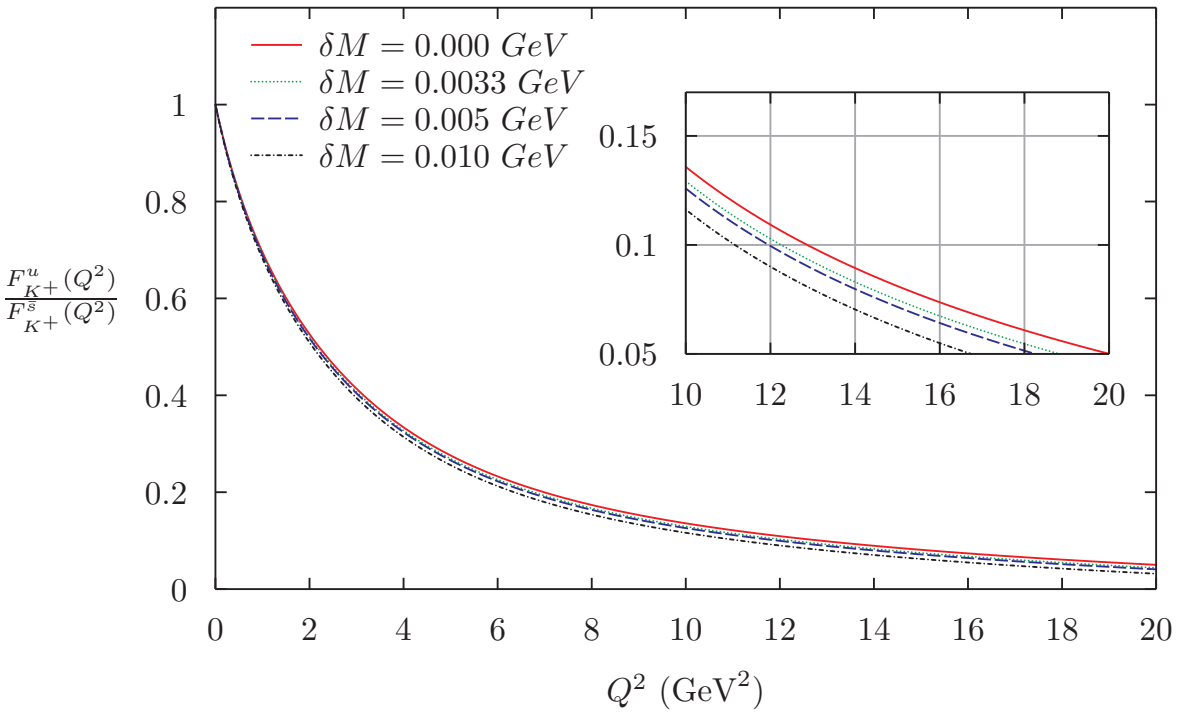

Figure 6.2.8: The CSV effect for the u- quark sector form factor in the kaon plus (K^+) as a function of the virtual squared four momentum transfer, Q^2.

Therefore, this implies that $F^s_{K^+}(Q^2) > F^s_{K^0}(Q^2)$.

Finally, our numerical results on the CSV show its significant contribution to the quark sector form factors in the kaon, This would be of great interest to confirm our results with the new experimental data in the future. Unfortunately, at present, there is no data available yet to test our results for the CSV effect in the quark sector form factors, in particular for the kaon form factors. However, our result can be used as a guide tool for the future experiments, other sophisticated models and lattice QCD studies.

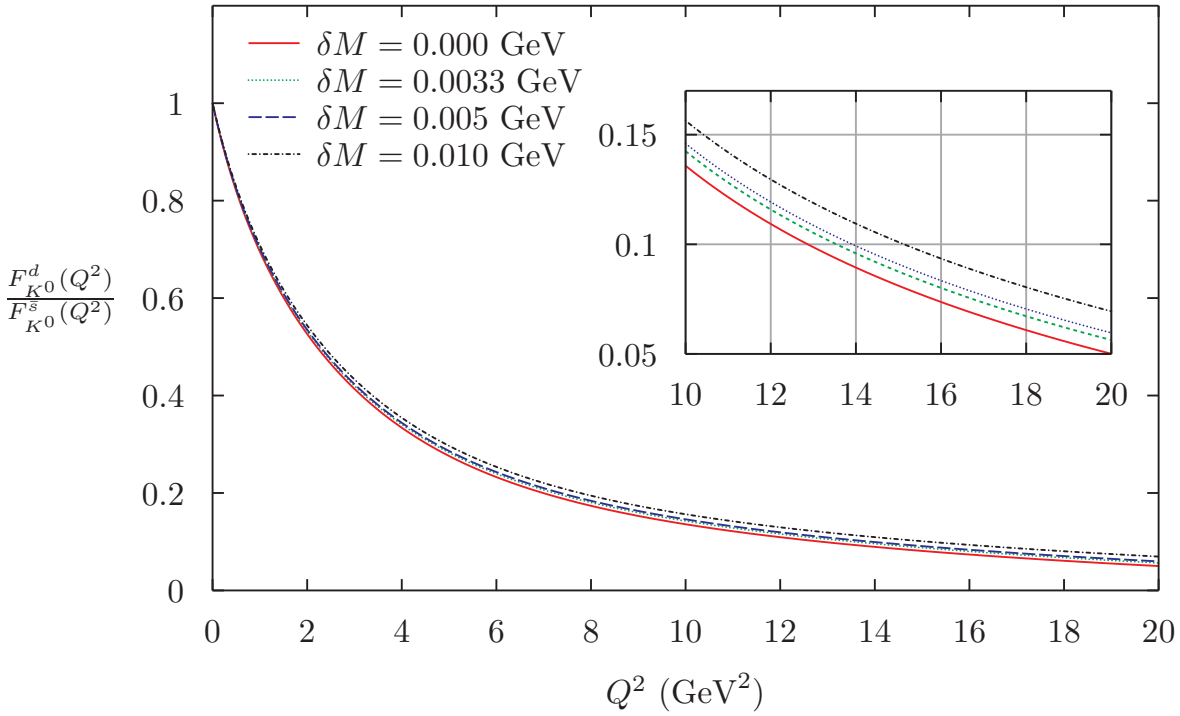

Figure 6.2.9: As in Fig. 6.2.8, but for K^0.

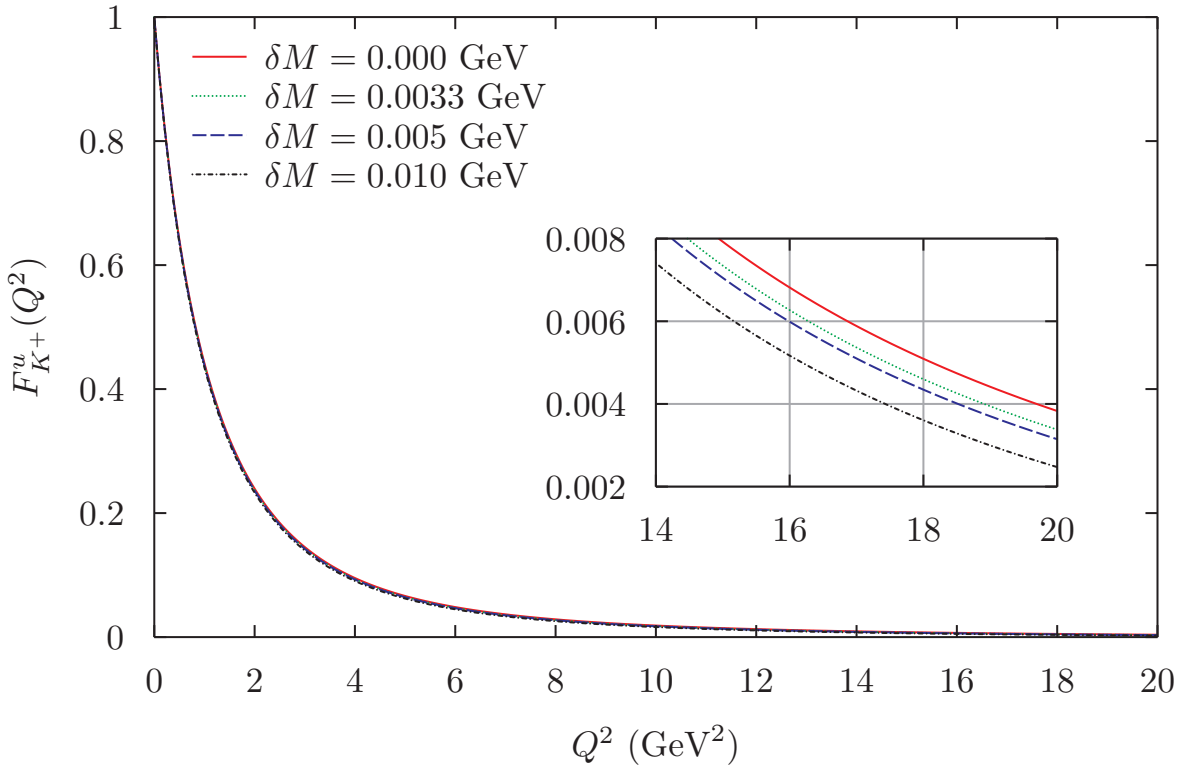

Figure 6.2.10: The effect of CSV for the u- quark sector form factor in the K^+, for the various δM, as a function of the Q^2.

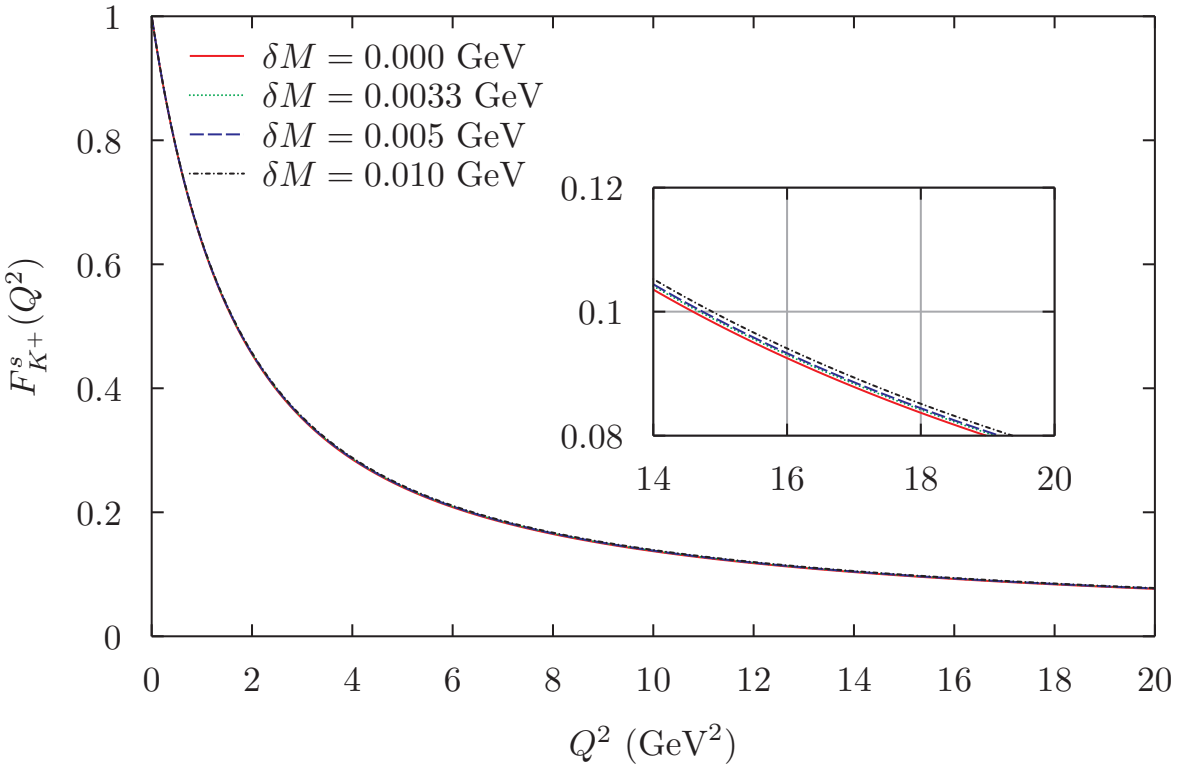

Figure 6.2.11: As in Fig. 6.2.10, but for the s-quark sector form factor.

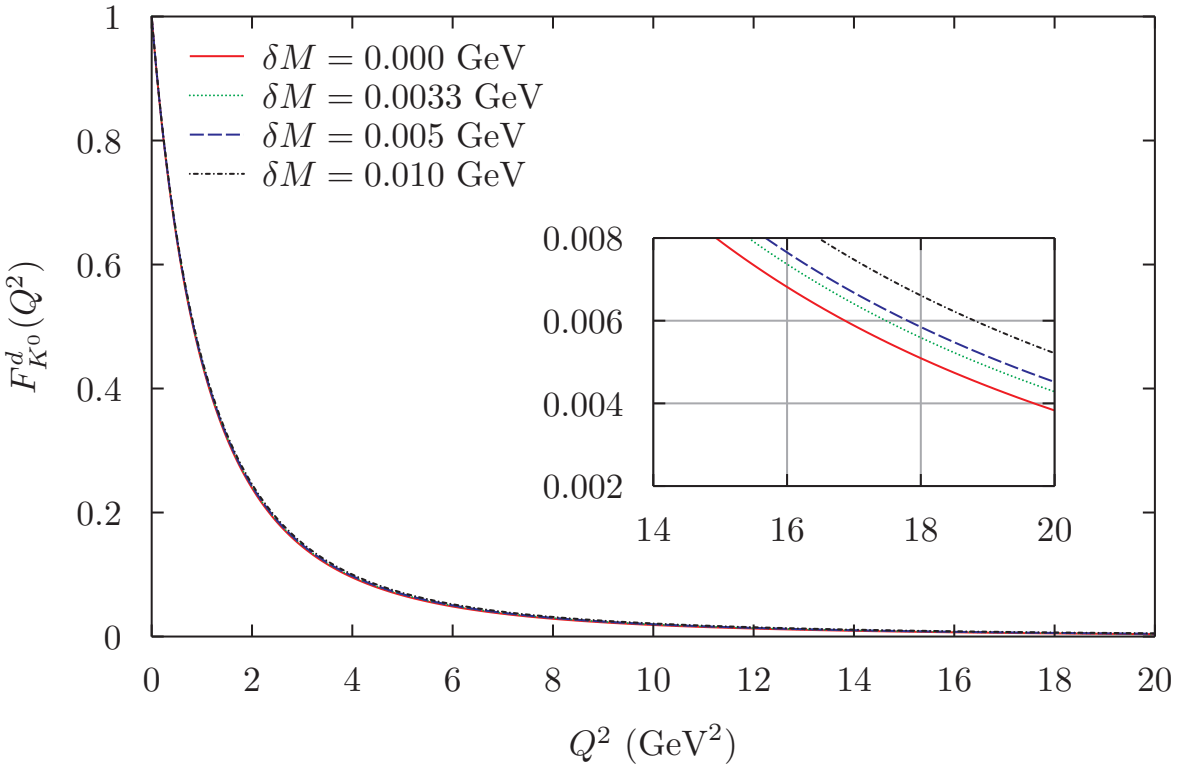

Figure 6.2.12: The effect of CSV for the d-quark sector form factor in the K^0, for the various δM, as a function of the Q^2.

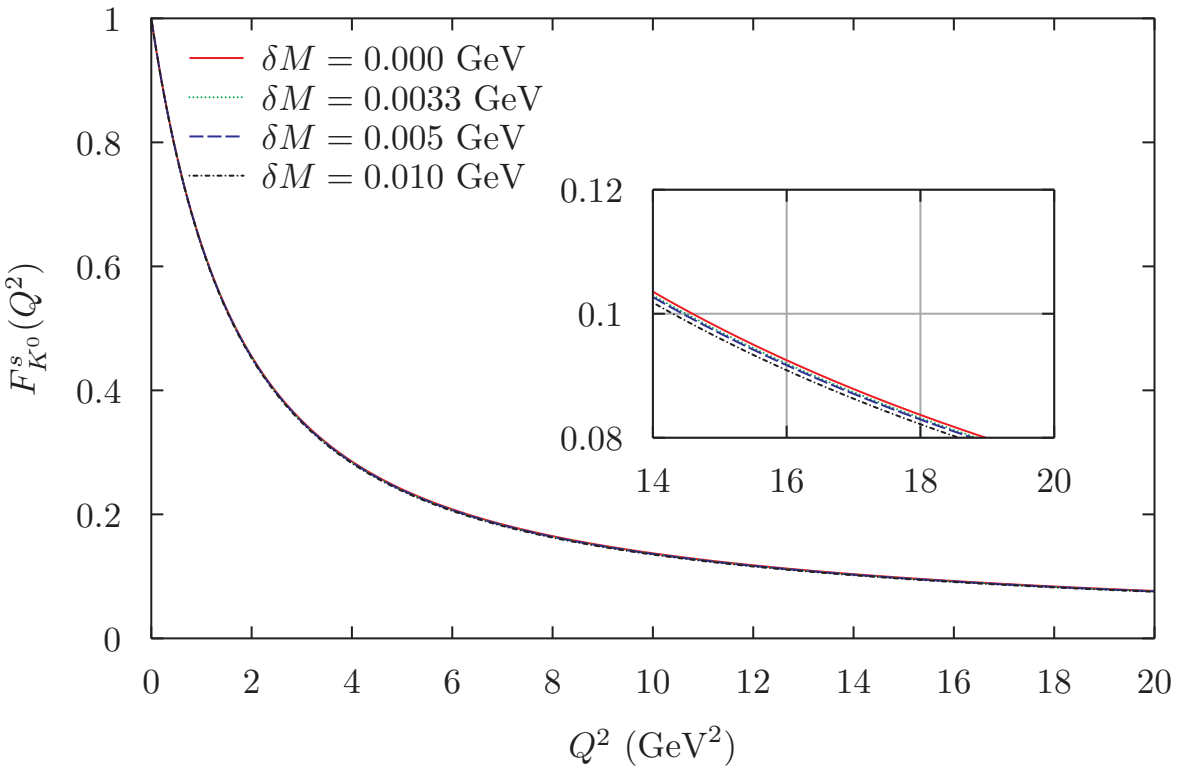

Figure 6.2.13: As in Fig. 6.2.12, but for the s-quark sector form factor.

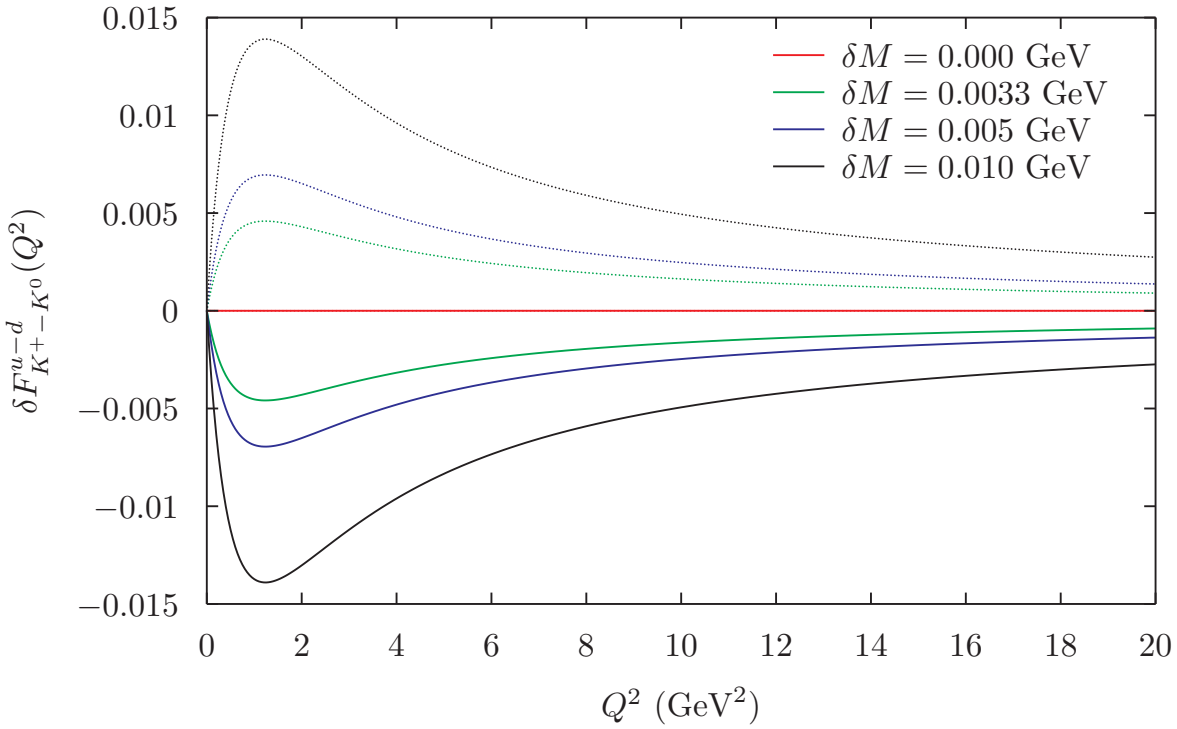

Figure 6.2.14: The difference between the u-quark sector form factor in the K^+ and the d-quark sector form factor in the K^0, $\delta F^{u-d}_{K^+-K^0}(Q^2) = F^u_{K^+}(Q^2) - F^d_{K^0}(Q^2)$ (solid line) and $\delta F^{d-u}_{K^0-K^+}(Q^2) = F^d_{K^0}(Q^2) - F^u_{K^+}(Q^2)$ (dashed line).

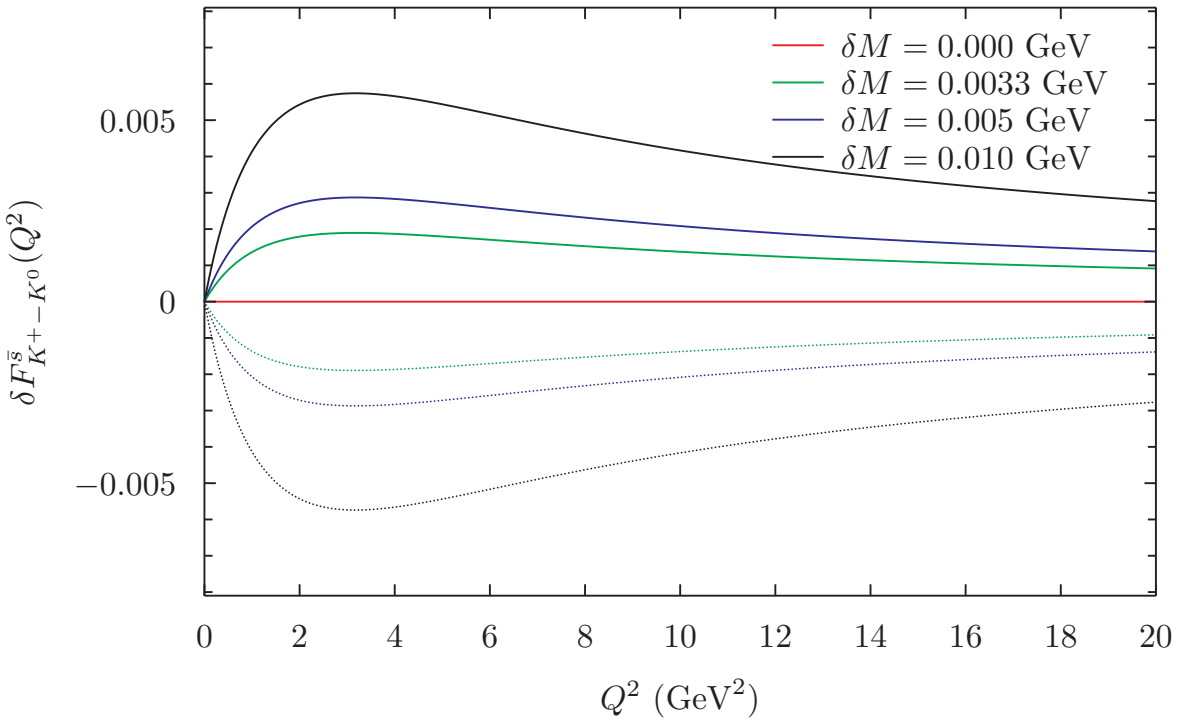

Figure 6.2.15: As in Fig. 6.2.14, but for the s-quark sector form factors in the K^+ and K^0, respectively, $\delta F^s_{K^+-K^0}(Q^2) = F^s_{K^+}(Q^2) - F^s_{K^0}(Q^2)$ is represented by the solid line and $\delta F^s_{K^0-K^+}(Q^2) = F^s_{K^0}(Q^2) - F^s_{K^+}(Q^2)$ is the dotted line.

To clearly understand the the CSV effect in the kaons. The difference between the u-quark sector form factor in the K^+ and d-quark sector form factor in the K^0, for the various δM, as a function of the Q^2 is depicted in Fig. 6.2.14 and the difference $\delta F^s_{K^+}(Q^2) - F^s_{K^0}(Q^2) = F^s_{K^+-K^0}(Q^2)$ and plot it for the various δM in Fig. 6.2.15. Again, there is unfortunately no experimental data available for the CSV in the form factors at the moment. However, the possibilities are open in the future experiments to test our results. This results can also be used as guide tool for other sophisticated models such as the DSE model and lattice QCD studies. Overall, our results show that CSV has a quite significant contribution to the kaon form factors. Apart from the investigation of the CSV in the quark sector form factors, we now turn to a discussion of the CSV effect in the parton distribution function of the kaon and pion.

6.3 Charge Symmetry Violation in Parton Distribution Functions

In this section, charge symmetry violation in the parton distribution functions of the kaon and pion is discussed. To investigate the effect of the quark mass difference δM, we recall the formula of the parton distribution function of the kaon and pion expression in Eqs. (4.2.8), (5.3.5) and (5.1.10), respectively, that is

$$q(x) = \frac{N_C g_{P\bar{q}q}^2}{4\pi^2} \int_{\frac{1}{\Lambda_{\rm UV}^2}}^{\frac{1}{\Lambda_{\rm IR}^2}} d\tau \frac{1}{\tau} e^{-\tau(k^2(x^2-x)+xM_2^2-M_1^2(x-1))} \times \left[1+\tau\left[k^2(x-x^2)-(x-x^2)(M_2-M_1)^2\right]\right], \quad (6.3.1)$$

$$\bar{q}(x) = \frac{N_C g_{P\bar{q}q}^2}{4\pi^2} \int_{\frac{1}{\Lambda_{\rm UV}^2}}^{\frac{1}{\Lambda_{\rm IR}^2}} d\tau \frac{1}{\tau} e^{-\tau(k^2(x^2-x)+xM_1^2-M_2^2(x-1))} \times \left[1+\tau\left[k^2(x-x^2)-(x-x^2)(M_1-M_2)^2\right]\right], \quad (6.3.2)$$

here M_1, M_2 are the constituent quark masses of the quark and anti-quark, respectively and N_C denotes the number of colors. Note that the valence quark distribution formulation is $q_v(x) = q(x) - \bar{q}(x)$, where $q(x)$ and $\bar{q}(x)$ are, respectively, the quark and anti-quark distributions. The valence quark distributions within the kaon and pion must satisfy the baryon number conservation, $\int_0^1 dx\ u_v(x) = 1$ and momentum sum rules, $\int_0^1 dx\ x[u_v(x) + d_v(x)] = 1$, as explained earlier. A more comprehensive explanation about the PDF can be found in our previous paper [159].

Londergan et al. in Ref. [264] proposed that the values for the pion valence quark distribution and the sea quark distribution can be extracted through the pion-induced Drell-Yan processes. From this experiment, the Drell-Yan cross section for the positively and negatively charged pions on deuterium can be measured. Having these valence quark distributions, we can formulate the ratios of the Drell-Yan cross sections:

$$R_{\pi D}^{DY}(x_\pi, x) = \frac{4\sigma_{\pi^+ D}^{DY} - \sigma_{\pi^- D}^{DY}}{\sigma_{\pi^- D}^{DY} - \sigma_{\pi^+ D}^{DY}}, \quad (6.3.3)$$

where $\sigma_{\pi^+ D}^{DY}$ and $\sigma_{\pi^- D}^{DY}$ denote the lowest order Drell-Yan cross sections, which have the form

$$\sigma_{\pi^+ D}^{DY} \equiv \frac{1}{9}\left[d_p(x) + d_n(x)\right] \bar{d}_{\pi^+}(x_\pi)$$
$$\sigma_{\pi^- D}^{DY} \equiv \frac{4}{9}\left[u_p(x) + u_n(x)\right] \bar{u}_{\pi^-}(x_\pi), \quad (6.3.4)$$

In the $\pi - D$ process, the pion PDF can be extracted directly from the Drell-Yan experiment, as suggested in Ref. [264]. Apart from the importance of the determination of the nucleon PDF to understand the CSV effects, they also argued that there is an additional terms to contribute, namely $\delta R_{\pi D}^{DY}(x_\pi, x)$, to the Drell-Yan ratio of Eq. (6.3.4). This additional term arises from the CSV in the parton distribution function of the pion. The largest CSV effect emerges from differences between the $\bar{d}$-quark in the π^+ and u-quark in the π^-. This is another strong motivation for exploring the

CSV effect in the valence quark distribution of the pion (or kaon). The additional term has the form

$$\delta R^{DY}_{\pi D}(x_\pi, x) \equiv \frac{4\left[\bar{d}^{\pi^+}_v(x) - \bar{u}^{\pi^-}_V(x)\right]}{3\pi_v(x_\pi)}, \tag{6.3.5}$$

where $\pi_v(x_\pi)$ stands for $u^{\pi^+}_v(x) = \bar{d}^{\pi^+}_v(x) = d^{\pi^-}_v(x) = \bar{u}^{\pi^-}_v(x)$. These distribution functions can be calculated using Eq. (6.3.1). With all these explanations above, next we will explore the CSV effects in the parton distribution functions of the pion. Similarly, the CSV effects in the parton distribution of the different kaons will be investigated in the next section.

By following the analysis procedure on the kaon form factor, in our PDF analysis, we firstly calculate the PDF of the kaon through Eq. (6.3.1) by using the new constituent quark masses in Eq. (6.0.1) as an input, where $M_1 = M_u$ for the kaon and pion, and $M_2 = M_d$ for the pion case and $M_2 = M_s$ for the kaon case. Then, our numerical results for the CSV effect in the parton distribution functions of the kaon and pion will be discussed in Section 6.4.

6.4 Results for the CSV in Parton Distribution Functions

In this section we discuss our numerical results on CSV effects in the parton distribution function of the kaon and pion. The parton distribution functions have been calculated using the NJL model with help of the proper-time regularization scheme. The parameter used is similar as previous calculation. The PDF of the kaon has been independently calculated using NJL model. We numerically compute the PDF of the K^+ and K^0, respectively, in our calculation. Thus, our numerical results for the ratio $\frac{xu_{K^+}(x)}{xd_{K^0}(x)}$ and the difference $x\delta u(x) = xu_{K^+}(x) - xd_{K^0}(x)$ at the NJL model scale $Q_0^2 =$ 0.16 GeV^2 are illustrated in Figs. 6.4.1 and 6.4.2.

Figure 6.4.1 provides our numerical result for the ratio, $\frac{xu_{\rm K^+}(x)}{xd_{\rm K^0}(x)}$, at the NJL model scale, $Q_0^2 = 0.16$ GeV^2. The ratios are computed for the $\delta M = 0.000$ GeV (red solid line), $\delta M = 0.0033$ GeV (blue dotted line), $\delta M = 0.0050$ GeV (green dashed line) and $\delta M = 0.010$ GeV (black dot-dashed line), respectively. This shows that the ratios increase with increasing quark mass difference, δM, but it decreases with increasing x and the trend of the ratios change at around $x \sim 0.4$, when it has one crossing. This indicates that the d-quark valence distribution in the K^0 is quite a bit smaller than the u-quark valence distribution in the K^+ over the range the longitudinal momentum, $x = 0.0 - 0.4$. Then at $x > 0.4$ the u quark valence distribution becomes smaller and the d-quark distribution becomes dominant with increasing the quark mass difference, δM. Consequently the ratios become less than one. Explicitly, in Fig. 6.4.1, the CSV effects are clearly seen from the difference between the PDFs with the charge symmetry ($\delta M = 0$) and the PDF with the CSV ($\delta M \neq 0$). The individual valence CSV u-quark distributions in the K^+ decreases with increasing δM. The CSV effect shifts down the

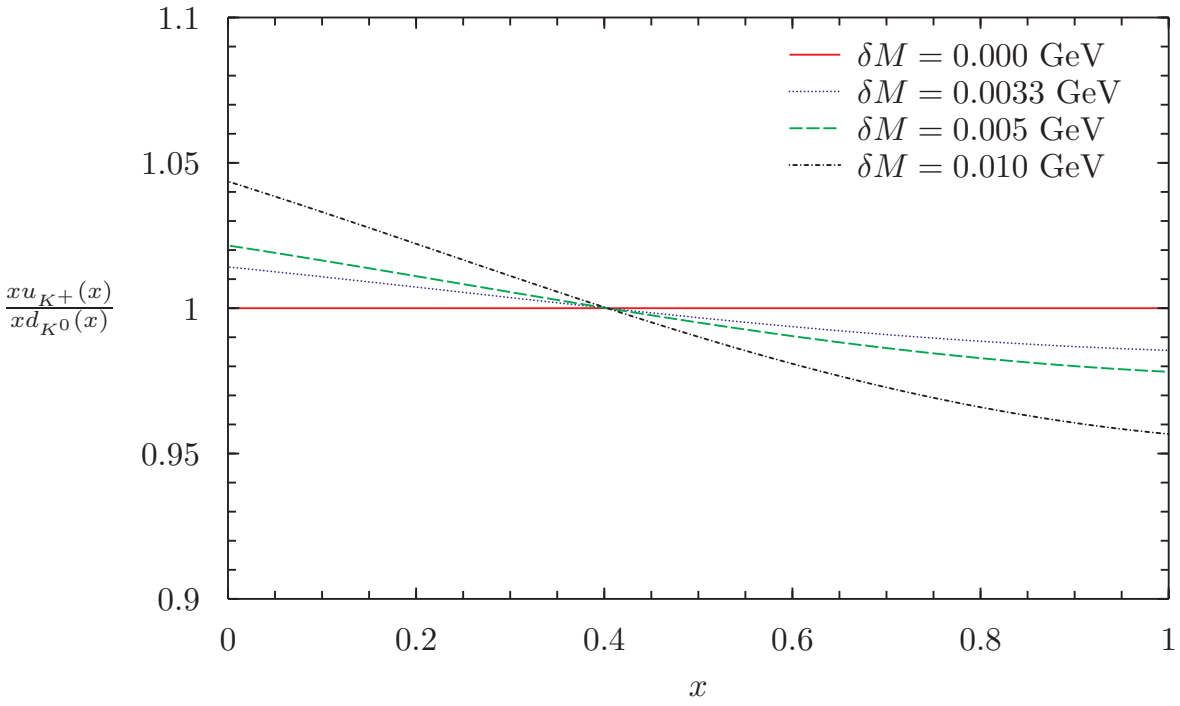

Figure 6.4.1: Ratio of the u-quark distribution in the positively charged kaon to the d-quark distribution in the neutral kaon as a function of x. The ratio, $\frac{xu_{K^+}(x)}{xd_{K^0}(x)}$ is represented by the dotted line and $\frac{xd_{K^0}(x)}{xu_{K^+}(x)}$ is represented by the dot-dashed line.

valence CSV u-quark distribution, as clearly seen in Fig. 6.4.3. On the contrary, the valence CSV d-quark distribution of the K^0 increases with increasing δM as depicted in Fig. 6.4.4.

In Fig. 6.4.2, we show that the difference, $x\delta u(x) = xu_{K^+}(x) - xd_{K^0}(x)$, represented by the solid line, whereas the difference, $x\delta d(x) = xd_{K^0}(x) - xu_{K^+}(x)$ denoted by the dotted line. The valence $x\delta u(x)$ has a negative value. This indicates that the valence CSV u-quark distribution in the K^+ is smaller than the valence CSV d-quark distributions in the K^0. This also implies that the $x\delta d(x)$ has a positive value. Thus, their relation is simply introduced as $\delta u(x) = -\ \delta d(x)$. This relation is the same with the findings on other calculation in Refs. [270–272].

To understand clearly the quark distribution in different kaons, we compute the moments of the difference in Fig. 6.4.2. We find that the first moment of the valence CSV distributions is zero because of the valence quark normalization ($\langle \delta u(x) \rangle = 1$). In addition, we also calculate the second and higher moments of the valence CSV quark distributions in Fig. 6.4.5. The value of the moments of the valence CSV quark distribution for the various δM at the NJL model scale, $Q_0^2 = 0.16$ GeV^2 are summarized in Table 6.4.1. Moreover, the individual valence u- and s-quark distributions of the K^+ and d- and s-quark distributions of the K^0 and the value of their moments for each δM are provided in Appendix A.18. Our first and second moments results of the valence CSV distributions are consistent with the lattice and other model predictions,

for nucleon case, in Refs. [270–272].

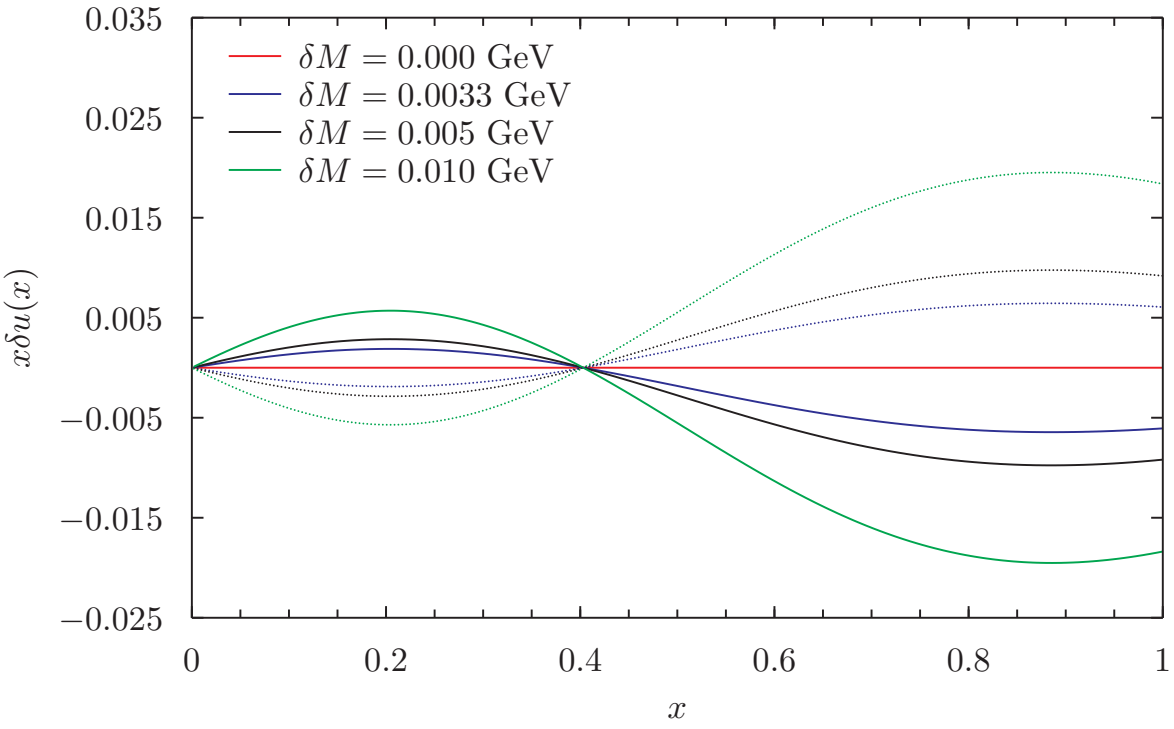

Figure 6.4.2: The difference $x\delta u(x) = xu_{K^+}(x) - xd_{K^0}(x)$ as a function of x. This is calculated at the NJL model scale $Q_0^2 = 0.16$ GeV^2.

Table 6.4.1: The moments of the $x\delta u(x) = xu_{K^+}(x) - xd_{K^0}(x)$ distribution at the NJL model scale, $Q_0^2 = 0.16$ GeV^2, where n denotes moments.

n	$\delta M = 0.000$ GeV	$\delta M = 0.0033$ GeV	$\delta M = 0.005$ GeV	$\delta M = 0.010$ GeV
1	0.0000	0.0000	0.0000	0.0001
2	0.0000	0.0022	0.0033	0.0066
3	0.0000	0.0020	0.0030	0.0060
4	0.0000	0.0016	0.0025	0.0049
5	0.0000	0.0014	0.0021	0.0041

To clearly see the CSV effect in PDFs, we also calculate the ratio and difference between the valence CSV u-quark distribution in the K^+ and d-quark distribution in the K^0, after they evolves. We evolve the valence CSV quark distribution using the DGLAP at scale $Q^2 = 5$ GeV^2.

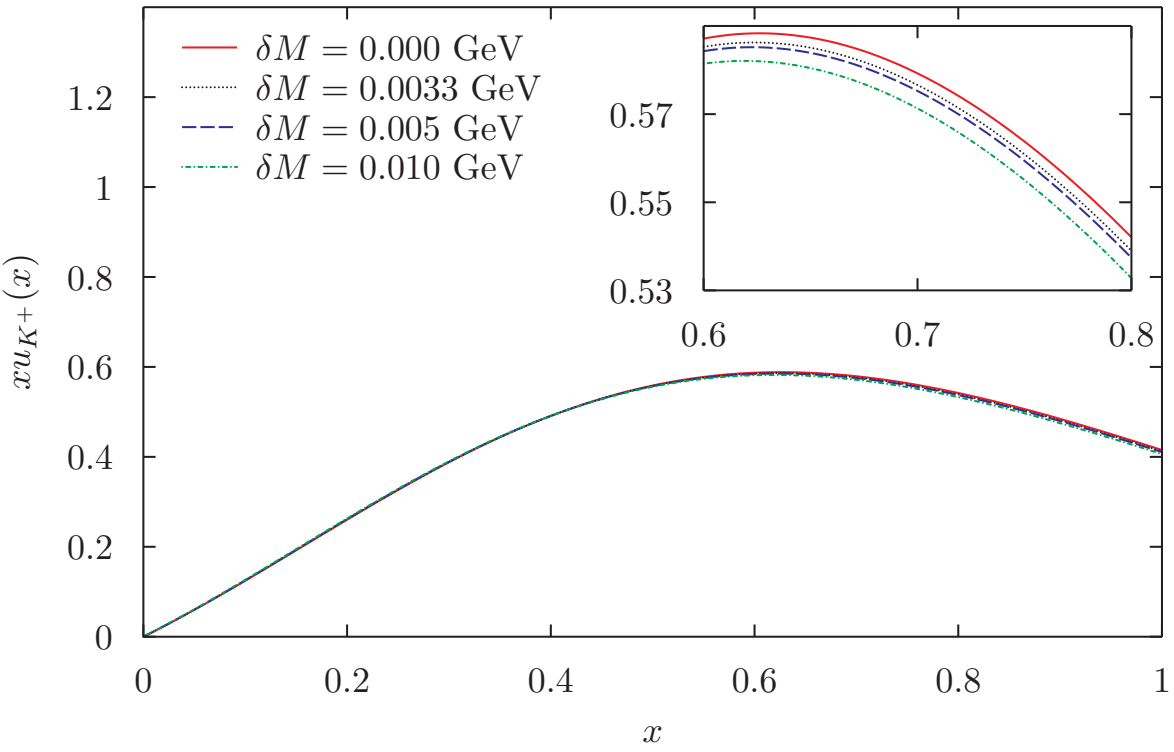

Figure 6.4.3: The PDF $xu_{K^+}(x)$ as a function of x. This is calculated at the NJL model scale $Q_0^2 = 0.16$ GeV^2.

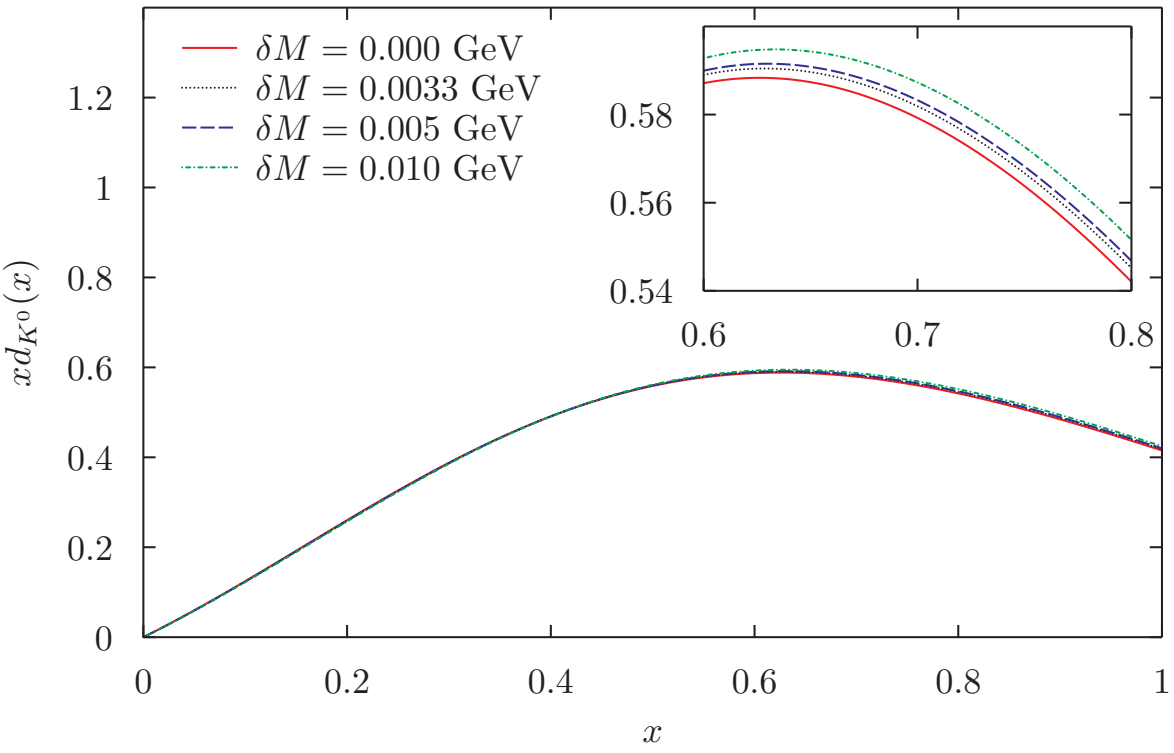

Figure 6.4.4: The PDF $xd_{K^0}(x)$ as a function of x. This is calculated at the NJL model scale $Q_0^2 = 0.16$ GeV^2.

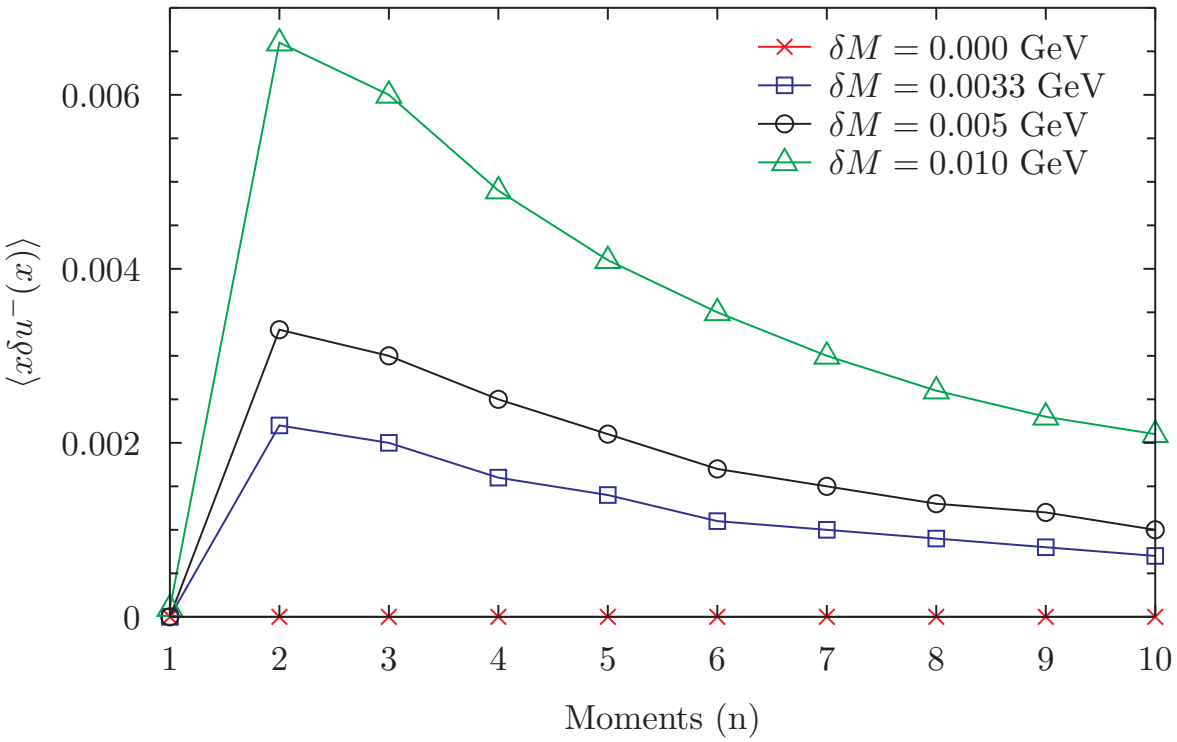

Figure 6.4.5: The moment of $\delta u(x)$ distribution at the NJL model scale, $Q_0^2 = 0.16$ GeV^2.

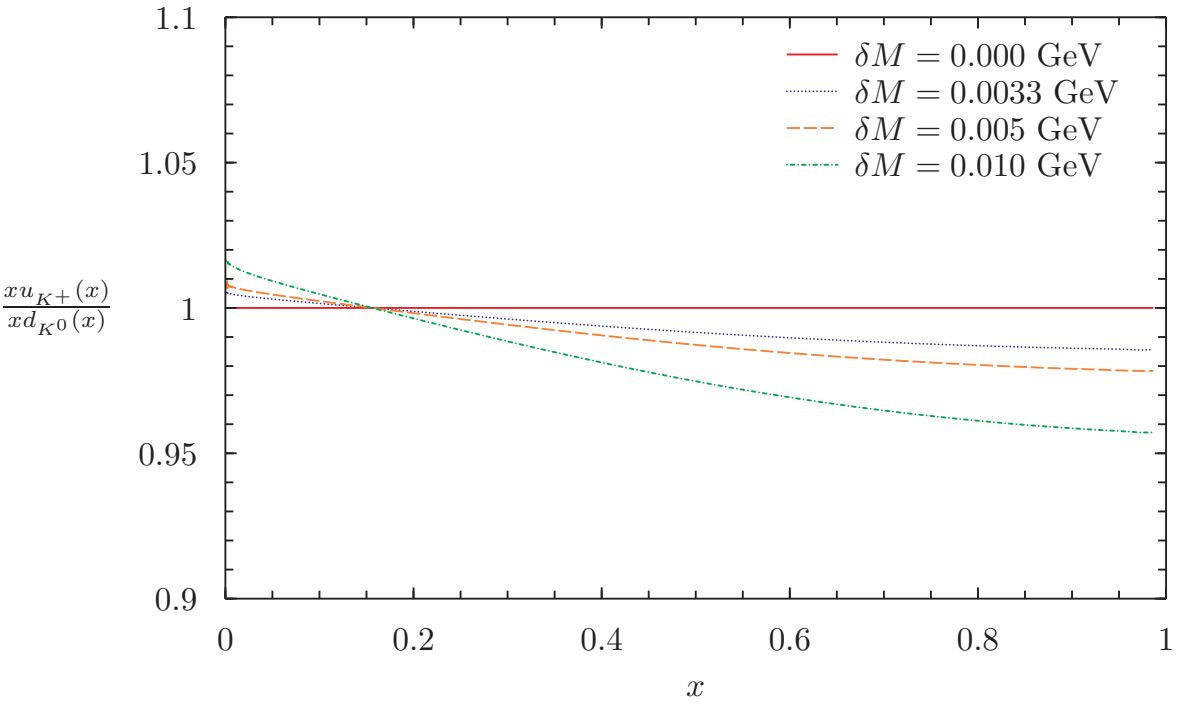

Figure 6.4.6: Ratio of the PDF $xu_{K^0}(x)$ to the PDF $xd_{K^0}(x)$ as a function of x, after QCD evolution using DGLAP at NLO to a scale $Q^2 = 5$ GeV^2.

In Fig. 6.4.6, we shows our numerical results for the ratio, $\frac{xu_{\mathrm{K}^+}(x)}{xd_{\mathrm{K}^0}(x)}$, after QCD evolution using the DGLAP at NLO to a scale, $Q^2 = 5$ GeV^2. This results indicates that the trend of the ratios seems similar to the ratio calculated at the NJL model scale in Fig. 6.4.1, but their magnitudes and the crossing point are different. This has a crossing point at $x \sim 0.16$. This may be caused the gluon distributions included in the DGLAP evolution. Additionally, this clearly shows that the ratios increase with increasing quark mass differences, δM, but they decrease with increasing x. Similar interpretation to Fig. 6.4.1, this indicates that the valence d-quark distributions in the K^0 are a bit larger than the valence u-quark distributions within the K^+ at $x > 0.16$. Inversely, the valence d-quark distributions in the K^0 are a bit smaller than the valence u-quark distributions within the K^+ at $x < 0.16$.

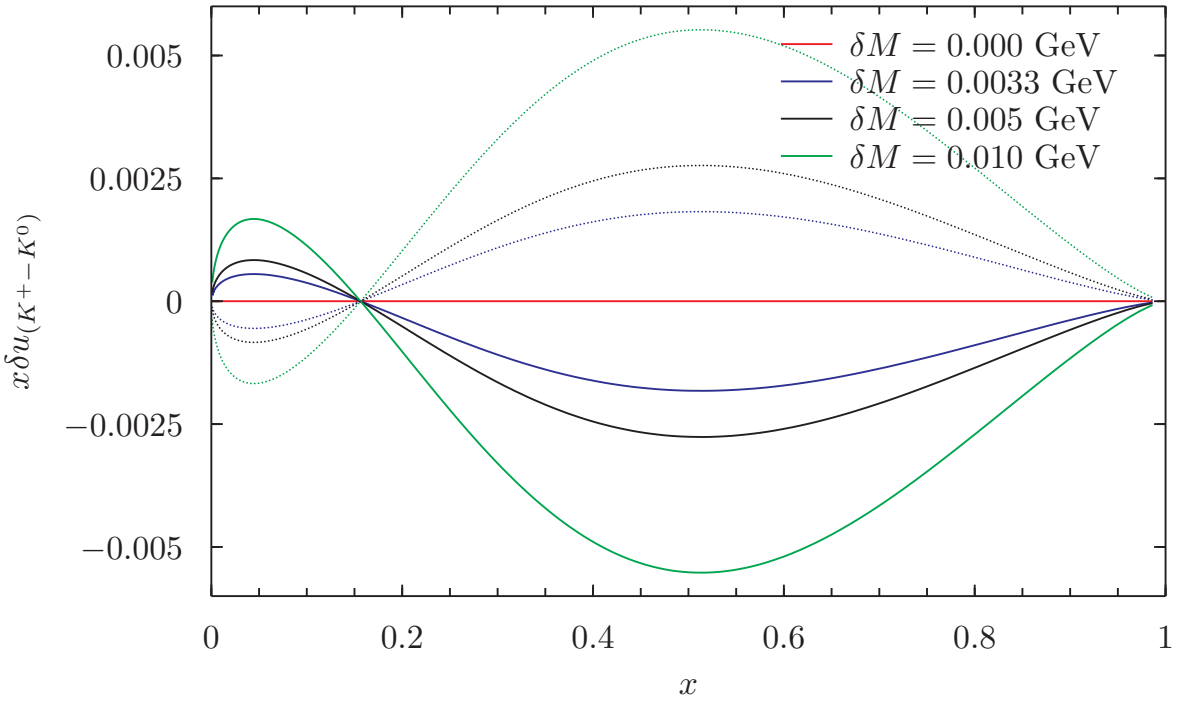

Figure 6.4.7: The difference $xu_{K^0}(x) - xd_{K^0}(x)$ as a function of x, after QCD evolution using DGLAP at NLO to a scale $Q^2 = 5$ GeV^2.

We also calculate the difference between the valence CSV u-quark distribution in the K^+ and the valence CSV d-quark distribution in the K^0 after we evolved them using the DGLAP evolution. Our results for the difference, $x\delta u_{K^+-K^0}(x) = xu_{K^0}(x) - xd_{K^0}(x)$ as a function of x, after QCD evolution using DGLAP at NLO to a scale $Q^2 = 5$ GeV^2, is depicted in Fig. 6.4.7. Then we calculate the moments of the difference, $x\delta u_{K^+-K^0}(x)$. The summary results of the difference moments is shown in Table 6.4.2.

Figure 6.4.8 displays our numerical result for the ratio of the up and anti-down distributions in the pion as a function of the Bjorken variable, x. The CSV effects are observed on the valence quark distributions in the pion for the various quark mass differences, $\delta M = 0.000$ GeV is represented by the red solid line, $\delta M = 0.0033$ GeV is represented by the blue dotted line, $\delta M = 0.0050$ GeV is represented by the black

dotted line and $\delta M = 0.010$ GeV is represented by the green dotted line. The valence $x\delta d$ is represented by the solid line. The ratio of the quark distributions in the pion has been computed at the NJL model scale, $Q_0^2 = 0.16$ GeV^2. This indicates that the ratio, $\dfrac{xu_\pi(x)}{x\bar{d}_\pi(x)}$, decreases with increasing x and passes through one for different δM at around $x \sim 0.43$. This result is consistent with the prediction in Ref. [264].

Similarly for the kaon case, we also calculate the difference of the quark distribution in the pion at the model scale, $Q_0^2 = 0.16$ GeV^2. Our result for the difference quark distribution in the pion is illustrated in Fig. 6.4.9. This shows that the crossing point is at $x \sim 0.48$. For $x < 0.43$ the value of the $x\delta u_\pi(x)$ is small, but for $x > 0.48$, the values of $x\delta u_\pi$ becomes large with increasing δM.

In Fig. 6.4.10 we show our numerical results for the ratio of the up quark distribution to anti-down quark distribution in the pion, after QCD evolution using DGLAP at NLO to a scale, $Q^2 = 5$ GeV^2 as a function of x. The ratios are calculated for the $\delta M = 0.000$ GeV (black solid line), $\delta M = 0.0033$ GeV (blue dashed line), $\delta M = 0.0050$ GeV (red dotted line) and $\delta M = 0.010$ GeV (green dot-dashed line). By increasing the light quark mass differences (CSV effect), the magnitude of the ratio $\dfrac{xu_\pi(x)}{x\bar{d}_\pi(x)}$ decreases rapidly above at $x \sim 0.2$. The ratios generally decrease with increasing x as in Fig. 6.4.8. Our result for the difference quark distribution in the pion at a scale, $Q^2 = 5$ GeV^2 is illustrated in Fig. 6.4.11. This shows that the crossing point is at $x \sim 0.2$. For $x < 0.2$ the value of the $x\delta u_\pi(x)$ is small, but for $x > 0.2$, the values of $x\delta u_\pi$ is large with increasing δM. Note that the solid line represent the difference between the d-quark distribution and the u-quark distribution in the pion (positive value) and the dotted lines is the difference between the u-quark distribution and the d-quark distribution in the pion (negative value).

Table 6.4.2: The moments of the $x\delta u_{K^{+-}K^0}(x) = xu_{K^+}(x) - xd_{K^0}(x)$ distribution at a scale, $Q^2 = 5$ GeV^2, where n denotes moments.

n	$\delta M = 0.000$ GeV	$\delta M = 0.0033$ GeV	$\delta M = 0.005$ GeV	$\delta M = 0.010$ GeV
1	0.0000	0.0004	0.0007	0.0013
2	0.0000	0.0010	0.0016	0.0031
3	0.0000	0.0006	0.0010	0.0019
4	0.0000	0.0004	0.0006	0.0013
5	0.0000	0.0003	0.0005	0.0009

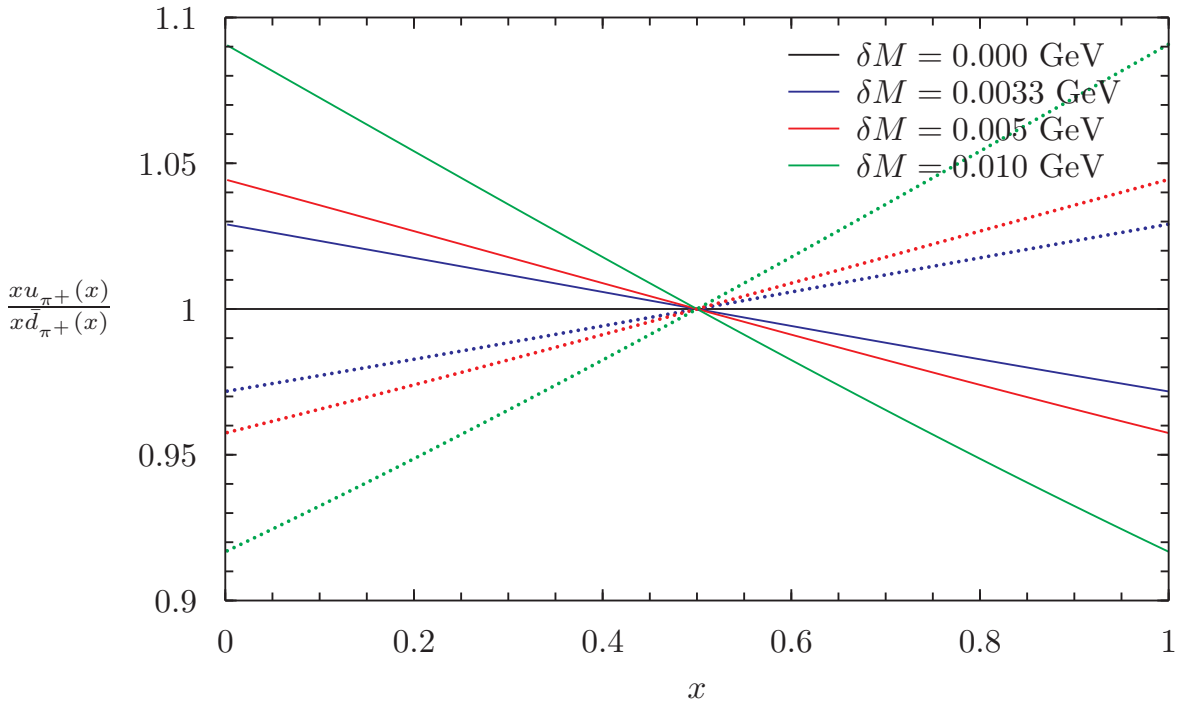

Figure 6.4.8: Ratio of the up quark distribution to the anti-down quark distribution in the pion versus x at the NJL model scale, $Q_0^2 = 0.16$ GeV^2.

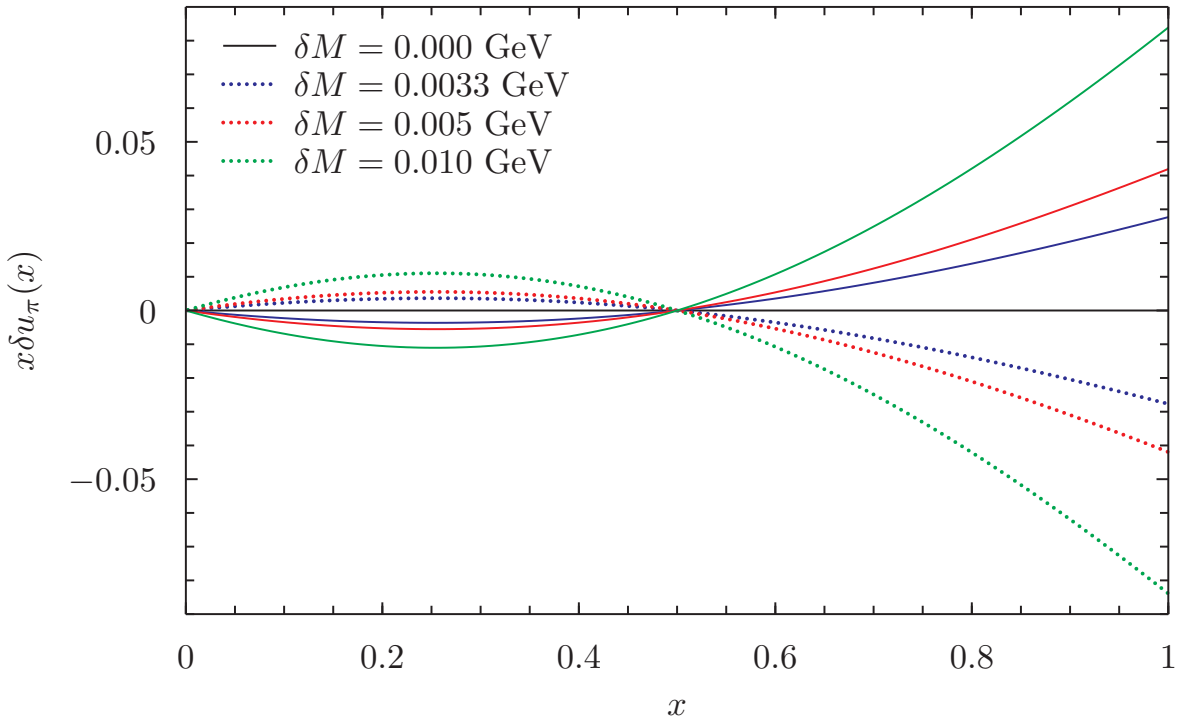

Figure 6.4.9: As Fig. 6.4.8, but for the difference between the u-quark distribution and the $\bar{d}$-quark distribution in the pion.

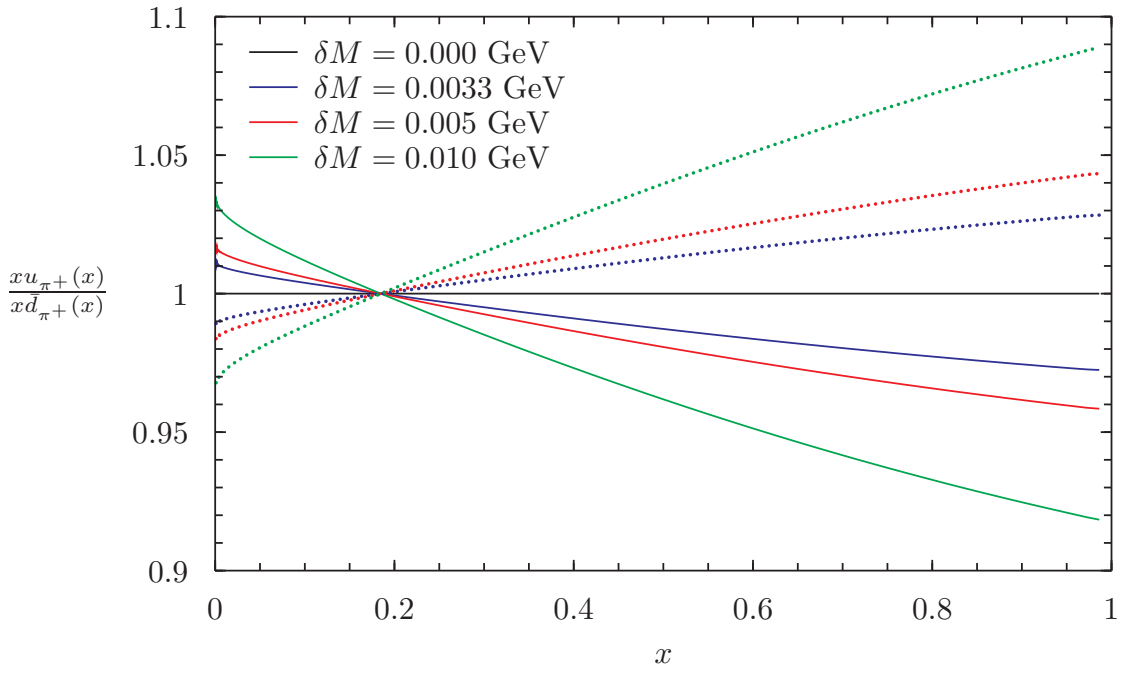

Figure 6.4.10: As in Fig. 6.4.8, but at a scale, $Q^2 = 5$ GeV^2 as a function of x.

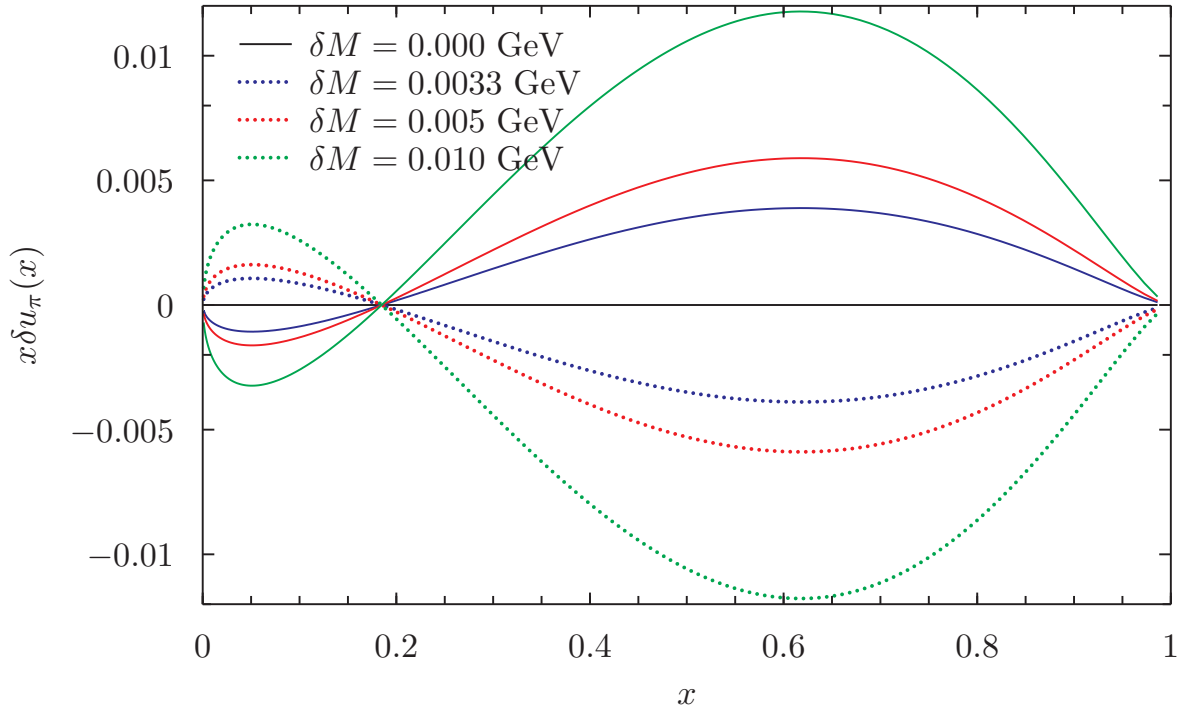

Figure 6.4.11: As in Fig. 6.4.10, but for the difference between the u-quark distribution and the $\bar{d}$-quark distribution in the pion.

6.5 Conclusion

In this last section, we have discussed the CSV in the form factors and parton distribution functions in the kaon and pion using the SU(3) Nambu-Jona-Lasinio model with the help of the PTR scheme. From our calculation result, we found that the effect of CSV, which arises from the light quark mass differences, significantly change the momentum distribution of the valence light quarks in the kaon and pion. Such a change indicates their sensitivity to the nuclear environment. Unfortunately there is no yet available of the experimental data at the moment. However, in the future, we will compare our model prediction on CSV to the forthcoming experimental data from JLAB [274–276]. Our results can be used as a guide tool for the future experiment, other sophisticated models and lattice QCD studies, in particular for the kaon and pion.

7
Summary and Outlook

Exploring the strong interaction in QCD is of fundamental importance in hadronic physics. Using probes of increasing energy, scattering experiments have revealed the quark and gluon structure of the hadron in DIS. These experimental discoveries have led to the development of QCD as the accepted theory describing the physics of strong interactions. The quark and gluon structure of the hadron can be parameterized with the help of PDFs, which describe the momentum distributions of partons inside the hadron. There has been significant progress in both experiment and theory. These are necessary not only to reveal the internal structure of the hadron in unprecedented depth and precision but also to explore ways of connecting the underlying parton distributions with other hadron properties.

In the SM the kaon consists of a quark-anti-quark pair. The internal structure of the kaon is simpler than the nucleon. Therefore the dynamics of quarks and gluons inside the kaon and pion may be easier to study than inside the nucleon. Understanding the dynamics of the quarks and gluons in the kaon and pion will lead us to extract new knowledge of QCD as the underlying strong interaction theory. Nowadays we are still far from fully understanding the behavior of the kaon internal structure, in part because of a lack of experimental data.

In this work we begin our studies by modeling the parton interactions inside the kaon and pion in the framework of the Nambu-Jona-Lasinio model − chiral effective quark theory of QCD − regularized with the help of the proper-time regularization scheme. This regularization scheme simulates some important aspects of confinement. The BSE has been used to described a bound state of the quark-antiquark pair in the kaon. After introducing the BSE, the meson statics and dynamics properties were derived in the NJL model. The meson properties considered are the pseudoscalar meson quark-antiquark coupling, pseudoscalar meson masses. pseudoscalar meson decay constant and GMOR relation for the kaon and pion in the NJL model. These properties are then used to compute the kaon FFs and PDFs.

The electromagnetic elastic form factor of the kaon and pion provide important and

useful information concerning their internal structure. In pQCD, the electromagnetic form factor at large Q^2 provides information to test the validity of pQCD. From the experimental point of view , the availability of the kaon electromagnetic form factor data in the space like region ($Q^2 < 0$) is considerably rare. Therefore more studies are required to have more complete information about the kaon internal structure. We have determined the kaon electromagnetic form factor in the space like region in the NJL model with help of the PTR scheme. The separate contributions of each quark flavour sector form factor to the total elastic form factor of the kaon has been explored, with and without the effect of the dressing at the quark-photon vertex. While at the present time one does not know the separate flavor contributions to the kaon elastic form factor, one may hope that it will prove possible to measure them in future. We find that the anti-strange quark sector form factor multiplied by Q^2 grows with increasing Q^2. On the contrary the u-quark sector form factor of the kaon multiplied by Q^2 decreases with increasing Q^2. Both asymptotically become flat to the region up to $Q^2 = 20$ GeV^2, where the different shows on the asymptotic value. This clearly shows that the anti-strange quark sector form factor has a larger contribution than the u-quark sector form factor to the total bare kaon form factor at both small and large Q^2. However, overall our kaon form factor with a bare quark is in disagreement with the experimental data and empirical monopole function. Similarly, we find that our form factor of the pion does not agree well with either the experimental data and the phenomenological monopole. This is because we treat the quark as a point like particle. We then improve our kaon and pion form factor by including a dressed quark via the quark-photon vertex, which is given by solving an inhomogeneous BSE self-consistently. We find that the anti-strange quark sector form factor of the kaon with the dressed quark is larger than the up quark sector form factor with the dressed quark in the whole Q^2 region. An immediate consequence of this result is that our kaon form factor shows an excellent agreement with the experimental data and the empirical monopole (VMD) and the quark sector form factors of the kaon has a good improvement. Similarly the pion form factor with the dressed quark also has an excellent agreement with the experimental data and the empirical monopole prediction. In addition, our pion form factor has similar prediction to that obtained with the DSE-RLT model at around $Q^2 \sim 6$ GeV^2.

We also investigated the ratio of the up quark sector form factor to the anti-strange quark sector form factor of the kaon in order to understand the sensitivity of the local hadronic environment of the valence quark in the kaon. We find that the ratio of the up quark and anti-strange quark sector form factor in the positively charged kaon decreases rapidly with increasing Q^2. This indicates that the up quark distribution is much smaller than the anti-strange quark distribution in the kaon. Our ratio results between the kaon form factor and the pion form factor, with and without dressed quarks, show excellent agreement with the experimental data at lower Q^2. We also find that the vector mesons make a significant contribution to the form factors. Then we compute the pion form factor with the pion cloud, we find that our result is in remarkable agreement with the experimental data and the DSE rainbow-ladder truncation. An excellent result for the elastic form factor has an implication to the charge radius squared. We find that the charge radius squared of the kaon is consistent with the experimental data. At large Q^2, the pion form factor plateau, we find that $Q^2 F_\pi^{(vmd+pc)}(Q^2) \sim 0.39$,

$Q^2F_\pi^{(vmd)}(Q^2) \sim 0.48$ and $Q^2F_\pi^{(bare)}(Q^2) \sim 0.52$, respectively.

We calculated the PDFs, which are basic nonperturbative ingredients for QCD hard scattering processes, involving the kaon and pion. We found that the evolved valence u-quark distribution of the pion has a remarkable agreement with the experimental data as well as both experimental fit models (E615 experimental fit and NA10 experimental fit), in particular at large x. The ratio of the valence u-quark distribution of the kaon to the pion at $x \sim 1$, $\dfrac{u_K(x \sim 1)}{u_\pi(x \sim 1)}$, is approximately 0.4. This result is in good agreement with the existing experimental data.

Possible charge symmetry violation in the form factors and parton distribution functions were also investigated. We found that the charge symmetry violation has a sizable contribution to the kaon and pion form factors and their quark sector form factors. We determine the kaon form factor by taking the quark mass difference to be $\delta M = (0.000, 0.0033, 0.005, 0.010)$ GeV, respectively. Unfortunately, at present, there is no data available yet to reveal the CSV effect in the quark sector form factors. However, our results can be used as a guide for the future experiments, other sophisticated models and lattice QCD studies, particularly for the kaon and pion. However, in the future we will compare our model prediction on CSV to forthcoming experimental data from JLAB.

Overall, we conclude that our kaon form factor and parton distribution functions show excellent agreement with the existing experimental data and other models. Our results in this thesis can be used as a guide tool in future experiment, sophisticated models and lattice QCD studies. It can also be applied in many interesting and important related topics of nuclear physics. This formalism used here can be straightforwardly extended to calculate the general parton distribution of the kaon and pion, where generalized parton distribution is a combination of the parton distributions and form factors, transverse momentum distribution (TMD) and SIDIS. The NJL formula can be also used to study more complex feature of the internal structure of hadrons such as nucleon and nuclear matter as well as phase transition with help of the QMC or RMF models. In this thesis, we have reported important results for understanding the internal structure of the kaon and pion.

From the experimental point of view, experimental data for the pion and the kaon are very rare. This is of course caused target difficulties for the pion and kaon. However, this becomes accessible through the Drell Yan experiments. The Jefferson Laboratory (JLAB), Newport News, USA is in the process of upgrading their experimental energy range up to 12 GeV. Thus the theoretical results in this thesis can be potentially be tested using new experimental data from JLAB. Additionally, in the near future the new data are expected from CLAS on DVCS, as well as the HERMES collaboration and COMPASS experiment at CERN.

A
Appendix

A.1 Generators of SU(2)

The definitions of generators of SU(2) can be defined as

$$\hat{\tau}_1 = \begin{pmatrix} 0 & 1 \\ 1 & 0 \end{pmatrix}, \qquad \hat{\tau}_2 = \begin{pmatrix} 0 & -i \\ i & 0 \end{pmatrix}, \qquad \hat{\tau}_3 = \begin{pmatrix} 1 & 0 \\ 0 & -1 \end{pmatrix}. \tag{A.1.1}$$

A.2 Generators of SU(3)

The generators of SU(3) can be written as

$$\hat{\lambda}_1 = \begin{pmatrix} 0 & 1 & 0 \\ 1 & 0 & 0 \\ 0 & 0 & 0 \end{pmatrix}, \quad \hat{\lambda}_2 = \begin{pmatrix} 0 & -i & 0 \\ i & 0 & 0 \\ 0 & 0 & 0 \end{pmatrix}, \quad \hat{\lambda}_3 = \begin{pmatrix} 1 & 0 & 0 \\ 0 & -1 & 0 \\ 0 & 0 & 0 \end{pmatrix}$$
$$\hat{\lambda}_4 = \begin{pmatrix} 0 & 0 & 1 \\ 0 & 0 & 0 \\ 1 & 0 & 0 \end{pmatrix}, \quad \hat{\lambda}_5 = \begin{pmatrix} 0 & 0 & -i \\ 0 & 0 & 0 \\ i & 0 & 0 \end{pmatrix}, \quad \hat{\lambda}_6 = \begin{pmatrix} 0 & 0 & 0 \\ 0 & 0 & 1 \\ 0 & 1 & 0 \end{pmatrix}, \quad \hat{\lambda}_7 = \begin{pmatrix} 0 & 0 & 0 \\ 0 & 0 & -i \\ 0 & i & 0 \end{pmatrix}$$
$$\hat{\lambda}_8 = \frac{1}{\sqrt{3}} \begin{pmatrix} 1 & 0 & 0 \\ 0 & 1 & 0 \\ 0 & 0 & -2 \end{pmatrix}. \tag{A.2.1}$$

A.3 Dirac δ-function

The Dirac δ-function [1] is introduced by

$$\delta(x) = \begin{cases} 0 & \text{if } x \neq 0 \\ \infty & \text{if } x = 0 \end{cases} \tag{A.3.1}$$

where the integration of the $\delta(x)$ can be written as $\int_{-\infty}^{\infty} \delta(x)dx = 1$. For $x \to 0$, we then can define $f(x)\delta(x) = f(0)\delta(x)$, this implies

$$\int_{\infty}^{\infty} f(x)\delta(x)dx = f(0), \tag{A.3.2}$$

$$\int_{\infty}^{\infty} f(x)\delta(x-a)dx = f(a), \tag{A.3.3}$$

For the linear transformation equation, for instance, $y = k(x-a)$, so that we can write

$$\delta(y) = \frac{1}{\mid k \mid}\delta(x-a), \tag{A.3.4}$$

where the $\delta(x)$ satisfies the δ-function definition in Eq. A.3.2 and this equation is straightforward to prove. Assume that we have the set points, $\{x_i\}$ and $f(x_i) = 0$, the delta function can be easily showed by employing a Taylor series expansion around the x_i, it then gives

$$\delta\left[f(x)\right] = \sum_i \frac{1}{\mid f'(x_i) \mid}\delta(x-x_i), \tag{A.3.5}$$

Another representations of the δ-function are defined as

$$\delta(\mathbf{r}) = \frac{1}{(2\pi)^3}\int e^{i\mathbf{k}.\mathbf{r}}d^2\mathbf{k} \qquad or \qquad \delta(x) = \frac{d\Theta(x)}{dx}, \tag{A.3.6}$$

where Heaviside step function, $\Theta(x)$, can be defined as

$$\Theta(x) = \begin{cases} 0 & \text{if } x < 0 \\ 1 & \text{if } x \geq 0 \end{cases} \tag{A.3.7}$$

A.4 Feynman Parametrization

$$\frac{1}{\mathbf{AB}} = \int_0^1 dx \frac{1}{\left[x\mathbf{A} + (1-x)\mathbf{B}\right]^2}, \tag{A.4.1}$$

$$\frac{1}{\mathbf{AB}^n} = \int_0^1 dx \frac{n(1-x)^{n-1}}{\left[x\mathbf{A} + (1-x)\mathbf{B}\right]^{n+1}}. \tag{A.4.2}$$

[1] In three dimension (3D), the delta can be written as, $\delta(\mathbf{r}) \equiv \delta(x)\delta(y)\delta(z)$.

A.5 Fierz Transformation

To yield the interaction Lagrangian of the three flavor NJL model in Eq. (3.1.6), we evaluate the interaction Lagrangian in Eq. (3.1.3) using Fierz transformation. It has the form

$$\mathcal{L}_{interaction} = G_q \left[\bar{\psi}\Gamma^q\psi\right]^2 = G_q\Gamma^q_{ij}\Gamma^q_{kl}\bar{\psi}_i\psi_j\bar{\psi}_k\psi_l, \tag{A.5.1}$$

with q denotes appropriate channel such as scalar $(\bar{\psi}\mathbb{1}\psi)$, pseudoscalar $(\bar{\psi}\gamma_5\psi)$, vector $(\bar{\psi}\gamma_\mu\psi)$, axial vector $(\bar{\psi}\gamma_5\gamma_\mu\psi)$ and tensor $(\bar{\psi}\sigma_{\mu\nu}\psi)$. Γ stand for a local operators in Dirac, flavor and color space. Then performing the Fierz transformation to Eq. (A.5.1), it has the form

$$\mathcal{F}\left[\mathcal{L}_{interaction}\right] = -G_q\Gamma^q_{ij}\Gamma^q_{kl}\bar{\psi}_i\psi_l\bar{\psi}_k\psi_j, \tag{A.5.2}$$

where $\mathcal{F}$ is an operator symbol for the Fierz transformation. Performing the Fierz transformation to the interaction Lagrangian in Eq. (A.5.1), it yields a new Lagrangian in Eq. (A.5.2), by exchanging the particle $\psi_j \to \psi_l$ and $\psi l \to \psi_j$, as seen in Eq. (A.2.1). In Fierz transformation, a contraction of the $\Gamma^q_{ik}\Gamma^q_{kl}$ can be defined as

$$\Gamma^q_{ik}\Gamma^q_{kl} = \sum_M \mathcal{C}^q_M\Gamma^M_{il}\Gamma^M_{kj}, \tag{A.5.3}$$

where $\mathcal{C}^q_M$ is unknown coefficients which are need to be solved. By evaluating Eq. (A.5.2) by means of the result in Eq. (A.5.3), it then gives

$$\mathcal{L}_{exchange} = -G_q\sum_M \mathcal{C}^q_M\Gamma^M_{il}\Gamma^M_{kj}\bar{\psi}_i\psi_l\bar{\psi}_k\bar{\psi}_j = -G_q\sum_M \mathcal{C}^q_M\left(\bar{\psi}\Gamma^M\psi\right)^2. \tag{A.5.4}$$

By summing the $\mathcal{L}_{interaction}$ and $\mathcal{F}\left[\mathcal{L}_{interaction}\right]$, a total Lagrangian of the quark-antiquark interaction can be written as

$$\mathcal{L}_{\bar{q}q} = \mathcal{L}_{interaction} + \mathcal{F}\left[\mathcal{L}_{interaction}\right], \tag{A.5.5}$$

In Dirac space, the exchange Lagrangian $\mathcal{L}_{exhange}$ of the quark-antiquark channel are defined by

$$\begin{pmatrix} (\mathbb{1})_{ij}(\mathbb{1})_{kl} \\ (i\gamma_5)_{ij}(i\gamma_5)_{kl} \\ (\gamma_\mu)_{ij}(\gamma_\mu)_{kl} \\ (\gamma_\mu\gamma_5)_{ij}(\gamma_\mu\gamma_5)_{kl} \\ (\sigma^{\mu\nu})_{ij}(\sigma_{\mu\nu})_{kl} \end{pmatrix} = \begin{pmatrix} \frac{1}{4} & -\frac{1}{4} & \frac{1}{4} & -\frac{1}{4} & \frac{1}{8} \\ -\frac{1}{4} & \frac{1}{4} & \frac{1}{4} & -\frac{1}{4} & -\frac{1}{8} \\ 1 & 1 & -\frac{1}{2} & -\frac{1}{2} & 0 \\ -1 & -1 & -\frac{1}{2} & -\frac{1}{2} & 0 \\ 3 & -3 & 0 & 0 & -\frac{1}{2} \end{pmatrix} \begin{pmatrix} (\mathbb{1})_{il}(\mathbb{1})_{kj} \\ (i\gamma_5)_{il}(i\gamma_5)_{kj} \\ (\gamma_\mu)_{il}(\gamma_\mu)_{kj} \\ (\gamma_\mu\gamma_5)_{il}(\gamma_\mu\gamma_5)_{kj} \\ (\sigma^{\mu\nu})_{il}(\sigma_{\mu\nu})_{kj} \end{pmatrix}, \tag{A.5.6}$$

In flavor and color for U(N) λ_a interaction can be written as

$$\begin{pmatrix} (\mathbb{1}_{ij})(\mathbb{1}_{kl}) \\ (\lambda_a)_{ij}(\lambda_a)_{kl} \end{pmatrix} = \begin{pmatrix} \frac{1}{2} & \frac{1}{2} \\ 2\frac{N^2-1}{N^2} & -\frac{1}{N} \end{pmatrix} \begin{pmatrix} (\mathbb{1})_{il}(\mathbb{1})_{kj} \\ (\lambda_a)_{il}(\lambda_a)_{kj} \end{pmatrix} \tag{A.5.7}$$

where λ_a are the generator of the SU(N), where $a = 1, \cdots, N^2-1$.

A.6 Integral Relations

$$\int \frac{d^4p}{(2\pi)^4}\frac{p^\mu}{[p^2-\Sigma+i\epsilon]^n}=0, \tag{A.6.1}$$

$$\int \frac{d^4p}{(2\pi)^4}\frac{p^\mu p^\nu}{[p^2-\Sigma+i\epsilon]^n}=\frac{1}{4}g^{\mu\nu}\int \frac{d^4p}{(2\pi)^4}\frac{p^2}{[p^2-\Sigma+i\epsilon]^n}, \tag{A.6.2}$$

$$\int \frac{d^4p}{(2\pi)^4}\frac{p^\mu p^\nu p^\rho p^\sigma}{[p^2-\Sigma+i\epsilon]^n}=\frac{1}{24}(g^{\mu\nu}g^{\rho\sigma}+g^{\mu\rho}g^{\nu\sigma}+g^{\mu\sigma}g^{\nu\rho})\int \frac{d^4p}{(2\pi)^4}\frac{p^4}{[p^2-\Sigma+i\epsilon]^n}, \tag{A.6.3}$$

$$\int \frac{d^4p}{(2\pi)^4}\frac{p^2}{[p^2-\Sigma+i\epsilon]^{n+1}}=\frac{2}{n}\int \frac{d^4p}{(2\pi)^4}\frac{1}{[p^2-\Sigma+i\epsilon]^n}, \tag{A.6.4}$$

with $n \geq 1$ and the function Σ has no p dependence.

A.7 Quark Propagators

$$S_0^{-1}(k)=\not{k}-m_{\rm q}+i\epsilon, \tag{A.7.1}$$

$$S_0(k)=\frac{\not{k}+m_{\rm q}}{k^2+m_{\rm q}^2+i\epsilon}, \tag{A.7.2}$$

$$S^{-1}(k)=\not{k}-M_{\rm q}+i\epsilon, \tag{A.7.3}$$

$$S(k)=\frac{\not{k}+M_{\rm q}}{k^2+M_{\rm q}^2+i\epsilon}, \tag{A.7.4}$$

$$\tau_\pi(q)=\frac{-2iG_\pi}{1+2G_\pi\Pi_S(q^2)}\rightarrow -2iG_\pi+\frac{ig_\pi}{[q^2-m_\pi^2+i\epsilon]}, \tag{A.7.5}$$

$$\tau_S(q)=\frac{-4iG_S}{1+2G_S\Pi_S(q^2)}\rightarrow 4iG_S+\frac{ig_S}{[q^2-M_S^2+i\epsilon]}. \tag{A.7.6}$$

A.8 Useful Integrals for the PTR Scheme

$$\int_0^\infty dp^2p^2e^{-\tau(p^2+\mathbf{A})}=\frac{e^{-\tau\mathbf{A}}}{\tau^2}, \tag{A.8.1}$$

$$\int_0^\infty dp^2p^4e^{-\tau(p^2+\mathbf{A})}=\frac{2e^{-\tau\mathbf{A}}}{\tau^3}, \tag{A.8.2}$$

$$\int_0^\infty dp^2p^6e^{-\tau(p^2+\mathbf{A})}=\frac{6e^{-\tau\mathbf{A}}}{\tau^4}. \tag{A.8.3}$$

A.9 Wick Rotation

$$\int \frac{d^4q}{(2\pi)^4}\rightarrow i\int \frac{d^4q_E}{(2\pi)4}=\frac{i}{16\pi^2}\int_0^\infty dq_E^2q_E^2. \tag{A.9.1}$$

Where $(q_0, \mathbf{q}) \to (iq_E^0, \mathbf{q}_E)$ and $q^2 \to -q_E^2$. In an $\mathcal{O}(4)$ invariant regularization, it can be defined as

$$q_- q_+ \to -\frac{1}{4} q_E^2, \tag{A.9.2}$$

$$q_- q_+ q_- q_+ \to -\frac{1}{24} q_E^2. \tag{A.9.3}$$

A.10 Derivation of the NJL gap equation

$$iS(k) = iS_0(k) + iS_0(k)\left[-i\Sigma(k)\right] iS(k), \tag{A.10.1}$$

$$\tag{A.10.2}$$

where Σ is defined as

$$\begin{aligned} -i\Sigma(k) &= -2iG_\pi \left\{ \sum_M \Gamma_M \int \frac{d^4p}{(2\pi)^4} \mathrm{Tr}\left[\Gamma_{\mathrm{M}}.\mathrm{S(k)}\right] \mathrm{S(k)} \right\} \\ &= -2iG_\pi \left\{ \mathbb{1} \int \frac{d^4p}{(2\pi)^4} \mathrm{Tr}\left[\mathbb{1}\mathrm{iS(k)}\right] + \mathrm{i}\gamma_5\tau_{\mathrm{a}} \int \frac{\mathrm{d^4p}}{(2\pi)^4} \mathrm{Tr}\left[\mathrm{i}\gamma_5\tau_{\mathrm{a}}\mathrm{iS(k)}\right] \right\}, \end{aligned} \tag{A.10.3}$$

where Γ_π is given by

$$\Gamma_\pi^i = i\mathbb{1}_c \otimes \gamma_5 \otimes \tau^i, \tag{A.10.4}$$

$$\Gamma_\sigma = \mathbb{1}_c \otimes \mathbb{1}_f \otimes \mathbb{1}_D. \tag{A.10.5}$$

Multiplying Eq. (A.10.1) with $S_0^{-1}(k)$ from the left side and then multiplying with $S^{-1}(k)$ from the right side, one obtains

$$\begin{aligned} S_0^{-1}(k)S(k) &= S_0^{-1}(k)S_0(k) + S_0^{-1}(k)S_0(k)\Sigma(k)S(k) \\ S_0^{-1}(k)S(k)S^{-1}(k) &= S_0^{-1}(k)S_0(k)S^{-1}(k) + S_0^{-1}(k)S_0(k)\Sigma(k)S(k)S^{-1}(k) \\ S_0^{-1}(k) &= S^{-1}(k) + \Sigma(k), \end{aligned} \tag{A.10.6}$$

Substituting the definition of the propagators in Eq. (A.7.1) into Eq. (A.10.6), it then gives

$$\begin{aligned} \not{k} - m_q + i\epsilon &= \not{k} - M_q + i\epsilon + \Sigma(k) \\ M_q &= m_q + \Sigma(k), \end{aligned} \tag{A.10.7}$$

with $\Sigma(k)$ can be rewritten as

$$\Sigma(k) = 8iG_\pi N_F N_C \int \frac{d^4p}{(2\pi)^4} \frac{M_q}{p^2 - M_q^2 + i\epsilon}, \tag{A.10.8}$$

where $\mathrm{Tr}\left[\mathbb{1}\right] = 4\mathrm{N_F N_C}$.

A.11 Derivation of the Mass of the Pion

Consider the scattering of a quark of flavor i from a quark of flavor j illustrated in Fig. 1.11.1,

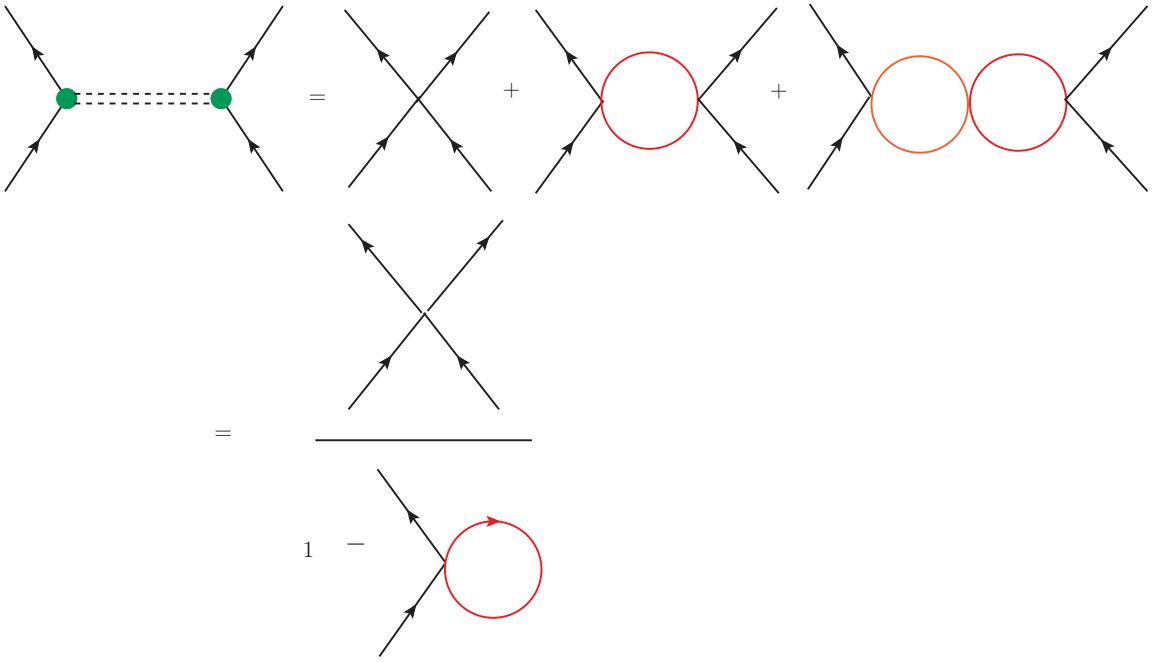

Figure 1.11.1: Diagrammatic of Bethe-Salpeter equation (BSE) for quark-antiquark interaction. The solid lines is a dressed quark propagator and the dashed lines is the meson T-matrix.

The total scattering amplitude $\mathcal{U}_{\rm ij}(k^2)$ is given as

$$
\begin{aligned}
i\mathcal{U}_{ij}(k^2) &= (i\gamma_5)T_i\left(2iG + 2iG(\frac{1}{i}\Pi_{ps}(k^2))2iG + 2iG(\frac{1}{i}\Pi_{ps}(k^2))2iG(\frac{1}{i}\Pi_{ps}(k^2))2iG + ...\right)(i\gamma_5)T_j \\
&= (i\gamma_5)T_i\left(\frac{2iG}{1-2G\Pi_{ps}(k^2)}\right)(i\gamma_5)T_j, \qquad \text{(A.11.1)}
\end{aligned}
$$

where k stands for the four momentum of the meson and $T_i = T_j = \tau_3$ for the π^0 or $T_i = \tau^{(\pm)}$, $T_j = \tau^{(\mp)}$ for creating a π^+ or π^- and the bubble graph has the form

$$
\Pi_{ps}(k^2) = -i\int\frac{d^4p}{(2\pi)^4}\mathrm{Tr}\left[\mathrm{i}\gamma_5\mathrm{T_i}\mathrm{S}(\mathrm{p}+\frac{\mathrm{k}}{2})\mathrm{i}\gamma_5\mathrm{T_j}\mathrm{S}(\mathrm{p}-\frac{\mathrm{k}}{2})\right]. \qquad \text{(A.11.2)}
$$

On the other hand, Eq. (A.11.2) can be written into the form

$$
\Pi_{ps}(k^2) = 4iN_CN_F\mathscr{I}_0 - 2iN_CN_Fk^2\mathscr{I}(k^2), \qquad \text{(A.11.3)}
$$

The mass of the pion is then given by the pole structure of the T-matrix as

$$
1 - 2G_\pi\Pi_{ps}(k^2) = 0. \qquad \text{(A.11.4)}
$$

Using the gap equation, which has the same integral, $\mathscr{I}_0$, with the first term on the RHS in Eq. (A.11.3), we obtain

$$1 - 2G_\pi \Pi_{ps}(k^2) = \frac{m}{M} + 4iG_\pi N_C N_F k^2 \mathscr{I}(k^2) = 0 \tag{A.11.5}$$

Setting $k^2 = m_\pi^2$, the mass of the pion is determined as

$$m_\pi^2 = -\frac{m}{M} \frac{1}{4iG_\pi N_C N_F \mathscr{I}(m_\pi^2)}. \tag{A.11.6}$$

A.12 Derivation of Meson Quark-AntiQuark Coupling

In Eq. (A.11.1), we evaluate that the scattering matrix is generated by the exchange of a pion and the bound state is defined as the iteration of the bubble graphs $\Pi_{\rm ps}(k^2)$. Then the scattering matrix is written as

$$i\mathcal{U}_{\rm ij}(k^2) = (i\gamma_5)\, T_{\rm i} \left(\frac{2iG}{1 - 2G\Pi_{\rm ps}(k^2)} \right) (i\gamma_5)\, T_{\rm j}, \tag{A.12.1}$$

Expanding the expression in Eq. (A.12.1) about its pole at $k^2 = m_\pi^2$ and satisfying $1 + 2G\Pi_{\rm ps}(k^2) = 0$, then it gives

$$i\mathcal{U}_{\rm ij}(k^2) \equiv (i\gamma_5) T_{\rm i} \frac{-i(\frac{\partial \Pi_{\rm ps}}{\partial k^2})^{-1}}{k^2 - m_\pi^2} (i\gamma_5) T_{\rm j}. \tag{A.12.2}$$

On the other hand, the scattering matrix can be obtained from the minimal local interaction Lagrangian. It describes the coupling of a pion field to quark fields. The effective interaction (pion exchange) can be written as

$$i\mathcal{U}_{ij}(k^2) = (i\gamma_5) T_i \frac{-ig^2_{\pi q\bar{q}}}{k^2 - m_\pi^2} (i\gamma_5) T_j. \tag{A.12.3}$$

Then the quark pion coupling constant can be obtained by comparing between Eqs. (A.12.2) and (A.12.3) that is

$$g^2_{\pi q\bar{q}} = \left(\frac{\partial \Pi_{ps}}{\partial k^2} \right)^{-1} |_{k^2 = m_\pi^2}, \tag{A.12.4}$$

where *ps* stands for pseudoscalar meson such as pion, kaon. Similarly, the meson quark-antiquark coupling constant, for other meson, can be computed in the same way.

A.13 Derivation of the Kaon Mass

The mass of the kaon is given by the pole of the T-matrix, that is

$$1 - 2K_6^+ \Pi_{ps}(k^2) = 0, \tag{A.13.1}$$

where $K_6^+ = G_\pi + \frac{1}{2}N_C K i tr[S_1] = G_\pi + \frac{1}{2}N_C K i(4M_1\mathcal{I}_1) = G_\pi + 2N_C K i M_1\mathscr{I}_1$ is the flavor dependent effective coupling constant. Additionally, the familiar expression of the bubble graph is obtained as

$$\begin{aligned}\Pi_{ps}(k^2) &= 4iN_C\frac{2M_2}{(M_2+M_1)}\mathscr{I}_2 + 4iN_C\frac{2M_1}{(M_2+M_1)}\mathscr{I}_1 - 4iN_Ck^2\mathscr{I}_{21}(k^2)\\ &= \frac{8iN_C}{(M_2+M_1)}\left(M_2\mathscr{I}_2 + M_1\mathscr{I}_1\right) - 4iN_Ck^2\mathscr{I}_{12}(k^2),\end{aligned} \tag{A.13.2}$$

with the gap equation for M_1 and M_2 are introduced here,

$$\begin{aligned}M_1 &= m_1 + 4iG_\pi N_C tr[S_1] - 2N_C^2 K tr[S_2]tr[S_1]\\ &= m_1 + 4iG_\pi N_C(4M_1\mathscr{I}_1) - 2N_C^2K(4M_2\mathscr{I}_2)4(M_1\mathscr{I}_2)\\ &= m_1 + 16iG_\pi N_C M_1\mathscr{I}_1 - 32N_C^2KM_2M_1\mathscr{I}_2\mathscr{I}_1,\end{aligned} \tag{A.13.3}$$

where the relationship between $\mathrm{Tr}\,[\mathrm{S}_2]$ and $\mathscr{I}_2$ is given by

$$\int\frac{d^4p}{(2\pi)^4}\frac{1}{p^2-M_2^2} = \frac{\mathrm{Tr}\,[\mathrm{S}_2]}{4M_2} = \mathscr{I}_2. \tag{A.13.4}$$

The relationship between $\mathrm{Tr}\,[\mathrm{S}_1]$ and $\mathscr{I}_1$ can be easily obtained using the similar way. Thus expression for the gap equation, M_2 is obtained as

$$\begin{aligned}M_2 &= m_2 + 4iG_\pi N_C tr[S_2] - 2N_C^2 K tr[S_1]tr[S_1]\\ &= m_2 + 4iG_\pi N_C(4M_2\mathscr{I}_2) - 2N_C^2K(4M_1\mathscr{I}_1)(4M_1\mathscr{I}_1)\\ &= m_2 + 16iG_\pi N_C M_2\mathscr{I}_2 - 32N_C^2KM_1^2\mathscr{I}_1\mathscr{I}_1.\end{aligned} \tag{A.13.5}$$

Then summing Eqs. (A.13.3) and (A.13.5) then we obtain

$$\begin{aligned}M_1+M_2 &= m_1+m_2 + 16iG_\pi N_C\left(M_1\mathscr{I}_1 + M_2\mathscr{I}_2\right)\\ &\quad + 32i^2N_C^2KM_1\mathscr{I}_1\left(M_2\mathscr{I}_2 + M_1\mathscr{I}_1\right)\\ &= m_1+m_2 + 16iN_C\left(G_\pi + 2iN_CK\right)\left(M_2\mathscr{I}_2 + M_1\mathscr{I}_1\right)\\ &= m_1+m_2 + 16iN_CK_6^+\left(M_2\mathscr{I}_2 + M_1\mathscr{I}_1\right)\\ (M_1+M_2)-(m_1+m_2) &= 16iN_CK_6^+\left(M_2\mathscr{I}_2 + M_1\mathscr{I}_1\right),\end{aligned} \tag{A.13.6}$$

where $K_6^+ = \left(G_\pi + 2iN_CK\right)$ [2]. In our calculation, we set the coupling constant, $K = 0$ for simple mathematics expression, therefore $K_6^+ = G_\pi$ for K = 0. [3].

Then eliminating the propagator in the bubble graph in Eq. (A.13.2) with the result in Eq. (A.13.6), one has

$$\Pi_{ps}(k^2) = \frac{(M_1+M_2)-(m_1+m_2)}{2K_6^+\left(M_2+M_1\right)} - 4iN_Ck^2\mathscr{I}_{21}(k^2), \tag{A.13.7}$$

[2] K_6^+ is the coupling constant of the six-fermion term.

[3] In our case, we do not include this term, so it does not change the physical interest in our work.

Plugging the bubble graph in Eq. (A.13.7) into the pole structure of the T-matrix in Eq. (A.13.1), this gives the form

$$\begin{aligned} 1 - 2K_6^+\Pi_{ps}(k^2) &= 0 \\ 1 - 2K_6^+\left(\frac{(M_1+M_2)-(m_1+m_2)}{2K_6^+\,(M_2+M_1)} - 4iN_Ck^2\mathscr{I}_{21}(k^2)\right) &= 0 \\ 1 - 1 + \frac{(m_1+m_2)}{2K_6^+\,(M_2+M_1)} + 8iN_Ck^2K_6^+\mathscr{I}_{21}(k^2) &= 0 \\ 8iN_Ck^2K_6^+\mathscr{I}_{21}(k^2) &= -\frac{(m_1+m_2)}{(M_2+M_1)}. \end{aligned} \tag{A.13.8}$$

From Eq. (A.13.8), the kaon mass is straightforwardly determined by taking $k^2 = m_\pi^2$,

$$\begin{aligned} k^2 &= -\frac{(m_1+m_2)}{(M_2+M_1)}\frac{1}{8iN_CK_6^+\mathscr{I}_{21}(k^2)} \\ m_K^2 &= -\frac{(m_1+m_2)}{(M_2+M_1)}\frac{1}{8iN_CK_6^+\mathscr{I}_{21}(k^2)} \\ &= -\frac{(m_1+m_2)}{(M_2+M_1)}\frac{1}{8iN_CG_\pi\mathscr{I}_{21}(k^2)}. \end{aligned} \tag{A.13.9}$$

A.14 Derivation of the Kaon Form Factor

In this appendix, the derivation of $\Lambda_{\rm u}^\mu(k.k')$ in Eq. (4.2.5) will presented. Also, the derivation of the trace in Eq. (4.2.5) will evaluated.

A.14.1 Derivation of $\Lambda_u^\mu(k,k')$

Recall $\Lambda_{\rm u}^\mu(k,k')$ in Eq. (4.2.5) and evaluate it, one has the form

$$\Lambda_u^\mu(k,k') = 2iN_Cg_{\rm Kq\bar{q}}^2\int\frac{d^4p}{(2\pi)^4}{\rm Tr}\left[\gamma_5{\rm S_u(p+k')}\gamma^\mu{\rm S_u(p+k)}\gamma_5{\rm S_{\bar{s}}(p)}\right], \tag{A.14.1}$$

with the dressed quark propagators can be defined as

$$S_u(p+k') = \frac{\not{p}+\not{k}'+M_u}{[(p+k')^2-M_u^2+i\epsilon]}, \tag{A.14.2}$$

$$S_{\bar{s}}(p) = \frac{\not{p}+M_{\bar{s}}}{[p^2-M_{\bar{s}}^2+i\epsilon]}, \tag{A.14.3}$$

By plugging the appropriate dressed quark propagators into Eq. (A.14.2), it then gives

$$\Lambda_u^\mu(k,k') = 2iN_Cg_{Kq\bar{q}}^2\int\frac{d^4p}{(2\pi)^4}{\rm Tr}[\gamma_5\left(\frac{\not{\rm p}+\not{\rm k}'+{\rm M_u}}{[{\rm (p+k')^2-M_u^2+i\epsilon}]}\right)$$

$$\times \gamma^{\mu}\left(\frac{\not{p}' + \not{k}' + M_u}{[(p+k)^2 - M_u^2 + i\epsilon]}\right)\gamma_5\left(\frac{\not{p}' + M_{\bar{s}}}{[p^2 - M_{\bar{s}}^2 + i\epsilon]}\right)]. \tag{A.14.4}$$

Later on, we evaluate the numerator (trace) and the denominator separately.

A.14.2 Evaluation of the Trace

Recall the numerator of Eq. (A.14.4) here, the trace is separately written as

$$\begin{aligned}
\mathcal{N} &= \mathrm{Tr}\,[\gamma_5(\not{p}' + \not{k}' + \mathrm{M_u})\gamma_\mu(\not{p}' + \not{k}' + \mathrm{M_u})\gamma_5(\not{p}' + \mathrm{M_{\bar{s}}})] \\
&= \mathrm{Tr}[\gamma_5\not{p}'\gamma_\mu\not{p}'\gamma_5\not{p}'] + \mathrm{Tr}[\gamma_5\not{p}'\gamma_\mu\not{p}'\gamma_5\mathrm{M_{\bar{s}}}] + \mathrm{Tr}[\gamma_5\not{p}'\gamma_\mu\not{k}'\gamma_5\not{p}'] + \mathrm{Tr}[\gamma_5\not{p}'\gamma_\mu\not{k}'\gamma_5\mathrm{M_{\bar{s}}}] \\
&+ \mathrm{Tr}[\gamma_5\not{p}'\gamma_\mu\mathrm{M_u}\gamma_5\not{p}'] + \mathrm{Tr}[\gamma_5\not{p}'\gamma_\mu\mathrm{M_u}\gamma_5\mathrm{M_{\bar{s}}}] + \mathrm{Tr}[\gamma_5\not{k}'\gamma_\mu\not{p}'\gamma_5\not{p}'] + \mathrm{Tr}[\gamma_5\not{k}'\gamma_\mu\not{p}'\gamma_5\mathrm{M_{\bar{s}}}] \\
&+ \mathrm{Tr}[\gamma_5\not{k}'\gamma_\mu\not{k}'\gamma_5\not{p}'] + \mathrm{Tr}[\gamma_5\not{k}'\gamma_\mu\not{k}'\gamma_5\mathrm{M_{\bar{s}}}] + \mathrm{Tr}[\gamma_5\not{k}'\gamma_\mu\mathrm{M_u}\gamma_5\not{p}'] + \mathrm{Tr}[\gamma_5\not{k}'\gamma_\mu\mathrm{M_u}\gamma_5\mathrm{M_{\bar{s}}}] \\
&+ \mathrm{Tr}[\gamma_5\mathrm{M_u}\gamma\mu\not{p}'\gamma_5\not{p}'] + \mathrm{Tr}[\gamma_5\mathrm{M_u}\gamma_\mu\not{p}'\gamma_5\mathrm{M_{\bar{s}}}] + \mathrm{Tr}[\gamma_5\mathrm{M_u}\gamma_\mu\not{k}'\gamma_5\not{p}'] + \mathrm{Tr}[\gamma_5\mathrm{M_u}\gamma_\mu\not{k}'\gamma_5\mathrm{M_{\bar{s}}}] \\
&+ \mathrm{Tr}[\gamma_5\mathrm{M_u}\gamma_\mu\mathrm{M_u}\gamma_5\not{p}'] + \mathrm{Tr}[\gamma_5\mathrm{M_u}\gamma_\mu\mathrm{M_u}\gamma_5\mathrm{M_{\bar{s}}}]
\end{aligned} \tag{A.14.5}$$

Using the $\mathrm{Tr}\,[\mathrm{odd's}\gamma] = 0$, $\mathrm{Tr}\,[\gamma_\mu\gamma_\nu\gamma_\lambda\gamma_\sigma] = 4[\mathrm{g}_{\mu\nu}\mathrm{g}_{\lambda\sigma} - \mathrm{g}_{\mu\lambda}\mathrm{g}_{\nu\sigma} + \mathrm{g}_{\mu\sigma}\mathrm{g}_{\nu\lambda}]$, and $\mathrm{Tr}[\gamma_\mu\gamma_\nu] = 4\mathrm{g}_{\mu\nu}$, so that the trace in Eq. (A.14.5) can be rewritten as

$$\begin{aligned}
&\rightarrow p^\rho p^\nu p^\beta \mathrm{Tr}[\gamma_5\gamma_\rho\gamma_\mu\gamma_\nu\gamma_5\gamma_\beta] + \mathrm{p^\rho p^\nu k^\beta Tr}[\gamma_5\gamma_\rho\gamma_\mu\gamma_\nu\gamma_5\gamma_\beta] + \mathrm{p^\rho M_u M_{\bar{s}} Tr}[\gamma_5\gamma_\rho\gamma_\mu\gamma_5] \\
&+ p^\rho p^\nu k'^\beta \mathrm{Tr}[\gamma_5\gamma_\rho\gamma_\mu\gamma_\nu\gamma_5\gamma_\beta] + \mathrm{k'^\rho k^\nu p^\beta Tr}[\gamma_5\gamma_\rho\gamma_\mu\gamma_\nu\gamma_5\gamma_\beta] + \mathrm{k'^\rho M_u M_{\bar{s}} Tr}[\gamma_5\gamma_\rho\gamma_\mu\gamma_5] \\
&+ p^\rho M_u M_{\bar{s}} \mathrm{Tr}[\gamma_5\gamma_\mu\gamma_\rho\gamma_5] + \mathrm{k^\rho M_u M_{\bar{s}} Tr}[\gamma_5\gamma_\mu\gamma_\rho\gamma_5] + \mathrm{p^\rho M_u^2 Tr}[\gamma_5\gamma_\mu\gamma_5\gamma_\rho] \\
&= -4[(p^2 - M_{\bar{s}}^2)(p_\mu + k'_\mu + k_\mu) - M_u^2(k'_\mu + k_\mu) + (M_{\bar{s}} - M_u)^2(p_\mu + k'_\mu + k_\mu) \\
&+ p.kk'_\mu - k'.kp_\mu + p.k'k_\mu + M_u M_{\bar{s}}(k'_\mu + k_\mu)] \\
&= -4[(p^2 - M_{\bar{s}}^2)\mathcal{N}_u + \mathcal{N}_{\bar{s}}].
\end{aligned} \tag{A.14.6}$$

we will cancel the $(p^2 - M^2)$ term, therefore the numerator is expressed as

$$\mathcal{N} = -4[(p^2 - M_u^2)\mathcal{N}_1 + \mathcal{N}_2], \tag{A.14.7}$$

$$\mathcal{N}_1 = (p_\mu + k_\mu + k'_\mu), \tag{A.14.8}$$

$$\begin{aligned}
\mathcal{N}_2 = (&-M_u^2(k'_\mu + k_\mu) + (M_{\bar{s}} - M_u)^2(p_\mu + k'_\mu + k_\mu) + p.kk'_\mu - k'.kp_\mu + p.k'k_\mu \\
&+ M_u M_{\bar{s}}(k'_\mu + k_\mu)).
\end{aligned} \tag{A.14.9}$$

A.14.3 Evaluation of the propagators

Propagator for $\mathcal{N}_1$

In this appendix, after we cancel $(p^2 - M_u^2)$ term, we straightforwardly evaluate the propagator in Eq. (A.14.1) using a Feynman parameterization. By assuming that $A = [(p+k')^2 - M_u^2 + i\epsilon]$ and $B = [(p+k)^2 - M_u^2 + i\epsilon]$, One finds that

$$\frac{1}{[(p+k')^2 - M_u^2 + i\epsilon][(p+k)^2 - M_u^2 + i\epsilon]} = \int_0^1 dx \frac{1}{[Ax + (1-x)B]^2}, \tag{A.14.10}$$

and the denominator ($\mathcal{D}_0$) in above equation can be calculated as

$$\mathcal{D}_0 = [xA + (1-x)B]^2$$

$$
\begin{aligned}
&= [x[(p+k')^2 - M_u^2 + i\epsilon] + (1-x)[(p+k)^2 - M_u^2 + i\epsilon]]^2 \\
&= [x[(p^2 + k'^2 + 2p.k') - M_u^2 + i\epsilon] + (1-x)[(p^2 + k^2 + 2p.k) - M_u^2 + i\epsilon]]^2 \\
&= [xp^2 + xk'^2 + 2xp.k' - xM_u^2 + ix\epsilon + p^2 + k^2 + 2p.k - M_u^2 + i\epsilon \\
&- xp^2 - xk^2 - 2xp.k + xM_u^2 - ix\epsilon]^2 \\
&= [p^2 + 2xp.k' - 2xp.k + 2p.k - M_u^2 + k^2 - xk^2 + xk'^2 + i\epsilon]^2 \\
&= [p^2 + 2p.[xk' - xk + k] - M_u^2 + k^2 - xk^2 + xk'^2 + i\epsilon]^2 \\
&= [(p + [xk' - xk + k])^2 - (xk' - xk + k)^2 - M_u^2 + k^2 - xk^2 + xk'^2 + i\epsilon]^2,
\end{aligned}
\tag{A.14.11}
$$

shifting the $p \to p - [xk' - xk + k]$ this result can be written as

$$
\begin{aligned}
\mathcal{D}_0 &= [p^2 - (xk' - xk + k)^2 - M_u^2 + k^2 - xk^2 + xk'^2 + i\epsilon]^2 \\
&= [p^2 - (xk' - xk + k)^2 - M_u^2 + k^2 - xk^2 + xk'^2 + i\epsilon]^2 \\
&= [p^2 - (k^2 - 2xk^2 + x^2k^2 + 2xk.k' - 2x^2k.k' + x^2k'^2) - M_u^2 + k^2 - xk^2 + xk'^2 + i\epsilon]^2 \\
&= [p^2 - k^2 + 2xk^2 - x^2k^2 - 2xk.k' + 2x^2k.k' - x^2k'^2 - M_u^2 + k^2 - xk^2 + xk'^2 + i\epsilon]^2 \\
&= [p^2 + 2xk^2 - x^2k^2 - 2xk.k' + 2x^2k.k' - x^2k'^2 - M_u^2 - xk^2 + xk'^2 + i\epsilon]^2 \\
&= [p^2 + 2xk^2 - x^2k^2 - 2x(k^2 - \frac{q^2}{2}) + 2x^2(k^2 - \frac{q^2}{2}) - x^2k'^2 - M_u^2 - xk^2 + xk'^2 + i\epsilon]^2 \\
&= [p^2 + xq^2 - x^2q^2 - M_u^2 + i\epsilon]^2 \\
&= [p^2 + q^2(x - x^2) - M_u^2 + i\epsilon]^2,
\end{aligned}
\tag{A.14.12}
$$

where $k'^2 = k^2$ and $k\dot{k}' = (k^2 - \frac{q^2}{2})$. The propagator for $\mathcal{N}_u$ after applying the Feynman parameterization becomes

$$
\frac{1}{[(p+k')^2 - M_u^2 + i\epsilon][(p+k)^2 - M_u^2 + i\epsilon]} = \int_0^1 dx \frac{1}{[p^2 + q^2(x - x^2) - M_u^2 + i\epsilon]^2}.
\tag{A.14.13}
$$

Recall $\mathcal{N}_1$ and performing the shift variable $p \to p - (xk' - xk + k) = p - xq - k$ to the numerator $\mathcal{N}_1$, the final expression then gives

$$
\begin{aligned}
\mathcal{N}_1 &= (p_\mu + k_\mu + k'_\mu) = (p_\mu - xk'_\mu + xk_\mu - k_\mu + k_\mu + k'_\mu) = (p_\mu - x(k'_\mu - k_\mu) + k'_\mu) \\
&= (p_\mu - xq_\mu + k'_\mu) = (-xq_\mu + k'_\mu) = (-\frac{1}{2}q_\mu + k'_\mu) = -\frac{1}{2}(k'_\mu - k_\mu) + k'_\mu = \frac{1}{2}(k'_\mu + k_\mu).
\end{aligned}
\tag{A.14.14}
$$

where we have ignored the terms in p and the factor one half are taken from the symmetry in the denominators under $x \to (1-x)$.

Propagators for $\mathcal{N}_2$

Now, the three propagators for numerator, $\mathcal{N}_2$ are evaluated using a Feynman paramaterization, that is

$$
\to \frac{1}{((p+k')^2 - M_1^2)\,[(p+k)^2 - M_u^2]\,[p^2 - M_{\bar{s}}^2]}
$$

$$\rightarrow \frac{1}{ABC} = 2\int_0^1 dx \int_0^{1-x} dz \frac{1}{[A+(B-A)x+(C-A)z]^3}. \tag{A.14.15}$$

By setting $A = p^2 - M_{\bar{s}}^2 + i\epsilon$, $B = (p+k)^2 - M_u^2 + i\epsilon$ and $C = (p+k')^2 - M_u^2 + i\epsilon$. Then plugging A, B and C into Eq. (A.14.15), the three propagators for the numerator $\mathcal{N}_2$ is written as

$$\begin{aligned}
\mathcal{D}_1 &= [A+(B-A)x+(C-A)z]^3 \\
&= [p^2 - M_{\bar{s}}^2 + i\epsilon + ((p+k)^2 - M_u^2 + i\epsilon - (p^2 - M_{\bar{s}}^2 + i\epsilon))x + ((p+k')^2 - M_u^2 + i\epsilon \\
&- (p^2 - M_{\bar{s}}^2 + i\epsilon))z]^3 \\
&= [p^2 - M_{\bar{s}}^2 + i\epsilon + (p^2 + k^2 + 2p.k - M_u^2 + i\epsilon - p^2 + M_{\bar{s}}^2 - i\epsilon)x \\
&+ (p^2 + k'^2 + 2p.k' - M_u^2 + i\epsilon - p^2 + M_{\bar{s}}^2 - i\epsilon)z]^3 \\
&= [p^2 - M_2^2 + i\epsilon + (k^2 + 2p.k - M_u^2 + M_{\bar{s}}^2)x + (k'^2 + 2p.k' - M_u^2 + M_{\bar{s}}^2)z]^3 \\
&= [p^2 - M_{\bar{s}}^2 + xk^2 + 2xp.k - xM_u^2 + xM_{\bar{s}}^2 + zk'^2 + 2zp.k' - zM_u^2 + zM_{\bar{s}}^2 + i\epsilon]^3 \\
&= [p^2 + 2p.(xk + zk') - M_2^2 + xk^2 + zk'^2 - xM_u^2 + xM_{\bar{s}}^2 - zM_u^2 + zM_{\bar{s}}^2 + i\epsilon]^3 \\
&= [(p + (xk + zk'))^2 - (xk + zk')^2 - M_{\bar{s}}^2 + xk^2 + zk'^2 - xM_u^2 + xM_{\bar{s}}^2 \\
&- zM_u^2 + zM_{\bar{s}}^2 + i\epsilon]^3,
\end{aligned} \tag{A.14.16}$$

Applying shift to the results in Eq. (A.14.16) by using $p \rightarrow p - [xk + zk']$, it gives

$$\begin{aligned}
\mathcal{D}_2 &= [p^2 - (xk + zk')^2 - M_{\bar{s}}^2 + xk^2 + zk'^2 - xM_u^2 + xM_{\bar{s}}^2 - zM_u^2 + zM_{\bar{s}}^2 + i\epsilon]^3 \\
&= [p^2 - (x^2k^2 + z^2k'^2 + 2xzk.k') - M_{\bar{s}}^2 + xk^2 + zk'^2 - xM_u^2 + xM_{\bar{s}}^2 - zM_u^2 \\
&+ zM_{\bar{s}}^2 + i\epsilon]^3 \\
&= [p^2 - x^2k^2 + xk^2 - z^2k'^2 + zk'^2 - 2xzk.q - 2xzk.k - M_{\bar{s}}^2 - xM_u^2 + xM_{\bar{s}}^2 \\
&- zM_u^2 + zM_{\bar{s}}^2 + i\epsilon]^3 \\
&= [p^2 - x^2k^2 + xk^2 - z^2k'^2 + zk'^2 + xzq^2 - 2xzk^2 - M_{\bar{s}}^2 - xM_u^2 + xM_{\bar{s}}^2 \\
&- zM_u^2 + zM_{\bar{s}}^2 + i\epsilon]^3 \\
&= [p^2 - k^2(x^2 - x) - k^2(z^2 - z) - 2xzk^2 + xzq^2 - M_{\bar{s}}^2 - xM_u^2 + xM_{\bar{s}}^2 \\
&- zM_u^2 + zM_{\bar{s}}^2 + i\epsilon]^3 \\
&= [p^2 - k^2[(x^2 - x) + (z^2 - z) + 2xz] + xzq^2 - M_{\bar{s}}^2 - xM_u^2 + xM_{\bar{s}}^2 \\
&- zM_u^2 + zM_{\bar{s}}^2 + i\epsilon]^3 \\
&= [p^2 - k^2[x^2 - x + z^2 - z + 2xz] + xzq^2 - M_{\bar{s}}^2 - xM_u^2 + xM_{\bar{s}}^2 \\
&- zM_u^2 + zM_{\bar{s}}^2 + i\epsilon]^3 \\
&= [p^2 - k^2[x^2 + z^2 + 2xz - x - z] + xzq^2 - M_{\bar{s}}^2 - xM_u^2 + xM_{\bar{s}}^2 \\
&- zM_u^2 + zM_{\bar{s}}^2 + i\epsilon]^3 \\
&= [p^2 - k^2[(x+z)^2 - (x+z)] + xzq^2 - M_{\bar{s}}^2 - xM_u^2 + xM_{\bar{s}}^2 \\
&- zM_u^2 + zM_{\bar{s}}^2 + i\epsilon]^3,
\end{aligned} \tag{A.14.17}$$

where $q.k = -\frac{q^2}{2}$ or $2q.k = -q^2$, $k^2 = k'^2$ and $q = k' - k$. The propagator for $\mathcal{N}_2$ after applying the Feynman parameterization becomes

$$\rightarrow \frac{1}{((p+k')^2 - M_1^2)\,[(p+k)^2 - M_u^2]\,[p^2 - M_{\bar{s}}^2]}$$

$$\rightarrow 2\int_0^1 dx \int_0^{1-x} dz$$
$$\times \frac{1}{[p^2 - k^2[(x+z)^2 - (x+z)] + xzq^2 - M_{\bar{s}}^2 - xM_u^2 + xM_{\bar{s}}^2 - zM_u^2 + zM_{\bar{s}}^2 + i\epsilon]^3}, \tag{A.14.18}$$

Now, recall the numerator $\mathcal{N}_2$ and applying shift $p \rightarrow p - (xk + zk')$ to the numerator $\mathcal{N}_2$, it then gives

$$\begin{aligned}
\mathcal{N}_2 &= p.kk'_\mu + p.k'k_\mu - k'.kp_\mu - M_u^2(k'_\mu + k_\mu) + (M_{\bar{s}} - M_u)^2(p_\mu + k'_\mu + k_\mu) + M_uM_{\bar{s}}(k'_\mu + k_\mu) \\
&= (p_\mu - xk - zk').kk'_\mu + (p_\mu - xk - zk').k'k_\mu - k'.k(p_\mu - xk_\mu - zk'_\mu) \\
&- M_u^2(k'_\mu + k_\mu) + (M_{\bar{s}} - M_u)^2((p_\mu - xk_\mu - zk'_\mu) \\
&+ k'_\mu + k_\mu) + M_uM_{\bar{s}}(k'_\mu + k_\mu),
\end{aligned} \tag{A.14.19}$$

Dropping p_μ term, which gives zero in the integral. It then gives

$$\begin{aligned}
\mathcal{N}_2 &= -xk.kk'_\mu - zk'.kk'_\mu - xk.k'k_\mu - zk'.k'k_\mu + xk'.kk_\mu + zk'.kk'_\mu - M_u^2(k'_\mu + k_\mu) \\
&+ (M_{\bar{s}} - M_u)^2(1-x)k_\mu + (M_{\bar{s}} - M_u)^2(1-z)k'_\mu + M_uM_{\bar{s}}(k'_\mu + k_\mu) \\
&= -xk^2k'_\mu - zk'^2k_\mu - M_u^2(k'_\mu + k_\mu) + (M_{\bar{s}} - M_u)^2(1-x)k_\mu \\
&+ (M_{\bar{s}} - M_u)^2(1-z)k'_\mu + M_uM_{\bar{s}}(k'_\mu + k_\mu),
\end{aligned} \tag{A.14.20}$$

where the odd terms in p is ignored. Introducing the equation $k'_\mu = \frac{1}{2}(k'_\mu + k_\mu) + \frac{1}{2}(k'_\mu - k_\mu)$ and $k_\mu = \frac{1}{2}(k'_\mu + k_\mu) - \frac{1}{2}(k'_\mu - k_\mu)$. By putting these expressions into Eq. (A.14.19), one has

$$\begin{aligned}
\mathcal{N}_2 &= -xk^2[\frac{1}{2}(k'_\mu + k_\mu) + \frac{1}{2}(k'_\mu - k_\mu)] - zk'^2[\frac{1}{2}(k'_\mu + k_\mu) - \frac{1}{2}(k'_\mu - k_\mu)] \\
&+ (M_{\bar{s}} - M_u)^2[(1-x)[\frac{1}{2}(k'_\mu + k_\mu) - \frac{1}{2}(k'_\mu - k_\mu)] + (1-z)[\frac{1}{2}(k'_\mu + k_\mu) + \frac{1}{2}(k'_\mu - k_\mu)]], \\
&- M_u^2(k'_\mu + k_\mu) + M_uM_{\bar{s}}(k'_\mu + k_\mu), \\
&= -\frac{xk^2}{2}(k'_\mu + k_\mu) - \frac{xk^2}{2}(k'_\mu - k_\mu)] - [\frac{zk'^2}{2}(k'_\mu + k_\mu) + \frac{zk'^2}{2}(k'_\mu - k_\mu)] \\
&+ (M_{\bar{s}} - M_u)^2[(1-x)[\frac{1}{2}(k'_\mu + k_\mu) - \frac{1}{2}(k'_\mu - k_\mu)] + (1-z)[\frac{1}{2}(k'_\mu + k_\mu) + \frac{1}{2}(k'_\mu - k_\mu)]] \\
&- M_u^2(k'_\mu + k_\mu) + M_uM_2(k'_\mu + k_\mu) \\
&= -\frac{xk^2}{2}(k'_\mu + k_\mu) - [\frac{zk'^2}{2}(k'_\mu + k_\mu) - \frac{xk^2}{2}(k'_\mu - k_\mu)] + \frac{zk'^2}{2}(k'_\mu - k_\mu)] \\
&+ (M_{\bar{s}} - M_u)^2[\frac{1}{2}(k'_\mu + k_\mu) - \frac{x}{2}(k'_\mu + k_\mu) - \frac{1}{2}(k'_\mu - k_\mu) + \frac{x}{2}(k'_\mu + k_\mu) + \frac{1}{2}(k'_\mu + k_\mu) \\
&- \frac{z}{2}(k'_\mu + k_\mu) + \frac{1}{2}(k'_\mu + k_\mu) - \frac{z}{2}(k'_\mu - k_\mu)] \\
&- M_u^2(k'_\mu + k_\mu) + M_uM_2(k'_\mu + k_\mu) \\
&= -\frac{xk^2 + zk'^2}{2}(k'^\mu + k^\mu) + \frac{zk'^2 - xk^2}{2}(k'^\mu - k^\mu)
\end{aligned}$$

$$
\begin{aligned}
&+ (M_{\bar{s}} - M_u)^2[(k'_\mu + k_\mu) - \frac{x}{2}(k'_\mu + k_\mu) - \frac{z}{2}(k'_\mu + k_\mu) + \frac{x}{2}(k'_\mu - k_\mu) - \frac{z}{2}(k'_\mu - k_\mu)] \\
&- M_u^2(k'_\mu + k_\mu) + M_u M_2(k'_\mu + k_\mu) \\
&= -\frac{xk^2 + zk'^2}{2}(k'^\mu + k^\mu) + \frac{zk'^2 - xk^2}{2}(k'^\mu - k^\mu) \\
&+ (M_{\bar{s}} - M_u)^2[(1 - \frac{x}{2} - \frac{z}{2})(k'_\mu + k_\mu) + (\frac{x}{2} - \frac{z}{2}) \\
&\times (k'_\mu - k_\mu)] \\
&- M_u^2(k'_\mu + k_\mu) + M_u M_{\bar{s}}(k'_\mu + k_\mu), \qquad \text{(A.14.21)}
\end{aligned}
$$

Note that the last term in Eq. (A.14.21) is vanished because the variable transformation $x \to \frac{1}{2}(x+z)$ and $z \to \frac{1}{2}(x-z)$, which evaluates being zero. This is because the numerator odds in z. In another reason, once we evaluate the integral over z or x, separately, it will gives the same answer, therefore the integral over the terms of $x - z$ equals to zero. Then, the final result of the numerator, $\mathcal{N}_2$ becomes

$$
\begin{aligned}
\mathcal{N}_2 &= -\frac{1}{2}k^2(x+z)(k'^\mu + k^\mu) + (M_{\bar{s}} - M_u)^2[(1 - \frac{x}{2} - \frac{z}{2})(k'_\mu + k_\mu)] \\
&- M_u^2(k'_\mu + k_\mu) + M_1 M_{\bar{s}}(k'_\mu + k_\mu) \\
&= [-\frac{1}{2}k^2(x+z) + (M_{\bar{s}} - M_u)^2(1 - \frac{x}{2} - \frac{z}{2}) - M_u^2 + M_u M_{\bar{s}}](k'_\mu + k_\mu) \\
&= [-\frac{1}{2}k^2(x+z) + M_{\bar{s}}^2 + M_u^2 - 2M_2 M_u - \frac{1}{2}(M_{\bar{s}} - M_u)^2(x+z) - M_u^2 + M_u M_{\bar{s}}](k'_\mu + k_\mu) \\
&= [-\frac{1}{2}k^2(x+z) - \frac{1}{2}(M_{\bar{s}} - M_u)^2(x+z) + M_2^2 - M_u M_{\bar{s}}](k'_\mu + k_\mu), \qquad \text{(A.14.22)}
\end{aligned}
$$

By putting the result of the numerator and the denominator together, the electromagnetic current of the kaon can be written as

$$
\begin{aligned}
\Lambda_u^\mu(k,k') &= 2iN_C g_{Kq\bar{q}}^2 \int \frac{d^4p}{(2\pi)^4} \frac{Tr\left[\gamma_5(\not{p} + \not{k}'' + M_u)\gamma_\mu(\not{p} + \not{k}' + M_u)\gamma_5(\not{p} + M_{\bar{s}})\right]}{[(p+k')^2 - M_u^2 + i\epsilon]\,[(p+k)^2 - M_u^2 + i\epsilon]\,[p^2 - M_{\bar{s}}^2 + i\epsilon]} \\
&= -8iN_C g_{Kq\bar{q}}^2 \int \frac{d^4p}{(2\pi)^4} \frac{(p^2 - M_{\bar{s}}^2)\mathcal{N}_u}{[(p+k')^2 - M_u^2 + i\epsilon]\,[(p+k)^2 - M_u^2 + i\epsilon]\,[p^2 - M_{\bar{s}}^2 + i\epsilon]} \\
&- 8iN_C g_{Kq\bar{q}}^2 \int \frac{d^4p}{(2\pi)^4} \frac{\mathcal{N}_{\bar{s}}}{[(p+k')^2 - M_u^2 + i\epsilon]\,[(p+k)^2 - M_u^2 + i\epsilon]\,[p^2 - M_{\bar{s}}^2 + i\epsilon]}, \qquad \text{(A.14.23)}
\end{aligned}
$$

The $(p^2 - M^2)$ in the first term are canceled. One has the form

$$
\begin{aligned}
\Lambda_u^\mu(k,k') &= -8iN_C g_{Kq\bar{q}}^2 \int \frac{d^4p}{(2\pi)^4} \frac{\mathcal{N}_1}{[(p+k')^2 - M_u^2 + i\epsilon]\,[(p+k)^2 - M_u^2 + i\epsilon]} \\
&- 8iN_C g_{Kq\bar{q}}^2 \int \frac{d^4p}{(2\pi)^4} \frac{\mathcal{N}_2}{[(p+k')^2 - M_u^2 + i\epsilon]\,[(p+k)^2 - M_u^2 + i\epsilon]\,[p^2 - M_{\bar{s}}^2 + i\epsilon]} \\
&= -8iN_C g_{Kq\bar{q}}^2 \int \frac{d^4p}{(2\pi)^4} \int_0^1 dx \frac{\frac{1}{2}(k'^\mu + k^\mu)}{[p^2 + q^2(x - x^2) - M_u^2 + i\epsilon]^2} \\
&- 8iN_C g_{Kq\bar{q}}^2 \int \frac{d^4p}{(2\pi)^4} 2 \int_0^1 dx \int_0^{1-x} dz
\end{aligned}
$$

$$\times \frac{\mathcal{N}_2}{[p^2-k^2[(x+z)^2-(x+z)]+xzq^2-M_{\bar{s}}^2(1-x-z)-M_u^2(x+z)+i\epsilon]^3}$$
$$= -4iN_C g_{Kq\bar{q}}^2 \int \frac{d^4p}{(2\pi)^4}\int_0^1 dx \frac{(k'^\mu+k^\mu)}{[p^2+q^2(x-x^2)-M_u^2+i\epsilon]^2}$$
$$+ 16iN_C g_{Kq\bar{q}}^2 \int \frac{d^4p}{(2\pi)^4}\int_0^1 dx \int_0^{1-x} dz$$
$$\times \frac{[\frac{1}{2}k^2(x+z)+\frac{1}{2}(M_{\bar{s}}-M_u)^2(x+z)-M_{\bar{s}}^2+M_uM_{\bar{s}}](k'_\mu+k_\mu)}{[p^2-k^2[(x+z)^2-(x+z)]+xzq^2-M_{\bar{s}}^2(1-x-z)-M_1^2(x+z)+i\epsilon]^3}$$
$$= -4iN_C g_{Kq\bar{q}}^2 \int \frac{d^4p}{(2\pi)^4}\int_0^1 dx \frac{(k'^\mu+k^\mu)}{[p^2+q^2(x-x^2)-M_u^2+i\epsilon]^2},$$
$$+ 8iN_C g_{Kq\bar{q}}^2 \int \frac{d^4p}{(2\pi)^4}\int_0^1 dx \int_0^{1-x} dz$$
$$\times \frac{[k^2(x+z)+(M_{\bar{s}}-M_u)^2(x+z)-2M_{\bar{s}}^2+2M_uM_{\bar{s}}](k'_\mu+k_\mu)}{[p^2-k^2[(x+z)^2-(x+z)]+xzq^2-M_{\bar{s}}^2(1-x-z)-M_u^2(x+z)+i\epsilon]^3}. \quad (A.14.24)$$

A.15 Derivation of $\Lambda_{\bar{s}}^{\mu}(-k,-k')$

Recalling $\Lambda_{\bar{s}}^{\mu}(-k,-k')$, gives

$$\Lambda_{\bar{s}}^{\mu}(-k,-k') = 2iN_C g_{Kq\bar{q}}^2 \int \frac{d^4p}{(2\pi)^4}\mathrm{Tr}[\gamma_5 \mathrm{S}_{\bar{\mathrm{s}}}(\mathrm{p}-\mathrm{k})\gamma_\mu \mathrm{S}_{\bar{\mathrm{s}}}(\mathrm{p}-\mathrm{k}')\gamma_5 \mathrm{S}_{\mathrm{u}}(\mathrm{p})], \quad (A.15.1)$$

where the propagators can be defined as

$$S_{\bar{s}}(p-k) = \frac{\not{p}-\not{k}+M_{\bar{s}}}{[(p-k)^2-M_{\bar{s}}^2+i\epsilon]}, \quad (A.15.2)$$
$$S_{\bar{s}}(p-k') = \frac{\not{p}-\not{k}'+M_{\bar{s}}}{[(p-k')^2-M_{\bar{s}}^2+i\epsilon]}, \quad (A.15.3)$$
$$S_u(p) = \frac{\not{p}+M_u}{[p^2-M_u^2+i\epsilon]}, \quad (A.15.4)$$

Putting the $S_{\bar{s}}(p-k)$, $S_{\bar{s}}(p-k')$ and $S_u(p)$ propagators into the $\Lambda_{\bar{s}}^{\mu}(-k,-k')$, it then gives

$$\Lambda_{\bar{s}}^{\mu}(-k,-k') = 2iN_C g_{Kq\bar{q}}^2 \int \frac{d^4p}{(2\pi)^4}\mathrm{Tr}[\gamma_5\left(\frac{\not{\mathrm{p}}-\not{\mathrm{k}}+\mathrm{M}_{\bar{\mathrm{s}}}}{[(\mathrm{p}-\mathrm{k})^2-\mathrm{M}_{\bar{\mathrm{s}}}^2+\mathrm{i}\epsilon]}\right)$$
$$\times \gamma_\mu\left(\frac{\not{p}-\not{k}'+M_{\bar{s}}}{[(p-k')^2-M_{\bar{s}}^2+i\epsilon]}\right)\gamma_5\left(\frac{\not{p}+M_u}{[p^2-M_u^2+i\epsilon]}\right)]. \quad (A.15.5)$$

For sake of the simplicity, the trace in the numerator in Eq. (A.15.5) and propagators in the denominator are evaluated separately. The trace in the numerator will calculated in the next subsection.

A.15.1 Evaluation of the Trace

The trace in the numerator, which is symbolized $\mathcal{N}_2^2$, can be written as

$$\begin{aligned}
\mathcal{N}_2^2 \rightarrow & \mathrm{Tr}[\gamma_5(\not{p}-\not{k}+\mathrm{M}_{\bar{s}})\gamma_\mu(\not{p}-\not{k}'+\mathrm{M}_{\bar{s}})\gamma_5(\not{p}'+\mathrm{M}_{\mathrm{u}})] \\
&= \mathrm{Tr}[\gamma_5\not{p}\gamma_\mu\not{p}'\gamma_5\not{p}'] + \underbrace{\mathrm{Tr}[\gamma_5\not{p}\gamma_\mu\not{p}\gamma_5\mathrm{M}_{\mathrm{u}}]} - \mathrm{Tr}[\gamma_5\not{p}\gamma_\mu\not{k}'\gamma_5\not{p}'] - \underbrace{\mathrm{Tr}[\gamma_5\not{p}'\gamma_\mu\not{k}'\mathrm{M}_{\mathrm{u}}]} \\
&+ \underbrace{\mathrm{Tr}[\gamma_5\not{p}'\gamma_\mu\mathrm{M}_{\bar{s}}\gamma_5\not{p}']} + \mathrm{Tr}[\gamma_5\not{p}'\gamma_\mu\mathrm{M}_{\bar{s}}\gamma_5\mathrm{M}_{\mathrm{u}}] - \mathrm{Tr}[\gamma_5\not{k}'\gamma_\mu\not{p}'\gamma_5\not{p}'] - \underbrace{\mathrm{Tr}[\gamma_5\not{k}'\gamma_\mu\not{p}'\gamma_5\mathrm{M}_{\mathrm{u}}]} \\
&+ \mathrm{Tr}[\gamma_5\not{k}'\gamma_\mu\not{k}'\gamma_5\not{p}'] + \underbrace{\mathrm{Tr}[\gamma_5\not{k}'\gamma_\mu\not{k}'\gamma_5\mathrm{M}_{\mathrm{u}}]} - \underbrace{\mathrm{Tr}[\gamma_5\not{k}'\gamma_\mu\mathrm{M}_{\bar{s}}\gamma_5\not{p}']} - \mathrm{Tr}[\gamma_5\not{k}'\gamma_\mu\mathrm{M}_{\bar{s}}\gamma_5\mathrm{M}_{\mathrm{u}}] \\
&+ \underbrace{\mathrm{Tr}[\gamma_5\mathrm{M}_{\bar{s}}\gamma_\mu\not{p}'\gamma_5\not{p}']} + \mathrm{Tr}[\gamma_5\mathrm{M}_{\bar{s}}\gamma_\mu\not{p}'\gamma_5\mathrm{M}_{\mathrm{u}}] - \underbrace{\mathrm{Tr}[\gamma_5\mathrm{M}_{\bar{s}}\gamma_\mu\not{k}'\gamma_5\not{p}']} - \mathrm{Tr}[\gamma_5\mathrm{M}_{\bar{s}}\gamma_\mu\not{k}'\gamma_5\mathrm{M}_{\mathrm{u}}] \\
&+ \mathrm{Tr}[\gamma_5\mathrm{M}_{\bar{s}}\gamma_\mu\mathrm{M}_{\bar{s}}\gamma_5\not{p}'] + \underbrace{\mathrm{Tr}[\gamma_5\mathrm{M}_{\bar{s}}\gamma_\mu\mathrm{M}_{\bar{s}}\gamma_5\mathrm{M}_{\mathrm{u}}]}, \qquad (A.15.6)
\end{aligned}$$

By using trace identities some of the trace will vanish and the remaining traces are

$$\begin{aligned}
\mathcal{N}_2^2 \rightarrow & \mathrm{Tr}[\gamma_5\not{p}\gamma_\mu\not{p}'\gamma_5\not{p}'] - \mathrm{Tr}[\gamma_5\not{p}'\gamma_\mu\not{k}'\gamma_5\not{p}'] + \mathrm{Tr}[\gamma_5\not{p}'\gamma_\mu\mathrm{M}_{\bar{s}}\gamma_5\mathrm{M}_{\mathrm{u}}] - \mathrm{Tr}[\gamma_5\not{k}'\gamma_\mu\not{p}'\gamma_5\not{p}'] \\
&+ \mathrm{Tr}[\gamma_5\not{k}'\gamma_\mu\not{k}'\gamma_5\not{p}'] - \mathrm{Tr}[\gamma_5\not{k}'\gamma_\mu\mathrm{M}_{\bar{s}}\gamma_5\mathrm{M}_{\mathrm{u}}] + \mathrm{Tr}[\gamma_5\mathrm{M}_{\bar{s}}\gamma_\mu\not{p}'\gamma_5\mathrm{M}_{\mathrm{u}}] \\
&- \mathrm{Tr}[\gamma_5\mathrm{M}_{\bar{s}}\gamma_\mu\not{k}'\gamma_5\mathrm{M}_{\mathrm{u}}] + \mathrm{Tr}[\gamma_5\mathrm{M}_{\bar{s}}\gamma_\mu\mathrm{M}_{\bar{s}}\gamma_5\not{p}'] \\
&= -4[(p^2-(M_u^2+M_{\bar{s}}^2-(M_{\bar{s}}-M_u)^2))(p_\mu-k_\mu-k'_\mu)+k_\mu k'.p-k.k'p_\mu \\
&+ k.pk'_\mu + M_{\bar{s}}^2 p_\mu - M_u M_{\bar{s}} k_\mu - M_u M_{\bar{s}} k'_\mu] \\
&= -4[(p^2-M_u^2)(p_\mu-k_\mu-k'_\mu) - M_{\bar{s}}^2(p_\mu-k_\mu-k'_\mu) + (M_{\bar{s}}-M_u)^2(p_\mu-k_\mu-k'_\mu) \\
&+ k_\mu k'.p - k.k'p_\mu + k.pk'_\mu + M_{\bar{s}}^2 p_\mu - M_u M_{\bar{s}} k_\mu - M_u M_{\bar{s}} k'_\mu] \\
&= -4[(p^2-M_u^2)(p_\mu-k_\mu-k'_\mu) + M_{\bar{s}}^2(k_\mu+k'_\mu) + (M_{\bar{s}}-M_u)^2(p_\mu-k_\mu-k'_\mu) \\
&+ k_\mu k'.p - k.k'p_\mu + k.pk'_\mu - M_u M_{\bar{s}} k_\mu - M_u M_{\bar{s}} k'_\mu] \\
&= -4[(p^2-M_u^2)\mathcal{N}_2^{2a} + \mathcal{N}_2^{2b}, \qquad (A.15.7)
\end{aligned}$$

where $\mathcal{N}_2^{2a}$ and $\mathcal{N}_2^{2b}$ can be written as

$$\mathcal{N}_2^{2a} = (p_\mu - k_\mu - k'_\mu) \qquad (A.15.8)$$

$$\begin{aligned}
\mathcal{N}_2^{2b} = & (M_{\bar{s}}^2(k_\mu+k'_\mu) + (M_{\bar{s}}-M_u)^2(p_\mu-k_\mu-k'_\mu) \\
& + k_\mu k'.p - k.k'p_\mu + k.pk'_\mu - M_u M_{\bar{s}}(k_\mu+k'_\mu)). \qquad (A.15.9)
\end{aligned}$$

A.15.2 Evaluation of the propagators

propagator for $\mathcal{N}_2^{2a}$

After we cancel $(p^2-M_u^2)$ term, using Feynman paramaterization we easily evaluate the propagators. By setting $A=[(p-k)^2-M_{\bar{s}}^2+i\epsilon]$ and $B=[(p-k')^2-M_{\bar{s}}^2+i\epsilon]$, we find

$$\frac{1}{[(p-k)^2-M_{\bar{s}}^2+i\epsilon][(p-k')^2-M_{\bar{s}}^2+i\epsilon][p^2-M_u^2+i\epsilon]} \rightarrow \int_0^1 dx \frac{1}{[Ax+(1-x)B]^2}, \qquad (A.15.10)$$

and the denominator ($\mathcal{D}_2$) can be calculated as

$$\begin{aligned}
\mathcal{D}_2 &= [xA + (1-x)B]^2 \\
&= [x[(p-k)^2 - M_{\bar{s}}^2 + i\epsilon] + (1-x)[(p-k')^2 - M_{\bar{s}}^2 + i\epsilon]]^2 \\
&= [x[p^2 + k^2 - 2p.k - M_{\bar{s}}^2 + i\epsilon] + (1-x)[p^2 + k'^2 - 2p.k' - M_{\bar{s}}^2 + i\epsilon]]^2 \\
&= [xp^2 + xk^2 - 2xp.k - xM_{\bar{s}}^2 + ix\epsilon + p^2 + k'^2 - 2p.k' - M_{\bar{s}}^2 + i\epsilon - xp^2 \\
&- xk'^2 + 2xp.k' + xM_{\bar{s}}^2 - ix\epsilon]^2 \\
&= [p^2 - 2p.(xk - xk' + k') + k'^2(1-x) - M_{\bar{s}}^2 + xk^2 + i\epsilon]^2 \\
&= [(p - (xk - xk' + k'))^2 - (xk - xk' + k')^2 + k'^2(1-x) - M_{\bar{s}}^2 + xk^2 + i\epsilon]^2,
\end{aligned} \tag{A.15.11}$$

Shifting the $p \to p + (xk - xk' + k')$, the $\mathcal{D}_2$ can be written as

$$\begin{aligned}
\mathcal{D}_2 &= [p^2 - (xk - xk' + k')^2 + k'^2(1-x) - M_{\bar{s}}^2 + xk^2 + i\epsilon]^2 \\
&= [p^2 - (k'^2 + 2xk.k' - 2k'^2x + k^2x^2 - 2k.k'x^2 + k'^2x^2) + k'^2(1-x) - M_{\bar{s}}^2 + xk^2 + i\epsilon]^2 \\
&= [p^2 - 2xk.k' + 2k'^2x - k^2x^2 + 2k.k'x^2 - k'^2x^2 - xk'^2 - M_{\bar{s}}^2 + xk^2 + i\epsilon]^2 \\
&= [p^2 - 2x(k^2 - \frac{q^2}{2} + 2k'^2x - k^2x^2 + 2(k^2 - \frac{q^2}{2}x^2 - k'^2x^2 - xk'^2 - M_{\bar{s}}^2 + xk^2 + i\epsilon]^2 \\
&= [p^2 + q^2(x - x^2) - M_{\bar{s}}^2 + i\epsilon]^2,
\end{aligned} \tag{A.15.12}$$

where $k'^2 = k^2$ and $k.k' = (k^2 - \frac{q^2}{2})$. The propagator for the numerator $\mathcal{N}_2^2$, after performing the Feynman paramaterization, it becomes

$$\frac{1}{[(p-k)^2 - M_{\bar{s}}^2 + i\epsilon][(p-k')^2 - M_{\bar{s}}^2 + i\epsilon]} \to \int_0^1 dx \frac{1}{[p^2 + q^2(x - x^2) - M_{\bar{s}}^2 + i\epsilon]^2}. \tag{A.15.13}$$

Recall $\mathcal{N}_2^{2a}$ and performing the shift $p \to p + (xk - xk' + k') = p + xk - xk' + k' = p + x(k - k') + k' = p - xq^2 + k'$ to the $\mathcal{N}_1$ numerator, it then gives

$$\begin{aligned}
\mathcal{N}_2^{2a} &= (p_\mu - k_\mu - k'_\mu) = (p_\mu + xk_\mu - xk'_\mu + k'_\mu - k_\mu - k'_\mu) \\
&= (p_\mu + x(k_\mu - k'_\mu) - k_\mu) \\
&= (p_\mu - xq_\mu - k_\mu) = (-xq_\mu - k_\mu) = (-\frac{1}{2}q_\mu - k_\mu) \\
&= -\frac{1}{2}(k'_\mu - k_\mu) + k_\mu = -\frac{1}{2}(k'_\mu + k_\mu),
\end{aligned} \tag{A.15.14}$$

where we have ignored the terms in p and the factor one half are taken from the symmetry in the denominators under $x \to (1-x)$.

Propagators for $\mathcal{N}_2^{2b}$

Now the three propagators for numerator, $\mathcal{N}_2$ are evaluated using Feynman paramaterization, that is

$$\to \frac{1}{((p-k)^2 - M_{\bar{s}}^2)\,[(p-k')^2 - M_{\bar{s}}^2]\,[p^2 - M_u^2]}$$

$$\rightarrow \frac{1}{ABC} = 2\int_0^1 dx \int_0^{1-x} dz \frac{1}{[A+(B-A)x+(C-A)z]^3}, \tag{A.15.15}$$

By setting $A = p^2 - M_u^2 + i\epsilon$, $B = (p-k)^2 - M_{\bar{s}}^2 + i\epsilon$ and $C = (p-k')^2 - M_{\bar{s}}^2 + i\epsilon$. Then plugging A, B and C into equation above, three propagators for $\mathcal{N}_2^{2b}$ becomes

$$\begin{aligned}
\mathcal{D}_3 &= [A+(B-A)x+(C-A)z]^3 \\
&= [p^2 - M_u^2 + i\epsilon + ((p-k)^2 - M_{\bar{s}}^2 + i\epsilon - (p^2 - M_u^2 + i\epsilon))x + ((p-k')^2 \\
&- M_{\bar{s}}^2 + i\epsilon - (p^2 - M_u^2 + i\epsilon))z]^3 \\
&= [p^2 - M_u^2 + i\epsilon + (p^2 + k^2 - 2p.k - M_{\bar{s}}^2 + i\epsilon - p^2 + M_u^2 - i\epsilon)x + (p^2 + k'^2 \\
&- 2p.k' - M_{\bar{s}}^2 + i\epsilon - p^2 + M_u^2 - i\epsilon)z]^3 \\
&= [p^2 - M_u^2 + i\epsilon + (k^2 - 2p.k - M_{\bar{s}}^2 + M_u^2)x + (k'^2 - 2p.k' + M_u^2 - M_{\bar{s}}^2)z]^3 \\
&= [p^2 - M_u^2 + xk^2 - 2xp.k - xM_{\bar{s}}^2 + xM_u^2 + zk'^2 - 2zp.k' + zM_u^2 - zM_{\bar{s}}^2 + i\epsilon]^3 \\
&= [p^2 - 2p.(xk+zk') - M_u^2 + xk^2 + zk'^2 - xM_{\bar{s}}^2 + xM_u^2 + zM_u^2 - zM_{\bar{s}}^2 + i\epsilon]^3 \\
&= [(p-(xk+zk'))^2 - (xk+zk')^2 - M_u^2 + xk^2 + zk'^2 - xM_{\bar{s}}^2 + xM_u^2 - zM_2^2, \quad + zM_u^2 + i\epsilon]^3,
\end{aligned} \tag{A.15.16}$$

Applying shift to the results by using p $\rightarrow p + [xk + zk']$, it gives

$$\begin{aligned}
\mathcal{D}_3 &= [p^2 - (xk+zk')^2 - M_u^2 + xk^2 + zk'^2 - xM_{\bar{s}}^2 + xM_u^2 - zM_{\bar{s}}^2 + zM_u^2 + i\epsilon]^3 \\
&= [p^2 - (x^2k^2 + z^2k'^2 + 2xzk.k') - M_u^2 + xk^2 + zk'^2 - xM_{\bar{s}}^2 + xM_u^2 - zM_{\bar{s}}^2 \\
&+ zM_u^2 + i\epsilon]^3 \\
&= [p^2 - x^2k^2 + xk^2 - z^2k'^2 + zk'^2 - 2xzk.q - 2xzk.k - M_u^2 - xM_{\bar{s}}^2 + xM_u^2 - zM_{\bar{s}}^2 \\
&+ zM_u^2 + i\epsilon]^3 \\
&= [p^2 - x^2k^2 + xk^2 - z^2k'^2 + zk'^2 + xzq^2 - 2xzk^2 - M_u^2 - xM_{\bar{s}}^2 + xM_u^2 - zM_{\bar{s}}^2 \\
&+ zM_u^2 + i\epsilon]^3 \\
&= [p^2 - k^2(x^2-x) - k^2(z^2-z) - 2xzk^2 + xzq^2 - M_u^2 - xM_{\bar{s}}^2 + xM_u^2 - zM_{\bar{s}}^2 \\
&+ zM_u^2 + i\epsilon]^3 \\
&= [p^2 - k^2[(x^2-x) + (z^2-z) + 2xz] + xzq^2 - M_u^2 - xM_{\bar{s}}^2 + xM_u^2 - zM_{\bar{s}}^2 \\
&+ zM_u^2 + i\epsilon]^3 \\
&= [p^2 - k^2[x^2 - x + z^2 - z + 2xz] + xzq^2 - M_u^2 - xM_{\bar{s}}^2 + xM_u^2 - zM_{\bar{s}}^2 \\
&+ zM_u^2 + i\epsilon]^3 \\
&= [p^2 - k^2[x^2 + z^2 + 2xz - x - z] + xzq^2 - M_{\bar{s}}^2 - xM_u^2 + xM_{\bar{s}}^2 - zM_u^2 \\
&+ zM_{\bar{s}}^2 + i\epsilon]^3 \\
&= [p^2 - k^2[(x+z)^2 - (x+z)] + xzq^2 - M_u^2 - xM_{\bar{s}}^2 + xM_u^2 - zM_{\bar{s}}^2 \\
&+ zM_u^2 + i\epsilon]^3 \\
&= [p^2 - k^2[(x+z)^2 - (x+z)] + xzq^2 - M_u^2(1-x-z) \\
&- M_{\bar{s}}^2(x+z) + i\epsilon]^3,
\end{aligned} \tag{A.15.17}$$

where $q.k = -\frac{q^2}{2}$ or $2q.k = -q^2$, $k^2 = k'^2$ and $q = k' - k$.

The propagator for $\mathcal{N}_2^{2b}$ after applying the Feynman parameterization becomes

$$\begin{aligned}
&\rightarrow \frac{1}{((p+k')^2-M_u^2)\,[(p+k)^2-M_u^2]\,[p^2-M_{\bar{s}}^2]} \\
&\rightarrow 2\int_0^1 dx \int_0^{1-x} dz \\
&\times \frac{1}{[p^2-k^2[(x+z)^2-(x+z)]+xzq^2-M_u^2(1-x-z)-M_{\bar{s}}^2(x+z)+i\epsilon]^3},
\end{aligned} \tag{A.15.18}$$

Now recall $\mathcal{N}_2^{2b}$ numerator and applying shift $p \rightarrow p+(xk+zk')$ to $\mathcal{N}_2^{2b}$ numerator, it gives

$$\begin{aligned}
\mathcal{N}_2^{2b} &= (M_{\bar{s}}^2(k_\mu+k'_\mu)+(M_{\bar{s}}-M_u)^2(p_\mu-k_\mu-k'_\mu)+k_\mu k'.p-k.k'p_\mu \\
&\quad + k.pk'_\mu - M_uM_{\bar{s}}(k_\mu+k'_\mu)) \\
&= p.kk'_\mu + p.k'k_\mu - k'.kp_\mu + M_{\bar{s}}^2(k'_\mu+k_\mu)+(M_{\bar{s}}-M_u)^2(p_\mu-k'_\mu-k_\mu) \\
&\quad - M_uM_{\bar{s}}(k'_\mu+k_\mu) \\
&= (p_\mu+xk+zk').kk'_\mu + (p_\mu+xk+zk').k'k_\mu - k'.k(p_\mu+xk_\mu+zk'_\mu)+M_{\bar{s}}^2(k'_\mu+k_\mu) \\
&\quad + (M_{\bar{s}}-M_u)^2((p_\mu+xk_\mu+zk'_\mu)-k'_\mu-k_\mu) - M_uM_{\bar{s}}(k'_\mu+k_\mu),
\end{aligned} \tag{A.15.19}$$

Dropping p_μ term which gives zero in the integral. it then gives

$$\begin{aligned}
\mathcal{N}_2^{2b} &= xk.kk'_\mu + zk'.kk'_\mu + xk.k'k_\mu + zk'.k'k_\mu - xk'.kk_\mu - zk'.kk'_\mu + M_{\bar{s}}^2(k'_\mu+k_\mu) \\
&\quad + (M_{\bar{s}}-M_u)^2(x-1)k_\mu + (M_{\bar{s}}-M_u)^2(z-1)k'_\mu - M_uM_{\bar{s}}(k'_\mu+k_\mu) \\
&= xk^2k'_\mu + zk'^2k_\mu + M_{\bar{s}}^2(k'_\mu+k_\mu)+(M_{\bar{s}}-M_u)^2(x-1)k_\mu \\
&\quad + (M_{\bar{s}}-M_u)^2(z-1)k'_\mu - M_uM_{\bar{s}}(k'_\mu+k_\mu),
\end{aligned} \tag{A.15.20}$$

where the odd terms in p is ignored. Using $k'_\mu = \frac{1}{2}(k'_\mu+k_\mu)+\frac{1}{2}(k'_\mu-k_\mu)$ and $k_\mu = \frac{1}{2}(k'_\mu+k_\mu)-\frac{1}{2}(k'_\mu-k_\mu)$. By putting these relations into Eq. (A.15.20), it gives

$$\begin{aligned}
\mathcal{N}_2 &= xk^2[\frac{1}{2}(k'_\mu+k_\mu)+\frac{1}{2}(k'_\mu-k_\mu)]+zk'^2[\frac{1}{2}(k'_\mu+k_\mu)-\frac{1}{2}(k'_\mu-k_\mu)] \\
&\quad + (M_{\bar{s}}-M_u)^2[(x-1)[\frac{1}{2}(k'_\mu+k_\mu)-\frac{1}{2}(k'_\mu-k_\mu)]+(z-1)[\frac{1}{2}(k'_\mu+k_\mu)+\frac{1}{2}(k'_\mu-k_\mu)]] \\
&\quad + M_{\bar{s}}^2(k'_\mu+k_\mu) - M_uM_{\bar{s}}(k'_\mu+k_\mu) \\
&= \frac{xk^2}{2}(k'_\mu+k_\mu)+\frac{xk^2}{2}(k'_\mu-k_\mu)]+[\frac{zk'^2}{2}(k'_\mu+k_\mu)-\frac{zk'^2}{2}(k'_\mu-k_\mu)] \\
&\quad + (M_{\bar{s}}-M_u)^2[(x-1)[\frac{1}{2}(k'_\mu+k_\mu)-\frac{1}{2}(k'_\mu-k_\mu)]+(z-1)[\frac{1}{2}(k'_\mu+k_\mu)+\frac{1}{2}(k'_\mu-k_\mu)]] \\
&\quad + M_{\bar{s}}^2(k'_\mu+k_\mu) - M_uM_{\bar{s}}(k'_\mu+k_\mu) \\
&= \frac{xk^2}{2}(k'_\mu+k_\mu)+[\frac{zk'^2}{2}(k'_\mu+k_\mu)+\frac{xk^2}{2}(k'_\mu-k_\mu)]-\frac{zk'^2}{2}(k'_\mu-k_\mu)] \\
&\quad + (M_{\bar{s}}-M_u)^2[\frac{x}{2}(k'_\mu+k_\mu)-\frac{1}{2}(k'_\mu+k_\mu)-\frac{x}{2}(k'_\mu-k_\mu)+\frac{1}{2}(k'_\mu-k_\mu)+\frac{z}{2}(k'_\mu+k_\mu)
\end{aligned}$$

$$
\begin{aligned}
&-\frac{1}{2}(k'_\mu+k_\mu)+\frac{z}{2}(k'_\mu-k_\mu)-\frac{1}{2}(k'_\mu-k_\mu)]\\
&+M^2_{\bar{s}}(k'_\mu+k_\mu)-M_uM_{\bar{s}}(k'_\mu+k_\mu)\\
&=\frac{xk^2+zk'^2}{2}(k'^\mu+k^\mu)+\frac{xk^2-zk'^2}{2}(k'^\mu-k^\mu)\\
&+(M_{\bar{s}}-M_u)^2[-(k'_\mu+k_\mu)+\frac{x}{2}(k'_\mu+k_\mu)+\frac{z}{2}(k'_\mu+k_\mu)-\frac{x}{2}(k'_\mu-k_\mu)+\frac{z}{2}(k'_\mu-k_\mu)]\\
&+M^2_{\bar{s}}(k'_\mu+k_\mu)-M_uM_{\bar{s}}(k'_\mu+k_\mu)\\
&=\frac{xk^2+zk'^2}{2}(k'^\mu+k^\mu)+\frac{xk^2-zk'^2}{2}(k'^\mu-k^\mu)\\
&+(M_{\bar{s}}-M_u)^2[(-1+\frac{x}{2}+\frac{z}{2})(k'_\mu+k_\mu)-(\frac{x}{2}-\frac{z}{2})(k'_\mu-k_\mu)]\\
&+M^2_{\bar{s}}(k'_\mu+k_\mu)-M_uM_{\bar{s}}(k'_\mu+k_\mu), \qquad \text{(A.15.21)}
\end{aligned}
$$

The last term is vanished because after variable transformation $x\to\frac{1}{2}(x+z)$ and $z\to\frac{1}{2}(x-z)$ which then evaluates to zero because the numerator is odd in z. Another reason is when we evaluate for z or x separately in integral, it will gives the same result, therefore the terms $x-z$ in integral equal to zero. Therefore the final results for the numerator, $\mathcal{N}_2^{2b}$ becomes

$$
\begin{aligned}
\mathcal{N}_2^{2b}&=\frac{1}{2}k^2(x+z)(k'^\mu+k^\mu)+(M_{\bar{s}}-M_u)^2[(-1+\frac{x}{2}+\frac{z}{2})(k'_\mu+k_\mu)]+M^2_{\bar{s}}(k'_\mu+k_\mu)\\
&\quad-M_uM_{\bar{s}}(k'_\mu+k_\mu)\\
&=[\frac{1}{2}k^2(x+z)+(M_{\bar{s}}-M_u)^2(-1+\frac{x}{2}+\frac{z}{2})+M^2_{\bar{s}}-M_uM_{\bar{s}}](k'_\mu+k_\mu)\\
&=[\frac{1}{2}k^2(x+z)-M^2_{\bar{s}}-M^2_u+2M_{\bar{s}}M_u+\frac{1}{2}(M_{\bar{s}}-M_u)^2(x+z)+M^2_{\bar{s}}-M_uM_{\bar{s}}](k'_\mu+k_\mu)\\
&=[\frac{1}{2}k^2(x+z)+\frac{1}{2}(M_{\bar{s}}-M_u)^2(x+z)-M^2_u+M_uM_{\bar{s}}](k'_\mu+k_\mu). \qquad \text{(A.15.22)}
\end{aligned}
$$

By putting the result of the numerator in Eqs. (A.15.14), (A.15.22) and the denominator in Eqs. (A.15.12), (A.15.17) the kaon form factor can be written as

$$
\begin{aligned}
\Lambda^{\mu}_2(k,k')&=2iN_Cg^2_{Kq\bar{q}}\int\frac{d^4p}{(2\pi)^4}\frac{\mathrm{Tr}\left[\gamma_5(\not{p}-\not{k}'+\mathrm{M}_{\bar{\mathrm{s}}})\gamma_\mu(\not{p}-\not{k}'+\mathrm{M}_{\bar{\mathrm{s}}})\gamma_5(\not{p}+\mathrm{M}_{\mathrm{u}})\right]}{[(p-k)^2-M^2_{\bar{s}}+i\epsilon]\,[(p-k')^2-M^2_{\bar{s}}+i\epsilon]\,[p^2-M^2_u+i\epsilon]}\\
&=-8iN_Cg^2_{Kq\bar{q}}\int\frac{d^4p}{(2\pi)^4}\frac{(p^2-M^2_u)\mathcal{N}_2^2}{[(p-k)^2-M^2_{\bar{s}}+i\epsilon]\,[(p-k')^2-M^2_{\bar{s}}+i\epsilon]\,[p^2-M^2_u+i\epsilon]}\\
&\quad-8iN_Cg^2_{Kq\bar{q}}\int\frac{d^4p}{(2\pi)^4}\frac{\mathcal{N}_2^2}{[(p-k)^2-M^2_{\bar{s}}+i\epsilon]\,[(p-k')^2-M^2_{\bar{s}}+i\epsilon]\,[p^2-M^2_u+i\epsilon]},
\end{aligned}
\qquad \text{(A.15.23)}
$$

The $(p^2-M^2_u)$ in the first term are canceled. Therefore it becomes

$$
\Lambda^{\mu}_{\bar{s}}(-k,-k')=-8iN_Cg^2_{Kq\bar{q}}\int\frac{d^4p}{(2\pi)^4}\frac{\mathcal{N}_2^{2a}}{[(p-k)^2-M^2_{\bar{s}}+i\epsilon]\,[(p-k')^2-M^2_{\bar{s}}+i\epsilon]}
$$

$$
\begin{aligned}
&- 8iN_C g^2_{Kq\bar{q}} \int \frac{d^4p}{(2\pi)^4} \frac{\mathcal{N}_2^{2b}}{[(p-k)^2 - M_{\bar{s}}^2 + i\epsilon]\,[(p-k')^2 - M_{\bar{s}}^2 + i\epsilon]\,[p^2 - M_u^2 + i\epsilon]} \\
&= -8iN_C g^2_{Kq\bar{q}} \int \frac{d^4p}{(2\pi)^4} \int_0^1 dx \frac{-\frac{1}{2}(k'^\mu + k^\mu)}{[p^2 + q^2(x-x^2) - M_{\bar{s}}^2 + i\epsilon]^2} \\
&- 8iN_C g^2_{Kq\bar{q}} \int \frac{d^4p}{(2\pi)^4} 2 \int_0^1 dx \int_0^{1-x} dz \\
&\times \frac{\mathcal{N}_2^{2b}}{[p^2 - k^2[(x+z)^2 - (x+z)] + xzq^2 - M_u^2(1-x-z) - M_{\bar{s}}^2(x+z) + i\epsilon]^3} \\
&= 4iN_C g^2_{Kq\bar{q}} \int \frac{d^4p}{(2\pi)^4} \int_0^1 dx \frac{(k'^\mu + k^\mu)}{[p^2 + q^2(x-x^2) - M_{\bar{s}}^2 + i\epsilon]^2} \\
&- 16iN_C g^2_{Kq\bar{q}} \int \frac{d^4p}{(2\pi)^4} \int_0^1 dx \int_0^{1-x} dz \\
&\times \frac{[\frac{1}{2}k^2(x+z) + \frac{1}{2}(M_{\bar{s}} - M_u)^2(x+z) - M_u^2 + M_u M_{\bar{s}}](k'_\mu + k_\mu)}{[p^2 - k^2[(x+z)^2 - (x+z)] + xzq^2 - M_u^2(1-x-z) - M_{\bar{s}}^2(x+z) + i\epsilon]^3} \\
&= 4iN_C g^2_{Kq\bar{q}} \int \frac{d^4p}{(2\pi)^4} \int_0^1 dx \frac{(k'^\mu + k^\mu)}{[p^2 + q^2(x-x^2) - M_{\bar{s}}^2 + i\epsilon]^2} \\
&- 8iN_C g^2_{Kq\bar{q}} \int \frac{d^4p}{(2\pi)^4} \int_0^1 dx \int_0^{1-x} dz \\
&\times \frac{[k^2(x+z) + (M_{\bar{s}} - M_1)^2(x+z) - 2M_u^2 + 2M_u M_{\bar{s}}](k'_\mu + k_\mu)}{[p^2 - k^2[(x+z)^2 - (x+z)] + xzq^2 - M_u^2(1-x-z) - M_{\bar{s}}^2(x+z) + i\epsilon]^3}.
\end{aligned}
\tag{A.15.24}
$$

Generally the definition of the electromagnetic current is expressed in terms of the local matrix elements of the electromagnetic quark currents which is symbolized by $\mathcal{J}^\mu$

$$
\mathcal{J}_K^\mu(k,k') = \langle K(k) \mid \mathcal{J}^\mu \mid K(k') \rangle = (k^\mu + k'^\mu)\, F_K(Q^2), \tag{A.15.25}
$$

where K is the kaon field operator and virtual momentum transfer $\mathrm{Q}^2 = -\mathrm{q}^2$ and kaon electromagnetic current $\mathcal{J}_{\mathrm{K}}^\mu(k,k')$ can be written as

$$
\mathcal{J}_K^{\mu,i,j}(k,k') = e_u \Lambda_u^\mu(k,k') + e_{\bar{s}} \Lambda_{\bar{s}}^\mu(-k,-k'), \tag{A.15.26}
$$

Using the definition of the electromagnetic current in Eq. (A.15.25) and taking the value of $e_u = \dfrac{2}{3}$ and $e_{\mathrm{s}} = -\dfrac{1}{3}$ and putting the $\Lambda_u^\mu(k,k')$ and $\Lambda_{\bar{s}}^\mu(-k,-k')$ into Eq.(A.15.26), we obtain the form factor of the kaon, which is expressed as

$$
\begin{aligned}
F_{K^+}(q^2) &= e_u F_{K^+}^u(q^2) + e_{\bar{s}} F_{K^+}^{\bar{s}}(q^2) \\
&= -4iN_C g^2_{Kq\bar{q}} e_u \int \frac{d^4p}{(2\pi)^4} \int_0^1 dx \frac{1}{[p^2 + q^2(x-x^2) - M_u^2 + i\epsilon]^2} \\
&+ 8iN_C g^2_{Kq\bar{q}} e_u \int \frac{d^4p}{(2\pi)^4} \int_0^1 dx \int_0^{1-x} dz \\
&\times \frac{[k^2(x+z) + (M_{\bar{s}} - M_u)^2(x+z) - 2M_{\bar{s}}^2 + 2M_u M_{\bar{s}}]}{[p^2 - k^2[(x+z)^2 - (x+z)] + xzq^2 - M_{\bar{s}}^2(1-x-z) - M_u^2(x+z) + i\epsilon]^3}
\end{aligned}
$$

$$
\begin{aligned}
&+4iN_C g^2_{Kq\bar{q}} e_{\bar{s}} \int \frac{d^4p}{(2\pi)^4} \int_0^1 dx \frac{1}{[p^2+q^2(x-x^2)-M^2_{\bar{s}}+i\epsilon]^2} \\
&-8iN_C g^2_{Kq\bar{q}} e_{\bar{s}} \int \frac{d^4p}{(2\pi)^4} \int_0^1 dx \int_0^{1-x} dz \\
&\times \frac{[k^2(x+z)+(M_{\bar{s}}-M_u)^2(x+z)-2M^2_u+2M_uM_{\bar{s}}]}{[p^2-k^2[(x+z)^2-(x+z)]+xzq^2-M^2_u(1-x-z)-M^2_{\bar{s}}(x+z)+i\epsilon]^3},
\end{aligned}
\tag{A.15.27}
$$

Performing a Wick rotation and introducing the 4-D polar, it then gives

$$
\begin{aligned}
F_{K^+}(q^2) =& \frac{N_C g^2_{Kq\bar{q}} e_u}{4\pi^2} \int p^2_E dp^2_E \int_0^1 dx \frac{1}{[p^2_E-q^2(x-x^2)+M^2_u-i\epsilon]^2} \\
&+\frac{N_C g^2_{Kq\bar{q}} e_u}{2\pi^2} \int p^2_E dp^2_E \int_0^1 dx \int_0^{1-x} dz \\
&\times \frac{[k^2(x+z)+(M_{\bar{s}}-M_u)^2(x+z)-2M^2_{\bar{s}}+2M_uM_{\bar{s}}]}{[p^2_E+k^2[(x+z)^2-(x+z)]-xzq^2+M^2_{\bar{s}}(1-x-z)+M^2_u(x+z)-i\epsilon]^3} \\
&-\frac{N_C g^2_{Kq\bar{q}} e_{\bar{s}}}{4\pi^2} \int p^2_E dp^2_E \int_0^1 dx \frac{1}{[p^2_E-q^2(x-x^2)+M^2_{\bar{s}}-i\epsilon]^2} \\
&-\frac{N_C g^2_{Kq\bar{q}} e_{\bar{s}}}{2\pi^2} \int p^2_E dp^2_E \int_0^1 dx \int_0^{1-x} dz \\
&\times \frac{[k^2(x+z)+(M_{\bar{s}}-M_u)^2(x+z)-2M^2_u+2M_uM_{\bar{s}}]}{[p^2_E+k^2[(x+z)^2-(x+z)]-xzq^2+M^2_u(1-x-z)+M^2_{\bar{s}}(x+z)-i\epsilon]^3},
\end{aligned}
\tag{A.15.28}
$$

Performing the proper-time regularization into Eq. (A.15.28), it becomes

$$
\begin{aligned}
F_{K^+}(q^2) =& \frac{N_C g^2_{Kq\bar{q}} e_u}{4\pi^2} \int_0^1 dx \int_{\frac{1}{(\Lambda_{\rm UV})^2}}^{\frac{1}{(\Lambda_{\rm IR})^2}} \frac{d\tau}{\tau} e^{-\tau(q^2(x^2-x)+M^2_u)} \\
&+\frac{N_C g^2_{Kq\bar{q}} e_u}{4\pi^2} \int_0^1 dx \int_0^{1-x} dz \int_{\frac{1}{(\Lambda_{\rm UV})^2}}^{\frac{1}{(\Lambda_{\rm IR})^2}} d\tau e^{-\tau(k^2[(x+z)^2-(x+z)]-xzq^2+M^2_{\bar{s}}(1-x-z)+M^2_u(x+z))} \\
&\times [k^2(x+z)+(M_u-M_{\bar{s}})^2(x+z)-2M^2_{\bar{s}}+2M_{\bar{s}}M_u] \\
&-\frac{N_C g^2_{Kq\bar{q}} e_{\bar{s}}}{4\pi^2} \int_0^1 dx \int_{\frac{1}{(\Lambda_{\rm UV})^2}}^{\frac{1}{(\Lambda_{\rm IR})^2}} \frac{d\tau}{\tau} e^{-\tau(q^2(x^2-x)+M^2_{\bar{s}})} \\
&-\frac{N_C g^2_{Kq\bar{q}} e_{\bar{s}}}{4\pi^2} \int_0^1 dx \int_0^{1-x} dz \int_{\frac{1}{(\Lambda_{\rm UV})^2}}^{\frac{1}{(\Lambda_{\rm IR})^2}} d\tau e^{-\tau(k^2[(x+z)^2-(x+z)]-xzq^2+M^2_u(1-x-z)+M^2_{\bar{s}}(x+z))} \\
&\times [k^2(x+z)+(M_{\bar{s}}-M_u)^2(x+z)-2M^2_u+2M_uM_{\bar{s}}].
\end{aligned}
\tag{A.15.29}
$$

The final result of the kaon form factor can be written as

$$
F_{K^+}(q^2) = e_u \frac{N_C g^2_{Kq\bar{q}}}{4\pi^2} \int_0^1 dx \int_{\frac{1}{(\Lambda_{\rm UV})^2}}^{\frac{1}{(\Lambda_{\rm IR})^2}} \frac{d\tau}{\tau} e^{-\tau(q^2(x^2-x)+M^2_u)}
$$

$$
\begin{aligned}
&+ e_u \frac{N_C g_{Kq\bar{q}}^2}{4\pi^2} \int_0^1 dx \int_0^{1-x} dz \int_{\frac{1}{(\Lambda_{\rm UV})^2}}^{\frac{1}{(\Lambda_{\rm IR})^2}} d\tau e^{-\tau(k^2[(x+z)^2-(x+z)]-xzq^2+M_{\bar{s}}^2(1-x-z)+M_u^2(x+z))} \\
&\times [k^2(x+z)+(M_u-M_{\bar{s}})^2(x+z)-2M_{\bar{s}}^2+2M_{\bar{s}}M_u] \\
&+ e_{\bar{s}} \frac{N_C g_{Kq\bar{q}}^2}{4\pi^2} \int_0^1 dx \int_{\frac{1}{(\Lambda_{\rm UV})^2}}^{\frac{1}{(\Lambda_{\rm IR})^2}} \frac{d\tau}{\tau} e^{-\tau(q^2(x^2-x)+M_{\bar{s}}^2)} \\
&+ e_{\bar{s}} \frac{N_C g_{Kq\bar{q}}^2}{4\pi^2} \int_0^1 dx \int_0^{1-x} dz \int_{\frac{1}{(\Lambda_{\rm UV})^2}}^{\frac{1}{(\Lambda_{\rm IR})^2}} d\tau e^{-\tau(k^2[(x+z)^2-(x+z)]-xzq^2+M_u^2(1-x-z)+M_{\bar{s}}^2(x+z))} \\
&\times [k^2(x+z)+(M_{\bar{s}}-M_u)^2(x+z)-2M_u^2+2M_uM_{\bar{s}}]. \qquad \text{(A.15.30)}
\end{aligned}
$$

Note that to check normalization of the kaon form factor $F_{K^+}(Q^2)$ by setting $Q^2=0$, it will give $F_{K^+}(0)=1$. Similarly, the pion form factor can be written as

$$
\begin{aligned}
F_{\pi^+}(q^2) &= e_u \frac{N_C g_{\pi q\bar{q}}^2}{4\pi^2} \int_0^1 dx \int_{\frac{1}{(\Lambda_{\rm UV})^2}}^{\frac{1}{(\Lambda_{\rm IR})^2}} \frac{d\tau}{\tau} e^{-\tau(-Q^2(x^2-x)+M_u^2)} \\
&+ e_u \frac{N_C g_{\pi q\bar{q}}^2}{4\pi^2} \int_0^1 dx \int_0^{1-x} dz \int_{\frac{1}{(\Lambda_{\rm UV})^2}}^{\frac{1}{(\Lambda_{\rm IR})^2}} d\tau e^{-\tau(k^2[(x+z)^2-(x+z)]+xzQ^2+M_{\bar{d}}^2(1-x-z)+M_u^2(x+z))} \\
&\times [k^2(x+z)+(M_u-M_{\bar{d}})^2(x+z)-2M_{\bar{d}}^2+2M_{\bar{d}}M_u] \\
&+ e_{\bar{d}} \frac{N_C g_{\pi q\bar{q}}^2}{4\pi^2} \int_0^1 dx \int_{\frac{1}{(\Lambda_{\rm UV})^2}}^{\frac{1}{(\Lambda_{\rm IR})^2}} \frac{d\tau}{\tau} e^{-\tau(-Q^2(x^2-x)+M_{\bar{d}}^2)} \\
&+ e_{\bar{d}} \frac{N_C g_{\pi q\bar{q}}^2}{4\pi^2} \int_0^1 dx \int_0^{1-x} dz \int_{\frac{1}{(\Lambda_{\rm UV})^2}}^{\frac{1}{(\Lambda_{\rm IR})^2}} d\tau e^{-\tau(k^2[(x+z)^2-(x+z)]+xzQ^2+M_u^2(1-x-z)+M_{\bar{d}}^2(x+z))} \\
&\times [k^2(x+z)+(M_{\bar{d}}-M_u)^2(x+z)-2M_u^2+2M_uM_{\bar{d}}], \qquad \text{(A.15.31)}
\end{aligned}
$$

where $q^2=-Q^2$.

A.16 Derivation for the kaon PDFs

We derive the quark distribution of the kaon in Eq. (5.1.7) , that is

$$
q_K(x) = -2iN_C g_{Kqq}^2 \frac{\partial}{\partial p^2} \int \frac{d^4q}{(2\pi)^4} \delta\left(x - \frac{q_-}{k_-}\right) Tr\left[\gamma_5 S_1(q) \gamma_5 S_2(q-k)\right], \qquad \text{(A.16.1)}
$$

where N_C denotes color numbers, $g_{\pi qq}$ is the pion quark-anti-quark coupling constant, and $S(q)$ is the quark propagator which can be defined as

$$
\begin{aligned}
S_1(q) &= \frac{\not{q} + M_1}{[q^2 - M_1^2 + i\epsilon]} \qquad \text{(A.16.2)} \\
S_2(q-k) &= \frac{\not{q} - \not{k} + M_2}{[(q-k)^2 - M_2^2 + i\epsilon]}, \qquad \text{(A.16.3)}
\end{aligned}
$$

where q is four momentum transfer, k is pion four momentum and M_1 and M_2 stand for the dynamical quark mass of kaon constituent.

Then plugging the propagators in Eq. (A.16.2) into Eq. (A.16.1), it gives

$$q_K(x) = -2iN_C g^2_{Kqq}\frac{\partial}{\partial p^2}\int \frac{d^4q}{(2\pi)^4}\delta\left(x-\frac{q_-}{k_-}\right) \times Tr\left[\gamma_5\left(\frac{\not{q}+M_1}{[q^2-M_1^2+i\epsilon]}\gamma_5\frac{\not{q}-\not{k}+M_2}{[(q-k)^2-M_2^2+i\epsilon]}\right)\right]. \quad (1.16.4)$$

We then evaluate the quark distribution of the kaon in Eq. (1.16.4) via moments, it gives

$$\mathcal{A}_n = \int_0^1 dx x^{n-1} q_K(x), \quad (1.16.5)$$

where n denotes a moment of the quark distribution of the kaon. It starts from n =1, 2, ... Plugging the quark distribution of the kaon in Eq.(1.16.4) into moments equation in Eq.(1.16.5). it has the form

$$\begin{aligned} A_n &= -2iN_C g^2_{Kqq}\frac{\partial}{\partial k^2}\int\frac{d^4q}{(2\pi)^4}\int_0^1 dx x^{n-1}\delta(x-\frac{q_-}{k_-})Tr_D[\gamma_5 S_1(q)\gamma_5 S_2(q-k)] \\ &= -2iN_C g^2_{Kqq}\frac{\partial}{\partial k^2}\left[\int\frac{d^4q}{(2\pi)^4}\int_0^1 dx\left(\frac{q_-}{k_-}\right)^{n-1}\delta(x-\frac{q_-}{k_-})Tr_D[\gamma_5 S_1(q)\gamma_5 S_2(q-k)]\right] \\ &= -2iN_C g^2_{Kqq}\frac{\partial}{\partial k^2}\left[\int\frac{d^4q}{(2\pi)^4}\int_0^1 dx\left(\frac{q_-}{k_-}\right)^{n-1} Tr_D[\gamma_5 S_1(q)\gamma_5 S_2(q-k)]\right], \quad (1.16.6) \end{aligned}$$

with the quark dressed propagators are defined in Eq. (A.16.2) and plugging the propagators into Eq.(1.16.6), then moments has the form

$$\begin{aligned} A_n \quad &= -2iN_C g^2_{Kqq}\frac{\partial}{\partial k^2}[\int\frac{d^4q}{(2\pi)^4}\int_0^1 dx\left(\frac{q_-}{k_-}\right)^{n-1} \\ &\times Tr_D[\gamma_5\left(\frac{\not{q}+M_1}{q^2-M_1^2+i\epsilon}\right)\gamma_5\left(\frac{\not{q}-\not{k}+M_2}{(q-k)^2-M_2^2+i\epsilon}\right)]]. \quad (1.16.7) \end{aligned}$$

By evaluating the trace, it then gives

$$\begin{aligned} Tr[\gamma_5(\not{q}+M_1)\gamma_5(\not{q}-\not{k}+M_2] &= Tr[\gamma_5\not{q}\gamma_5\not{q}] - Tr[\gamma_5\not{q}\gamma_5\not{k}] + Tr[\gamma_5\not{q}\gamma_5 M_2] \\ &+ Tr[\gamma_5 M_1\gamma_5\not{q}] - Tr[\gamma_5 M_1\gamma_5\not{k}] + Tr[\gamma_5 M_1\gamma_5 M_2] \\ &= -Tr[\not{q}\not{q}] + Tr[\not{q}\not{k}] + M_1M_2Tr[\mathcal{I}] \\ &= -4q^2 + 4q.k - 4M_1M_2 = 4[-q^2 + q.k + M_1M_2], \end{aligned} \quad (1.16.8)$$

where $\mathcal{I}$ is identity matrix. Then pefroming a little trick calculation to the denominator before the Feynman paramaterization applies, it then gives

$$\rightarrow \frac{1}{[q^2 - M_1^2 + i\epsilon]\,[(q-k)^2 - M_2^2 + i\epsilon]}$$
$$= \frac{1}{2q^2 - 2k.q + k^2 - M_1^2 - M_2^2}\left[\frac{1}{[q^2 - M_1^2 + i\epsilon]} + \frac{1}{[(q-k)^2 - M_2^2 + i\epsilon]}\right], \quad (1.16.9)$$

Similarly the numerator can be expressed as

$$\begin{aligned} -q^2 + q.k + M_1M_2 &= \left[-q^2 + q.k + M_1M_2 - \frac{k^2}{2}\right] + \frac{k^2}{2} \\ -2q^2 + 2q.k + 2M_2M_1 &= \left[-2q^2 + 2q.k + 2M_1M_2 - k^2\right] + k^2 \\ &= \left[-2q^2 + 2q.k + M_2^2 + M_1^2 - (M_2 - M_1)^2 - k^2\right] + k^2 \\ &= \left[-2q^2 + 2q.k + M_2^2 + M_1^2 - k^2\right] + k^2 - (M_2 - M_1)^2. \end{aligned} \quad (1.16.10)$$

Putting the numerator in Eq.(1.16.10) and denominator in Eq.(1.16.9) into the trace part of Eq.(1.16.8), one has the form

$$\begin{aligned} A_n &= -2iN_Cg_{Kqq}^2\frac{\partial}{\partial k^2}\left[\int \frac{d^4q}{(2\pi)^4}\int_0^1 dx\left(\frac{q_-}{k_-}\right)^{n-1}\frac{4[-q^2 + q.k + M_1M_2]}{[q^2 - M_1^2 + i\epsilon][(q-k)^2 - M_2^2 + i\epsilon]}\right] \\ &= -4iN_Cg_{Kqq}^2\frac{\partial}{\partial k^2}\left[\int \frac{d^4q}{(2\pi)^4}\int_0^1 dx\left(\frac{q_-}{k_-}\right)^{n-1}\frac{2[-q^2 + q.k + M_1M_2]}{[q^2 - M_1^2 + i\epsilon][(q-k)^2 - M_2^2 + i\epsilon]}\right] \\ &= -4iN_Cg_{Kqq}^2\frac{\partial}{\partial k^2} \\ &\times\left[\int \frac{d^4q}{(2\pi)^4}\int_0^1 dx\left(\frac{q_-}{k_-}\right)^{n-1}\frac{-2q^2 + 2q.k + M_2^2 + M_1^2 - k^2 + k^2 - (M_2 - M_1)^2}{[q^2 - M_1^2 + i\epsilon][(q-k)^2 - M_2^2 + i\epsilon]}\right] \\ &= -4iN_Cg_{Kqq}^2\frac{\partial}{\partial k^2} \\ &\times[\int \frac{d^4q}{(2\pi)^4}\int_0^1 dx\left(\frac{q_-}{k_-}\right)^{n-1}\frac{-2q^2 + 2q.k + M_2^2 + M_1^2 - k^2}{[q^2 - M_1^2 + i\epsilon][(q-k)^2 - M_2^2 + i\epsilon]} \\ &+ \frac{k^2 - (M_2 - M_1)^2}{[q^2 - M_1^2 + i\epsilon][(q-k)^2 - M_2^2 + i\epsilon]}], \end{aligned} \quad (1.16.11)$$

Then the final quark distribution of the kaon is obtained after applying the Wick rotation and proper-time regularisation scheme, one has

$$\begin{aligned} q_K(x,k^2) &= \frac{N_Cg_{Kqq}^2}{4\pi^2}\int d\tau\frac{1}{\tau}e^{-\tau(k^2(x^2-x)+xM_2^2-M_1^2(x-1))} \\ &\times\left[1 + \tau\left[k^2(x-x^2) - (x-x^2)(M_2 - M_1)^2\right]\right], \end{aligned} \quad (1.16.12)$$

where $k^2 = m_K^2$. This result satisfies the baryon number and momentum sum rules. This is analogous relation with the anti-quark distribution.

A.17 Derivation for the charge radius squared of the kaon and pion and their quark sector

Here we can evaluate the derivation of the kaon form factor and its quark sector form factor, it is given as

$$\begin{aligned}
\frac{d\mathcal{F}_{u}^{K^+}}{dQ^2} &= \frac{d}{dQ^2}\left[\frac{N_C g_{Kqq}^2}{4\pi^2}\int_0^1 dx\int\frac{d\tau}{\tau}e^{-\tau(Q^2(x-x^2)+M_1^2)}\right] \\
&+ \frac{d}{dQ^2}[\frac{N_C g_{Kqq}^2}{4\pi^2}\int_0^1 dx\int_0^{1-x} dz\int d\tau e^{-\tau(k^2((x+z)^2-(x+z))+xzQ^2+M_2^2(1-x-z)+M_1^2(x+z))} \\
&\times [k^2(x+z)+(M_1-M_2)^2(x+z)-2M_2^2+2M_2M_1]] \\
&= \frac{N_C g_{Kqq}^2}{4\pi^2}\int_0^1 dx\int\frac{d\tau}{\tau}\frac{d}{dQ^2}\left[e^{-\tau(Q^2(x-x^2)+M_1^2)}\right] \\
&+ \frac{N_C g_{Kqq}^2}{4\pi^2}\int_0^1 dx\int_0^{1-x} dz\int d\tau\left[k^2(x+z)+(M_1-M_2)^2(x+z)-2M_2^2+2M_2M_1\right] \\
&\times \frac{d}{dQ^2}\left[e^{-\tau(k^2((x+z)^2-(x+z))+xzQ^2+M_2^2(1-x-z)+M_1^2(x+z))}\right] \\
&= \frac{N_C g_{Kqq}^2}{4\pi^2}\int_0^1 dx\int\frac{d\tau}{\tau}\left[-(x-x^2)\tau e^{-\tau(Q^2(x-x^2)+M_1^2)}\right] \\
&+ \frac{N_C g_{Kqq}^2}{4\pi^2}\int_0^1 dx\int_0^{1-x} dz\int d\tau\left[k^2(x+z)+(M_1-M_2)^2(x+z)-2M_2^2+2M_2M_1\right] \\
&\times \left[-xz\tau e^{-\tau(k^2((x+z)^2-(x+z))+xzQ^2+M_2^2(1-x-z)+M_1^2(x+z))}\right], \qquad (1.17.1)
\end{aligned}$$

Then the charge radii of the up quark sector form factor can be written as

$$\begin{aligned}
\langle r^2\rangle_{u/K^+} &= \frac{3N_C g_{Kqq}^2}{2\pi^2}\int_0^1 dx\int\frac{d\tau}{\tau}(x-x^2)\tau e^{-\tau(M_1^2)} \\
&+ \frac{3N_C g_{Kqq}^2}{2\pi^2}\int_0^1 dx\int_0^{1-x} dz\int d\tau \\
&\times\left[k^2(x+z)+(M_1-M_2)^2(x+z)-2M_2^2+2M_2M_1\right] \\
&\times xz\tau e^{-\tau(k^2((x+z)^2-(x+z))+M_2^2(1-x-z)+M_1^2(x+z))}, \qquad (1.17.2)
\end{aligned}$$

and for the anti-strange quark sector form factor contribution can be expressed as

$$\begin{aligned}
\frac{d\mathcal{F}_{\bar{s}}^{K^+}(Q^2)}{dQ^2} &= \frac{N_C g_{Kqq}^2}{4\pi^2}\int_0^1 dx\int\frac{d\tau}{\tau}\frac{d}{dQ^2}\left[e^{-\tau(Q^2(x-x^2)+M_2^2)}\right] \\
&+ \frac{N_C g_{Kqq}^2}{4\pi^2}\int_0^1 dx\int_0^{1-x} dz\int d\tau \\
&\times\left[k^2(x+z)+(M_2-M_1)^2(x+z)-2M_1^2+2M_1M_2\right] \\
&\times \frac{d}{dQ^2}\left[e^{-\tau(k^2((x+z)^2-(x+z))+xzQ^2+M_1^2(1-x-z)+M_2^2(x+z))}\right] \\
&= \frac{N_C g_{Kqq}^2}{4\pi^2}\int_0^1 dx\int\frac{d\tau}{\tau}\left[-\tau(x-x^2)e^{-\tau(Q^2(x-x^2)+M_2^2)}\right]
\end{aligned}$$

$$
\begin{aligned}
&+ \frac{N_C g_{Kqq}^2}{4\pi^2} \int_0^1 dx \int_0^{1-x} dz \int d\tau \\
&\times \left[k^2(x+z) + (M_2 - M_1)^2(x+z) - 2M_1^2 + 2M_1 M_2\right] \\
&\times \left[-\tau x z e^{-\tau(k^2((x+z)^2-(x+z)) + xzQ^2 + M_1^2(1-x-z) + M_2^2(x+z))}\right], \qquad (1.17.3)
\end{aligned}
$$

The charge radii of the anti-strange quark sector form factor can be defined as

$$
\begin{aligned}
\langle r^2 \rangle_{\bar{s}/K^+} &= \frac{3N_C g_{Kqq}^2}{2\pi^2} \int_0^1 dx \int \frac{d\tau}{\tau} \tau (x - x^2) e^{-\tau(M_2^2)} \\
&+ \frac{3N_C g_{Kqq}^2}{2\pi^2} \int_0^1 dx \int_0^{1-x} dz \int d\tau \\
&\times \left[k^2(x+z) + (M_2 - M_1)^2(x+z) - 2M_1^2 + 2M_1 M_2\right] \\
&\times \tau x z e^{-\tau(k^2((x+z)^2-(x+z)) + M_1^2(1-x-z) + M_2^2(x+z))}. \qquad (1.17.4)
\end{aligned}
$$

The total kaon charge radii can be written as

$$
\begin{aligned}
\langle r^2 \rangle_{K^+} &= e_u \langle r^2 \rangle_u^{K^+} + e_d \langle r^2 \rangle_{\bar{s}}^{K^+} \\
&= e_u \frac{3N_C g_{Kqq}^2}{2\pi^2} \int_0^1 dx \int \frac{d\tau}{\tau} (x - x^2) \tau e^{-\tau(M_1^2)} \\
&+ e_u \frac{3N_C g_{Kqq}^2}{2\pi^2} \int_0^1 dx \int_0^{1-x} dz \int d\tau \\
&\times \left[k^2(x+z) + (M_1 - M_2)^2(x+z) - 2M_2^2 + 2M_2 M_1\right] \\
&\times x z \tau e^{-\tau(k^2((x+z)^2-(x+z)) + M_2^2(1-x-z) + M_1^2(x+z))} \\
&+ e_{\bar{s}} \frac{3N_C g_{Kqq}^2}{2\pi^2} \int_0^1 dx \int \frac{d\tau}{\tau} \tau (x - x^2) e^{-\tau(M_2^2)} \\
&+ e_{\bar{s}} \frac{3N_C g_{Kqq}^2}{2\pi^2} \int_0^1 dx \int_0^{1-x} dz \int d\tau \\
&\times \left[k^2(x+z) + (M_2 - M_1)^2(x+z) - 2M_1^2 + 2M_1 M_2\right] \\
&\times \tau x z e^{-\tau(k^2((x+z)^2-(x+z)) + M_1^2(1-x-z) + M_2^2(x+z))}. \qquad (1.17.5)
\end{aligned}
$$

A.18 Additional Figures for Section 6.4

In this section we present the extra figures for the CSV in Parton Distribution Functions.

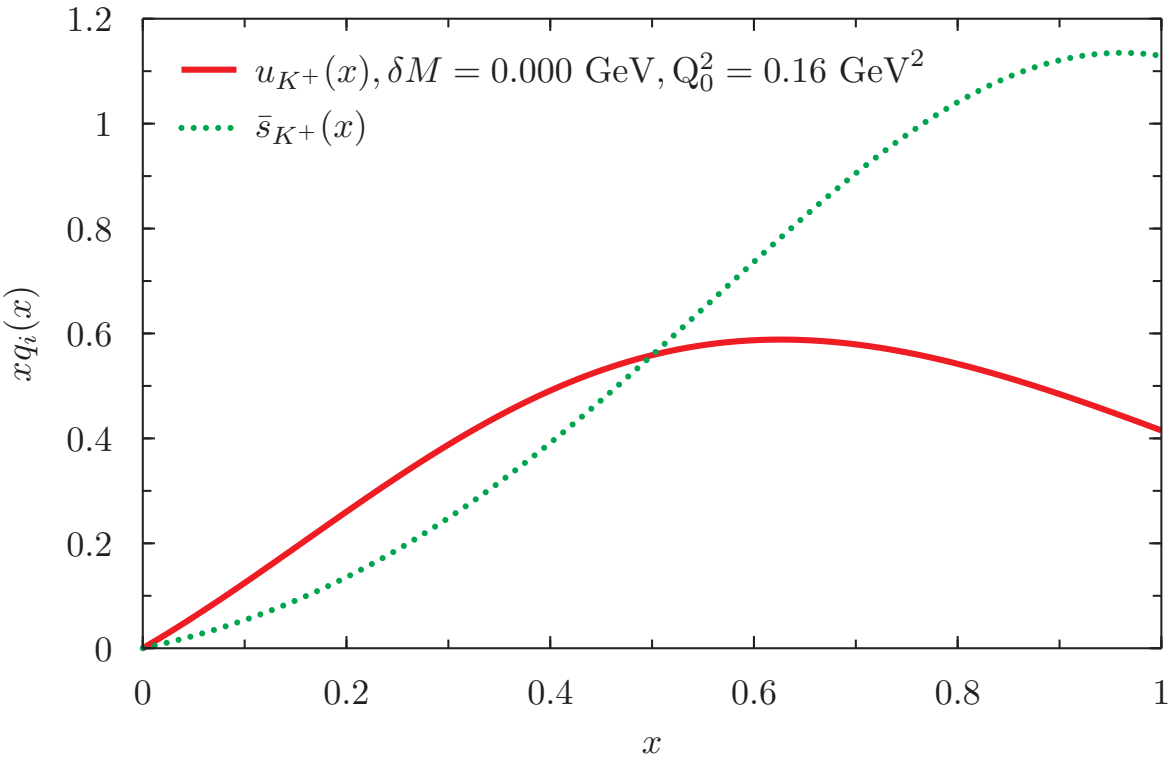

Figure 1.18.1: The parton distribution function of the positively charged kaon for $\delta M = 0.000$ GeV.

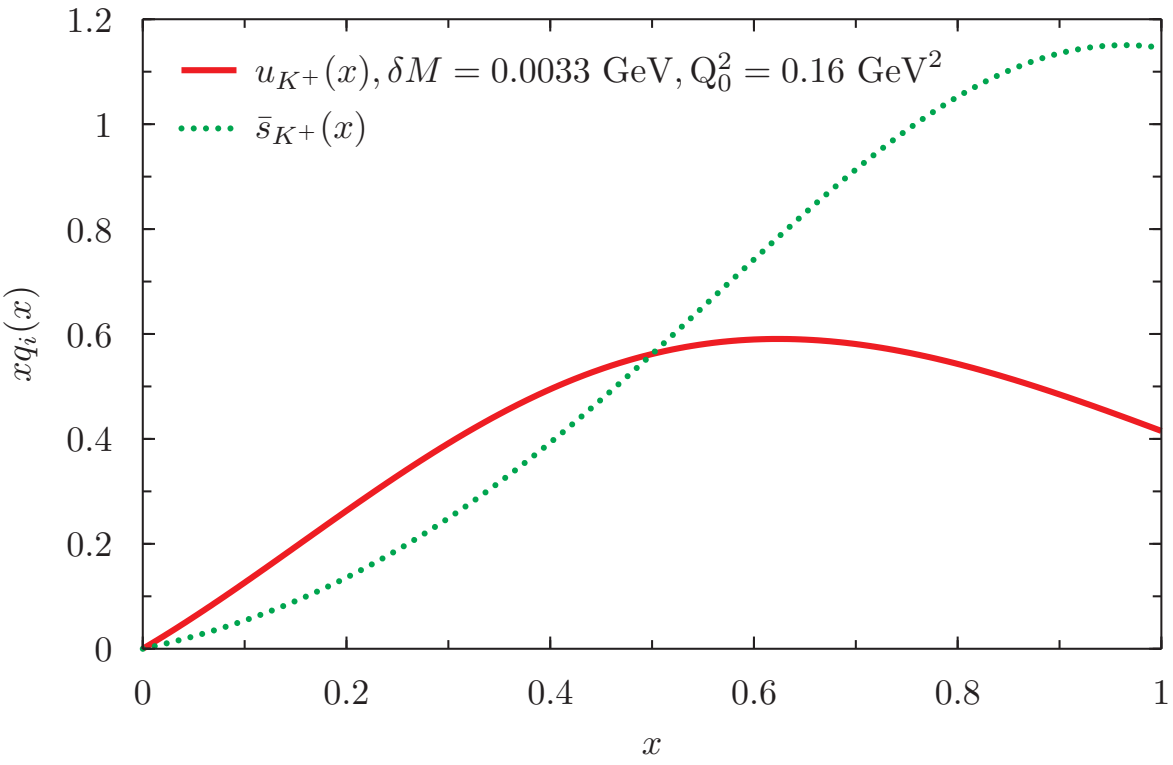

Figure 1.18.2: As in Fig. 1.18.1 but for $\delta M = 0.0033$ GeV.

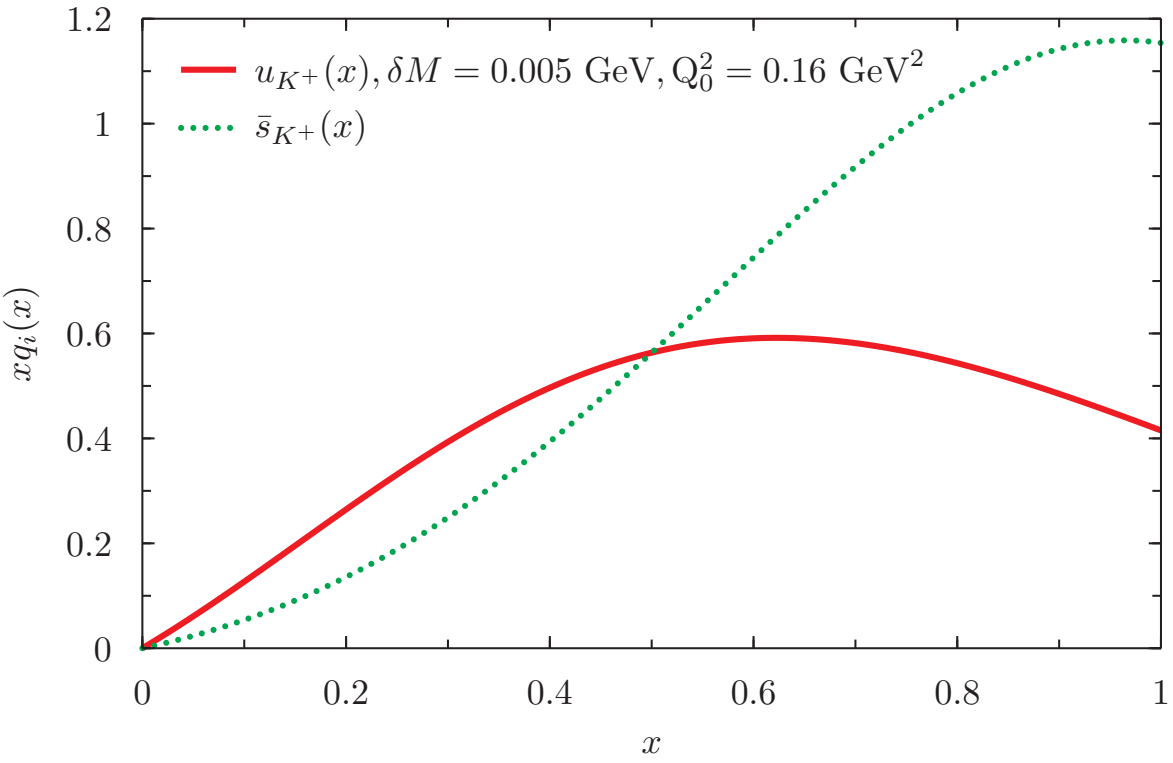

Figure 1.18.3: As in Fig. 1.18.1 but for $\delta M = 0.005$ GeV.

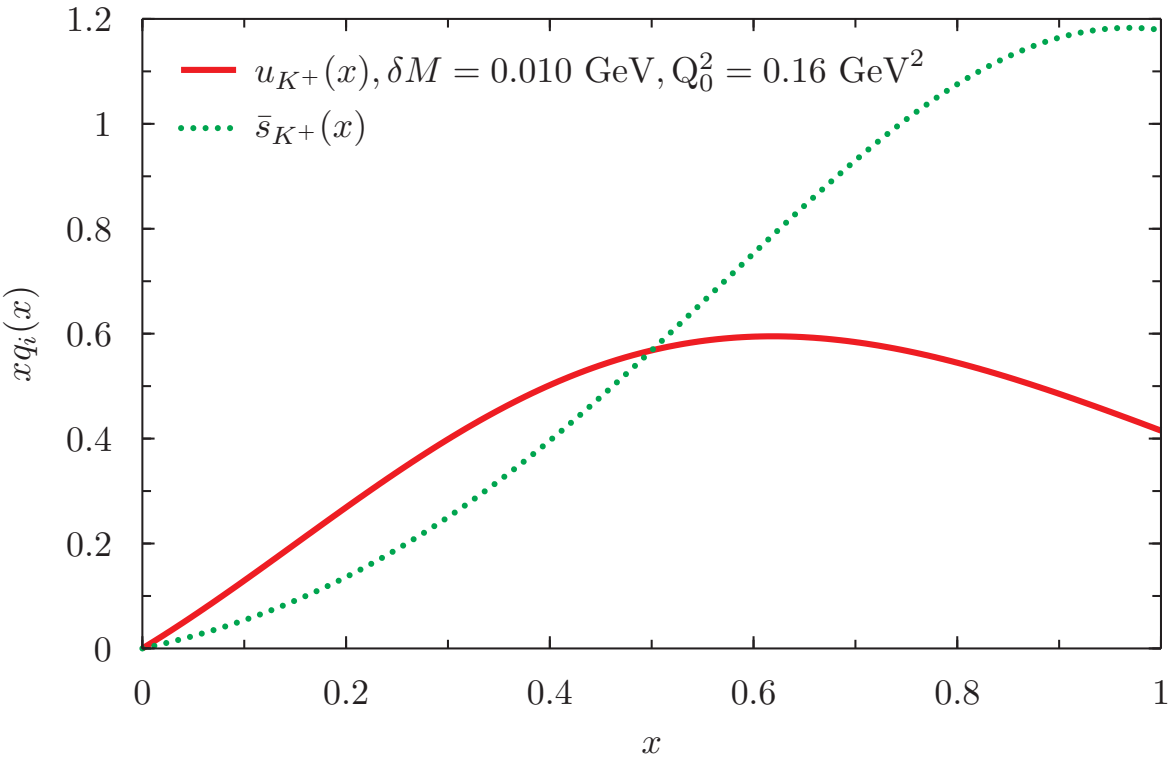

Figure 1.18.4: As in Fig. 1.18.1 but for $\delta M = 0.010$ GeV.

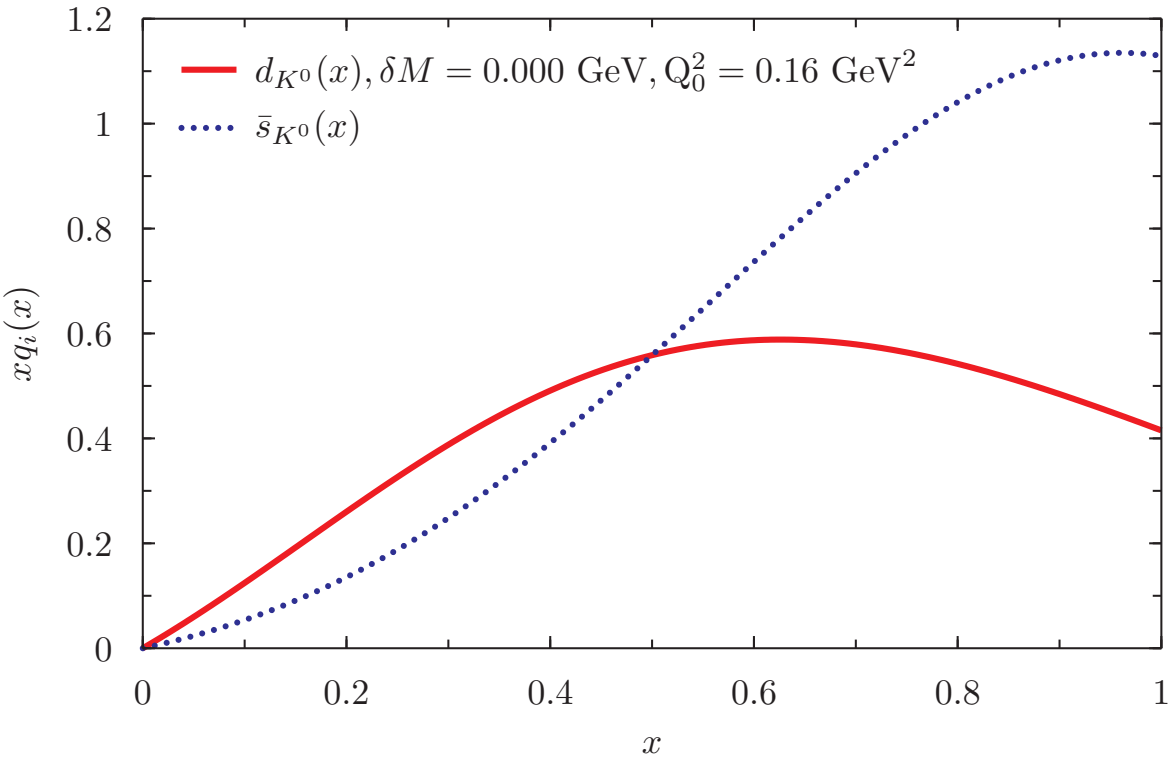

Figure 1.18.5: The parton distribution function of the neutral kaon for $\delta M = 0.000$ GeV.

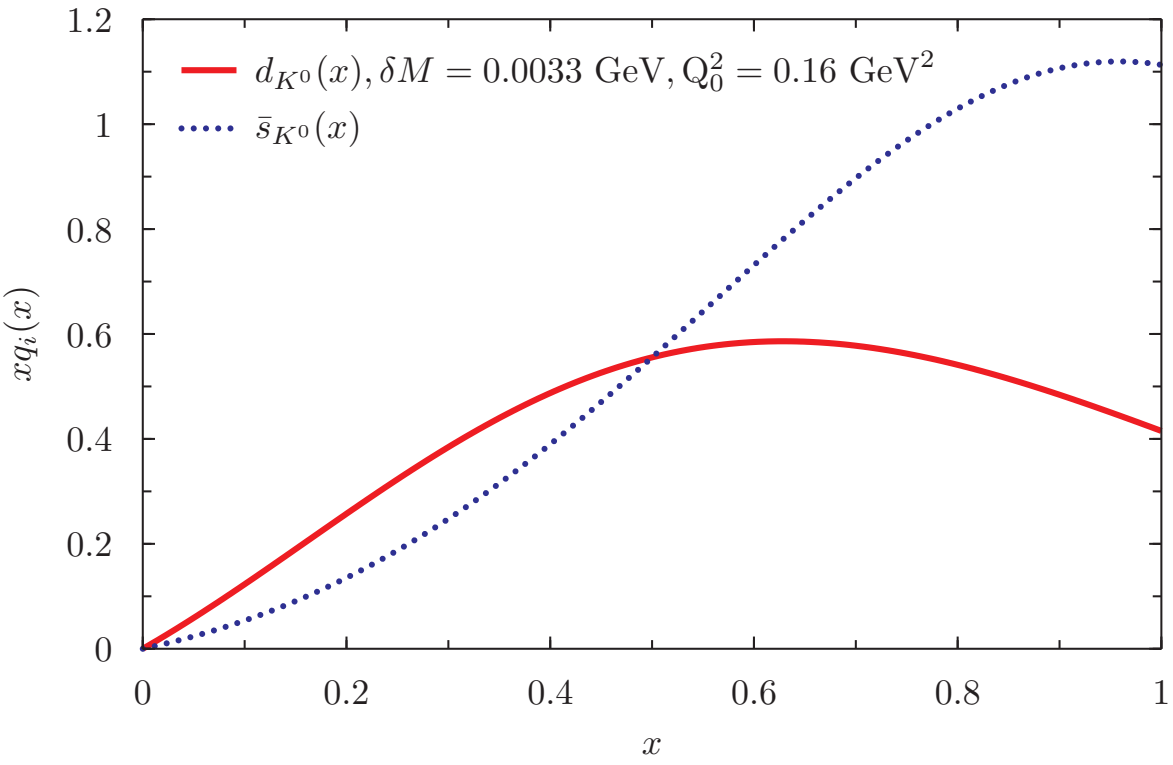

Figure 1.18.6: As in Fig. 1.18.5 but for $\delta M = 0.0033$ GeV.

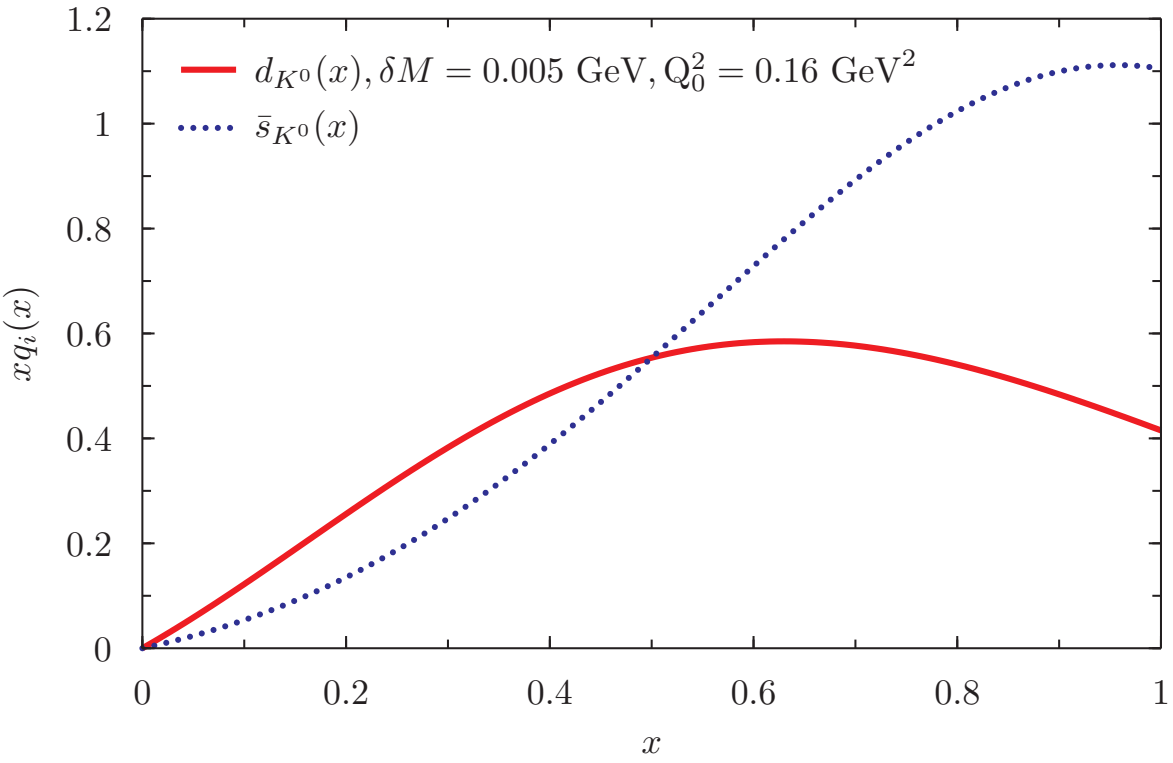

Figure 1.18.7: As in Fig. 1.18.5 but for $\delta M = 0.005$ GeV.

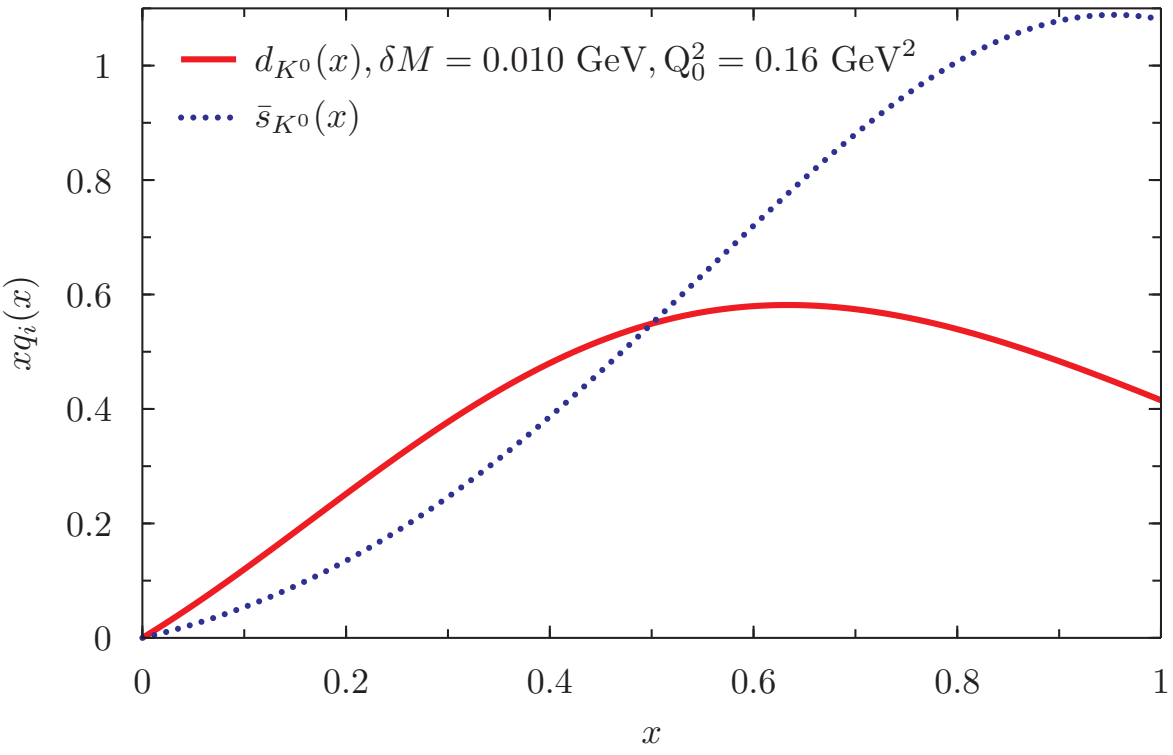

Figure 1.18.8: As in Fig. 1.18.5 but for $\delta M = 0.010$ GeV.

Table 1.18.1: The moments of the positively charged kaon valence u-quark distribution at the NJL model scale, $Q_0^2 = 0.16$ GeV^2, where n denotes moments.

n	$\delta M = 0.000$ GeV	$\delta M = 0.0033$ GeV	$\delta M = 0.005$ GeV	$\delta M = 0.010$ GeV
1	1.0000	1.0000	1.0000	1.0000
2	0.4238	0.4227	0.4222	0.4206
3	0.2494	0.2484	0.2479	0.2465
4	0.1706	0.1698	0.1694	0.1682
5	0.1273	0.1267	0.1263	0.1253
6	0.1006	0.1000	0.0997	0.0989
7	0.0827	0.0822	0.0819	0.0812
8	0.0699	0.0695	0.0692	0.0686
9	0.0604	0.0600	0.0598	0.0593
10	0.0531	0.0528	0.0526	0.0521

Table 1.18.2: The moments of the positively charged kaon valence s-quark distribution at the NJL model scale, $Q_0^2 = 0.16$ GeV^2, where n denotes moments.

n	$\delta M = 0.000$ GeV	$\delta M = 0.0033$ GeV	$\delta M = 0.005$ GeV	$\delta M = 0.010$ GeV
1	1.0000	1.0000	1.0000	1.0000
2	0.5762	0.5772	0.5778	0.5794
3	0.4017	0.4029	0.4035	0.4053
4	0.3061	0.3073	0.3079	0.3096
5	0.2461	0.2471	0.2477	0.2492
6	0.2051	0.2060	0.2065	0.2079
7	0.1754	0.1763	0.1767	0.1780
8	0.1530	0.1538	0.1542	0.1554
9	0.1356	0.1363	0.1367	0.1378
10	0.1216	0.1223	0.1226	0.1236

Table 1.18.3: The moments of the neutral kaon valence d-quark distribution at the NJL model scale, $Q_0^2 = 0.16$ GeV^2, where n denotes moments.

n	$\delta M = 0.000$ GeV	$\delta M = 0.0033$ GeV	$\delta M = 0.005$ GeV	$\delta M = 0.010$ GeV
1	1.0000	1.0000	1.0000	1.0000
2	0.4238	0.4249	0.4255	0.4271
3	0.2494	0.2504	0.2509	0.2524
4	0.1706	0.1714	0.1718	0.1731
5	0.1273	0.1280	0.1284	0.1294
6	0.1006	0.1012	0.1015	0.1024
7	0.0827	0.0831	0.0834	0.0842
8	0.0699	0.0703	0.0706	0.0712
9	0.0604	0.0608	0.0610	0.0616
10	0.0531	0.0535	0.0536	0.0542

Table 1.18.4: The moments of the neutral kaon valence s-quark distribution at the NJL model scale, $Q_0^2 = 0.16$ GeV^2, where n denotes moments.

n	$\delta M = 0.000$ GeV	$\delta M = 0.0033$ GeV	$\delta M = 0.005$ GeV	$\delta M = 0.010$ GeV
1	1.0000	1.0000	1.0000	1.0000
2	0.5762	0.5751	0.5745	0.5728
3	0.4017	0.4006	0.3999	0.3981
4	0.3061	0.3050	0.3044	0.3027
5	0.2461	0.2451	0.2445	0.2430
6	0.2051	0.2042	0.2037	0.2023
7	0.1754	0.1746	0.1741	0.1729
8	0.1530	0.1523	0.1519	0.1507
9	0.1356	0.1349	0.1345	0.1334
10	0.1216	0.1209	0.1206	0.1196

Bibliography

[1] S. L. Glashow, "Partial Symmetries of Weak Interactions," Nucl. Phys. **22**, 579 (1961).

[2] S. Weinberg, "A Model of Leptons," Phys. Rev. Lett. **19**, 1264 (1967).

[3] A. Salam, "Elementary Particle Physics: Relativistic Groups and Analitcity", Eight Nobel Symposium, 367 (1968).

[4] G. Aad *et al.* [ATLAS Collaboration], "Observation of a new particle in the search for the Standard Model Higgs boson with the ATLAS detector at the LHC," Phys. Lett. B **716**, 1 (2013) [arXiv:1207.7214 [hep-ex]].

[5] S. Chatrchyan *et al.* [CMS Collaboration], "Observation of a new boson at a mass of 125 GeV with the CMS experiment at the LHC," Phys. Lett. B **716**, 30 (2012) [arXiv:1207.7235 [hep-ex]].

[6] M. Gell-Mann, "A Schematic Model of Baryons and Mesons," Phys. Lett. **8**, 214 (1964).

[7] G. Zweig, "An SU(3) model for strong interaction symmetry and its breaking. Version 1," CERN-TH-401.

[8] G. Zweig, "An SU(3) model for strong interaction symmetry and its breaking. Version 2," Developments in the Quark Theory of Hadrons, Volume 1. Edited by D. Lichtenberg and S. Rosen. pp. 22-101

[9] R. P. Feynman, M. Gell-Mann and G. Zweig, "Group U(6) x U(6) generated by current components," Phys. Rev. Lett. **13**, 678 (1964).

[10] D. J. Gross, "The discovery of asymptotic freedom and the emergence of QCD," Proc. Nat. Acad. Sci. **102**, 9099 (2005) [Int. J. Mod. Phys. A **20**, 5717 (2005)] [Rev. Mod. Phys. **77**, 837 (2005)].

[11] W. J. Marciano and H. Pagels, "Quantum Chromodynamics: A Review," Phys. Rept. **36**, 137 (1978).

[12] H. Fritzsch, M. Gell-Mann and H. Leutwyler, "Advantages of the Color Octet Gluon Picture," Phys. Lett. B **47**, 365 (1973).

[13] D. J. Gross and F. Wilczek, "Ultraviolet Behavior of Nonabelian Gauge Theories," Phys. Rev. Lett. **30**, 1343 (1973).

[14] D. J. Gross and F. Wilczek, "Asymptotically Free Gauge Theories. 1," Phys. Rev. D **8**, 3633 (1973).

[15] H. D. Politzer, "Reliable Perturbative Results for Strong Interactions?," Phys. Rev. Lett. **30**, 1346 (1973).

[16] J. Beringer *et al.* [Particle Data Group Collaboration], "Review of Particle Physics (RPP)," Phys. Rev. D **86**, 010001 (2012).

[17] K. G. Wilson, "Confinement of Quarks," Phys. Rev. D **10**, 2445 (1974).

[18] W. Detmold, W. Melnitchouk and A. W. Thomas, "Extraction of parton distributions from lattice QCD," Mod. Phys. Lett. A **18**, 2681 (2003) [hep-lat/0310003].

[19] W. Detmold, W. Melnitchouk and A. W. Thomas, "Parton distribution functions in the pion from lattice QCD," Phys. Rev. D **68**, 034025 (2003) [hep-lat/0303015].

[20] W. Detmold, W. Melnitchouk and A. W. Thomas, "Connecting structure functions on the lattice with phenomenology," Int. J. Mod. Phys. A **18**, 1343 (2003) [hep-ph/0201288].

[21] F. J. Dyson, "The Radiation theories of Tomonaga, Schwinger, and Feynman," Phys. Rev. **75**, 486 (1949).

[22] F. J. Dyson, "The S matrix in quantum electrodynamics," Phys. Rev. **75**, 1736 (1949).

[23] J. S. Schwinger, "On the Green's functions of quantized fields. 1.," Proc. Nat. Acad. Sci. **37**, 452 (1951).

[24] J. S. Schwinger, "On the Green's functions of quantized fields. 2.," Proc. Nat. Acad. Sci. **37**, 455 (1951).

[25] J. S. Schwinger, "On gauge invariance and vacuum polarization," Phys. Rev. **82**, 664 (1951).

[26] M. A. Shifman, A. I. Vainshtein and V. I. Zakharov, "QCD and Resonance Physics. Theoretical Foundations," Nucl. Phys. B **147**, 385 (1979).

[27] M. A. Shifman, A. I. Vainshtein and V. I. Zakharov, "QCD and Resonance Physics: Applications," Nucl. Phys. B **147**, 448 (1979).

[28] M. A. Shifman, A. I. Vainshtein and V. I. Zakharov, "QCD and Resonance Physics. The rho-omega Mixing," Nucl. Phys. B **147**, 519 (1979).

[29] G. V. Korenblit, V. A. Naumov and V. L. Chernyak, "Asymptotics Of Hadron Exclusive Electroproduction Amplitudes. (in Russian)," Sov. J. Nucl. Phys. **29**, 77 (1979) [Yad. Fiz. **29**, 153 (1979)].

[30] D. Ebert, L. Kaschluhn and G. Kastelewicz, "Effective meson - diquark Lagrangian and mass formulas from the Nambu-Jona-Lasinio model," Phys. Lett. B **264**, 420 (1991).

[31] T. Horikawa and W. Bentz, "Medium modifications of nucleon electromagnetic form-factors," Nucl. Phys. A **762**, 102 (2005) [nucl-th/0506021].

[32] N. Ishii, W. Bentz and K. Yazaki, "Baryons in the NJL model as solutions of the relativistic Faddeev equation," Nucl. Phys. A **587**, 617 (1995).

[33] H. Asami, N. Ishii, W. Bentz and K. Yazaki, "Static properties of the nucleon in the Faddeev approach based on the Nambu-Jona-Lasinio model," Phys. Rev. C **51**, 3388 (1995).

[34] T. Hatsuda and T. Kunihiro, "QCD phenomenology based on a chiral effective Lagrangian," Phys. Rept. **247**, 221 (1994) [hep-ph/9401310].

[35] S. P. Klevansky, "The Nambu-Jona-Lasinio model of quantum chromodynamics," Rev. Mod. Phys. **64**, 649 (1992).

[36] U. Vogl and W. Weise, "The Nambu and Jona Lasinio model: Its implications for hadrons and nuclei," Prog. Part. Nucl. Phys. **27**, 195 (1991).

[37] S. Klimt, M. F. M. Lutz, U. Vogl and W. Weise, "GENERALIZED SU(3) NAMBU-JONA-LASINIO MODEL. Part. 1. MESONIC MODES," Nucl. Phys. A **516**, 429 (1990).

[38] U. Vogl, M. F. M. Lutz, S. Klimt and W. Weise, "Generalized SU(3) Nambu-Jona-Lasinio Model. Part 2. From Current to Constituent Quarks," Nucl. Phys. A **516**, 469 (1990).

[39] M. Buballa, "NJL model analysis of quark matter at large density," Phys. Rept. **407**, 205 (2005) [hep-ph/0402234].

[40] T. Klhn, R. astowiecki and D. B. Blaschke, "Implications of the measurement of pulsars with two solar masses for quark matter in compact stars and heavy-ion collisions: A NambuJona-Lasinio model case study," Phys. Rev. D **88**, 085001 (2013) [arXiv:1307.6996].

[41] S. Lawley, W. Bentz and A. W. Thomas, "Neutron star properties from an NJL model modified to simulate confinement," Nucl. Phys. Proc. Suppl. **141**, 29 (2005) [nucl-th/0409073].

[42] M. Baldo, G. F. Burgio, P. Castorina, S. Plumari and D. Zappala, "Quark matter in neutron stars within the Nambu - Jona-Lasinio model and confinement," Phys. Rev. C **75**, 035804 (2007) [hep-ph/0607343].

[43] A. Blotz, M. Praszalowicz and K. Goeke, "Axial properties of the nucleon with 1/N(c) corrections in the solitonic SU(3) NJL model," Phys. Rev. D **53**, 485 (1996) [hep-ph/9403314].

[44] M. E. Carrillo-Serrano, I. C. Clot and A. W. Thomas, "SU(3)-flavor breaking in octet baryon masses and axial couplings," Phys. Rev. C **90**, no. 6, 064316 (2014) [arXiv:1409.1653 [nucl-th]].

[45] T. Ito, W. Bentz, I. C. Cloet, A. W. Thomas and K. Yazaki, "The NJL-jet model for quark fragmentation functions," Phys. Rev. D **80**, 074008 (2009) [arXiv:0906.5362 [nucl-th]].

[46] H. H. Matevosyan, A. W. Thomas and W. Bentz, "Dihadron fragmentation functions within the NambuJona-Lasiniojet model," Phys. Rev. D **88**, no. 9, 094022 (2013) [arXiv:1310.1917 [hep-ph]].

[47] H. H. Matevosyan, W. Bentz, I. C. Cloet and A. W. Thomas, "Transverse Momentum Dependent Fragmentation and Quark Distribution Functions from the NJL-jet Model," Phys. Rev. D **85**, 014021 (2012) [arXiv:1111.1740 [hep-ph]].

[48] I. C. Cloet, W. Bentz and A. W. Thomas, "Transversity quark distributions in a covariant quark-diquark model," Phys. Lett. B **659**, 214 (2008) [arXiv:0708.3246 [hep-ph]].

[49] C. Weiss, A. Buck, R. Alkofer and H. Reinhardt, "Diquark electromagnetic form-factors in a Nambu-Jona-Lasinio model," Phys. Lett. B **312**, 6 (1993) [hep-ph/9305215].

[50] M. Kato, W. Bentz, K. Yazaki and K. Tanaka, "A Modified Nambu-Jona-Lasinio model for mesons and baryons," Nucl. Phys. A **551**, 541 (1993).

[51] H. Weigel, R. Alkofer and H. Reinhardt, "Hyperons in the bound state approach to the Nambu-Jona-Lasinio chiral soliton," Nucl. Phys. A **576**, 477 (1994) [hep-ph/9310309].

[52] G. Ripka, "Introduction to Nambu-Jona-Lasinio models of hadrons," Czech. J. Phys. **46**, 721 (1996).

[53] W. Broniowski, G. Ripka, E. Nikolov and K. Goeke, "Analytic structure of meson propagators in the proper time regularized Nambu-Jona-Lasinio model," Z. Phys. A **354**, 421 (1996) [hep-ph/9509363].

[54] A. Buck, R. Alkofer and H. Reinhardt, "Baryons as bound states of diquarks and quarks in the Nambu-Jona-Lasinio model," Phys. Lett. B **286**, 29 (1992).

[55] H. Asami, "Electromagnetic properties of the nucleon as a solution of the relativistic Faddeev equation," CNS-REP-18.

[56] I. C. Cloet, W. Bentz and A. W. Thomas, "Nucleon quark distributions in a covariant quark-diquark model," Phys. Lett. B **621**, 246 (2005) [hep-ph/0504229].

[57] W. Bentz and A. W. Thomas, "The Stability of nuclear matter in the Nambu-Jona-Lasinio model," Nucl. Phys. A **696**, 138 (2001) [nucl-th/0105022].

[58] H. L. L. Roberts, A. Bashir, L. X. Gutierrez-Guerrero, C. D. Roberts and D. J. Wilson, "pi- and rho-mesons, and their diquark partners, from a contact interaction," Phys. Rev. C **83**, 065206 (2011) [arXiv:1102.4376 [nucl-th]].

[59] P. Rehberg, S. P. Klevansky and J. Hufner, "Hadronization in the SU(3) Nambu-Jona-Lasinio model," Phys. Rev. C **53**, 410 (1996) [hep-ph/9506436].

[60] D. Ebert, T. Feldmann and H. Reinhardt, "Extended NJL model for light and heavy mesons without q - anti-q thresholds," Phys. Lett. B **388**, 154 (1996) [hep-ph/9608223].

[61] A. A. Andrianov, D. Ebert, T. Feldmann and V. A. Andrianov, "Dimensional structural constants from chiral and conformal bosonization of QCD," Int. J. Mod. Phys. A **12**, 5589 (1997) [hep-ph/9702338].

[62] A. A. Andrianov, V. A. Andrianov and D. Ebert, "QCD bosonization 96: Recent developments," In *St. Petersburg 1996, High energy physics and quantum field theory* 297-303

[63] H. C. Kim, M. V. Polyakov, A. Blotz and K. Goeke, "Magnetic moments of the SU(3) octet baryons in the semibosonized SU(3) Nambu-Jona-Lasinio model," Nucl. Phys. A **598**, 379 (1996) [hep-ph/9506422].

[64] H. C. Kim, A. Blotz, M. V. Polyakov and K. Goeke, "Electromagnetic form-factors of the SU(3) Octet baryons in the semibosonized SU(3) Nambu-Jona-Lasinio model," Phys. Rev. D **53**, 4013 (1996) [hep-ph/9504363].

[65] K. Goeke, C. V. Christov and A. Blotz, "Baryons in the SU(2) and SU(3) NJL model: A review of results," Prog. Part. Nucl. Phys. **36**, 207 (1996).

[66] T. Inagaki, D. Kimura, H. Kohyama and A. Kvinikhidze, "Nonet meson properties in Nambu–Jona-Lasinio model with dimensional versus cutoff regularization," Phys. Rev. D **83**, 034005 (2011) [arXiv:1010.0309 [hep-ph]].

[67] H. Kohyama, D. Kimura and T. Inagaki, "Regularization dependence on phase diagram in NambuJona-Lasinio model," Nucl. Phys. B **896**, 682 (2015) [arXiv:1501.00449 [hep-ph]].

[68] T. Inagaki, D. Kimura and H. Kohyama, "Next to leading order calculation with dimensional regularization in Nambu-Jona-Lasinio model," Int. J. Mod. Phys. A **29**, 1450048 (2014) [arXiv:1401.7399 [hep-ph]].

[69] T. Inagaki, D. Kimura, H. Kohyama and A. Kvinikhidze, "Regularization parameter independent analysis in Nambu-Jona-Lasinio model," Int. J. Mod. Phys. A **28**, 1350164 (2013) [arXiv:1302.5667 [hep-ph]].

[70] T. Inagaki, D. Kimura, H. Kohyama and A. Kvinikhidze, "Nonet meson properties in Nambu-Jona-Lasinio model with dimensional regularization at finite temperature and chemical potential," Phys. Rev. D **85**, 076002 (2012) [arXiv:1110.5898 [hep-ph]].

[71] H. Weigel, E. Ruiz Arriola and L. P. Gamberg, "Hadron structure functions in a chiral quark model: Regularization, scaling and sum rules," Nucl. Phys. B **560**, 383 (1999) [hep-ph/9905329].

[72] G. Hellstern, R. Alkofer and H. Reinhardt, "Diquark confinement in an extended NJL model," Nucl. Phys. A **625**, 697 (1997) [hep-ph/9706551].

[73] G. Hellstern, R. Alkofer, M. Oettel and H. Reinhardt, "Nucleon form-factors in a covariant diquark - quark model," Nucl. Phys. A **627**, 679 (1997) [hep-ph/9705267].

[74] J. Bijnens, "Chiral Lagrangians and Nambu-Jona-Lasinio - like models," Phys. Rept. **265**, 369 (1996) [hep-ph/9502335].

[75] J. Bijnens and P. Gosdzinsky, "Electromagnetic contributions to vector meson masses and mixings," Phys. Lett. B **388**, 203 (1996) [hep-ph/9607462].

[76] D. Ebert and H. Reinhardt, "Effective Chiral Hadron Lagrangian with Anomalies and Skyrme Terms from Quark Flavor Dynamics," Nucl. Phys. B **271**, 188 (1986).

[77] D. Ebert, T. Feldmann, R. Friedrich and H. Reinhardt, "Effective meson Lagrangian with chiral and heavy quark symmetries from quark flavor dynamics," Nucl. Phys. B **434**, 619 (1995) [hep-ph/9406220].

[78] Y. Ninomiya, W. Bentz and I. C. Clot, "Dressed Quark Mass Dependence of Pion and Kaon Form Factors," Phys. Rev. C **91**, no. 2, 025202 (2015) [arXiv:1406.7212 [nucl-th]].

[79] A. J. Buras, "Asymptotic Freedom in Deep Inelastic Processes in the Leading Order and Beyond," Rev. Mod. Phys. **52**, 199 (1980).

[80] T. Frederico and G. A. Miller, "Deep inelastic structure function of the pion in the null plane phenomenology," Phys. Rev. D **50**, 210 (1994).

[81] N. E. Ligterink and B. L. G. Bakker, "Renormalization of light front Hamiltonian field theory," Phys. Rev. D **52**, 5917 (1995).

[82] N. E. Ligterink and B. L. G. Bakker, "Equivalence of light front and covariant field theory," Phys. Rev. D **52**, 5954 (1995) [hep-ph/9412315].

[83] K. Kusaka, G. Piller, A. W. Thomas and A. G. Williams, "Deep inelastic structure functions in a covariant spectator model," Phys. Rev. D **55**, 5299 (1997) [hep-ph/9609277].

[84] K. Kusaka, G. Piller, A. W. Thomas and A. G. Williams, "Structure functions of the nucleon in a covariant scalar spectator model," Austral. J. Phys. **50**, 139 (1997) [hep-ph/9603260].

[85] T. Shigetani, K. Suzuki and H. Toki, "Pion structure function in the Nambu and Jona-Lasinio model," Phys. Lett. B **308**, 383 (1993) [hep-ph/9402286].

[86] T. Shigetani, K. Suzuki and H. Toki, "Meson structure in deep inelastic scattering," Nucl. Phys. A **579**, 413 (1994) [hep-ph/9402277].

[87] R. M. Davidson and E. Ruiz Arriola, "Structure functions of pseudoscalar mesons in the SU(3) NJL model," Phys. Lett. B **348**, 163 (1995).

[88] R. M. Davidson and E. Ruiz Arriola, "Mesonic correlation functions in the NJL model with vector mesons," Phys. Lett. B **359**, 273 (1995).

[89] A. De Rujula and F. Martin, "The Structure of Hadron Structure Functions," Phys. Rev. D **22**, 1787 (1980).

[90] C. J. Benesh and G. A. Miller, "Valence Quark Distributions in the Soliton Bag Model," Phys. Lett. B **215**, 381 (1988).

[91] C. J. Benesh and G. A. Miller, "Deep Inelastic Scattering in a Modified Bag Model," Phys. Rev. D **38**, 48 (1988).

[92] G. Altarelli and G. Parisi, "Asymptotic Freedom in Parton Language," Nucl. Phys. B **126**, 298 (1977).

[93] A. Van Dyck, T. Van Cauteren, J. Ryckebusch and B. C. Metsch, "Generalized parton distributions of pseudoscalar mesons in a covariant constituent quark model," arXiv:0808.0429 [hep-ph].

[94] M. Gluck, E. Reya and A. Vogt, "Pionic parton distributions," Z. Phys. C **53**, 651 (1992).

[95] Annelies Van Dyck, PhD Thesis, "Generalized Parton Distributions of pseudoscalar mesons in relativistic Bethe-Salpeter framework", Universiteit Gent, Belgium (2008).

[96] I. C. Cloet, PhD Thesis, "Nucleon Structure Functions, their medium modification and the polarized EMC effect", The University of Adelaide, Adelaide-South Australia (2006).

[97] M. Diehl, T. Feldmann, R. Jakob and P. Kroll, "Linking parton distributions to form-factors and Compton scattering," Eur. Phys. J. C **8**, 409 (1999) [hep-ph/9811253].

[98] L. Chang and C. D. Roberts, "Empirically Charting Dynamical Chiral Symmetry Breaking," AIP Conf. Proc. **1261**, 25 (2010) [arXiv:1004.1848 [nucl-th]].

[99] H. L. L. Roberts, L. Chang and C. D. Roberts, "Impact of dynamical chiral symmetry breaking on meson structure and interactions," Int. J. Mod. Phys. A **26**, 371 (2011) [arXiv:1007.4318 [nucl-th]].

[100] M. Alberg and J. Tibbals, "Comparison of kaon and pion valence quark distributions in a statistical model," Phys. Lett. B **709**, 370 (2014) [arXiv:1110.1606 [nucl-th]].

[101] M. A. Alberg and E. M. Henley, "Parton distributions in the proton and pion," Phys. Lett. B **611**, 111 (2005) [hep-ph/0309188].

[180] B. El-Bennich, J. P. B. C. de Melo and T. Frederico, "A combined study of the pion's static properties and form factors," Few Body Syst. **54**, 1851 (2013) [arXiv:1211.2829 [nucl-th]].

[103] M. B. Hecht, C. D. Roberts and S. M. Schmidt, "Valence quark distributions in the pion," Phys. Rev. C **63**, 025213 (2001) [nucl-th/0008049].

[104] O. W. Greenberg, "Spin and Unitary Spin Independence in a Paraquark Model of Baryons and Mesons," Phys. Rev. Lett. **13**, 598 (1964).

[105] M. Y. Han and Y. Nambu, "Three Triplet Model with Double SU(3) Symmetry," Phys. Rev. **139**, B1006 (1965).

[106] Y. Nambu, "In preludes in Theoretical Physics", edited by. A. de Shalit, H. Feshbach and L. Van Hove, North Holland, Amsterdam (1966).

[107] E. D. Bloom *et al.*, "High-Energy Inelastic e p Scattering at 6-Degrees and 10-Degrees," Phys. Rev. Lett. **23**, 930 (1969).

[108] M. Breidenbach *et al.*, "Observed Behavior of Highly Inelastic electron-Proton Scattering," Phys. Rev. Lett. **23**, 935 (1969).

[109] T. Muta, "Foundations of quantum chromodynamics. Second edition," World Sci. Lect. Notes Phys. **57**, 1 (1998).

[110] W. Greiner, S. Schramm and E. Stein, "Quantum chromodynamics," Berlin, Germany: Springer (2002) 551 p

[111] G. 't Hooft, "Renormalizable Lagrangians for Massive Yang-Mills Fields," Nucl. Phys. B **35**, 167 (1971).

[112] M. Shifman, "Understanding Confinement in QCD: Elements of a Big Picture," Int. J. Mod. Phys. A **25**, 4015 (2010) [arXiv:1007.0531 [hep-th]].

[113] A. Casher, H. Neuberger and S. Nussinov, "Chromoelectric Flux Tube Model of Particle Production," Phys. Rev. D **20**, 179 (1979).

[114] J. Goldstone, A. Salam and S. Weinberg, "Broken Symmetries," Phys. Rev. **127**, 965 (1962).

[115] J. Goldstone, "Field Theories with Superconductor Solutions," Nuovo Cim. **19**, 154 (1961).

[116] K. Nakamura *et al.* [Particle Data Group Collaboration], "Review of particle physics," J. Phys. G **37**, 075021 (2010).

[117] M. Gell-Mann, R. J. Oakes and B. Renner, "Behavior of current divergences under SU(3) x SU(3)," Phys. Rev. **175**, 2195 (1968).

[118] R. G. Roberts, "The Structure of the proton: Deep inelastic scattering,"

[119] R. P. Feynman, "Very high-energy collisions of hadrons," Phys. Rev. Lett. **23**, 1415 (1969).

[120] R. P. Feynman, "The behavior of hadron collisions at extreme energies," Conf. Proc. C **690905**, 237 (1969).

[121] M. B. Johnson and A. Picklesimer, "Relativistic Dynamics And Quark Nuclear Physics. Proceedings, Workshop, Los Alamos, Usa, June 1985," NEW YORK, USA: WILEY (1986) 861p

[122] R. L. Jaffe, "Deep Inelastic Scattering With Application To Nuclear Targets," MIT-CTP-1261.

[123] R. L. Jaffe, "Spin, twist and hadron structure in deep inelastic processes," Lect. Notes Phys. **496**, 178 (1997) [hep-ph/9602236].

[124] C. G. Callan, Jr. and D. J. Gross, "High-energy electroproduction and the constitution of the electric current," Phys. Rev. Lett. **22**, 156 (1969).

[125] D. Amati, R. Petronzio and G. Veneziano, "Relating Hard QCD Processes Through Universality of Mass Singularities," Nucl. Phys. B **140**, 54 (1978).

[126] D. Amati, R. Petronzio and G. Veneziano, "Relating Hard QCD Processes Through Universality of Mass Singularities. 2.," Nucl. Phys. B **146**, 29 (1978).

[127] S. B. Libby and G. F. Sterman, "Mass Divergences in Two Particle Inelastic Scattering," Phys. Rev. D **18**, 4737 (1978).

[128] G. F. Sterman, "Mass Divergences in Annihilation Processes. 1. Origin and Nature of Divergences in Cut Vacuum Polarization Diagrams," Phys. Rev. D **17**, 2773 (1978).

[129] G. F. Sterman, "Mass Divergences in Annihilation Processes. 2. Cancellation of Divergences in Cut Vacuum Polarization Diagrams," Phys. Rev. D **17**, 2789 (1978).

[130] S. Coleman and R. E. Norton, "Singularities in the physical region," Nuovo Cim. **38**, 438 (1965).

[131] R. K. Ellis, H. Georgi, M. Machacek, H. D. Politzer and G. G. Ross, "Perturbation Theory and the Parton Model in QCD," Nucl. Phys. B **152**, 285 (1979).

[132] A. V. Efremov and A. V. Radyushkin, "Hard Processes, Parton Model And Qcd," Riv. Nuovo Cim. **3N2**, 1 (1980).

[133] A. V. Efremov and A. V. Radyushkin, "Asymptotical Behavior of Pion Electromagnetic Form-Factor in QCD," Theor. Math. Phys. **42**, 97 (1980) [Teor. Mat. Fiz. **42**, 147 (1980)].

[134] A. V. Efremov and A. V. Radyushkin, "Factorization and Asymptotical Behavior of Pion Form-Factor in QCD," Phys. Lett. B **94**, 245 (1980).

[135] A. V. Efremov and A. V. Radyushkin, "Field Theoretic Treatment of High Momentum Transfer Processes. 1. Deep Inelastic Scattering," Theor. Math. Phys. **44**, 573 (1980) [Teor. Mat. Fiz. **44**, 17 (1980)].

[136] A. V. Efremov and A. V. Radyushkin, "Field Theoretic Treatment of High Momentum Transfer Processes. 3. Gauge Theories," Theor. Math. Phys. **44**, 774 (1981) [Teor. Mat. Fiz. **44**, 327 (1980)].

[137] J. Collins, "Foundations of perturbative QCD," (Cambridge monographs on particle physics, nuclear physics and cosmology. 32)

[138] Y. L. Dokshitzer, "Calculation of the Structure Functions for Deep Inelastic Scattering and e+ e- Annihilation by Perturbation Theory in Quantum Chromodynamics.," Sov. Phys. JETP **46**, 641 (1977) [Zh. Eksp. Teor. Fiz. **73**, 1216 (1977)].

[139] V. N. Gribov and L. N. Lipatov, "Deep inelastic e p scattering in perturbation theory," Sov. J. Nucl. Phys. **15**, 438 (1972) [Yad. Fiz. **15**, 781 (1972)].

[140] W. Bentz, I. C. Cloet, T. Ito, A. W. Thomas and K. Yazaki, "Polarized structure functions of nucleons and nuclei," Prog. Part. Nucl. Phys. **61**, 238 (2008) [arXiv:0711.0392 [nucl-th]].

[141] I. C. Cloet, W. Bentz and A. W. Thomas, "Spin-dependent parton distributions in the nucleon," Nucl. Phys. Proc. Suppl. **141**, 225 (2005).

[142] H. Mineo, W. Bentz, N. Ishii, A. W. Thomas and K. Yazaki, "Quark distributions in nuclear matter and the EMC effect," Nucl. Phys. A **735**, 482 (2004) [nucl-th/0312097].

[143] T. Braunschweig, B. Geyer, J. Horejsi and D. Robaschik, "Hadron Operators on the Light Cone," Z. Phys. C **33**, 275 (1986).

[144] F. M. Dittes, D. Mueller, D. Robaschik, B. Geyer and J. Horejsi, "The Altarelli-Parisi Kernel as Asymptotic Limit of an Extended Brodsky-Lepage Kernel," Phys. Lett. B **209**, 325 (1988).

[145] I. I. Balitsky and A. V. Radyushkin, "Light ray evolution equations and leading twist parton helicity dependent nonforward distributions," Phys. Lett. B **413**, 114 (1997) [hep-ph/9706410].

[146] J. Blumlein, B. Geyer and D. Robaschik, "On the evolution kernels of twist-2 light ray operators for unpolarized and polarized deep inelastic scattering," Phys. Lett. B **406**, 161 (1997) [hep-ph/9705264].

[147] A. V. Belitsky and D. Mueller, "Next-to-leading order evolution of twist-2 conformal operators: The Abelian case," Nucl. Phys. B **527**, 207 (1998) [hep-ph/9802411].

[148] A. Cafarella, C. Coriano and M. Guzzi, "Nnlo logarithmic expansions and exact solutions of the DGLAP equations from x-space: New algorithms for precision studies at the lhc," Nucl. Phys. B **748**, 253 (2006) [hep-ph/0512358].

[149] A. Cafarella and C. Coriano, "Direct solution of renormalization group equations of QCD in x space: NLO implementations at leading twist," Comput. Phys. Commun. **160**, 213 (2004) [hep-ph/0311313].

[150] M. Traini, "Charge symmetry violation: A NNLO study of partonic observables," Phys. Lett. B **707**, 523 (2012) [arXiv:1110.3594 [hep-ph]].

[151] Y. Nambu and G. Jona-Lasinio, "Dynamical Model of Elementary Particles Based on an Analogy with Superconductivity. 1.," Phys. Rev. **122**, 345 (1961).

[152] Y. Nambu and G. Jona-Lasinio, "Dynamical Model Of Elementary Particles Based On An Analogy With Superconductivity. Ii," Phys. Rev. **124**, 246 (1961).

[153] J. Bardeen, L. N. Cooper and J. R. Schrieffer, "Microscopic theory of superconductivity," Phys. Rev. **106**, 162 (1957).

[154] V. Bernard, R. L. Jaffe and U. G. Meissner, "Strangeness Mixing and Quenching in the Nambu-Jona-Lasinio Model," Nucl. Phys. B **308**, 753 (1988).

[155] V. Bernard and U. G. Meissner, "Electromagnetic Structure of the Pion and the Kaon," Phys. Rev. Lett. **61**, 2296 (1988) [Phys. Rev. Lett. **61**, 2973 (1988)].

[156] V. Bernard and U. G. Meissner, "Properties of Vector and Axial Vector Mesons from a Generalized Nambu-Jona-Lasinio Model," Nucl. Phys. A **489**, 647 (1988).

[157] U. G. Meissner and V. Bernard, "The Nambu-Jona-Lasinio Model: Use and Misuse of a Strong Coupling Theory," Comments Nucl. Part. Phys. **19**, 67 (1989).

[158] G. 't Hooft, "Computation of the Quantum Effects Due to a Four-Dimensional Pseudoparticle," Phys. Rev. D **14**, 3432 (1976) [Phys. Rev. D **18**, 2199 (1978)].

[159] P. T. P. Hutauruk, I. C. Cloet, A. W. Thomas, "Kaon Form Factor and Parton Distribution Functions," Phys. Rev. C –, – (2015) [in preparation].

[160] K. Suzuki and W. Weise, "Chiral constituent quarks and their role in quark distribution functions of nucleon and pion," Nucl. Phys. A **634**, 141 (1998) [hep-ph/9711368].

[161] H. A. Bethe and E. E. Salpeter, Phys. Rev. **82**, 309 (1951).

[162] R. P. Feynman, "The Theory of positrons," Phys. Rev. **76**, 749 (1949).

[163] R. P. Feynman, "Space - time approach to quantum electrodynamics," Phys. Rev. **76**, 769 (1949).

[164] E. E. Salpeter and H. A. Bethe, "A Relativistic equation for bound state problems," Phys. Rev. **84**, 1232 (1951).

[165] S. M. Dancoff, "Nonadiabatic meson theory of nuclear forces," Phys. Rev. **78**, 382 (1950).

[166] A. W. Thomas and W. Weise, "The Structure of the Nucleon," Berlin, Germany: Wiley-VCH (2001) 389 p

[167] J. Volmer *et al.* [Jefferson Lab F(pi) Collaboration], "Measurement of the Charged Pion Electromagnetic Form-Factor," Phys. Rev. Lett. **86**, 1713 (2001) [nucl-ex/0010009].

[168] S. R. Amendolia *et al.* [NA7 Collaboration], "A Measurement of the Space - Like Pion Electromagnetic Form-Factor," Nucl. Phys. B **277**, 168 (1986).

[169] E. B. Dally *et al.*, "Elastic Scattering Measurement of the Negative Pion Radius," Phys. Rev. Lett. **48**, 375 (1982).

[170] G. T. Adylov *et al.*, "A Measurement of the Electromagnetic Size of the Pion from Direct Elastic Pion Scattering Data at 50-GeV/c," Nucl. Phys. B **128**, 461 (1977).

[171] E. B. Dally *et al.*, "Direct Measurement of the pi- Form-Factor.," Phys. Rev. Lett. **39**, 1176 (1977).

[172] E. B. Dally *et al.*, "Measurement of the π^- Form-factor," Phys. Rev. D **24**, 1718 (1981).

[173] E. Dally *et al.*, "Measurement of the Kaon Form Factor," FERMILAB-PROPOSAL-0456.

[174] G. Adylov *et al.*, "The Pion Radius," Phys. Lett. B **51**, 402 (1974).

[175] H. P. Blok *et al.* [Jefferson Lab Collaboration], "Charged pion form factor between Q^2=0.60 and 2.45 GeV^2. I. Measurements of the cross section for the ^{1}H$(e, e'\pi^+)n$ reaction," Phys. Rev. C **78**, 045202 (2008) [arXiv:0809.3161 [nucl-ex]].

[176] G. M. Huber *et al.* [Jefferson Lab Collaboration], "Charged pion form-factor between Q**2 = 0.60-GeV**2 and 2.45-GeV**2. II. Determination of, and results for, the pion form-factor," Phys. Rev. C **78**, 045203 (2008) [arXiv:0809.3052 [nucl-ex]].

[177] C. J. Bebek *et al.*, "Electroproduction of single pions at low epsilon and a measurement of the pion form-factor up to q^2 = 10-GeV^2," Phys. Rev. D **17**, 1693 (1978).

[178] L. Chang, I. C. Clot, C. D. Roberts, S. M. Schmidt and P. C. Tandy, "Pion electromagnetic form factor at spacelike momenta," Phys. Rev. Lett. **111**, 141802 (2013) [arXiv:1307.0026 [nucl-th]].

[179] C. S. Mello, J. P. C. Filho, E. O. da Silva, B. El-Bennich, J. P. B. C. de Melo and V. S. Filho, "Electromagnetic Structure of Pion," AIP Conf. Proc. **1520**, 333 (2013) [arXiv:1208.2021 [hep-ph]].

[180] B. El-Bennich, J. P. B. C. de Melo and T. Frederico, "A combined study of the pion's static properties and form factors," Few Body Syst. **54**, 1851 (2013) [arXiv:1211.2829 [nucl-th]].

[181] P. Maris, "Electromagnetic properties of diquarks," Few Body Syst. **35**, 117 (2004) [nucl-th/0409008].

[182] B. El-Bennich, J. P. B. C. de Melo, B. Loiseau, J.-P. Dedonder and T. Frederico, "Modeling electromagnetic form-factors of light and heavy pseudoscalar mesons," Braz. J. Phys. **38**, 465 (2008) [arXiv:0805.0768 [hep-ph]].

[183] S. R. Amendolia *et al.*, "A Measurement of the Kaon Charge Radius," Phys. Lett. B **178**, 435 (1986).

[184] P. Maris and P. C. Tandy, "The pi, K+, and K0 electromagnetic form-factors," Phys. Rev. C **62**, 055204 (2000) [nucl-th/0005015].

[185] P. C. Tandy, "Hadron physics from the global color model of QCD," Prog. Part. Nucl. Phys. **39**, 117 (1997) [nucl-th/9705018].

[186] W. W. Buck, R. A. Williams and H. Ito, "Elastic charge form-factors for K mesons," Phys. Lett. B **351**, 24 (1995).

[187] C. J. Burden, C. D. Roberts and M. J. Thomson, "Electromagnetic form-factors of charged and neutral kaons," Phys. Lett. B **371**, 163 (1996) [nucl-th/9511012].

[188] E. O. da Silva, J. P. B. C. de Melo, B. El-Bennich and V. S. Filho, "Pion and kaon elastic form factors in a refined light-front model," Phys. Rev. C **86**, 038202 (2012) [arXiv:1206.4721 [nucl-th]].

[189] E. O. da Silva, J. P. B. C. de Melo, V. S. Filho and B. El-Bennich, "The Electromagnetic Form Factor for the Kaon in the Light-Front Approach," AIP Conf. Proc. **1520**, 452 (2013) [arXiv:1208.2010 [hep-ph]].

[190] O. A. T. Dias, V. S. Filho and J. P. B. C. de Melo, "Kaon and Pion Electromagnetic Form Factor Ratios in the Light-Front," Nucl. Phys. Proc. Suppl. **199**, 281 (2010) [arXiv:1001.4039 [hep-ph]].

[191] U. Raha and H. Kohyama, "Space-and Time-like Electromagnetic Kaon Form Factors," Phys. Rev. D **82**, 114012 (2010) [arXiv:1005.1673 [hep-ph]].

[192] I. C. Clot, W. Bentz and A. W. Thomas, "Role of diquark correlations and the pion cloud in nucleon elastic form factors," Phys. Rev. C **90**, no. 4, 045202 (2014) [arXiv:1405.5542 [nucl-th]].

[193] R. Alkofer, A. Bender and C. D. Roberts, "Pion loop contribution to the electromagnetic pion charge radius," Int. J. Mod. Phys. A **10**, 3319 (1995) [hep-ph/9312243].

[194] P. Maris and P. C. Tandy, "The Quark photon vertex and the pion charge radius," Phys. Rev. C **61**, 045202 (2000) [nucl-th/9910033].

[195] P. Maris and P. C. Tandy, "The quark photon vertex and meson electromagnetic form-factors," Nucl. Phys. A **663**, 401 (2000) [nucl-th/9908045].

[196] P. Maris, "Dyson-Schwinger calculations of meson form-factors," Nucl. Phys. Proc. Suppl. **90**, 127 (2000) [nucl-th/0008048].

[197] A. W. Thomas, "The Pion cloud: Insights into hadron structure," Prog. Theor. Phys. **168** (2007) 614 [arXiv:0711.2259 [nucl-th]].

[198] B. Povh and M. Rosina, "The qq$\bar{\mathbf{q}}$ Component in the Constituent Quark Generates the Pion Cloud of the Nucleon," arXiv:1107.5977 [hep-ph].

[199] A. W. Thomas, "Interplay of Spin and Orbital Angular Momentum in the Proton," Phys. Rev. Lett. **101**, 102003 (2008) [arXiv:0803.2775 [hep-ph]].

[200] G. P. Lepage and S. J. Brodsky, "Exclusive Processes in Quantum Chromodynamics: Evolution Equations for Hadronic Wave Functions and the Form-Factors of Mesons," Phys. Lett. B **87**, 359 (1979).

[201] G. R. Farrar and D. R. Jackson, "The Pion Form-Factor," Phys. Rev. Lett. **43**, 246 (1979).

[202] G. P. Lepage and S. J. Brodsky, "Exclusive Processes in Perturbative Quantum Chromodynamics," Phys. Rev. D **22**, 2157 (1980).

[203] N. Isgur and C. H. Llewellyn Smith, "Asymptopia in High q**2 Exclusive Processes in QCD," Phys. Rev. Lett. **52**, 1080 (1984).

[204] N. Isgur and C. H. Llewellyn Smith, "Perturbative QCD in exclusive processes," Phys. Lett. B **217**, 535 (1989).

[205] N. Isgur and C. H. Llewellyn Smith, "The Applicability of Perturbative QCD to Exclusive Processes," Nucl. Phys. B **317**, 526 (1989).

[206] S. J. Brodsky and G. R. Farrar, "Scaling Laws at Large Transverse Momentum," Phys. Rev. Lett. **31**, 1153 (1973).

[207] D. W. Sivers, S. J. Brodsky and R. Blankenbecler, "Large Transverse Momentum Processes," Phys. Rept. **23**, 1 (1976).

[208] S. J. Brodsky and G. R. Farrar, "Scaling Laws for Large Momentum Transfer Processes," Phys. Rev. D **11**, 1309 (1975).

[209] V. A. Matveev, R. M. Muradian and A. N. Tavkhelidze, "Automodellism in the large - angle elastic scattering and structure of hadrons," Lett. Nuovo Cim. **7**, 719 (1973).

[210] V. A. Matveev, "Deep Inelastic Lepton - Hadron Interactions At High-energies. (in Russian)," In *Gomel 1973, Proceedings, High-energy Physics School*, Dubna 1973, 81-172

[211] V. L. Chernyak and A. R. Zhitnitsky, "Asymptotic Behavior of Exclusive Processes in QCD," Phys. Rept. **112**, 173 (1984).

[212] R. L. Jaffe and P. F. Mende, "When is field theory effective?," Nucl. Phys. B **369**, 189 (1992).

[213] S. i. Nam, "Parton-distribution functions for the pion and kaon in the gauge-invariant nonlocal chiral-quark model," Phys. Rev. D **86**, 074005 (2012) [arXiv:1205.4156 [hep-ph]].

[214] S. i. Nam and C. W. Kao, "Fragmentation and quark distribution functions for the pion and kaon with explicit flavor-SU(3)-symmetry breaking," Phys. Rev. D **85**, 094023 (2012) [arXiv:1202.3281 [hep-ph]].

[215] T. Nguyen, A. Bashir, C. D. Roberts and P. C. Tandy, "Pion and kaon valence-quark parton distribution functions," Phys. Rev. C **83**, 062201 (2011) [arXiv:1102.2448 [nucl-th]].

[216] C. Avila, J. C. Sanabria and J. Magnin, "Pion and kaon parton distribution functions in a meson cloud model," Phys. Rev. D **67**, 034022 (2003) [Phys. Rev. D **68**, 079902 (2003)] [hep-ph/0210421].

[217] C. Avila, J. Magnin and J. C. Sanabria, "Low Q**2 wave functions of pions and kaons and their parton distribution functions," Phys. Rev. D **66**, 034016 (2002) [hep-ph/0005287].

[218] A. I. Signal and A. W. Thomas, "Calculation of Quark Distribution Functions Using Bag Model Wave Functions," Phys. Rev. D **40**, 2832 (1989).

[219] A. W. Schreiber, P. J. Mulders, A. I. Signal and A. W. Thomas, "The Pion cloud of the nucleon and its effect on deep inelastic structure," Phys. Rev. D **45**, 3069 (1992).

[220] D. Diakonov, V. Y. Petrov, P. V. Pobylitsa, M. V. Polyakov and C. Weiss, "Unpolarized and polarized quark distributions in the large N(c) limit," Phys. Rev. D **56**, 4069 (1997) [hep-ph/9703420].

[221] R. J. Holt and C. D. Roberts, "Distribution Functions of the Nucleon and Pion in the Valence Region," Rev. Mod. Phys. **82**, 2991 (2010) [arXiv:1002.4666 [nucl-th]].

[222] M. Bonesini *et al.* [WA70 Collaboration], "High Transverse Momentum Prompt Photon Production by π^- and π^+ on Protons at 280-GeV/c," Z. Phys. C **37**, 535 (1988).

[223] B. Betev *et al.* [NA10 Collaboration], "Differential Cross-section of High Mass Muon Pairs Produced by a 194-GeV/$c\pi^-$ Beam on a Tungsten Target," Z. Phys. C **28**, 9 (1985).

[224] B. Betev *et al.* [NA10 Collaboration], "Observation of Anomalous Scaling Violation in Muon Pair Production by 194-GeV/$c\pi^-$ Tungsten Interactions," Z. Phys. C **28**, 15 (1985).

[225] J. Badier *et al.* [Saclay-CERN-College de France-Ecole Poly-Orsay Collaboration], "Measurement of the K^-/π^- Structure Function Ratio Using the Drell-Yan Process," Phys. Lett. B **93**, 354 (1980).

[226] J. Badier *et al.* [NA3 Collaboration], "Experimental Determination of the pi Meson Structure Functions by the Drell-Yan Mechanism," Z. Phys. C **18**, 281 (1983).

[227] J. S. Conway *et al.*, "Experimental Study of Muon Pairs Produced by 252-GeV Pions on Tungsten," Phys. Rev. D **39**, 92 (1989).

[228] P. J. Sutton, A. D. Martin, R. G. Roberts and W. J. Stirling, "Parton distributions for the pion extracted from Drell-Yan and prompt photon experiments," Phys. Rev. D **45**, 2349 (1992).

[229] W. Bentz, T. Hama, T. Matsuki and K. Yazaki, "NJL model on the light cone and pion structure function," Nucl. Phys. A **651**, 143 (1999) [hep-ph/9901377].

[230] T. Huang, B. Q. Ma and Q. X. Shen, "Analysis of the pion wave function in light cone formalism," Phys. Rev. D **49**, 1490 (1994) [hep-ph/9402285].

[231] H. Mineo, W. Bentz, N. Ishii and K. Yazaki, "Axial vector diquark correlations in the nucleon: Structure functions and static properties," Nucl. Phys. A **703**, 785 (2002) [nucl-th/0201082].

[232] H. Mineo, W. Bentz and K. Yazaki, "Quark distributions in the nucleon based on a relativistic three-body approach to the NJL model," Phys. Rev. C **60**, 065201 (1999) [nucl-th/9907043].

[233] A. W. Schreiber, A. I. Signal and A. W. Thomas, "Structure functions in the bag model," Phys. Rev. D **44**, 2653 (1991).

[234] M. Miyama and S. Kumano, "Numerical solution of Q**2 evolution equations in a brute force method," Comput. Phys. Commun. **94**, 185 (1996) [hep-ph/9508246].

[235] M. Aicher, A. Schafer and W. Vogelsang, "Soft-gluon resummation and the valence parton distribution function of the pion," Phys. Rev. Lett. **105**, 252003 (2010) [arXiv:1009.2481 [hep-ph]].

[236] G. Martinelli and C. T. Sachrajda, "A Lattice Calculation of the Pion's Form-Factor and Structure Function," Nucl. Phys. B **306**, 865 (1988).

[237] S. D. Drell and T. M. Yan, "Connection of Elastic Electromagnetic Nucleon Form-Factors at Large Q**2 and Deep Inelastic Structure Functions Near Threshold," Phys. Rev. Lett. **24**, 181 (1970). doi:10.1103/PhysRevLett.24.181

[238] G. B. West, "Phenomenological model for the electromagnetic structure of the proton," Phys. Rev. Lett. **24**, 1206 (1970). doi:10.1103/PhysRevLett.24.1206

[239] S. D. Drell and T. M. Yan, "Massive Lepton Pair Production in Hadron-Hadron Collisions at High-Energies," Phys. Rev. Lett. **25**, 316 (1970) [Phys. Rev. Lett. **25**, 902 (1970)]. doi:10.1103/PhysRevLett.25.316

[240] S. D. Drell and T. M. Yan, "Partons and their Applications at High-Energies," Annals Phys. **66**, 578 (1971) [Annals Phys. **281**, 450 (2000)]. doi:10.1016/0003-4916(71)90071-6

[241] E. M. Henley and G. Krein, "Nambu-Jona-Lasinio Model and Charge Independence," Phys. Rev. Lett. **62**, 2586 (1989).

[242] H. D. Politzer, "Effective Quark Masses in the Chiral Limit," Nucl. Phys. B **117**, 397 (1976).

[243] A. Barducci, R. Casalbuoni, S. De Curtis, D. Dominici and R. Gatto, "Calculation of the Pseudoscalar Masses From a QCD Effective Potential," Phys. Lett. B **147**, 460 (1984).

[244] J. Bijnens, "Violations of Dashen's theorem," Phys. Lett. B **306**, 343 (1993) [hep-ph/9302217].

[245] J. Bijnens and J. Prades, "Electromagnetic corrections for pions and kaons: Masses and polarizabilities," Nucl. Phys. B **490**, 239 (1997) [hep-ph/9610360].

[246] J. F. Donoghue, B. R. Holstein and D. Wyler, "Electromagnetic selfenergies of pseudoscalar mesons and Dashen's theorem," Phys. Rev. D **47**, 2089 (1993).

[247] J. Gasser and H. Leutwyler, "Quark Masses," Phys. Rept. **87**, 77 (1982).

[248] H. Leutwyler, "The Ratios of the light quark masses," Phys. Lett. B **378**, 313 (1996) [hep-ph/9602366].

[249] J. F. Donoghue and A. F. Perez, "The Electromagnetic mass differences of pions and kaons," Phys. Rev. D **55**, 7075 (1997) [hep-ph/9611331].

[250] D. E. Groom *et al.* [Particle Data Group Collaboration], "Review of particle physics. Particle Data Group," Eur. Phys. J. C **15**, 1 (2000).

[251] R. D. Young, "Nucleon structure in the search for new physics," AIP Conf. Proc. **1354**, 19 (2011) [arXiv:1102.3231 [hep-ph]].

[252] P. E. Shanahan *et al.*, "Charge symmetry violation in the electromagnetic form factors of the nucleon," Phys. Rev. D **91**, no. 11, 113006 (2015) [arXiv:1503.01142 [hep-lat]].

[253] J. A. Nolen, Jr. and J. P. Schiffer, "Coulomb energies," Ann. Rev. Nucl. Part. Sci. **19**, 471 (1969).

[254] J. W. Negele, Nucl. Phys. A **165**, 305 (1971).

[255] J. W. Negele, "The Coulomb Energy Anomaly and Charge Asymmetry," Comments Nucl. Part. Phys. **6**, no. 1, 15 (1974).

[256] R. Horsley *et al.*, "Charge Symmetry Breaking in Parton Distribution Functions from Lattice QCD," Phys. Rev. D **83**, 051501 (2011) [arXiv:1012.0215 [hep-lat]].

[257] G. A. Miller, A. K. Opper and E. J. Stephenson, "Charge symmetry breaking and QCD," Ann. Rev. Nucl. Part. Sci. **56**, 253 (2006) [nucl-ex/0602021].

[258] G. A. Miller, B. M. K. Nefkens and I. Slaus, "Charge symmetry, quarks and mesons," Phys. Rept. **194**, 1 (1990).

[259] G. A. Miller, "Charge symmetry breaking," Nucl. Phys. A **518**, 345 (1990).

[260] I. Slaus, B. M. K. Nefkens and G. A. Miller, "Quark mass difference and the origin of charge symmetry breaking," Nucl. Instrum. Meth. B **56-57**, 489 (1991).

[261] R. Horsley *et al.*, "QED effects in the pseudoscalar meson sector," arXiv:1509.00799 [hep-lat].

[262] B. Kubis, "Charge-symmetry-breaking nucleon form factors," Hyperfine Interact. **201**, 7 (2011) [arXiv:0910.2800 [nucl-th]].

[263] A. D. Martin, R. G. Roberts, W. J. Stirling and R. S. Thorne, "Uncertainties of predictions from parton distributions. 2. Theoretical errors," Eur. Phys. J. C **35**, 325 (2004) [hep-ph/0308087].

[264] J. T. Londergan, D. P. Murdock and A. W. Thomas, "Experimental tests of charge symmetry violation in parton distributions," Phys. Rev. D **72**, 036010 (2005) [hep-ph/0507029].

[265] S. A. Coon, "The u - d quark mass difference and nuclear charge symmetry breaking," Nucl. Phys. A **689**, 119 (2001) [nucl-th/0101004].

[266] J. T. Londergan and A. W. Thomas, "The Validity of charge symmetry for parton distributions," Prog. Part. Nucl. Phys. **41**, 49 (1998) [hep-ph/9806510].

[267] J. T. Londergan, J. C. Peng and A. W. Thomas, "Charge Symmetry at the Partonic Level," Rev. Mod. Phys. **82**, 2009 (2010) [arXiv:0907.2352 [hep-ph]].

[268] P. E. Shanahan, A. W. Thomas and R. D. Young, "Charge symmetry breaking from a chiral extrapolation of moments of quark distribution functions," Phys. Rev. D **87**, no. 9, 094515 (2013) [arXiv:1303.4806 [nucl-th]].

[269] M. Wagman and G. A. Miller, "Charge Symmetry Breaking and Parity Violating Electron-Proton Scattering," Phys. Rev. C **89**, no. 6, 065206 (2014) [Phys. Rev. C **91**, no. 1, 019903 (2015)] [arXiv:1402.7169 [nucl-th]].

[270] T. J. Hobbs, J. T. Londergan, D. P. Murdock and A. W. Thomas, "Testing Partonic Charge Symmetry at a High-Energy Electron Collider," Phys. Lett. B **698**, 123 (2011) [arXiv:1101.3923 [hep-ph]].

[271] E. N. Rodionov, A. W. Thomas and J. T. Londergan, "Charge asymmetry of parton distributions," Mod. Phys. Lett. A **9**, 1799 (1994).

[272] R. Horsley, J. Najjar, Y. Nakamura, D. Pleiter, P. E. L. Rakow, G. Schierholz and J. M. Zanotti, "Octet baryon mass splittings from up-down quark mass differences," PoS LATTICE **2012**, 135 (2012) [arXiv:1212.5507].

[273] E. Sather, "Isospin violating quark distributions in the nucleon," Phys. Lett. B **274**, 433 (1992).

[274] J. Arrington *et. al.*, (Jefferson Lab), "Precise Measurement of $\frac{\pi^+}{\pi^-}$ Ratios in Semi-Inclusive DIS, Part 1 : Charge Symmetry Violating Quark Distributions", Jefferson Lab PAC **34** Proposal, (2008)

[275] G. M. Huber *et. al.*, (Jefferson Lab), "Measurement of the charged Pion Form Factor to High Q^2", Jefferson Lab PAC **30** Proposal, (2006).

[276] T. Horn *et. al.*, (Jefferson Lab), "Studies of the L-T Separated Kaon Electroproduction Cross Section from 5-11 GeV", Jefferson Lab PAC **38** Proposal, (2011).

[277] E. M. Henley and G. A. Miller, "Excess of anti-D over anti-U in the proton sea quark distribution," Phys. Lett. B **251**, 453 (1990).

[278] B. Kubis and R. Lewis, "Isospin violation in the vector form factors of the nucleon," Phys. Rev. C **74**, 015204 (2006) [nucl-th/0605006].

[279] R. J. Holt, "Large x physics: recent results and future plans," arXiv:1311.1527 [nucl-ex].

[280] G. R. Farrar and D. R. Jackson, "Pion and Nucleon Structure Functions Near x=1," Phys. Rev. Lett. **35**, 1416 (1975).

[281] X. d. Ji, J. P. Ma and F. Yuan, "Factorization of large-x quark distributions in a hadron," Phys. Lett. B **610**, 247 (2005) [hep-ph/0411382].

[282] K. Wijesooriya, P. E. Reimer and R. J. Holt, "The pion parton distribution function in the valence region," Phys. Rev. C **72**, 065203 (2005) [nucl-ex/0509012].

[283] J. F. Donoghue and E. S. Na, "Asymptotic limits and structure of the pion form-factor," Phys. Rev. D **56**, 7073 (1997) [hep-ph/9611418].

[284] A. D. Martin, R. G. Roberts, W. J. Stirling and R. S. Thorne, "Parton distributions incorporating QED contributions," Eur. Phys. J. C **39**, 155 (2005) [hep-ph/0411040].